UTS UNIVERSITY OF TECHNOLOGY SYDNEY

Thermal Performance Analysis of Conventional and Enhanced Corrugated and Flat Plate Heat Exchangers

By

Salman Al zahrani

Thesis submitted in fulfilment of the requirements for the degree of

Doctor of Philosophy

University of Technology Sydney

School of Mechanical and Mechatronic Engineering

November 2020

CERTIFICATE OF ORIGINAL AUTHORSHIP

I, Salman Al zahrani, declare that this thesis is submitted in fulfilment of the requirements for the award of Doctor of Philosophy, in Mechanical Engineering at the University of Technology Sydney. This thesis is wholly my own work unless otherwise referenced or acknowledged. In addition, I certify that all information sources and literature used are indicated in the thesis. This document has not been submitted for qualifications at any other academic institution. This research is supported by the Australian Government Research Training Program.

Signature: Production Note:
Signature removed prior to publication.

Date: 11.11.2020

Keywords

Plate Heat Exchanger; Corrugated Plate Heat Exchanger; Flat Plate Heat Exchanger; Novel Design; Chevron Angle; CFD; Corrugation; Thermo-Hydraulic Characteristics; Overall Thermal Performance; Numerical Modelling; Turbulent; Laminar; Heat Transfer; Nusselt Number; Single-Phase; Reynolds Number; Basic Design; Heat Transfer Enhancement; Heat Exchanger; Flow Maldistribution; Pressure Drop; JF Factor; Flow Resistance; Flow Velocity; Modified Plate; Passive Technique; Compact; Conventional Plate Heat Exchanger.

Dedication

This thesis is dedicated to my deceased father, **Ahmed**, who passed away just one year before I started my PhD journey, to the one I love the most, my mother **Alia** with eternal appreciation, to my brothers and sisters, to my wife **Asrar** and to my children **Battal, Jassar,** and **Alia.**

Abstract

Plate heat exchangers (PHEs) have been extensively adopted for a large number of industrial applications, particularly systems that require high thermal efficiencies such as aerospace and heat recovery applications. Several studies have been performed on PHEs to disclose the impact of different geometrical parameters on heat transfer characteristics. However, the demand for energy is continuously increasing, and there is continuous development in industrial processes that require newly developed compact heat exchangers (HEs). Therefore, this thesis aims to introduce enhanced corrugated and flat PHEs. Passive enhancement techniques are adopted. Computational fluid dynamics (CFD) has been utilised to verify the superiority of the proposed enhanced PHEs. All turbulence models have been tested, and realizable $k-\varepsilon$ with scalable approach for wall treatment is found the best model that could provide the most accurate data. All PHEs that have been studied in the present thesis have identical geometrical and physical parameters. Full CAD approach is used, and all geometrical parameters are considered i.e. port effect and sinusoidal corrugations shape. The numerical approach has been extensively validated with benchmark studies from the literature, and an experiment is conducted for further validation. All studies are performed for water-water, 1-1 pass, U type, and counter-current flow arrangements. To assess the thermal performance of the enhanced PHEs, the findings have been compared with those of the conventional PHEs. Nusselt number (Nu), and fanning friction factor (*f*) are utilized as indicators of enhancement in the convective heat transfer and pressure drop, respectively. Moreover, turbulence kinetic energy, turbulence intensity, JF factor, intensity of flow maldistribution along with other parameters, are also employed to compare the thermal performance of the enhanced PHEs against the conventional ones. Generally, the thermal performance of the proposed corrugated and flat PHEs unequivocally outperforms that of the conventional PHEs. For instance, the enhancement in Nu data of the modified PHEs are up to 75%, 70%, 30%, and 175% with respect to the conventional PHEs. Hence the selection of the enhanced PHEs must be carefully performed, e.g. based on allowable pressure drop. Overall, these enhanced PHEs could pave the way for more compact HEs to be built and incorporated in applications that require more compact and durable HEs. They could be potential replacements of their counterparts of PHEs. In all studies, heat transfer correlations have been developed to assist the designers in predicting the HEs' thermal performance and to estimate the required heat transfer surface area.

Acknowledgements

I would like to express my heartfelt thanks to my principal supervisor and mentor, Dr Suvash C. Saha, for his unlimited support and guidance. He has always been the best example for me of how a professional researcher should be. Since the first day of my PhD journey, he has been a kind mentor, constructive, and with an encouraging attitude.

I would also like to express my sincere gratitude to my co-supervisor, Dr Mohammed S. Islam, for his endless support and guidance. I know a mere "thank you" is not enough to be said to those who have always been there to guide, inspire and assist me. However, it will always remind me that I am indebted to them.

My gratitude also goes to my sponsor Al Baha University for their financial support. I would also like to acknowledge professional editor, Diane Kolomeitz, for copyediting and proofreading services according to the guidelines laid out in the university-endorsed national 'Guidelines for editing research theses'.

I would like to stress how indebted I am to all of the UTS members, and to the members of my group in particular. Also, my gratitude goes to UTS interactive high performance computing members, for their technical services.

List of Publications

Journal Papers:

1. **S. Al-Zahrani**, M.S. Islam, F. Xu, S.C. Saha, Thermal performance investigation in a novel corrugated plate heat exchanger, **International Journal of Heat and Mass Transfer**, 148 (2020) 119095, [Q1], IF: 4.947
2. **S. Al-Zahrani**, M.S. Islam, S.C. Saha, Comparison of flow resistance and port maldistribution between novel and conventional plate heat exchangers, **International Communication in Heat and Mass Transfer**, 123 (2021) 105200, [Q1], IF: 3.971
3. **S. Al-Zahrani**, M.S. Islam, S.C. Saha, Heat transfer enhancement investigation in a novel flat plate heat exchanger. **International Journal of Thermal Sciences**, 161 (2021) 106763, [Q1], IF: 3.476
4. **S. Al-Zahrani**, M.S. Islam, S.C. Saha, Heat transfer augmentation in retrofitted corrugated plate heat exchanger, **International Journal of Heat and Mass Transfer**, 161 (2020) 120226, [Q1], IF: 4.947
5. **S. Al-Zahrani**, M.S. Islam, S.C. Saha, Heat transfer enhancement of modified flat plate heat exchanger, **Applied Thermal Engineering**, 186 (2021) 116533, [Q1], IF: 4.725

Peer Review Conference Paper:

S. Al-Zahrani, M.S. Islam, S.C. Saha, A thermo-hydraulic characteristics investigation in corrugated plate heat exchanger, Energy Procedia. 160 (2019) 597–605 .

Table of Contents

List of Figures

List of Tables

Symbols

A	Effective heat transfer area, m^2
$A_\circ$	Channel flow heat transfer area, m^2
A_h	Heat transfer area of the process fluid, m^2
A_P	Cross-sectional area of the inlet port, m^2
b	Corrugation depth, m
C_p	Specific heat, $J/kg.k$
d_e	Equivalent diameter, $d_e = 2b, m$
f	Fanning friction factor
h	Convective heat transfer coefficient, W/m^2K
G	Mass flux, kg/m^2s
L_h	Horizontal length from port to port, m
L_p	Plate's channel effective length, m
L_v	Vertical length from port to port, m
L_w	Flow channel width, m
$\dot{m}$	Mass flow rate, kg/s
N	Number of channels
Q	Heat transfer rate, W
P_m	Overall pressure drop, Pa
T	Temperature, K
t	Plate thickness, m
ΔTp	Temperature gradient of the plate
Tp,avg	Average temperature of the plate
Tp,max	Maximum temperature of the plate
Tp,min	Minimum temperature of the plate

S_k	User define source
S_ε	

Dimensionless quantities

j	Colburn factor, $j = \frac{Nu}{RePr^{1/3}}$
JF	JF factor
Nu	Nusselt number
Pr	Prandtl number
P_{mal}	Flow maldistribution intensity
Re	Reynolds number
Re_{cr}	Critical Reynolds number

Abbreviation

CPHE	Corrugated plate heat exchanger
FPHE	Flat plate heat exchanger
HE	Heat exchanger
HVAC	Heating, ventilation, and air conditioning
NTU	Number of transfer units
PHE	All types of plate heat exchanger
PHE^1	Basic plate heat exchanger
PHE^2	The modified plate heat exchanger

Greek letters

β	Chevron angle, °
μ	Dynamic viscosity, $Pa.s$
μ_t	Turbulent viscosity, $Pa.s$
ρ	Fluid density, kg/m^3
E	Effectiveness

Subscripts

avg	Average
b	Bulk fluid temperature
c	Cold stream
h	Hot stream
HTC	Heat transfer characteristics
i	Inlet condition
min	Minimum
max	Maximum
m	Measured
0	Outlet condition
w	Wall
mal	Maldistribution
i, j, k	Unit vectors for 3-space coordinates

Chapter 1: Introduction

1.1 Background

Plate heat exchanger (PHE) was introduced for the first time in the 1870s in Germany [1]. It was composed of a series of flat (also called smooth) thermal plates stacked one above the other. This heat exchanger (HE) is known as flat PHE (FPHE). A gasket is installed on the periphery of the front side of each plate, as presented in Fig. 1.1. The purposes of the gasket are to create space between each two consecutive thermal plates (channel), prevent leakage, and guide the flow into the required direction. There are four holes (ports) on the corners of each plate to allow the hot and the cold fluids to flow alternatively between the hot and the cold channels. Thus, each thermal plate is in contact with the hot fluid from one side and the cold fluid from the other side except the first and end plate, as shown in Fig. 1.2.

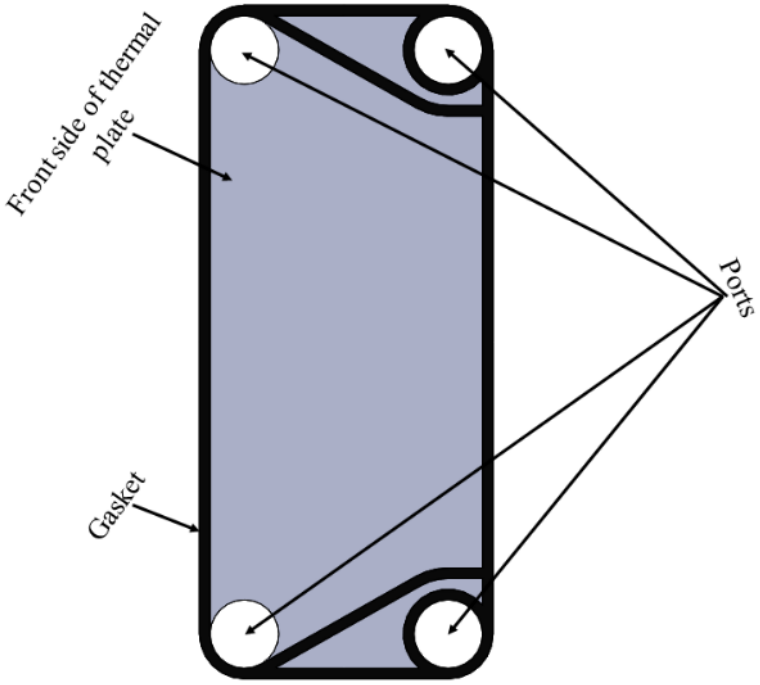

Fig. 1.1: Schematic drawing of thermal plate.

In the 1920s, PHEs were employed for milk pasteurization [2]. The plates were cast metal collected inside a frame [2]. The main drawbacks at that time were the limited operating pressure and temperature. Mainly, the maximum operating pressure and temperature were respectively 3 bar and 100 °C [2]. In 1933, Seligman [3] proposed the corrugated surface instead of the flat one. Both flat and corrugated plates are still utilized

up to this time [4-10]. However, corrugated plates are more popular and used on a wider range. That is because the corrugations promote the flow velocity/ flow mixing, boundary layer separation, and enhance the rigidity of the entire corrugated PHE (CPHE).

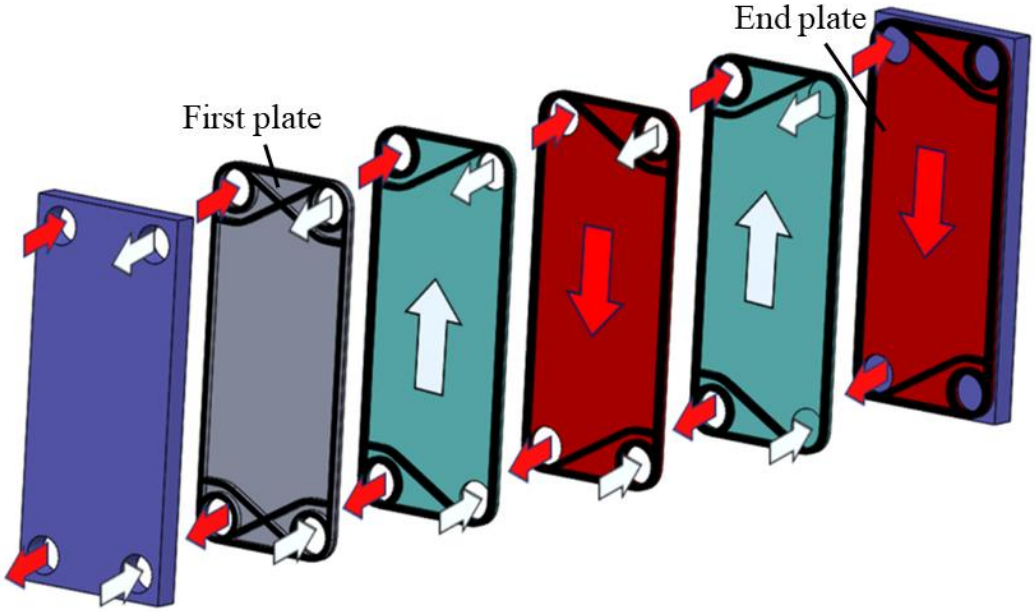

Fig. 1.2: Illustrative schematic for counter current flow mechanism of FPHE.

In the 1960s, new processes in the dairy industry was developed, and these required higher temperature and pressure, which stimulated manufacturers and researchers to develop the PHEs to meet these new processes. Since then, the development of PHEs has been set to meet the needs of several industrial applications. Nowadays, heat exchangers play a primary role in a large number of industrial and residential applications. PHEs have been incorporated in pharmaceutical industries, HVAC systems, water desalination plants, dairy processes, paper/pulp, acid coolers, power plants and oil coolers, along with a large number of applications. In 2019, the size of the global market of HEs was assessed at USD 15.9 billion and is anticipated to rise by 6% from 2020 to 2027 [11]. The size of the global market of PHEs was evaluated at USD 3.32 billion in 2019, and it is likely to rise by 6.9% over a short period [12]. This rise is directly proportional to the innovations that could improve the overall thermal-hydraulic performance of the PHEs [12].

Heat transfer surface area of the HE to its volume is called area density. The area density for compact HEs is usually greater than 700 m^2/m^3 [13], and all types of PHEs, i.e. brazed, welded, and gasketed PHEs, are compact [14]. One main task for the HEs'

manufacturers and researchers is to come up with novel approaches to boost the overall thermal performance of the HEs. Reducing fuel consumption, saving material for HE construction (making it compact), and reducing the required pumping power are stimulators to constantly improve the designs of HEs. Moreover, various applications, i.e. spacecraft, and automobiles require compact/small size, and lightweight HEs. Two techniques are used to achieve this aim, and they are known as active and passive techniques. Active enhancement methods involve external power such as surface vibration, jet impingement, and electric field. In comparison, passive enhancement methods are incorporated within the HE itself, such as using extended surfaces, dimples, rough surfaces, ribs, twisted tapes, and wire coils. Fixing a disturbance in the fluid path to break the thermal boundary layers, which would eventually increase the heat transfer coefficient, is very common in HEs. However, the pressure drop may increase significantly in the process, which would lead to a higher pumping cost. Generally, passive enhancement methods are better than active ones because they don't require external power, and they are simpler in design [15]. Therefore, based on the constant necessity to improve the thermal performance of HEs, PHEs in particular, and because of the continuous expend on energy demand [16], developing innovative PHEs is significantly important in order to meet these requirements.

1.2 Research Question

PHEs are compact in nature, and they yield high thermal performance. Nevertheless, several flaws are accompanied with these PHEs i.e. flow maldistribution. In addition, corrugated type PHE contains one of the most complicated channels with a large number of geometrical parameters. Therefore, this thesis arises the following questions:

- Is it feasible to develop sophisticated numerical models of PHEs that take into account the influence of all geometrical parameters on heat transfer and pressure drop?
- Can the design of the current conventional PHEs be improved by imposing new innovative passive techniques?
- What is the impact of the newly developed passive techniques of PHEs on the overall thermal performance with respect to the conventional PHEs?

1.3 Aim and Objectives

For any HE, it is an essential target to reduce its size and weight to save the required material, space, and fuel consumption for the same heat duty. Therefore, the present thesis aims to improve the thermal performance of the current flat and corrugated PHEs. Accordingly, the following objectives are to be fulfilled to achieve the aim of this thesis:

i. Develop sophisticated numerical models that can efficiently simulate the real physics that take place inside PHEs. More specifically, the effect of all geometrical parameters that impact the thermal performance of PHEs is to be considered when generating the numerical models.
ii. Verify the accuracy of the adopted numerical technique. Mainly, validate the numerical results with benchmark experimental studies.
iii. Develop innovative passive techniques that could boost the thermal performance of both corrugated and flat PHEs.
iv. Obtain the heat transfer data, and generalize those data by generating Nu, and *f* correlations to extend the quantitative understanding of the PHEs' thermal performance. In addition, analyse the impact of the new passive techniques on other physical phenomenon, and quantities such as temperature distribution, flow maldistribution, heat transfer effectiveness, turbulence kinetic energy (TKE), and shear stress.

1.3.1 Significance, scope and innovation

Heat exchangers are known as one of the most essential pieces of equipment in a wide range of industrial applications. They are used to regulate temperature, capture by-product heat that would be otherwise dumped into the atmosphere, for food pasteurization, and cooling/heating process fluids along with other utilizations. Generally, heat exchangers are the main parts in most energy sectors. Moreover, PHEs are the most utilized type among all compact heat exchangers [17]. The thermal performance of these PHEs would directly influence the efficiency of the entire cycle where these HEs are integrated. This thesis reveals the heat transfer characteristics of full CAD flat and corrugated PHEs. The numerical models are extensively validated with several experimental studies from the literature. Also, experiments have been carried out to verify

the validity of the adopted numerical technique.

In 1920s and 1930s, flat and corrugated PHEs were respectively invented [2, 18]. The same designs of these PHEs are still in use up to the present time. However, the industrial advancement and the continuous demand on energy require continuous improvement in the thermal performance of HEs. Therefore, this thesis introduces various innovative modifications to the design of both flat and corrugated PHEs. Thermal performance of these innovative PHEs surpasses that of the conventional PHEs. Consequently, this will allow for smaller PHEs (greater area density) to be constructed for the same heat duty, which would result in smaller floor space, lower fuel consumption, and material saving. Important applications such as rockets, ships, cars, and concentrated solar power require small lightweight heat exchangers with superior thermal and mechanical performance. The newly developed PHEs in this thesis could be potential solutions for such critical applications. This thesis studies these newly developed PHEs from the perspective of thermal performance. The contact area between the successive thermal plates of the newly developed PHEs is greater than that of the conventional PHEs. Therefore, the mechanical integrity and the maximum allowable pressure drop of these innovative PHEs are likely to be greater than those of the conventional PHEs. Thereby, this thesis paves the way for further studies to be conducted i.e. to verify the correctness of the latter point along with other suggested studies. The present thesis provides the heat transfer correlations of the newly developed and the conventional PHEs. These correlations will assist designers to calculate the required heat transfer surface area and to predict heat transfer rate and pressure drop of the newly developed and the conventional PHEs.

1.3.2 Thesis structure

The present thesis consists of eight chapters. The arrangement of these chapters is presented in Fig. 1.3.

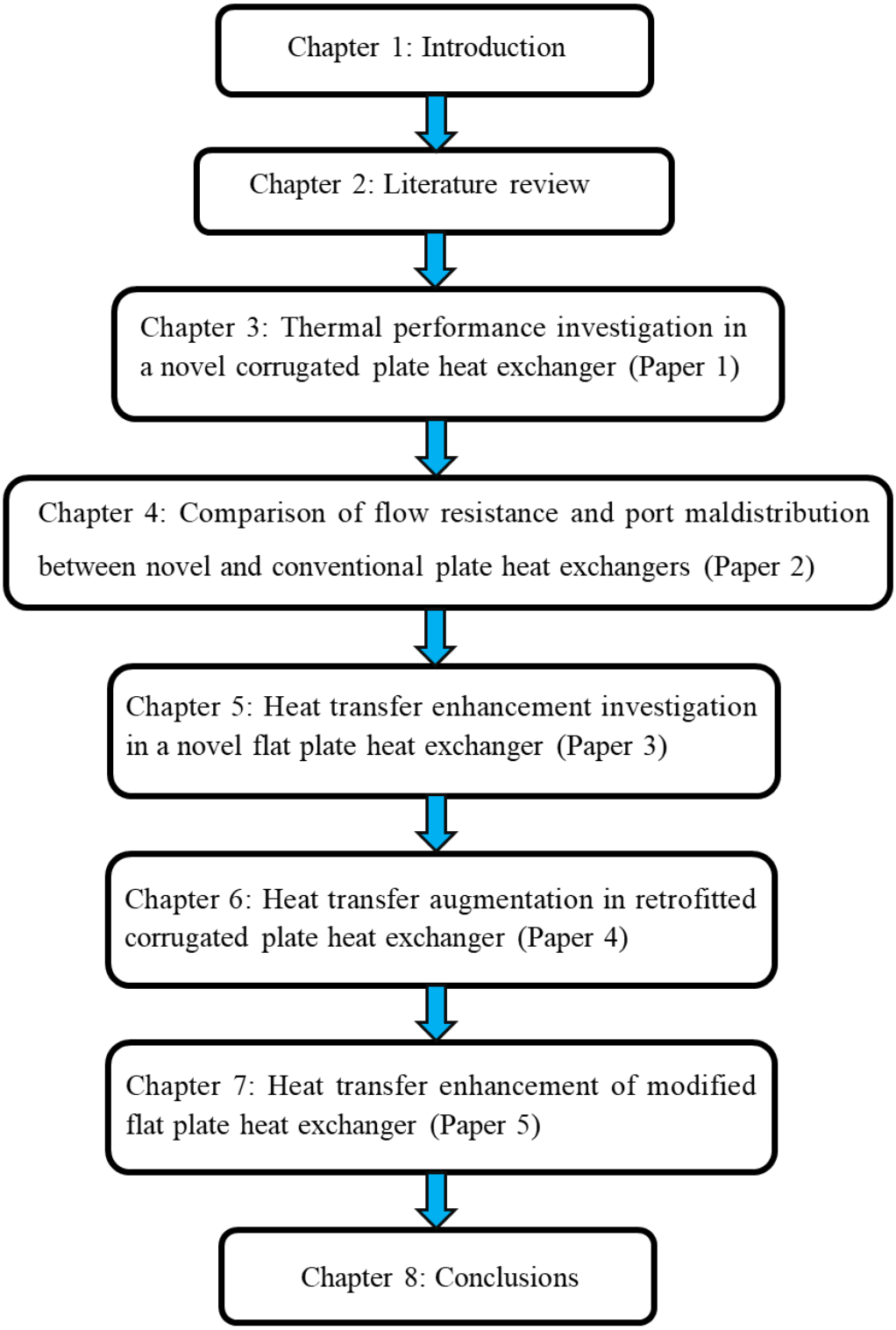

Fig. 1.3: Flowchart of this thesis.

Chapter 2: Literature Review

2.1 General Overview

The importance of energy in our modern life style is overtly perspicuous, and its growth is directly related to prosperity and welfare across the world. Heat exchangers are the major parts in most of the energy sectors. It is rare to find process plant without heat exchanger(s). Heat exchangers are critical, and they could directly impact the overall efficiency of the plants. They are incorporated with oil industries, HVAC systems, recovery applications, electric generation plants, aerospace industries, food and beverage processes, water desalination plants etc. An important point is this: energy sectors all over the globe have been constantly facing serious challenges, and a very small part of these challenges will be highlighted in the forthcoming discussion.

There is an increased demand on energy i.e. petrochemicals and transport are continuously pushing demand to higher levels. In 2013, the demand was 90 million barrels per day (mb/d), and this is expected to reach 104 mb/d in 2040 [16]. According to the International Energy Agency (IEA), $ 900 billion per year must be invested in energy development technologies to meet the projected demand by 2030 [16]. In addition, carbon dioxide (CO2) emissions were 33.9 billion metric tons in 2015, which is expected to reach to 39.3 billion metric tons by 2040 [19].

Furthermore, for many decades past and still until now, electricity is the fastest growing form of energy [19]. In 2015, the net electricity generation in the world was 23.4 trillion kWh, and it is expected to reach 34 trillion kWh in 2040 [16, 19]. Thus, in order to keep pace with the increased demand on electricity, 11 trillion kWh is needed to be generated in the next two decades. In sub-Saharan Africa, more than 600 million people are living without electricity [16]. Some people in that region have electricity, though it is unreliable, insufficient, and very costly [16]. Solid biomass represents the main source for cooking for more than 700 million people in sub-Saharan Africa [16]. Using this solid biomass attributes to 13% of global pollution and 600,000 premature deaths every year, although the energy demand of this region is only 4% of the global demand [16]. Therefore, the global agencies of energy (i.e. IEA) are demanding urgent actions to improve energy sectors in such areas.

PHEs occupy first rank in the global market among all types of compact HEs [17]. In

2009, the cost of global demand on HEs exceeded 9.5 million euro (M€), and ~22% of this demand was on PHEs (2.100 M€) [20]. There are several types of PHE, and two types will be investigated in this thesis: corrugated and flat PHEs. PHEs have been known of, for several decades. They have modular nature that makes the system flexible (Fig. 2.1 (a) and (b)) to meet the heat duty requirement very quickly, and they yield higher thermal performance in comparison with other conventional HEs [21]. For a given heat duty, the PHE's surface area needed is 30-50% with respect to that of shell and tube heat exchangers [22], hence the cost is reduced. PHEs' weight and volume are respectively 30% and 20% of the shell and tube HE [22, 23]. All the advantages of PHEs are explained in section 2.12. Because of these advantages, PHEs have been widely adopted for various industrial applications [24, 25].

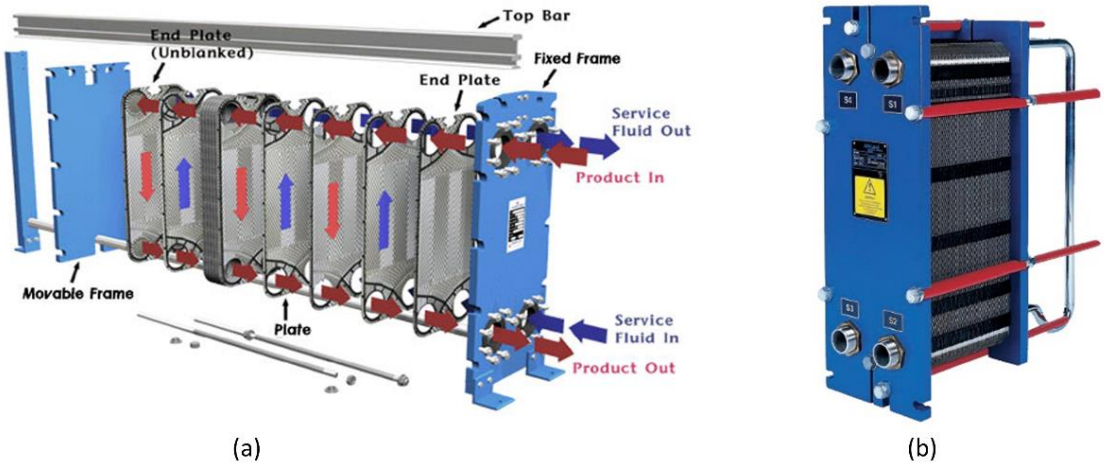

Fig. 2.1: (a) Disassembled CPHE, and (b) Assembled CPHE[1].

The thermo-hydraulic performance of PHE is high because of the small hydraulic diameter; also, PHEs have large surface areas, where fluids flow on both surfaces of each plate, except the first and the end plate. Over the last seven decades, the material technology of PHEs has been significantly improved. The current operating pressure can reach up to 40 bar, and the temperature can range from -50 °C to 350 °C [17]. In addition, PHEs are most efficient when they serve liquid-to-liquid applications with no change occurring in their phase [26]. Moreover, 1-1 pass flow arrangement yields the lowest pressure drop, lowest flow maldistribution, and the highest effectiveness for NTU > 5 [27-29]. Therefore, 1-1 pass flow arrangement, and water-water as base fluid have been

[1] Resources for figure 1.2 : http://www.separationequipment.com/m6-plate-heat-exchanger.html

adopted in this thesis for all cases.

2.2 PHE's Design Approaches

Despite the high thermal performance of PHE, there is no database for the design of PHE. The reason is due to the complexity of PHE channel geometry, diversity of flow and pass arrangements, and the large number of geometrical and physical parameters that affect the performance of the PHE. In fact, PHEs have the most complicated channel geometry of all ducts [30]. However, there have been several research works that have been carried out to draw a guideline for PHEs' design. Simplified methods [31-34] have been generated to calculate the required number of plates. Graphical procedures for optimizing the number of passes and the number of channels per pass have been conducted by Jarzebski and Wardas-Koziel [35]. A numerical study for counter current flow, and number of different pass arrangements have been performed by Kandlikar & Shah [29]. They investigated the impact of number of passes, and number of thermal plates on the number of transfer units (NTU), temperature effectiveness (P), and log mean temperature difference correction factor (F), and all data have been tabulated. An important finding is that the 1-1 pass arrangement was found to provide the highest effectiveness for NTU>5. However, in many industrial applications, multi passes are required due to the required heat duty and the differences in the fluids' heat capacities. In addition, similar studies with different approaches, such as experimental data-based [36], physically-based mathematical model [37], and numerical data-based [37-40] have been conducted to help the manufacturer and the designer of PHE to predict and analyse the performance of PHE.

2.3 Experimental Studies Overview

Most experimental studies have been carried out to investigate the impact of a specific parameter e.g. chevron angle (β). Through the last seven decades, heat transfer correlations have been generated. These are specific in nature because most of them were created during an investigation for either a specific geometry, experimental range of operations, or both. However, they are useful where you can choose the closest one to your application.

Okada et al. [41] studied the impact of different chevron angles range from 0° to 60°. Their study has been carried out on seven CPHEs. Reynolds number (Re) ranges from

400 to 15,000, and water-water were used as the working fluids. The result showed that, as the chevron angle decreases the heat transfer coefficient increases. The pressure drop is about 1.5 to 2 times higher compared with other conventional heat exchangers. The Nusselt correlations were generated as follows:

$$Nu = 0.14\, Re^{0.66} Pr^{0.4} \qquad \beta=60°$$

$$Nu = 0.22\, Re^{0.64} Pr^{0.4} \qquad \beta=45°$$

$$Nu = 0.34\, Re^{0.64} Pr^{0.4} \qquad \beta=30°$$

$$Nu = 0.42\, Re^{0.62} Pr^{0.4} \qquad \beta=15°$$

$$400 < Re < 15{,}000 \qquad (2.1)$$

Muley & Manglik [42] studied the heat transfer characteristics for single-phase (water-water). Thermal performance for CPHEs with U type counter-current flow and for three different chevron angles 30°/30°, 60°/60°, and mixed 30°/60° has been investigated. Nu and *f* correlations have been generated as a function of Re, Pr, surface enlargement factor (∅), and chevron angle. All correlations were incorporated in single equation. Yet, neither deviation was reported, nor were the equations for each chevron angle provided, in order to enable the reader to estimate the deviation between each single equation and the incorporated one. Similar attempts for incorporating equations under a range of chevron angles have been conducted by various authors [43-45]. However, because the channels of CPHE are composed of numerous geometrical parameters, the accuracy of an incorporated single equation for different parameters is an open issue in the literature. Results showed that Nu is directly proportional to the surface enlargement factor, and chevron angle. However, there is penalty for the increasing of heat transfer, which is an increasing in pressure drop at a given pumping power. The Muley & Manglik [42] incorporated equations for Nu and *f* are given as:

$$Nu = [0.2668 - 0.006967\boldsymbol{\beta} + 7.244 \times 10^{-5}\beta^2] \times Re^{\left[0.728+0.0543 \sin\left[\left(\frac{\pi\beta}{45}\right)+3.7\right]\right]} Pr^{\frac{1}{3}} \left(\frac{\mu}{\mu_w}\right)^{0.14} \qquad (2.2)$$

$$f = [2.917 - 0.1277\boldsymbol{\beta} + 2.016 \times 10^{-3}\boldsymbol{\beta}^2] \times Re^{-[0.2+0.0577 \sin\left(\left[\left(\frac{\pi\beta}{45}\right)+2.1\right]\right.} \qquad (2.3)$$

They are applicable for Re ≥ 1000, 30°≤ β ≤60°, and ∅ = 1.29.

Khan et al. [46] have investigated the heat transfer characteristics of two symmetric

chevron angles 30°, 60°, and one mixed chevron angle 30°/60° for $500 < Re < 2500$ and $3.5 \leq Pr \leq 6.5$. Because Re was the same on both sides, the heat transfer coefficient "h" was considered the same for both hot and cold sides. Thus, they assumed Nu would be the same on both sides. However, the same Re on both sides of the CPHE does not imply h will be the same, as h depends on many other factors i.e. fluid viscosity, fluid density, fluid velocity etc. For the cold side, h is likely greater than that of the hot side, because thermal boundary layer resistance is lower in the case of cold fluids [47]. In addition, heat capacity rate (C) of cold water is higher than that of hot water as the viscosity of cold water is higher than that of hot water. Hence the velocity of the cold water would be higher in order to meet the same Reynolds number. Consequently, the mass flow rate of cold water will be higher than that of hot water. Therefore, considering Nu the same on both sides is not an accurate assumption. Similar studies have been performed on CPHE to investigate the impact of different chevron angles [48-60].

Generally, the only geometrical parameter that was investigated in this study [46] is β. The findings showed that Nu increases with the increasing of the chevron angle and it increases linearly as Re increases. The impact of different $\beta's$ was represented in the form of Nu as:

$$Nu = 0.144\, Re^{0.8414} Pr^{0.35} (\mu/\mu_b)^{0.14} \qquad \beta=60°/60°$$

$$Nu = 0.1437\, Re^{0.7810} Pr^{0.35} (\mu/\mu_b)^{0.14} \qquad \beta=30°/60° \qquad (2.4)$$

$$Nu = 0.1368\, Re^{0.7424} Pr^{0.35} (\mu/\mu_b)^{0.14} \qquad \beta=30°/30°$$

An important note is this: some studies i.e. Okada et al. [41] reported that, as chevron angle decreases, Nu increases. Although it seems in contradiction with the findings of Khan et al. [46], both conclusions are identical. The reason is that, Okada et al. [41] considered β with respect to the horizontal axis, whereas Khan et al. [46]considered β with respect to the vertical axis. The latter point refers to an obstacle in the literature where there is no code or standards in case of PHE.

Cieśliński et al. [61] performed an experimental study to investigate the validity for some correlations that have been published in the literature. The result showed that, the correlations generated by Richter et al. [62] are not preferred to be used because they under-predict the heat transfer average values. The correlations of Muely & Manglik [42] showed the best consistency and hence can predict Nu values reasonably well. However,

the percentage of deviation with the result of Richter et al. [62] was not provided, and only one experiment was conducted with β = 61°. In addition, the differences in the geometrical parameters were not considered, which will contribute to the discrepancy between the results of these studies [63]. Thermal performance study of CPHE with three plates of herringbone type (two channels), and one chevron angle 60° has been carried out by Gherasim et al. [51]. Nu and f data have been calculated for the hot side; Re ranges from 400 up to 1500 and from 50 up to 850 for hot and cold sides, respectively. The corrugation shapes were trapezoidal. Therefore, the discrepancy between the results has been justified by the attribution of the trapezoidal shape and the number of the plates. Isotherms on the exterior plates were presented, to help to visualize the temperature gradient along the vertical and horizontal axes. Their study did not investigate the impact of any parameter. Also, f data against Re was plotted but the correlation of f was not provided. The flow rate for the cold side was fixed at Re = 800, and its average temperature also fixed at 25 °C. The flow rate for the hot side has been changed 11 times. The Nu correlation was generated as:

$$Nu = 0.377\, Re^{0.617} Pr^{0.33} \left(\frac{\mu_b}{\mu_w}\right)^{0.17} \tag{2.5}$$

The reason Re started at 400 for the hot side in this study [51] is to ensure the flow is turbulent However, there is disagreement upon the onset of the turbulence flow inside CPHE. Ciofalo et al. [64] studied the flow in narrow passages and concluded that transitional flow occurs when Re ranges from 500 to 1500. Vlasogiannis et al. [59] reported that, when Re > 650 the flow is turbulent. Lioumbas et al. [65] experimentally investigated the flow in CPHE for two phases, counter-current flow arrangement. They proposed the flow shares turbulent flow features even at low Reynolds numbers 500 ≤ Re ≤ 1200.

Khan et al [66] conducted an experiment on the same CPHEs that have been already tested in [46]. The same chevron angles and same Reynolds number range were adopted to investigate the impact of different chevron angles on the fanning friction factor. They developed their correlations using a power law approach. The correlations are given as:

$$f = 34.43Re^{-0.5} \qquad \beta = 60°/60°$$
$$f = 2.07Re^{-0.27} \qquad \beta = 30°/60° \qquad (2.6)$$
$$f = 1.76Re^{-0.26} \qquad \beta = 30°/30°$$

The findings were compared against other findings in the literature. Fock et al. [50], and the results of Chisolm and Wanniarachchi [67] were found to highly over predict the friction factor for $\beta = 60°/60°$. The average deviation was 57% and 94%, respectively. In addition, deviation was 25% to 32% with respect to the studies of Heavner and Kumar [26] and Muley and Manglik [42], respectively. This investigation highlighted an important parameter, which may greatly affect not only the friction factor but also the heat transfer characteristics, that being the effect of the corrugation depth for the same corrugation angle. However, it was not investigated. The result showed the pressure drop is increasing as the Re and chevron angle increase.

Study on CPHE with β ranges from 22.5° to 67°, and with water-water as the working fluid, has been carried out by Heavner and Kumar [26]. The purpose was to find the values of friction factor and the heat transfer group (j_{Nu}) as a function of Re. The impact of β on f and j_{Nu} was investigated. The heat transfer group and the fanning friction factor equations were expressed as follows:

$$j_{Nu} = bRe^{m} \qquad (2.7)$$

$$f = a/Re^{n} \qquad (2.8)$$

Where

$$j_{Nu} = \frac{Nu}{Pr^{\frac{1}{3}}\left(\frac{\mu_b}{\mu_w}\right)^{0.17}} \qquad (2.9)$$

The heat-transfer group relates to the well-known Coulborn J-factor as:

$$j = j_{Nu}/Re \qquad (2.10)$$

The experiments over the range of Re have been conducted; all were in the turbulent region for both sides. The unknown's values are listed in Table 2.1 and Table 2.2.

Table 2.1. Fanning friction factor values [26].

β	β_{avg}	least square fits
45° /0°	22.5°	$1.715/Re^{0.0838}$
67° /0°	33.5°	$1.645/Re^{0.1353}$
45° /45°	45°	$0.81/Re^{0.1405}$
67° /45°	56°	$0.649/Re^{0.1555}$
67° /67°	67°	$0.571/Re^{0.1814}$

Table 2.2. Heat-transfer group values [26].

β	β_{avg}	least square fits
45° /0°	22.5°	$0.287\ Re^{0.683}$
67° /0°	33.5°	$0.308\ Re^{0.667}$
45° /45°	45°	$0.195\ Re^{0.692}$
67° /45°	56°	$0.118\ Re^{0.720}$
67° /67°	67°	$0.118\ Re^{0.720}$

Essential data were not provided such as the flow arrangements, and the data reduction method.

2.4 Computational Fluid Dynamics

2.4.1 Introduction

In CPHEs, the fluid flows over troughs of cross-corrugated plates, which is essentially three dimensional and considered to be very complicated. Giving a full description of a fluid flow inside the channels of these PHEs analytically is very hard. Investigating different geometrical parameters to study their effect experimentally is quite difficult and time expensive. Computational fluid dynamics (CFD) has its superiority over other software to simulate the fluid flow using the appropriate model, i.e. $k-\omega, k-\varepsilon,$ LES etc. In addition to its ability to solve the essential heat transfer equations including Navier-Stokes equations, continuity, and energy equations, CFD is an effective and reliable tool

[68] with which to study different geometrical parameters. It uses numerical analysis to solve many types of fluid flow. It can provide a very complex interaction of fluids inside the heat exchangers that are defined by boundary conditions, such as turbulent flow. Also it has the ability to show the local behaviour anywhere you need to explore, such as temperature, velocity, and shear stresses. Several studies have been using CFD to disclose new findings about their devices/problems i.e. the impact of different geometrical parameters [69-71]. They validate their results by comparing them with experimental ones, but with more understanding and analysis such as finding out stagnant spots inside the plates, the shape of flow inside the channels, which is a hard task to be completed experimentally, and the temperature gradient through the plates. Several manufacturers are using CFD for improving and developing their products, however, their findings are not to be shared for marketing reasons. More specifically, CFD is the name given to the science of solving problems that involves fluid flow. To clarify the features of CFD, let's consider our model is an aircraft. Aircraft used to be designed by intuitive use of flow equations, trial and error, and experimentation. Today, understanding the physics of the flight has been enhanced by CFD. HE is another example where it is very difficult to achieve a good portrayal and full description of the changes in physical and chemical properties of the flow inside the HE, especially if it is a complicated one such as PHE. Hence, CFD is a very powerful tool in this regard, where it can assist to investigate the flow and heat transfer mechanisms inside the HE. The mesh for most complicated geometries usually consists of millions of grid points such as the grids generated for the models of this thesis. All governing equations of fluid dynamics are numerically solved at each point on this grid thousands of times in order to achieve converged solution. Furthermore, CFD helps medical engineers to design and test the performance of the targeted organs. An example of computer power is the aerospace plane that is designed to travel at high speed; it repeatedly changes the physics of flight and outruns the capabilities of wind tunnels.

In the present study, CFD solves Navier-Stock Eq. (NS), continuity Eq., and energy Eq. These equations describe all kinds of fluid flow, regardless if the flow is 1, 2, or 3 dimensional, laminar or turbulent, compressible or incompressible, and of constant or variable viscosity. These equations are nonlinear due the inertial term (e.g. $\frac{\partial u}{\partial x}$). Till now

theses equations have not had an analytical solution in their full form. Therefore, CFD is essential in order to perform the numerical solution.

2.4.2 Numerical studies overview

Due to the high capabilities of ANSYS Fluent to predict heat transfer mechanisms [72], it has been utilized to investigate the heat transfer and fluid flow features in PHEs . Jain et al. [73] have conducted analysis for small size CPHE using CFD, where flat periodic boundaries were used. In order to enable the use of the periodic boundary conditions, an infinite pack was assumed. A realizable $k-\varepsilon$ turbulence model with non-equilibrium wall function was adopted. To validate their numerical approach, the heat transfer and pressure drop data were collected experimentally with 14 plates for Re range from 400-1300. Kumar's empirical correlation [74] was also used to validate the data of the friction factor. Their study was conducted for $\beta = 60°/60°$. The average deviation between empirical friction factor and the experimental one was 23%. The numerical friction factor that was found under predicted by about 2.5% to 14.5% with respect to the empirical correlation data. Nu was under predicted by 3% to 18% in comparison with the data of Hewitt et al [75]. One among the possible other reasons for under prediction is due to the exclusion of ports in numerical modelling. Also, applying virtual flat boundaries is not realistic since the effect of the end plate was excluded, which is significant especially if the number of plates is less than 50 [76].

Thermal performance for CPHE with air-water as the working fluids, $100 \leq \mathrm{Re} \leq 1000$, and β = 45°/45° was investigated by Croce and d'Agaro [77]. The unitary cell method was adopted to conduct the simulations, and periodic boundary conditions were applied. Nu was used as a sign for the overall heat transfer effectiveness. The impacts of Re and Pr on heat transfer characteristics were investigated. The conclusion stated that, the dependence of temperature on Pr is not obvious, and Nu increases as Re increases but with accompanied increase in pressure drop. The validation of the unitary cell approach is an open issue in the literature because it cannot represent many physical and geometrical parameters. Additionally, the same mechanism is assumed to be identically repeated anywhere inside each channel of the CPHE.

O'Halloran and Jokar [78] conducted a numerical study for single-phase flow with three different β's (60°/60°, 27°/60°, and 27°/27°). Models were built by using

Pro/Engineer for solid modelling, Gambit was used to generate the meshes, and Fluent used to run the simulations. Three channels have been tested, two cold channels on the sides of the PHE and one hot channel in the middle. Shear stress transport (SST) $k-\omega$ turbulence model was adopted with turbulence intensity 5%. The simulations started with flat plates for simplicity and gradually, corrugated furrows have been added. The heat transfer rate and the pressure drop across the heat exchanger for each fluid were calculated. The corrugation shape was built to be rectangular. It has been reported that, getting sinusoidal shaped cross sectional areas for corrugations are almost impossible, which is incorrect. The important heat transfer characteristics such as Nu and *f* were not reported.

A two symmetric $\beta = 30°/30°$ and 60°/60° CPHEs were numerically studied using CFD by Asif et al. [79]. The thermo-hydraulic characteristics was investigated in the form of Nusselt number. Prnadtl numbers range from 3.5 to 7.5 and Reynolds numbers range from 500 to 2500. The numerical result was validated with experimental data conducted by Khan et al. [46]. However, the deviation is not reported. Essential details were not provided about the appropriateness of the used turbulence model, and the number of channels or plates was not provided.

Recently, Skočilas and Palaziuk [80] carried out a numerical study for a CPHE with three symmetrical chevron angles (30°, 45°, and 60°). CFD was employed, and SST $k-\omega$ was the used turbulence model. The geometry was created in Solidworks CAD. Mesh generation was performed by using ANSYS Meshing module. The result was compared with an experimental one from the literature. For $\beta = 60°$, 5.1% was the maximum deviation between heat transfer coefficient data, and 14% deviation regarding to the pressure drop data. For $\beta = 30°$ the deviation was 11.5% and 59.1% for heat transfer coefficients and pressure drop data, respectively. The range of Re and the flow arrangement type are not provided. An essential point that could have improved the results is using sinusoidal corrugation shapes, where orthogonal corrugations were implemented in this study. The distance between two consecutive corrugations is known as corrugation pitch "Pc" (also called wavelength). The geometrical parameters of chevron plate are explained in section 2.7.1. Wang et al. [81] have numerically studied the impact of the ratio of Pc to the corrugation depth (b), and various βs on heat transfer and pressure drop. Both β and Pc/b were found to have direct proportionality with the

heat transfer and pressure drop. The impact of Pc that ranges from 7-10 mm on Nu and *f* data has been studied by Guo et al. [82].The data of *f* were found increasing as Pc increases, and the highest Nu data were found at Pc = 9 mm. Zhao et al. [83] studied the impact of corrugation depth that ranges from 2-6 mm on Nu and *f* data. As b increases, Nu data was found to increase, while *f* data decreased. Yuan et al.[84] have conducted a similar numerical study, and they concluded that, b has the most impact on heat transfer characteristics. In addition, the influence of β on PHE's thermal performance has been widely investigated numerically [85-88]. In general, the findings are similar: Nu and *f* data have been found directly proportional to the chevron angle.

2.4.3 Validation of numerical approach

To assure the reliability and the robustness of the adopted numerical approach, the numerical results must be compared with benchmark experimental results. The deviation between the results must be in an acceptable range. The same methodology that has been used in the literature by several authors [39, 72, 73, 79, 89-93] to validate their numerical results is used in this thesis. Nusselt number data are to be calculated for the applied range of Reynolds number in each study. Also, the fanning friction factor data are to be calculated for the applied range of Reynolds numbers in each study. These numerical data are compared with one or more experimental results from the literature.

2.5 Heat Transfer Enhancement

Various attempts to enhance the convective heat transfer rate of PHEs have been made by several research groups. The most widely used technique is the passive one [15]. That is because it does not require external energy, and mostly it is feasible to be adopted for real applications. Various approaches that are applied on PHE to enhance its thermal performance are discussed in the following sub-section.

2.5.1 Passive heat transfer enhancement approaches

The thermal performance of staggered concave and convex embossed surface pattern (Fig. 2.2) has been studied by Zhang et al. [94]. Their study is conducted by using CFD. Unitary cell approach with shear stress $k-\omega$ turbulence model are adopted. The findings showed significant reduction in *f* data of the embossed surface in comparison with a

chevron plate type that has β = 60°/60°. The Nu data of both types of surfaces are found close to each other.

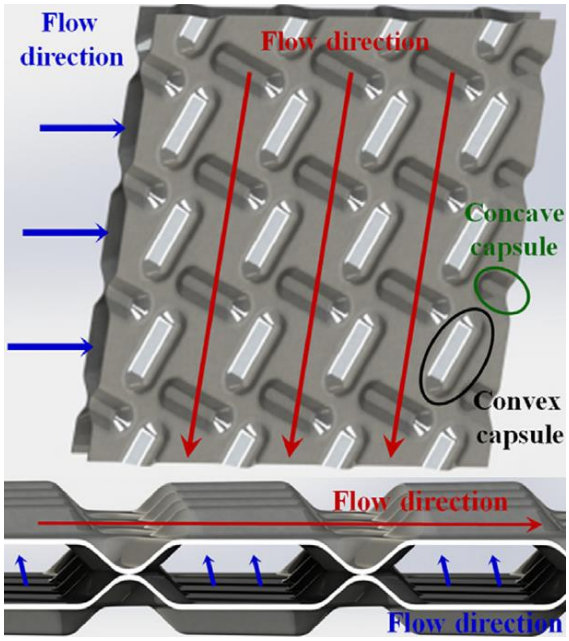

Fig. 2.2: Capsule type channel [94].

Another common surface passive technique is known as dimple surface. Song et al. [95] have generated a hexagon plate with dimples embossed on its surface, as shown in Fig. 2.3. Better thermal performance than that of the chevron plate type of β = 60°/60° has been claimed. However, neither the percentage of the improvement nor the comparison among the heat transfer characteristics of the two surfaces were provided in this study [95]. Similar studies have been performed on dimple-type surfaces [96-99].

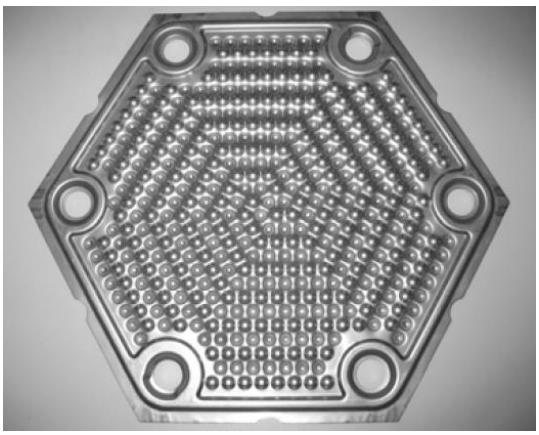

Fig. 2.3: Hexagon plate with dimple pattern [95].

All of these studies have reported an increase in Nu and *f* data, in comparison with those of the conventional chevron plate type.

Numerical studies on elliptic embossing, round embossing, and chevron plate type have been carried out by Jeong et al. [100]. The best thermal performance was found to take place in case of the elliptic embossing type, and the highest pressure drop was found in case of the conventional chevron plate type.

Energy and heat transfer analysis for three types of surface i.e. flat, corrugated (chevron) and asterisk, have been conducted by Durmus et al. [101]. Fig. 2.4 shows the shape of asterisk and corrugated plate types. The data of Nu and *f* of corrugated PHE were found to be 17% and 40% greater than those of the asterisk PHE. It also has been found that the pressure drops of corrugated and asterisk PHEs are respectively 3.5 and 2.5 times that of the flat PHE. Furthermore, similar embossing patterns have been suggested. Circular-spot pattern [102], bubble pattern [103], and horseshoe pattern [104, 105] have been proposed to enhance the thermal performance of the well-known PHE. Generally, there has been no clear evidence found in these studies [102-105] about the superiority of these surfaces patterns. On the contrary, it has been found [102] that the conventional chevron plate type is providing better thermal performance than the other patterns.

Fig. 2.4: Asterisk and chevron plates [101].

Nilpueng et al. [106, 107] have performed experimental studies on roughened surfaces to enhance the heat transfer coefficient. A sand blasting machine was used to roughen the surfaces. The surface roughness varies from 0.936 μm to 3.3 μm. The enhancement in

heat transfer coefficient was found ranging from 4.46% to 17.95%, and it was accompanied with an increase in pressure drop, ranging from 3.9% to 19.24% in comparison to the smooth surface.

In addition, Wajs and Mikielewicz [108, 109] have conducted experimental studies to evaluate the impact of surface roughness on heat transfer coefficient. Glass shot was used to increase the roughness of the surfaces. To assure identical test conditions, two experiments were conducted. The first one was performed without increasing the roughness of the surfaces, and the second one was performed on the roughened surfaces. The findings showed that the data of the heat transfer coefficient of the smooth PHE are higher in some ranges, and they are higher in case of the roughened surfaces for the rest. They concluded that the influence of the roughness on heat transfer characteristics cannot clearly be evaluated.

2.6 Heat Exchanger Theory

Heat exchangers are substantial units for a countless number of processes. They continuously enable heat exchange (enthalpy) between two or more fluids. The physics' laws allow the heat to be transferred from the hotter fluid to the colder one until equilibrium is reached. The energy gained by the cold fluid is always equal to the energy lost by the hot one. Finally, there should be temperature difference between the fluids. The process fluids could be liquids and gases, the heat could be transferred from gas to liquid, gas to gas, and liquid to liquid. In most applications, the two working fluids are separated by walls to prevent fluid mixing, and heat is conducted through the walls. This type is called indirect contact HE. On the other hand, there are direct contact HEs, in which the fluids are mixed together, such as cooling towers. The latter type is comparatively inexpensive. In addition, there are no fouling problems due to the absence of walls between the fluids.

2.6.1 Heat exchangers classification

There are many ways to classify HEs. They could be classified according to the surface compactness, number of fluids, and flow arrangement. From the perspective of surface compactness, there are gas-liquid and liquid-liquid HEs. Some authors [110, 111] classified the HEs' compactness based on the working fluids. The gas-liquid HE is considered to be compact if its surface area density is ≥ 700 m^2/m^3 or its hydraulic

diameter d_h is < 6 mm. For phase change liquid-liquid HE, it is considered compact if its surface area density is ≥ 400 m^2/m^3. Conventional HEs have less surface area density. Shell and tube HEs are very common; their surface area density is < 100 m^2/m^3 and d_h is > 6 mm [112]. They are usually used when a large amount of fluid is required either for cooling or heating. The thermal performance of compact PHE is greater than that for shell and tube HE [41]. The values of heat transfer coefficients have been reported as twice that of the shell and tube HE [30].

2.6.2 Heat exchanger thermal characteristics

The energy balance equation is always applicable regardless the type of HE (PHE, shell and tube, concentric, etc.), the flow arrangements, and whether there is phase change or not. The equation is given by:

$$Q = UA\Delta T_{LM} \tag{2.11}$$

Where A is the effective heat transfer area. U is a fundamental parameter represents the overall heat transfer coefficient, and its formula in the case of PHE is:

$$U = \frac{1}{\frac{1}{h_h} + \frac{t}{k_p} + \frac{1}{h_c} + R_{f,h} + R_{f,c}} \tag{2.12}$$

Where h and c subscripts refer to hot and cold fluids, respectively. Also, h represents heat transfer coefficient, R_f represents fouling resistance, t refers to plate thickness, and k_p refers to plate conductivity. ΔT_{LM} refers to the log mean temperature difference (LMTD). To clarify ΔT_{LM}, Fig. 2.5 shows temperature distribution for counter-current flow. On the inlet of the hot fluid side the temperature difference is between $T_{h,i}$ and $T_{c,o}$ is ΔT_1, and on the inlet of the cold fluid side the temperature difference is between $T_{h,o}$ and $T_{c,i}$ is ΔT_2. Now ΔT_{LM} is defined as:

$$\Delta T_{LM} = \frac{(\Delta T_1 - \Delta T_2)}{ln\left(\frac{\Delta T_1}{\Delta T_2}\right)} \tag{2.13}$$

From Eq.(2.13) it can be noticed that LMTD measures the logarithmic average temperature difference at each side of the HE between the cold and the hot fluids. Moreover, greater temperature difference between the cold and the hot sides yields faster and higher heat transfer coefficient. Consequently, a smaller heat transfer area will be

needed. However, LMTD is no more valid in particular cases e.g. phase change in condensation.

In HEs, the correction factor F sometimes is required to correct the ΔT_{LM} value, especially in cases of multipass flow arrangement and when the flow is not purely counter or co-current. Then the energy balance equation becomes:

$$Q = UA\Delta T_{LM}F \tag{2.14}$$

There are a number of different graphical correction factors for most types of HEs and common flow configuration can be found in HE design handbooks and in the open literature.

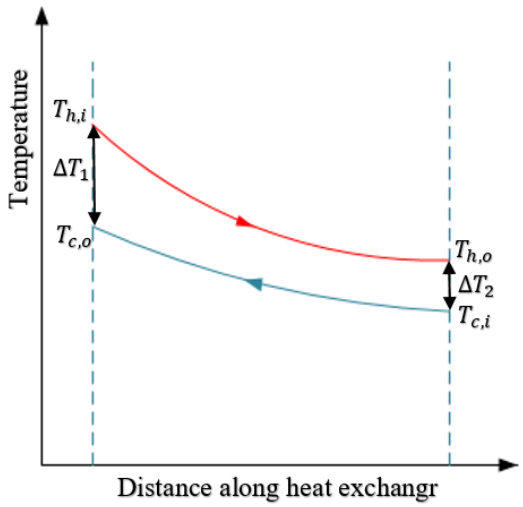

Fig. 2.5: Temperature distribution in counter-current arrangement.

There are various approaches for designing HEs. LMTD is very popular but it is iterative when it is used to calculate the performance, i.e. heat duty with unknown outlet temperatures. Another common approach is $\varepsilon - NTU$ which require neither iteration nor outlet temperatures to be known. The formula of the HE effectiveness (E) is:

$$\mathrm{E} = \frac{Q_{max}}{Q}, \qquad where \;\; 0 \leq \mathrm{E} \leq 1 \tag{2.15}$$

Where Q_{max} represents the maximum heat transfer rate that could be theoretically achieved from that HE, Q refers to the actual heat transfer rate, Q_{max} formula is:

$$Q_{max} = C_{\min}\,(T_{h,i} - T_{c,i}) \tag{2.16}$$

C is the heat capacity rate and its formula is:

$$C = \dot{m}c_p \tag{2.17}$$

$$C_{min} = \min(C_c \; or \; C_h) \tag{2.18}$$

$$where$$

$$C_c = \dot{m}_c c_{p,c} \tag{2.19}$$

$$C_h = \dot{m}_h c_{p,h} \tag{2.20}$$

NTU refers to the number of transfer units and is defined as:

$$NTU = \frac{UA}{C_{min}} \tag{2.21}$$

The value of NTU impacts the performance of the HE. It is proportional to the heat transfer rate. An important feature of this approach is that it is not necessary to know both values of E and NTU. If any value of them is known, the second one is easy to get, e.g. $\mathrm{E} = fun(NTU, C_r)$ and vice versa, where C_r stands for the critical heat capacity ratio and its formula is given as:

$$C_r = \frac{C_{min}}{C_{max}} \tag{2.22}$$

When $C_r = 0$ there exists a single relation between $\mathrm{E} - NTU$ which is applicable to all types of HEs and it is:

$$\mathrm{E} = 1 - \exp(-NTU) \tag{2.23}$$

Which is the same as:

$$NTU = -\ln\,(1 - \mathrm{E}) \tag{2.24}$$

2.7 Plate Geometry

In all types of PHEs, thermal plates represent the basic component of PHE. Each plate contains four ports at its corners, in addition to its surface, where heat transfer takes place. For CPHE, there are many kinds of corrugations e.g. chevron (herringbone), washboard, zig-zag, and wavy-groove. The chevron type proved to be the superior one over many

years and it has become the required pattern between research community and manufacturers [113]. Therefore, the investigated CPHEs in this thesis are of this type. The geometrical parameters will be explained in the following sub-sections due to their impact on the performance of the PHE. The plate's geometry of the FPHE and CPHE is identical, except in FPHE where there are no corrugations i.e. the plate is flat.

2.7.1 Chevron type corrugation

Fig. 2.6 shows geometrical parameters of chevron plate in CPHE. The chevron patterns are pressed on the plates. This pattern, of sinusoidal recurrent shape, forms an angle between the corrugation and the longitudinal axis (the flow axis) known as the chevron angle (β). It is noteworthy to highlight that some researchers consider the angle of corrugations with respect to the horizontal axis. However, it is more common to be considered with respect to the vertical axis.

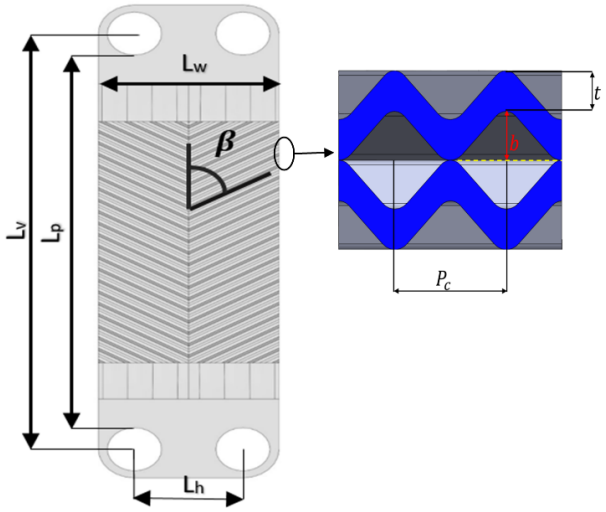

L_v- vertical length from port to port-m

L_p- plate's channel effective length-m

L_w- flow channel width-m

b- Channel gap for the mean flow-m

L_h- horizontal length from port to port-m

β- Chevron angle- degree

P_c- corrugation pitch-m

t- Plate thickness-m

Fig. 2.6: Chevron type plate.

The corrugations basically provide larger surface area and promote turbulence flow at low flow rates [42]. They also minimize the stagnant areas and fouling. The commercial types usually vary from 23° up to 65°. It can be seen from the aforementioned experimental and numerical literature that it is the most important geometrical parameter that impacts the thermal and hydraulic performance, which has also been verified by various authors [114-120].

2.7.2 Surface Enlargement Factor

The Surface Enlargement Factor ($\emptyset$) is an important geometrical parameter that represents the developed length over the projected length and it usually varies from 1.1 to 1.29. Martin [121] proposed an approximate correlation to calculate $\emptyset$ for a sinusoidal corrugated pattern; the formula is as follows:

$$\emptyset = \frac{1}{6}\left[1 + \sqrt{1 + \left(\frac{\pi b}{p_c}\right)^2} + 4\sqrt{1 + \frac{\left(\frac{\pi b}{p_c}\right)^2}{2}}\right] \tag{2.25}$$

Where b is the main flow channel gap between two consecutive plates, and Pc represents the wave pitch. There is also another important ratio in PHEs known as aspect ratio which is $A_r = \frac{L_p}{L_w}$ where L_P and L_w are port-to-port channel length and flow channel width, respectively. $L_p = L_v - D_p$, and $L_w = L_h + D_p$.

2.8 Flow in PHE Channels

In CPHEs, each plate is fixed 180° opposite to the adjacent plate to form a cross-corrugated channel, and to assure there is a channel gap between these two adjacent plates. Either these plates are to be sealed with gaskets or by welding at the edges. The important parameter in this case is the flow area, which is known as free flow area A_f and it is given by:

$$A_f = bL_wN_p \tag{2.26}$$

Where N_p is the number of the passages.

In FPHEs, the plates are simply stacked upon each other and sealed with gaskets inside a frame and tightened together either by bolts or by welding. The depth in this case equals the hydraulic diameter $b=d_h$. Therefore, the free flow area for the FPHEs is:

$$A_f = d_hL_wN_p \tag{2.27}$$

2.8.1 Equivalent diameter

There is a disagreement in the literature upon the right formula of the CPHE's hydraulic diameter. However, there are two common definitions and the difference

between them is insignificant. The first definition is often used and it is called equivalent diameter. It is double the corrugation depth $d_e=2b$. The second one is known as hydraulic diameter and it is defined in the traditional way for non-circular tube [111] as:

$$d_h = \frac{4A_f L_h}{A} \tag{2.28}$$

2.8.2 Pass arrangement

In PHEs the pass represents a group of channels that have the same flow direction. Fig. 2.7 shows 2-1 pass flow arrangement.

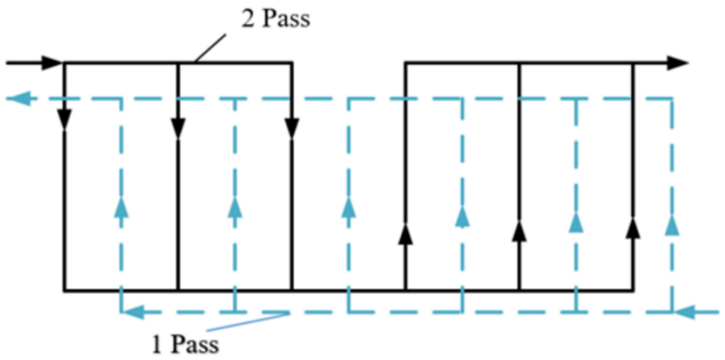

Fig. 2.7: 2-1 Pass arrangement.

In PHEs the flow arrangement is controllable and flexible. It is an important task to choose the best arrangement for your design in order to exploit the available heat transfer area to transfer the required heat load at the possible minimum pressure drop. The effect of the passes number and the flow arrangements on the temperature effectiveness and log mean temperature difference has been investigated by Kandlikar & Shah [29]. The findings showed that the highest effectiveness was achieved for 1-1 single pass with NTU > 5. However, if number of plates (*Np*) is large (e.g. *Np* > 40), the flow maldistribution may occur and the heat transfer characteristics may also be too low. In that case, n-n pass arrangement could be the solution with n > 1 based on the allowable pressure drop [29].

2.8.3 Vertical vs diagonal ports configurations

In PHEs, two port arrangements are available. The fluid could flow vertically, where it enters and exits from the ports that are located on the same side of the plate, as shown in Fig. 2.8(a). On the other hand, the fluid could flow diagonally, where it enters from

one port and exits from the opposite diagonal port, as shown in Fig. 2.8 (b). The comparison between the thermal performances for each port configuration need to be conducted. However, Cooper and Usher [122] referred to better thermal performance that takes place in diagonal ports configuration.

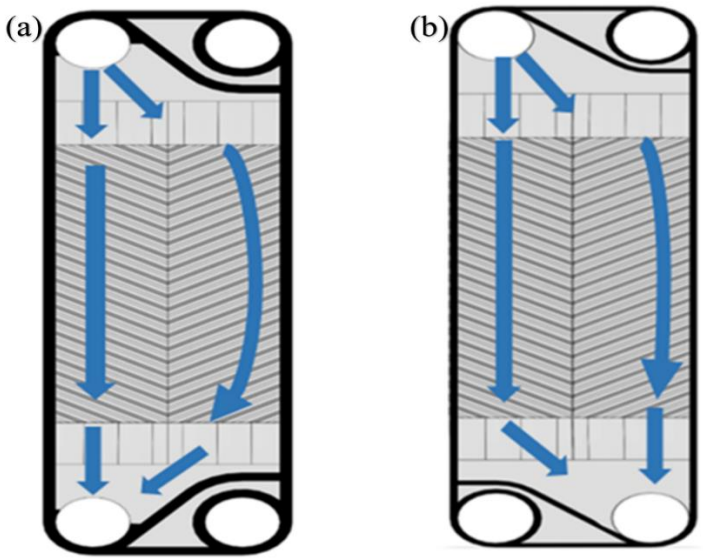

Fig. 2.8: (a) Vertical ports configuration, and (b) Diagonal ports configuration.

2.8.4 U and Z flow arrangements

Both U and Z arrangements are used in the 1-1 pass flow arrangement. In U type, both cold and hot fluid enter and exit from the same side. Also the flow could be either parallel or counter-current as shown in Fig. 2.9 (a) and (b), respectively. The temperature of the stream changes as it flows along the plates.

In parallel flow arrangement, the outlet cold temperature is always less than the outlet hot temperature (Fig. 2.9 (c)) unless for infinitely large HE, which is not realistic. This is not the case for counter-current flow arrangement (Fig. 2.9 (d)). That is because of its favourable temperature gradient, which consequently will require smaller surface area in comparison with other types of flow arrangements. In addition, in U type it is easier to clean and repair without disturbing the external pipes [123].

In Z flow arrangement, the fluid enters from one side and exits from the opposite side as shown in Fig. 2.9(e). The advantage of adopting this type is getting more uniform flow distribution on the surfaces of the plates [124].

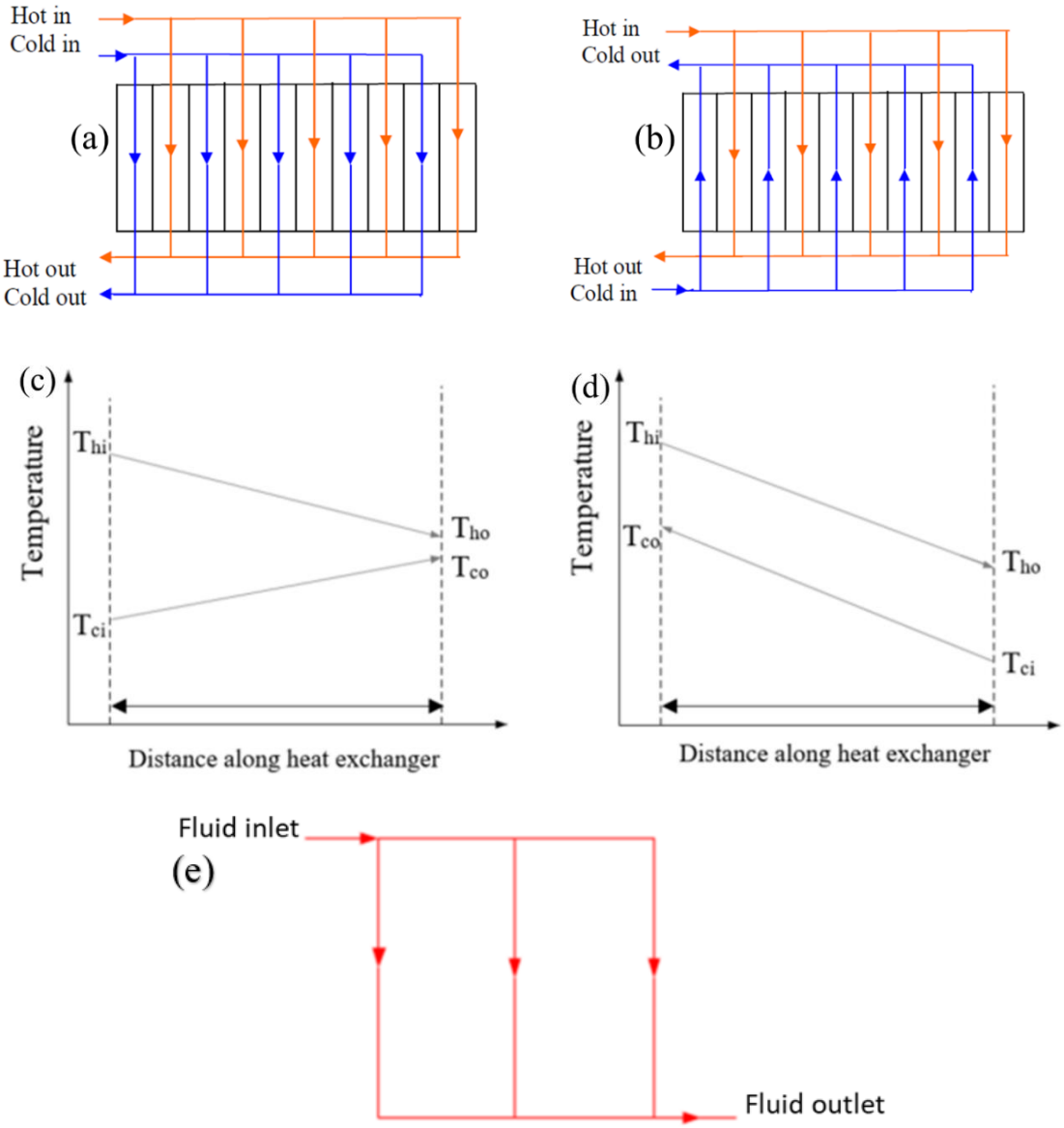

Fig. 2.9: (a) Parallel flow arrangement, and b) Counter current flow arrangement, (c) Temperature distribution in parallel-flow arrangement, (d) Temperature distribution in counter-flow arrangement, and (e) Z-flow arrangement.

2.9 Friction Factor

Friction factor is an important physical parameter, which refers to the resistance of the fluid to flow, either inside the channel or over specific geometry. Greater values of friction factor refer to greater pressure drops; consequently high pumping power would be required, which will increase the capital cost of that project. In PHEs, the friction factor is associated with the core pressure drop (plate passage) and is given by:

$$\Delta P_{core} = \frac{4flG^2}{2g_c D_e} \tag{2.29}$$

The friction factor in Eq. (2.30) represents fanning friction factor, which is the ratio between the local shear stress and the local dynamic pressure.

$$f = \frac{\tau}{\rho \frac{u^2}{2}} \tag{2.30}$$

Sometimes confusion takes place between the two well-known friction factors, Darcy and Fanning friction factor. Each researcher could use anyone and sometimes without referring to the kind of that friction factor. Care must be taken when interpreting any friction factor from literature. In this thesis (f) represents the fanning friction factor and f_D represents Darcy friction factor. For any case and condition $f_D = 4f$.

2.10 Types of PHE

Various types of PHE have been used for a large number of applications. There are four types of PHE; these types being gasketed PHE (GPHE), semi welded PHE, brazed PHE, and shell and plate heat exchanger. The first three types are the most popular and they all have similar geometrical shapes.

2.10.1 Gasket plate and frame HE

Gasket plate and frmae HE consists of number of plates. These plates are produced by different manufacturers with different sizes. They are very thin, rectangular in shape. Each plate contains a gasket on its periphery in order to prevent the leakage. Each plate consists of four ports, two of them usually open for the inlet and the outlet fluid, and the other two closed on their perimeter by the gasket. The materials of the gasket are illustrated in section 2.11. The gaskets are used for FPHE and CPHE. In CPHE, the plates are stacked upon each other, and each plate is reversely oriented by 180° with respect to the adjacent plate generating the corrugation depth. Therefore, the corrugations provide a numerous contact points. Then these plates and gaskets are fixed in their frame by tightening bolts as shown in Fig. 2.10. This type has a modular nature, while others don't have this feature. It enables us to disassemble the HE either for maintenance (cleaning or repairing), or to add or remove plates according to the required heat duty, which would enable the user to save the money of buying new unit. As the fluid flows in opposite

directions between two plates in counter-current flow, the high pressure side tends to bend the wall toward the low pressure side, which results in a narrowing passage and at some point it may block that passage [41]. Therefore, the corrugations on the surface of this type are made to increase the strength of the plates. In addition, these corrugations promote turbulence to take place at low flow rates, and also increase the effective surface. The highest temperature value depends on the gasket material but generally the pressure shouldn't exceed 25 bar and the temperature should not exceed 250 °C [125].

Fig. 2.10: Gasket and Frame PHEs.[2]

2.10.2 Semi-welded plate

In this type, each two adjacent plates are laser welded and known as twin plates or a plate cassette, as shown in Fig. 2.11. However, it is not gasket free. An O-ring gasket is used to maintain the seal. This type is used for aggressive fluid to ensure there is no leakage and also to handle higher pressure and temperature. Operating pressure can range from vacuum to 40 bar and temperature can range from -50 to 350 °C [126] .

[2] Source is: https://www.alfalaval.com/products/heat-transfer/plate-heat-exchangers/gasketed-plate-and-frame-heat-exchangers/

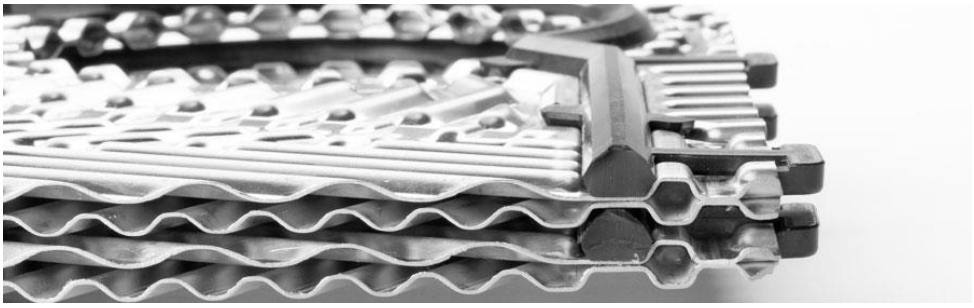

Fig. 2.11: Semi welded plates.[3]

2.10.3 Brazed PHE

Brazed PHE (BPHE) consists of a number of plates brazed together, eradicating the use of gaskets, and bolts. Therefore it is less complicated, more compact comparing to other kinds of PHE, and it has lighter weight. BPHE completely removes the limitation due to the gasket existence, which represents a significant weakness point in the design and applications. Due to its light weight and because it comes as one piece, as shown in Fig. 2.12 , it costs much less for shipping and installation [127]. In addition to the aforementioned features, BPHE exhibits an outstanding strength and durability. It can handle operating pressure reach to 45 bar, and temperature ranges from -195°C up to 350°C [23]. However, BPHEs are not allowed to be disassembled for cleaning or rearranging the plates. The cleaning process is usually performed by using different chemical approaches [128]. Because BPHEs are more reliable than gasket PHEs from the perspective of fluid leakage, primarily they have been employed for refrigeration/ heat pump applications as evaporators and condensers. Nowadays, they are used for heat recovery, chemical industries, pharmaceuticals and other sensitive applications [129].

2.11 Gaskets Characteristics

Each plate in PHE is grooved on its periphery to install the gasket on that plate, as shown in Fig. 2.13. There are two ways for installing the gasket: glue style, in which a gasket is installed on the grooves by help of an appropriate adhesive material, and clip style, which is conducted without the need to use any adhesive material. A gasket can be replaced when it is needed. The purpose of the gasket in PHE is to prevent leakage between the stream fluids, where they arranged in order to provide a double seal, so inter-

[3] Source from: http://www.sondex-usa.com/en-US/Products/Heat-Exchangers/Semi-Welded.aspx.

mixing between the working fluids is unlikely to take place. After the installing process, the gaskets are compressed by big bolts on the frame.

Fig. 2.12: Brazed PHE[4].

These gaskets are designed to stand a compression of about 25% of their original thickness [130] to provide a good joint without affecting the plates. There is a number of elastomer gasket materials, such as synthetic materials. These materials can easily deform, twist, compress and when released, they quickly revert totheir original shape and dimensions. However, sometimes choosing the appropriate gasket is critical, especially for aggressive fluids applications. NBR, HNBR, EPDM, and FPM are the most popular materials for gaskets. Table 2.3 shows the temperature range for different gasket materials. Before installing any material, it should be subjected to a number of tests. The hardening test is an essential one where the material's surface is subjected to a needle penetration and the more the penetration depth is, the less hard the material is and vice versa. The elongation test is another important test. It is performed to observe the ability of that material to stretch before it breaks, along with other kinds of important mechanical and chemical tests.

[4] Source from: http://www.coowor.com/p/20160106135558ZF0V/Brazed-phe-oil-cooler-oil-water-heat-exchanger.htm.

Fig. 2.13: Gasket installed on plate's periphery[5].

2.12 Advantages and Limitations of PHE

PHEs have various advantages over other types of heat exchangers [41]. Generally, the main advantages are as follows:

- The fluids flow over a large surface area. PHE uses metal plates in order to exchange heat between two fluids on both sides of the plate. The fluid spreads out over that plate (large surface area) and the plate is very thin in order to allow for more heat to be conducted between the two fluids on its right and left sides. Consequently, this will greatly decrease the time for temperature change.
- GPHE has a modular nature that enables us to perform cleaning and maintenance very easily. In addition, it enables us to increase/decrease the number of the plates when the heat duty task changes. In corrugated heat exchangers, high shear stresses and high turbulence could be achieved at low flow rates with respect to other conventional heat exchangers. The corrugations contribute in promoting secondary swirling flow [131], which consequently will promote the heat transfer coefficient. Also these corrugations contribute to supporting the plate strength and durability. They prevent the plate from getting distorted due to the pressure difference between the fluids on the right and left sides of the plate.
- Compactness - PHEs' weight is about $1/16^{th}$ the entire weight of shell and tube, and they occupy about $1/10^{th}$ the floor space [22]. Hence the cost of shipping,

[5] Source from: https://www.wcrhx.com/plate-heat-exchanger-service

handling, and installation will be reduced. Also, it is easy to detect leakage in PHEs.

Table 2.3. Temperature range for different gasket materials[6].

Chemical Description	abbreviation	temperature	
		low	high
Acrylonitrile-butadiene rubber	NBR	-30°C	100°C
Hydrogenated Acrylonitrile butadiene rubber	HNBR	-30°C	149°C
Ethylene propylene diene rubber	EPDM	-51°C	149°C
Fluorosilicone rubber	FVMQ	-59°C	232°C
Natural rubber	NR	-51°C	104°C
Ethylene Acrylic rubber	AEM	-40°C	149°C

PHEs have also some limitations and flaws; the most important disadvantages are:

- The pressure drop accompanied with the PHE is relatively high, which will affect the pumping power and consequently the capital cost must be considered.
- The main flaw of the gasket PHE is the necessity for long gaskets that are cemented into slots around the plate's edges. In spite of this drawback, plate and frame HEs held by tightened bolts have been successfully operated at different high pressures and temperatures. Note, this flaw is not applicable to brazed PHE since there are no gaskets in this type. However, brazed PHE is usually suitable for small heat duty tasks.
- The gaskets' lifetime is limited, especially if they were used for aggressive applications, e.g. erosive duties, and need to be replaced after a specific time.

[6] Source from: http://usa.datwyler.com/materials.html

2.13 Summary of Literature Review

A general overview about the the energy challenges across the world and the role of HEs in energy sections have been discussed. This chapter also discloses that, Most of the experimental studies are found specific in nature where they investigate either a specific geometry, experimental range of operations, or both. However, they are useful where you can choose the closest one to your application. The importance of CFD to assist in developing different branches of science in general and heat exchangers in particular i.e. giving a full description of a fluid flow inside the HEs have been highlighted. Additionally, the performance of various passive heat transfer techniques that have been introduced in the literature are reported. Essential concepts about various aspects of HEs in general have been highlighted. Also, important features of PHE such as geometirical parameters, flow configurations, and PHE types have been reported.

A review about the experiemental and numerical studies of PHE have been carried out. Most of these studies have investigated the impact of different geometrical parameters on the heat transfer process, and β was the most investigated parameter [132]. In addition, studies that have been performed to introduce new passive techniques to boost the thermal performance of PHEs are limited in comparison with the parametric studies. Generally, it can be unequivocally seen that most of these studies imply either embossing surface or roughened surface. Yet, chevron plate type is still the most common one [113]. Therefore, based on the challenges and limitations that are highlighted in this chapter, the main aim of this thesis is to contribute to improve the thermal performance of the current well-known PHEs. Mainly, find new passive methods that could either boost the convective heat transfer, reduce pressure drop, or both.

Chapter 3: Thermal Performance Investigation in a Novel Corrugated Plate Heat Exchanger

Research Paper One:

S. Al-Zahrani, M.S. Islam, F. Xu, S.C. Saha, Thermal performance investigation in a novel corrugated plate heat exchanger, International Journal of Heat and Mass Transfer, 148 (2020) 119095.

International Journal of Heat and Mass Transfer 148 (2020) 119095

Contents lists available at ScienceDirect

International Journal of Heat and Mass Transfer

journal homepage: www.elsevier.com/locate/hmt

Thermal performance investigation in a novel corrugated plate heat exchanger

Salman Al zahrani[a,b], Mohammad S. Islam[a], Feng Xu[c], Suvash C. Saha[a,*]

[a] School of Mechanical and Mechatronic Engineering, University of Technology Sydney, Ultimo, NSW 2007, Australia
[b] Department of Mechanical Engineering, Al baha University, Al baha, Saudi Arabia
[c] School of Civil Engineering, Beijing Jiaotong University, Beijing 100044, China

ARTICLE INFO

Article history:
Received 2 April 2019
Revised 15 November 2019
Accepted 21 November 2019

Keywords:
Corrugated plate heat exchanger
Thermal performance
Numerical modelling
Nusselt number

ABSTRACT

Compact heat exchangers have become an essential necessity for power production and multi other purposes on a daily basis. The corrugated plate heat exchangers (CPHEs) are well-known for their high thermal performance. This study proposes a unique CPHE with a simple modification that can boost its thermal performance significantly. The overall tests have been conducted on four CPHEs for two symmetric chevron angles (β) of 30°/30° and 60°/60° Two CPHEs belong to the newly CPHEs, and the other two belong to the well-known basic CPHE. Data are obtained for steady-state, single-phase (water-water), counter-current arrangements, and for Reynolds number (Re) ranges from 500 to 2500. Sophisticated mesh techniques have been adopted to develop the mesh for the plates and the fluids between the plates. An appropriate grid refinement test has been carried out for the accuracy of the numerical results. The results have been validated with benchmark experimental and numerical data. A realizable $k-\varepsilon$ turbulence model with scalable wall treatment found to provide the most consistent and accurate prediction of the thermal performance of CPHE. The numerical results showed that the Nusselt number (Nu) and the effectiveness (ϵ) of the newly developed CPHEs are much higher than that of the basic one, which can be very useful when a heavy heat duty is required. The enhancement for Nu is up to 75% and for ϵ is up to 42%, and generally both exhibit a direct proportional relationship with Re. Based on the numerical result, a new correlation to predict Nu has been developed.

3.1 Abstract

Compact heat exchangers have become essential for power production and multi other purposes on daily basis. The corrugated plate heat exchangers (CPHEs) are well-known for their high thermal performance. This study proposes a unique CPHE with a simple modification that can boost its thermal performance significantly. The overall tests have been conducted on four CPHEs for two symmetric chevron angles (β) of 30°/30° and 60°/60°. Two CPHEs belong to the newly CPHEs, and the other two belong to the well-known basic CPHE. Data are obtained for steady-state, single-phase (water-water), counter-current arrangements, and for Reynolds number (Re) ranges from 500 to 2500. Sophisticated mesh techniques have been adopted to develop the mesh for the plates and the fluids between the plates. An appropriate grid refinement test has been carried out for the accuracy of the numerical results. The results have been validated with benchmark experimental and numerical data. A realizable $k-\varepsilon$ turbulence model with scalable wall treatment was found to provide the most consistent and accurate prediction of the thermal performance of CPHE. The numerical results showed that, the Nusselt number (Nu) and the effectiveness (E) of the newly developed CPHEs are much higher than that of the basic one, which can be very useful when a heavy heat duty is required. The enhancement for Nu is up to 75% and for E is up to 42%, and generally both exhibit a direct proportional relationship with Re. Based on the numerical result, a new correlation to predict Nu has been developed.

Keywords: Corrugated plate heat exchanger; Thermal performance; Numerical modelling; Nusselt number.

3.2 Introduction

The use of CPHEs has become an essential necessity on daily basis. CPHE is the most efficient among other conventional types of heat exchangers (HEs). Many researchers have studied different approaches to enhance the flow mixing and the heat transfer i.e. introducing passive techniques to control the energy dissipation rate, and using vortex generators to reduce the wake region and enhance the turbulence intensity [133-136]. Other research has been conducted to optimize the performance for different types of the HEs [137, 138]. CPHEs are compact in nature, have high thermal effectiveness, and hence close approach temperatures (2 °C temperature difference) can be reached [14]. Therefore, CPHEs are important particularly for heat recovery and regeneration

applications. In addition, CPHEs have a modular nature that eases the cleaning process as well as making the system flexible, by adding or removing plates to meet the energy requirements quickly. CPHEs have been employed in food, paper/pulp, power, pharmaceutical industries, HVAC and many other applications [25].

In CPHEs, the turbulence flow can be achieved at low Re, Re$>$ 400 [111, 139]. In addition, CPHEs are lighter and require less space.

Troup et al. [140] performed one of the earliest studies on CPHE performance, who considered washboard plate type HE. However, later the chevron plate became the most popular due to its high thermal performance among other plate types (e.g. wavy, and zig-zag plate). The impact of different β on CPHE's thermal performance was investigated by Okada et al. [41], where the β was considered with respect to the horizontal centreline. However, it is more common that β to be considered with respect to the longitudinal centreline as shown in Fig. 3.1. Later Manglik et al. [42] studied heat transfer characteristics (HTC) in CPHE for $\beta = 30°/30°$, 60°/60° and 30°/60°. The correlations for the whole study were incorporated in one formula. Nevertheless, each correlation should be separately reported, in order to be able to test the agreement between each β correlation and the general formula. One-one pass, water-water fluids for the same β's have been tested by Khan et al. [46]. An equal heat transfer coefficient (h) and Nu were considered for both sides as the Reynolds number was the same at the cold and at the hot side. The same Re on both sides of the CPHE does not imply h will be the same, as h depends on many other factors i.e. fluid viscosity, fluid density, fluid velocity and many other parameters. For the cold side, h is likely greater than that of the hot side, because thermal boundary layer resistance is lower in case of cold fluids [47]. In addition, heat capacity rate (C) of cold water is higher than that of hot water as the viscosity of cold water is higher than that of hot water. Hence the velocity of the cold water would be higher in order to meet the same Re, and consequently the mass flow rate of cold water will be higher than that of hot water. Therefore, considering Nu as the same on both sides is not an accurate assumption. Similar studies have been performed on CPHE to investigate the impact of different chevron angles [50, 55].

The experimental and numerical studies have concluded that the flow inside the CPHE is non-uniform and tends to flow toward the lateral edges of the plate [141]. However,

the study did not consider the thermal performance of CPHEs. Kanaris et al. [89] carried out both experimental and numerical studies about thermo-hydraulic characteristics in CPHE with one corrugated plate ($\beta = 60°$). The study used one corrugated plate, while the other plate was flat. The port effect and the pressure drop were ignored. In fact, to be able to study heat transfer inside the CPHE, at least three plates should be considered (two channels) to allow heat transfer process to take place. One year later, Kanaris et al. [72] executed another numerical investigation using CFD, and three plates were generated with $\beta = 60°$. The shape of the corrugation they considered was trapezoidal. The real corrugation however is sinusoidal shape. Also, the port effect was neglected again.

A numerical study for CPHE with two channels was performed by Tsai et al. [142]. The flow maldistribution was investigated by applying the Bassiouny and Martin formula [28]. The heat transfer was ignored, and the range of Reynolds number was small ($Re \leq 1700$). A two symmetric $\beta = 30°/30°$ and $60°/60°$ CPHEs were numerically studied using CFD by Asif et al. [79]. The thermo-hydraulic characteristics were investigated in the form of Nusselt number. Essential details were not provided for supporting the appropriateness of adopting the turbulence model, and no information of the number of channels or plates. The Wilson plot technique was applied in their numerical study. However, a comprehensive understanding of CFD would help to avoid going through this long iterative process.

One good aspect of considering CFD study is that it enables the user to find the temperature at any spot on the model, and the average temperature for any side of the plate. Consequently h can directly be calculated from numerical data. This would be very hard to get from an experimental model. In all previous numerical studies reviewed in this research, the mesh dependency tests were not provided. In addition, the mesh statistics were also insufficient. Al zahrani et al. [47] have numerically investigated the effect of the Prandtl number (Pr) on the heat transfer and friction factor (*f*), by conducting two sets of tests at hot fluid side, while cold water was kept at the cold side for all cases. The first set was for hot air, and the second set was for hot water. The result concluded that both Nu and *f* increase as Pr increases.

An essential objective of the present study is to introduce a new passive technique that could enhance the thermal performance of the current CPHE, and consequently reduce its size and make the system more compact. Most research either studied the impact of

different β on HTC or studied the fluid flow pattern inside CPHE's channels. However, in order to be able to reduce its size and make the system more compact, there is ongoing effort to find new techniques to enhance the performance of the heat exchanger. In general, heat transfer enhancement methods are active, passive, and compound. Active technique requires an external power for the enhancement such as induced pulsation, and surface vibration. Passive technique involves a geometrical modification to the fluid flow passage, or using inserts in the flow passage, or both. An example for passive technique is inserting twisted tape to promote turbulence flow regime, adding fins, and extending surface. In the compound method, both active and passive techniques are used. In general, passive technique is the preferred one [143], because the potential of active technique is limited due to its design complexity [15].

The present study introduces a new modification in CPHE flow mechanism as described in the following section, which could enhance convective heat transfer significantly between the cold and the hot fluids, and consequently the fuel consumption can be reduced [144]. The numerical thermo-hydraulic performance tests were carried out on the counter-current flow arrangement, and for two symmetric $\beta = 30°/30°, \text{and } 60°/60°$. Nu is employed as an indicator for heat transfer improvement, and CPHE effectiveness (E) is employed to compare the thermal performance between the basic and the new CPHE design. The CPHE comprised of four channels (five plates): two of them pertaining to the cold side, which represent the utility fluid, and the other two pertaining to the hot side, which represent the product fluid. Therefore, the present study is performed on the hot side of CPHE. The port effect, and the corrugations' shape have been considered for all cases, in order to get as close as possible to simulating thermal-hydraulic performance in real CPHE.

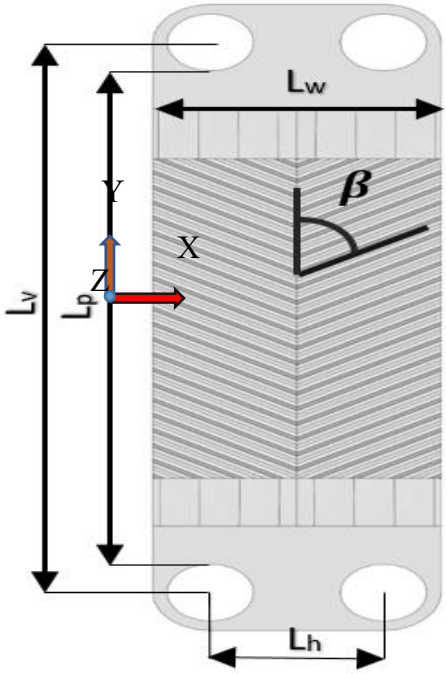

Fig. 3.1: Geometrical parameters illustration for chevron plate type.

3.3 The New CPHE Design Approach

The material technology of CPHE has been constantly improved, which allows the usage of CPHE for further applications such as chemical processes. In addition, the brazed CPHE has been introduced in order to resist higher pressures and temperatures. However, the basic design of CPHE has hardly been changed since it was invented in the 1920s. All studies of the CPHEs were to test the performance, flow patterns inside the CPHE, or to study the effect of a specific parameter. In the basic design, CPHE's thermal performance is higher in comparison with other types of HEs such as shell and tube HE [14, 145]. However, the current study introduces a new modification in the basic design that improves the CPHE's thermal performance significantly. Additionally, the fluid is distributed on the plate's surface randomly in the basic design. The modification implies more degree of control of the fluid flow on the plate's surface.

In the basic and new CPHEs, the gasket is used to regulate the fluid directions through the CPHE. The design of the new gasket is shown in Fig. 3.2, where the separator has been installed at the middle of the plate for two reasons. Firstly, it guides the fluid to the desired direction. Secondly, it replaces the contact points at the middle between every

two consecutive plates, where the heat transfer magnitude is negligible at this area [73]. In addition, it also assures equal fluid distribution on each plate side.

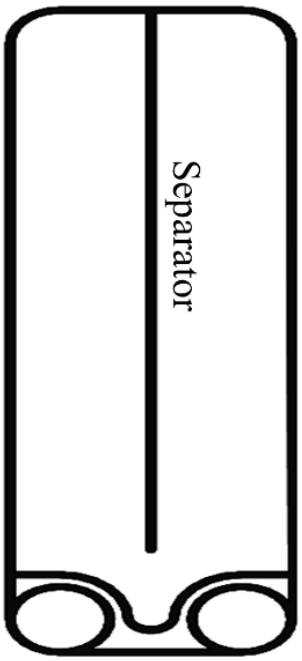

Fig. 3.2: The current gasket design.

The flow mechanism in the new CPHE is as follows; the hot fluid is flowing from bottom to top and then from top to bottom. At the same time on the adjacent plate, the cold fluid is flowing in the opposite direction with respect to the hot fluid, as shown in Fig. 3.3(b). In all well-known CPHEs configurations, the fluid enters from one side and exits from the opposite side either vertically (as shown in Fig. 3.3(a)) or diagonally. However, in the new design, the fluid enters and leaves from the port on the same side, in order to maximize the amount of heat recovery (reducing temperature gradient) between the cold and the hot fluids, consequently enhancing CPHE's thermal performance.

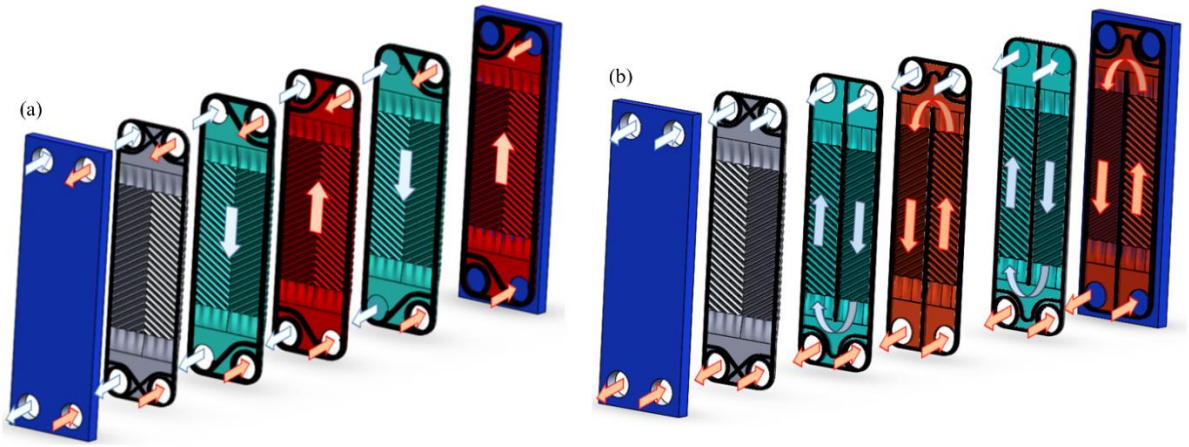

Fig. 3.3: Illustrative schematics of, (a) Flow arrangement for 1-1 pass in the basic CPHE, and (b) The current flow mechanism.

3.4 Numerical Method

3.4.1 Governing equations

Fluids inside CPHE are subjected to turbulent flow due to the change of flow velocity over the corrugations for the considered Reynolds number. In addition, heat transfer takes place between cold and hot sides, and consequently a transition of physical properties occurs, such as temperature, pressure, viscosity, density, and velocity. Therefore, Navier-Stockes Eq. (NS) (3.1) is employed to estimate changes on these properties during the thermal and dynamic interaction as shown below:

$$\frac{\partial}{\partial x_j}\left(\rho u_i u_j\right) = -\frac{\partial p}{\partial x_i} + \frac{\partial}{\partial x_j}\left[(\mu + \mu_t)\frac{\partial u_i}{\partial x_j}\right] \tag{3.1}$$

NS can be considered as Newton's second law applied to the fluid motion. Inertia, pressure, and viscous forces are estimated. ANSYS FLUENT 19.0 solves these equations along with continuity Eq. (3.2). Whereas NS refers to conservation of momentum, and continuity equation refers to conservation of mass.

$$\frac{\partial}{\partial x_i}(\rho u_i) = 0 \tag{3.2}$$

In addition, the energy equation is included to resolve heat transfer among the cold fluid, the hot fluid, and the plates as shown in Eq. (3.3):

$$\rho C_p \frac{\partial}{\partial x_j}\left(u_j T\right) = k_{eff} \frac{\partial^2 T}{\partial x_j^2} + (T_{ij})_{eff} \frac{\partial u_i}{\partial x_j} \tag{3.3}$$

SIMPLE algorithm scheme is enabled to resolve the pressure-velocity coupling. The finite volume based technique is used to discretize the governing Eqs. along with second order upwind scheme to discretize the convection term. Additionally, first order upwind is enabled to discretize the turbulent kinetic energy and dissipation rate.

3.4.2 Turbulence model

Up until today, there is no single or favorite turbulence model that can be applied for any turbulence flow modelling. ANSYS FLUENT provides a large selection of turbulence models, however, care must be taken during choosing an appropriate model. One of the most common turbulence model that is considered as an industry standard model is $k-\varepsilon$ model [146]. The turbulence kinetic energy, k represents the diversity of fluid fluctuations. The turbulence eddy dissipation, ε represents the dissipation rate of the velocity fluctuations. On the other hand, the shear stress transport (SST) $k-\omega$ turbulence model is also used to simulate some heat transfer processes [147, 148], whereas ω represents the dissipation rate between ε to k. The two equations' turbulence models, $k-\varepsilon$ and $k-\omega$ differ from each other. The SST $k-\omega$ model is the combination of $k-\omega$ and standard $k-\varepsilon$. Also, the SST $k-\omega$ model can resolve the boundary layers near the wall, whereas, the standard $k-\varepsilon$ model can resolve the boundary layer away from the wall. The realizable $k-\varepsilon$ model is a relatively new approach that differs from the standard one. It shows outstanding capabilities to capture the mean flow for very complicated structures [146]. In realizable $k-\varepsilon$ model, a new formulation approach for the calculation of eddy viscosity μ_t (3.4) (also called turbulent viscosity) has been developed, where C_μ is no longer constant.

$$\mu_t = \rho\, C_\mu \frac{k^2}{\epsilon} \tag{3.4}$$

The transport Eqs. (3.5) and (3.6) are used to obtain the turbulence kinetic energy k, and

the dissipation rate ε values, respectively.

$$\frac{\partial}{\partial t}(\rho k) + \frac{\partial}{\partial x_j}(\rho k u_j) = \frac{\partial}{\partial x_j}\left[\left(\mu + \frac{\mu_t}{\sigma_k}\right)\frac{\partial k}{\partial x_j}\right] + G_k + G_b - \rho\epsilon - Y_M + S_k \quad (3.5)$$

$$\begin{aligned} &\frac{\partial}{\partial t}(\rho\epsilon) + \frac{\partial}{\partial x_j}(\rho\epsilon u_j) \\ &= \frac{\partial}{\partial x_j}\left[\left(\mu + \frac{\mu_t}{\sigma_\epsilon}\right)\frac{\partial \epsilon}{\partial x_j}\right] + \rho C_1 S_\epsilon + C_{1\epsilon}\frac{\varepsilon}{k}C_{3\epsilon}G_b \\ &- C_2\,\rho\frac{\epsilon^2}{k + \sqrt{\epsilon\nu}} + S_\epsilon \end{aligned} \quad (3.6)$$

where G_k and G_b characterize the generation of k due to the mean velocity gradient and buoyancy, respectively. Y_M depicts the addition of fluctuating enlargement in compressible turbulence to the total dissipation. $C_{1\varepsilon}$, C_2, and $C_{3\varepsilon}$ are constants. σ_k, and σ_ϵ characterize the turbulence Prandtl numbers for turbulence kinetic energy k, and its dissipation ε, respectively. User-defined source terms S_k and S_ε can be implemented when needed.

A realizable $k-\varepsilon$ model satisfies a specific mathematical constraint as well as complying with turbulent flow physics. The spreading rate of planar and round jet can accurately be predicted. In addition, a realizable $k-\varepsilon$ model can provide a superior performance for simulating complex flows, which includes boundary layer reattachment, circulation, rotation, and strong adverse pressure gradient. Both $k-\varepsilon$ and $k-\omega$ are y^+ independent. However, adopting the most appropriate near wall function depends on the degree of mesh refinement near the wall. Near wall treatment methods are very useful when the prism boundary layers are not sufficient to resolve those layers. Standard wall treatment denotes that the whole boundary layer mesh is located within the log-law region. However, for engineering applications, this is difficult to be fulfilled. That is because of existing of different geometrical scales as well as arbitrary refinement, especially for geometries that contain narrow curves and passages. Enhanced and non-equilibrium wall functions can be adopted for ε based. However, the mesh resolution should be high, which is computationally expensive. Altogether, both enhanced and non-equilibrium approaches are not recommended if the viscous sub-layer region is the area

of interest. Instead SST $k-\omega$ can perform better in this region [146].

On the other hand, a scalable wall function introduces an elegant solution for the issue of arbitrary refinement, particularly in complicated geometries. The mesh is virtually shifted to the log-law region ($y^+ \approx 11.225$). Hence the invalid modelling of the laminar sub-layer and buffer region is avoided.

Generally, all turbulence models have been tested for this problem. The realizable $k-\varepsilon$ model with scalable wall function has been adopted, because it showed the most accurate result that is close to the experimental one as well as its consistency with different Re.

3.4.3 Data formulation

In the current study, Re was set as the same for both cold and hot fluids inside CPHE's channels. However, Nu was not considered to be the same.

$$Re = \frac{\dot{m}\, d_e}{\mu\, A_\circ\, N} \tag{3.7}$$

$Re, \mu, A_\circ, N,$ and d_e are known, $\dot{m}$ is calculated to meet the required Re. d_e is twice the plate's corrugation depth.

The essential measurements are the outlet temperatures of cold and hot fluids, and the hot walls' temperature. The fluids' inlet temperatures and velocities have been set in the initial boundary conditions. Two main non-dimensional parameters have been employed to express heat transfer data. Nu is used for a scale heat transfer improvement, and E is calculated to compare the enhancement in thermal performance between the new and the basic CPHEs for two symmetric β = 30°/30°, and 60°/60°. The hot side of CPHE is considered as the product fluid, while the cold side is considered as the utility fluid. Therefore, Nu, and E are considered for the hot side. Nu is given by:

$$Nu = \frac{h_h d_e}{k} \tag{3.8}$$

The heat transfer coefficient, h_h is calculated as follows:

$$Q_h = \dot{m}_h c_{p,h}\left(T_{h,i} - T_{h,o}\right) \tag{3.9}$$

$c_{p,h}$ has been extracted from the tables of thermodynamics at hot fluid bulk mean

temperature as follows:

$$T_{h,b} = \frac{(T_{h,i} + T_{h,o})}{2} \tag{3.10}$$

Note, Q_c is calculated from Eq. (3.11) below. $c_{p,c}$ is also extracted at the bulk mean cold fluid temperature as shown in Eq. (3.12) below. The difference between Q_h and Q_c should always be zero to fulfil the energy balance. However, the difference of about 95% of the simulations is less than ± 2%, and ±4-6% for the rest of the simulations. Therefore, Q_{avg} is taken as the average value of the hot and cold heat load and considered for the current calculations.

$$Q_c = \dot{m}_c c_{p,c}(T_{c,o} - T_{c,i}) \tag{3.11}$$

$$T_{c,b} = \frac{(T_{c,i} + T_{c,o})}{2} \tag{3.12}$$

Now Q_{avg} is known, and h_h is given by:

$$h_h = \frac{Q_{avg}}{A(T_{h,b} - T_{w,h})} \tag{3.13}$$

Q_{max} is the maximum possible amount of heat that could be exchanged between hot and cold fluids and is given by:

$$Q_{max} = C_{min}(T_{h,i} - T_{c,i}) \tag{3.14}$$

C_{min} is the minimum heat capacity. For all cases in the current study $C_h < C_c$:

$$C_h = \dot{m}_h c_{p,h} \tag{3.15}$$

$$C_c = \dot{m}_c c_{p,c} \tag{3.16}$$

Then, E is determined as follows:

$$E = \frac{Q_{avg}}{Q_{max}} \tag{3.17}$$

3.5 Model Setup

3.5.1 CAD geometry creation

Four CPHEs are drawn by using Solidworks CAD 2016. Two symmetric CPHEs with

$\beta = 30°/30°$, and $60°/60°$ are developed according to CPHE's basic design. The other two symmetric CPHEs with $\beta = 30°/30°$, and $60°/60°$ are drawn according to the new design criterion. Each CPHE consists of five plates, which generate four channels. Two channels belong to the cold side and the other two belong to the hot side. All CPHE's geometric parameters have been developed carefully. The corrugations have a sinusoidal shape similar to that one in real CPHE. The port effect is considered. The hot port is created and merged with the hot side, and the same is developed for the cold port side for both basic and new design CPHEs.

3.5.2 Mesh optimization

CPHE contains a large number of curved and tilted narrow passages. Therefore, in order to ensure sufficient mesh element in these narrow passages, unstructured tetrahedron mesh elements are adopted. An advanced technique has been employed to get a good quality mesh. Patch conforming and patch independent algorithms have been adopted simultaneously for the same geometry. The patch conforming is a Delaunay [146] mesher, where mesh refinement is carried out by using an advancing front point insertion technique. The meshing process uses the bottom-up approach, meshing edges, faces, and volume in sequence. In the patch conforming algorithm, excluding the de-featuring tolerance, all faces, and their boundaries are conformed.

On the other hand, a patch independent algorithm is based on spatial subdivision. The mesh refinement is carried out where necessary, particularly in holes, curves, and narrow passages. Large mesh elements are developed where possible such as on flat surfaces. Hence, one should look into covering the important complicated areas on the geometry and allowing for faster computation at the same time. The meshing process uses a top-down approach. The volume mesh is carried out first, and then the surface mesh is created by projecting the volume mesh onto faces and edges.

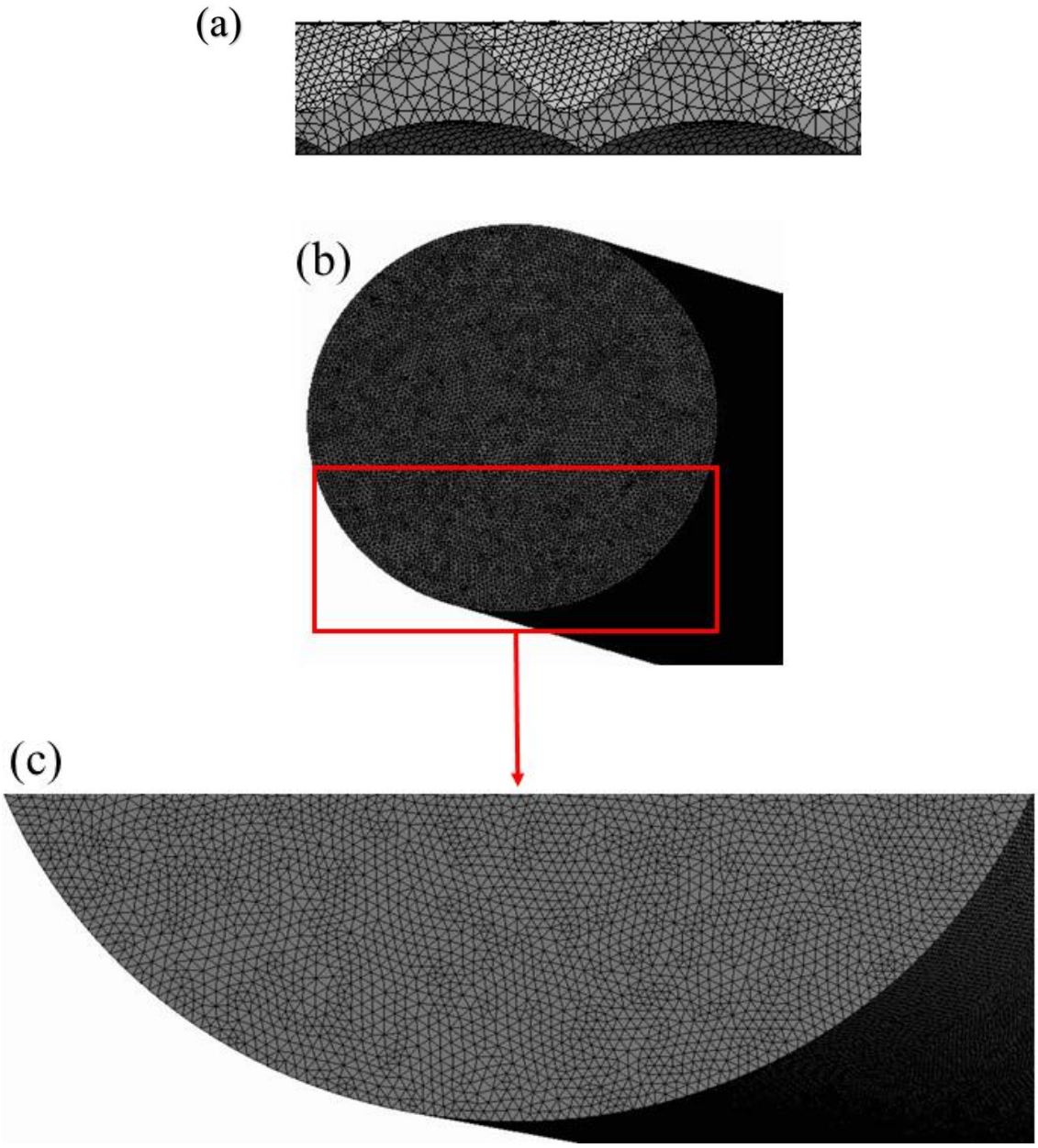

Fig. 3.4: (a) A side view for one corrugation mesh (The whole mesh is not visible due to the high-density elements), (b) Front view for mesh at the cold inlet port, and (c) Close viw at the bottom side of the cold inlet port.

Samples of the mesh are shown in Fig. 3.4(a) and (b). To ensure solution stability, the mesh dependency tests have been carried out for each CPHE as shown in Table 3.1. Mesh elements of 53.1 and 73 million for $\beta = 30°/30°$, for basic and new design CPHEs have been adopted, respectively. Mesh elements of 14.8 and 16.1 million for $\beta = 60°/60°$, for basic and new design CPHEs have been adopted, respectively.

Table 3.1. Mesh independent test for basic (CPHE[1]) and new (CPHE[2]) CPHEs.

	Mesh elements (million)	Outlet cold average temperature (K)	Outlet hot average temperature (K)
CPHE[1] β =30°/30°	44	295.44	305.32
	53.1	295.75	305.82
	62	295.79	305.84
CPHE[2] β =30°/30°	56.6	296.57	303.98
	73	296.78	304.02
	80	296.79	304.01
CPHE[1] β =60°/60°	8	293.62	308.45
	14.8	293.95	308.85
	32	293.89	308.87
CPHE[2] β =60°/60°	9.5	296.59	303.92
	16	296.75	303.82
	47	296.73	303.82

3.5.3 Boundary conditions and material properties specification

Both hot and cold fluids' inlet boundary conditions are set as velocity inlet. The mass flow rate ($\dot{m}$) is calculated from Eq. (3.7) to meet the required Re value. Thus, velocity at the inlet can be calculated from $\dot{m}$. The working fluid is water-water. The hot and the cold inlet water temperatures are set to 40 °C and 18°C respectively. The fluid's thermodynamics properties ($\rho, c_p, k_f,$ and μ) have been set for each fluid according to its temperature. Zero gauge pressure has been set at both cold and hot port outlets. According to the Ansys FLUENT user manual [146], the optimum value for turbulence intensity for the current flow pattern is 5%. The conjugate heat transfer is enabled, where the plate thickness is set to 0.5 mm. Stationary and no slip boundary conditions are set for all walls.

Since most of the studies that were conducted on CPHEs have used stainless steel, and to be able to validate the numerical study, stainless steel is defined as the plate's material. The plate's ρ, c_p, and k are 8030 kg/m^3, 502.48 $J/kg.k$, and 16.27 $W/m.k$, respectively. All simulations are carried out on a high performance computing cluster using nodes with 3.3 GHz, 28 processor, and with 128 GB of RAM. For the mesh that contains 14.8 and 16.1 million element, the simulation time is approximately10-13 hours. For the mesh that contains 53.1 and 73 million elements, the time for each simulation is approximately 48-55 hours.

3.6 Model Validation

The present study has been comprehensively validated with available experimental and CFD studies. The same working fluids and CPHE's material from the available literature are used in this study. Nu data of the current CFD study are compared with other Nu correlations of various studies from the literature. Fig. 3.5(a) shows the empirical Nu deviation for $\beta = 60°/60°$. The maximum and the minimum deviations are found + 9% and + 6% respectively with the findings of Okada et al. [41]. The findings of the CFD study also compared with the measurement obtained by Gherasim et al. [149] and Thonon et al. [150], and the numerical results show good agreement with the published literature.

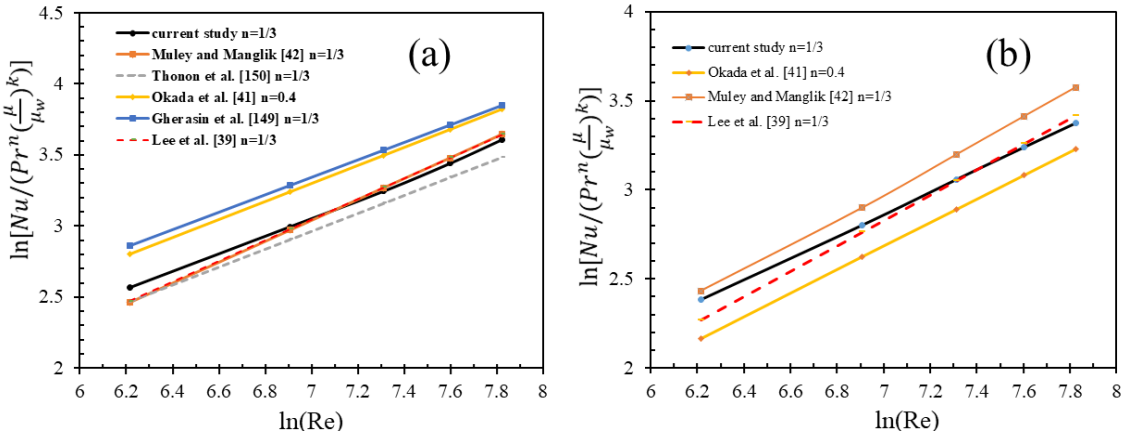

Fig. 3.5: Comparison of present Nu data with other experimental and numerical studies, (a) For $\beta = 60°/60°$, and (b) For $\beta = 30°/30°$.

The findings of the present study have also been compared with the results of Muley and Manglik [42] and Lee et al. [39], and found a negligible deviation with the published data. In the case of $\beta = 30°/30°$, as shown in Fig. 3.5(b), the maximum and the

minimum deviation with the study of Manglik et al. [42] are + 6% and + 2% respectively. The maximum and the minimum deviation are found - 9% and - 4% respectively with the findings of Okada et al. [41]. The maximum and the minimum deviation compared with Lee et al. [39] are - 4.7% and + 1.3%, respectively. The numerical correlations of the present study for both $\beta = 30°/30°$ and $60°/60°$ are consistent with all other published correlations and show an increasing trend.

Several reasons could contribute to the deviation between the results. Some studies calculated average Nu between the cold and the hot sides of the CPHE's [41] . Manglik et al. [42] calculated Nu for the hot side, hence the current results are very close to this one.

Janusz et al. [61] have investigated a number of published Nusselt number correlations to test their accuracy and reported that the Manglik et al. [42] correlation can predict Nu values reasonably well. Furthermore, the differences in the geometrical dimensions such as corrugation depth, aspect ratio (A_r), and even a small difference in the corrugation roundness may result in change in Nu values up to 18% [151]. However, the maximum deviation is always $\leq \pm$ 10% except in one case where the maximum deviation is 11%. The calculated Nu of the present study shows good agreement with the published literature, which sufficiently indicates that the present CFD model is accurate to predict the thermal performance of the CPHEs.

3.7 Results and Discussion

In the present study, four symmetric CPHEs have been employed. Two of them belong to the well-known basic design with $\beta = 30°/30°$, and $60°/60°$. The other two are based on the new design criterion with the same chevron angle of $\beta = 30°/30°$, and $60°/60°$. The numerical simulations have been carried out for the single phase (water-water). All four CPHEs have an identical geometrical dimension ($b, d_e, \beta,$ and A_r) and physical conditions ($T_{h,i} T_{c,i},$ and Re). Reynolds number ranges from 500 to 2500.

Nusselt number has been calculated for all CPHEs, as shown in Fig. 3.6. The results show that, Nu is directly proportional to the plate's chevron angle as well as to the Re. In addition, the new design exhibits significant heat transfer enhancement for all cases. At the same Reynolds number, Nusselt number for the new CPHE increases up to 75% with respect to the basic CPHE as shown in Table 3.2.

The non-uniformity of the CPHE's surfaces causes velocity fluctuation. The fluid has the maximum velocity at the corrugation's ridge and the minimum velocity at the corrugation's furrows as shown in Fig. 3.7. This fluctuation of velocity causes disruption, boundary layer re-attachment, and secondary flow development. Consequently, higher heat transfer rate is provided.

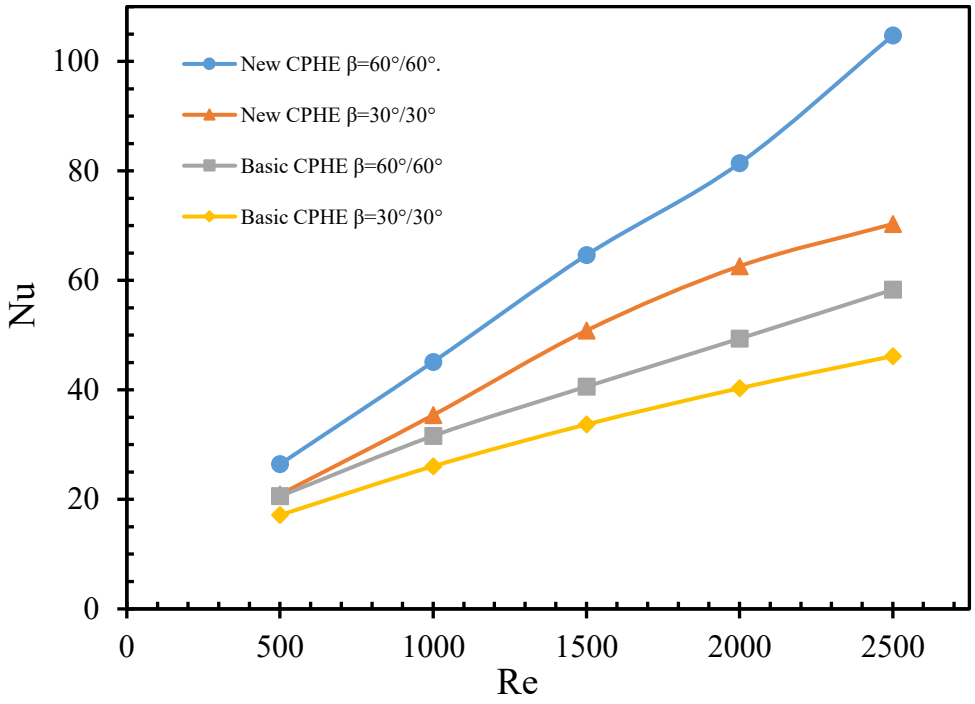

Fig. 3.6: Nu values versus Re for novel and basic CPHEs.

The longitudinal vortices in the corrugation's furrows are observed by Blomerius and Mitra [152]. In addition, Won and Ligrani [153] have carried out an instantaneous visualization of fluid flow inside the channel. The result showed a strong spanwise secondary flow, that moved in an opposite direction in the bottom and the top halves. The boundary layer re-attachment, and its rule in heat transfer augmentation, was also confirmed by Focke and Knibbe [154].

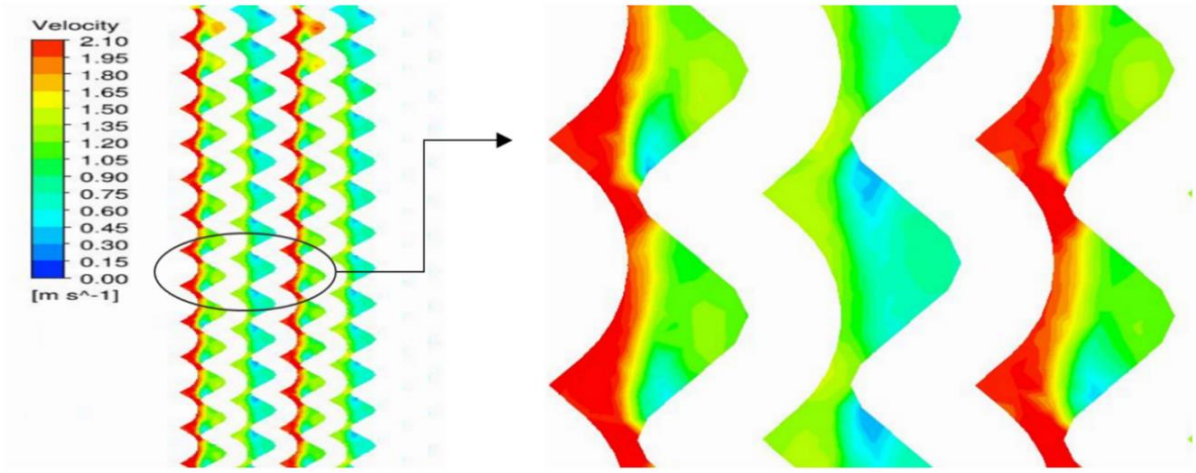

Fig. 3.7: ZY plane (side view) illustrates fluids velocity contour inside new CPHE's channels with β 30°/30° at Re = 500.

In the case of new CPHE, Fig. 3.9 shows that, Re varies significantly over the plate as the fluid is forced to flow along the specified half of the plate. The fluid velocity inside the modified channel is about three times higher than that of the basic channel. Thus, more turbulent flow is developed, which would contribute in heat transfer augmentation. Fig. 3.8 shows the velocity vectors inside the basic CPHE. For the same mass flow rate, the fluid velocity is lower than that of the new one, because in basic CPHE the fluid flows and distributes randomly over the plate.

Table 3.2. Comparison between Nu of the basic ($CPHE^1$) and the new ($CPHE^2$) CPHEs.

Re	**Nu $CPHE^1$ 60°/60°**	**Nu $CPHE^2$ 60°/60°**	**I %**	**Nu $CPHE^1$ 30°/30°**	**Nu $CPHE^2$ 30°/30°**	**I %**
500	20.6	26.7	29.8	17.1	20.9	22
1000	31.6	45.7	44.6	26	35.4	35.9
1500	40.6	65.1	60.2	33.7	50.8	50.9
2000	49.4	81.5	65.1	40.3	62.6	55.3
2500	58.3	102.2	75.3	46.2	72	56

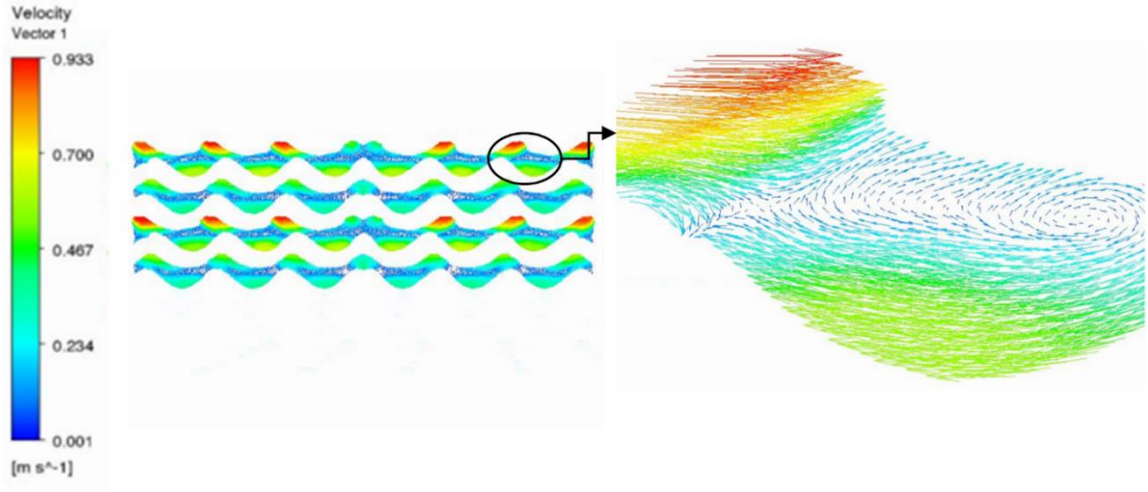

Fig. 3.8: ZX plane (Top view) for velocity vectors for basic CPHE with β 60°/60° at Re = 500.

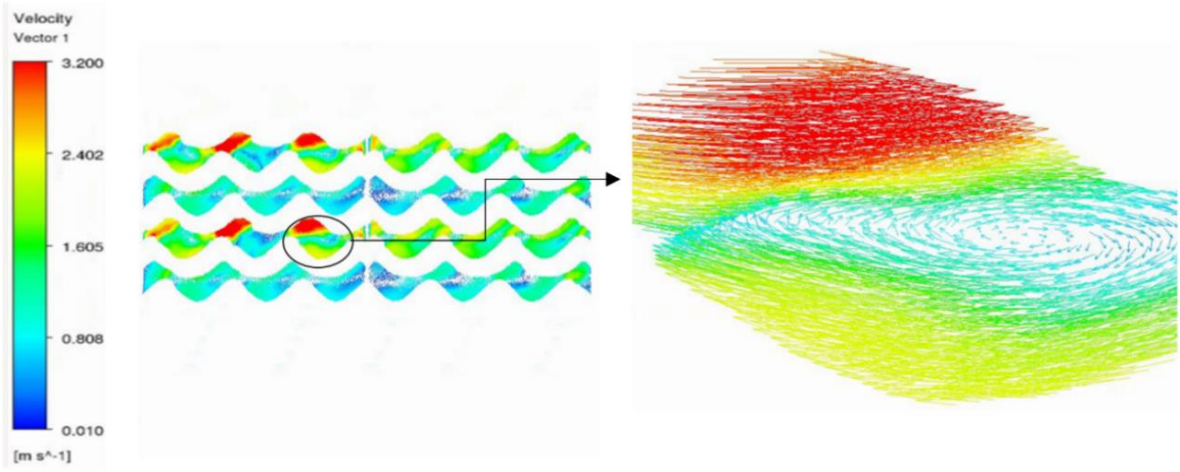

Fig. 3.9: ZX plane (Top view) for velocity vectors for new CPHE with β 60°/60° at Re = 500.

Thermal performance of basic and new CPHEs has been calculated in the form of CPHE's effectiveness (E). Fig. 3.10 shows the CPHE's E versus Reynold number for all cases. In addition, quantitative data of the E along with the enhancement percentage for the new CPHE's E compared with the E of the basic one is given in Table 3.3.

Table 3.3. Comparison between E of the basic (CPHE[1]) and the new (CPHE[2]) CPHEs.

Re	E CPHE[1] 60°/60°	ECPHE[2] 60°/60°	I %	E CPHE[1] 30°/30°	E CPHE[2] 30°/30°	I %
500	34.1	42	23	35.6	41.5	16.6
1000	26.4	34.3	30	27.7	34.2	23.5
1500	22.5	31.4	39.6	23.5	30.7	30.6
2000	20	28.6	42.5	20.8	28.5	36.8
2500	18	26.1	42.2	18.7	25.8	38

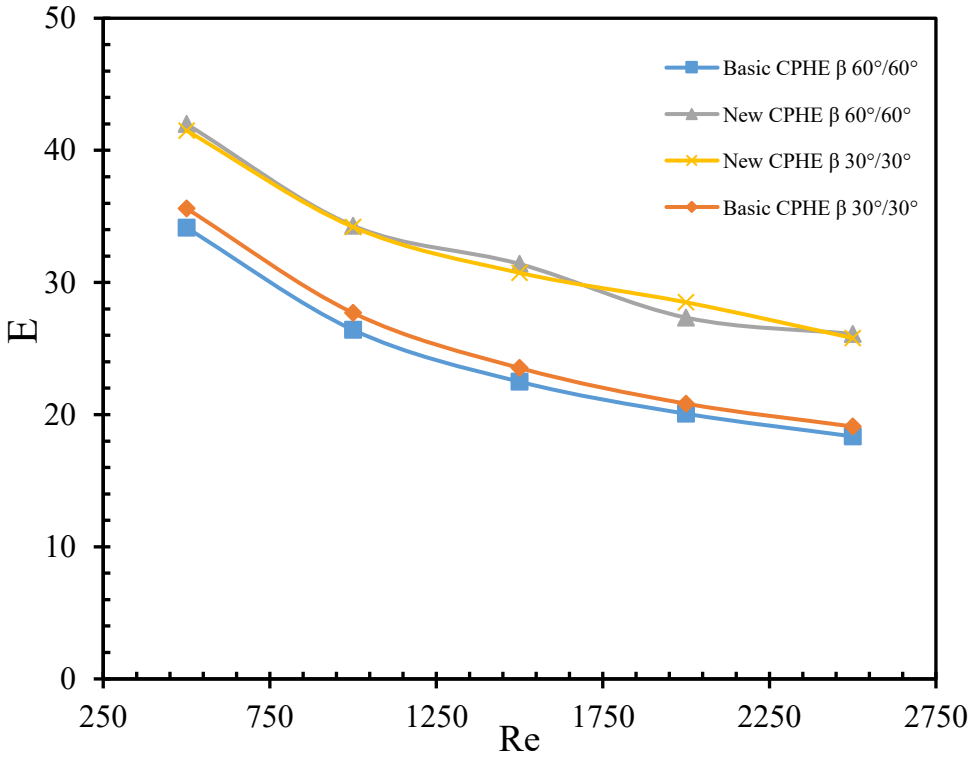

Fig. 3.10: Comparison between the effectiveness (E) of new and basic CPHEs versus Re.

Fig. 3.11(a) and (b) and Fig. 3.12(a) and (b) show temperature contour and profile on the hot channel that is located at the middle (see Fig. 3.13) of the new and the basic CPHE, respectively. In the case of new CPHE, the hot fluid's temperature decreasing rate is higher than that of the basic one. In addition, the hot fluid's temperature is more homogeneous. While in the case of basic CPHE, the hot fluid's temperature shows less homogeneity. In the basic CPHE, the temperature of the hot fluid on the left side is lower

than that on the right side, as shown in Fig. 3.12(a). That is because the cold fluid is entering from the left side in the fore and the next adjacent cold channel as shown in Fig. 3.13.

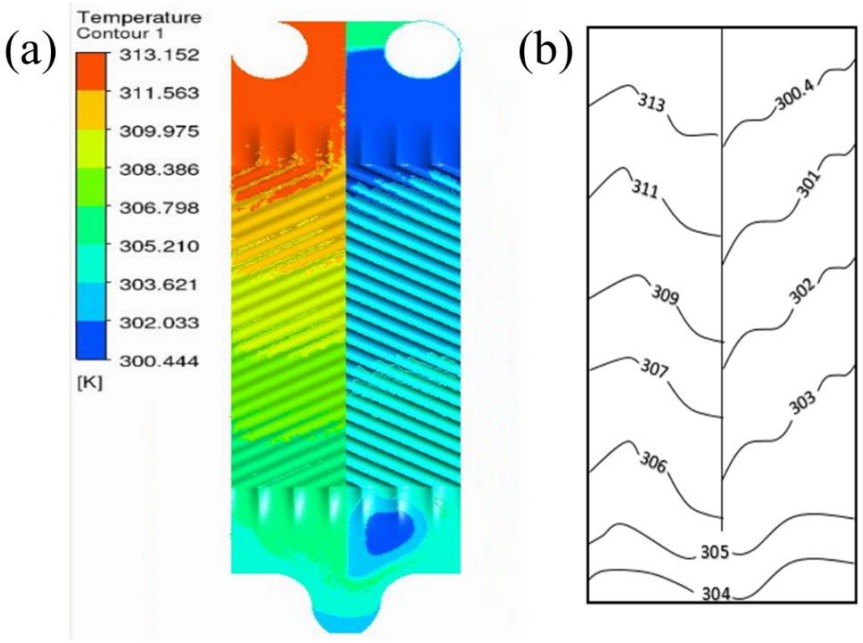

Fig. 3.11: For $\beta = 60°/60°$, and $Re = 500$ (a) Temperature contour of hot channel of the new CPHE, and (b) Temperature profile of hot channel of the new CPHE.

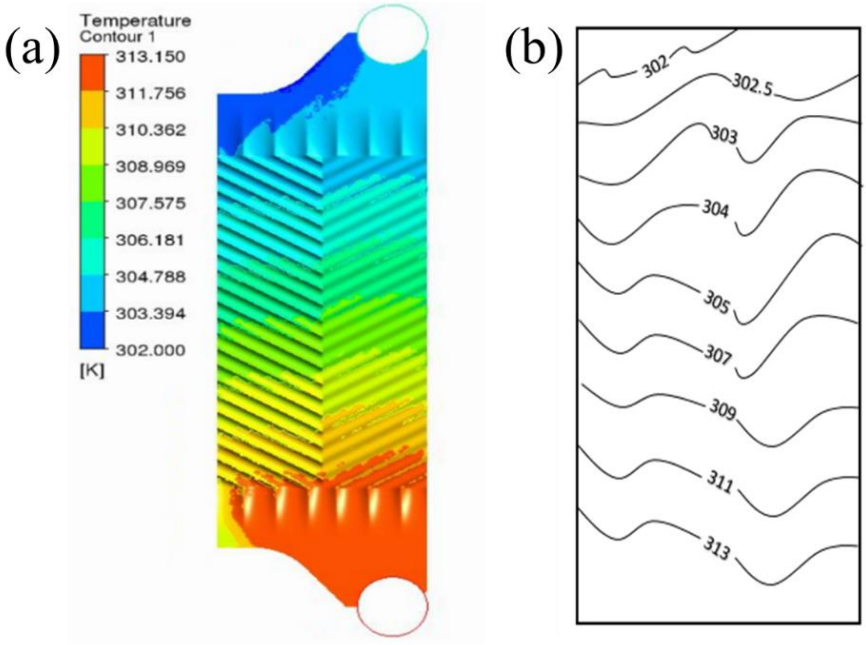

Fig. 3.12: For $\beta = 60°/60°$, and $Re = 500$ (a) Temperature contour of hot channel of the basic CPHE, and (b) Temperature profile of hot channel of the basic CPHE.

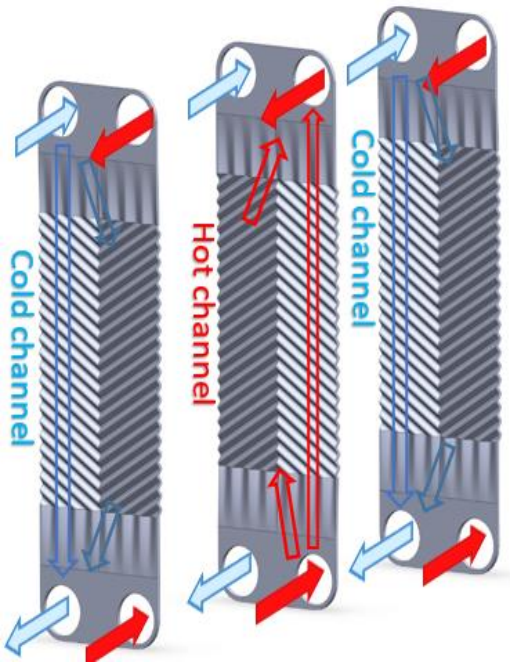

Fig. 3.13: Illustrative schematic for fluid flow arrangement in basic CPHE.

The temperature trend throughout the port of the hot channel outlet, as shown in Fig. 3.14, is presented in Fig. 3.15 (a) and (b). For all cases, the temperature of the last hot channel is higher than that of the first hot channel, whereas, the last hot channel transfers heat with cold fluid from one side only (the side that locates just before the last channel).

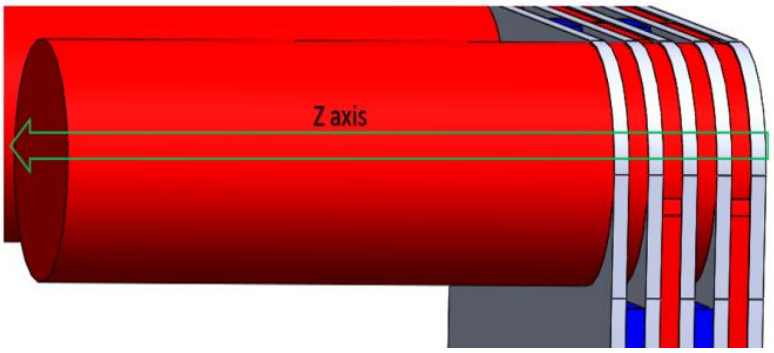

Fig. 3.14: Illustrative sketch for hot channel outlet port.

The first hot channel transfers heat with cold channels from the front and the back sides. Therefore, its temperature is always less than the temperature of the hot channel that locates at the end. All four trends at the beginning show descending temperature as hot fluid moves through z axis. Because the hot fluid of the last channel mixes with the hot fluid of the first channel, which has lower temperature, the temperature increases up to a specific limit, allowing for the temperature balance to take place.

In the newly modified CPHE, more degree of contact between the thermal plates is presented from the middle area of each plate where gaskets are installed, which would enhance the mechanical strength and integrity of the HE. Furthermore, the convective heat transfer and the effectiveness of the modified CPHE are considerably higher than those of the well-known CPHE, hence its size could be further reduced for the same heat duty allowing for more compact heat exchange to be constructed. Therefore, the newly modified CPHE could be implemented in applications that require superior performance such as the solar receiver powered systems. The design of the new generation of the solar receivers in the Concentrated Solar Power (CSP) systems is required to be very efficient. Whether the pressurized air or the carbon dioxide is the working fluid in the solar receiver, both would require an efficient thermo-hydraulic performance of the HE to guarantee the overall efficiency of the system. Additionally, the geometrical constraints in these systems represent an obstacle that needs to be solved [22], hence compact HEs are important to overcome such difficulties. Similarly, the new CPHE could be implemented in applications where area and weight are limited, such as in rockets to cool their nozzles and in ships to integrate with the power generation system and to control the lube oil temperature. In addition, it could be implemented for the heat recovery applications where a closer temperature approach could be achieved in comparison with the well-known CPHE as presented earlier in Fig. 3.11,Fig. 3.12, and Fig. 3.15.

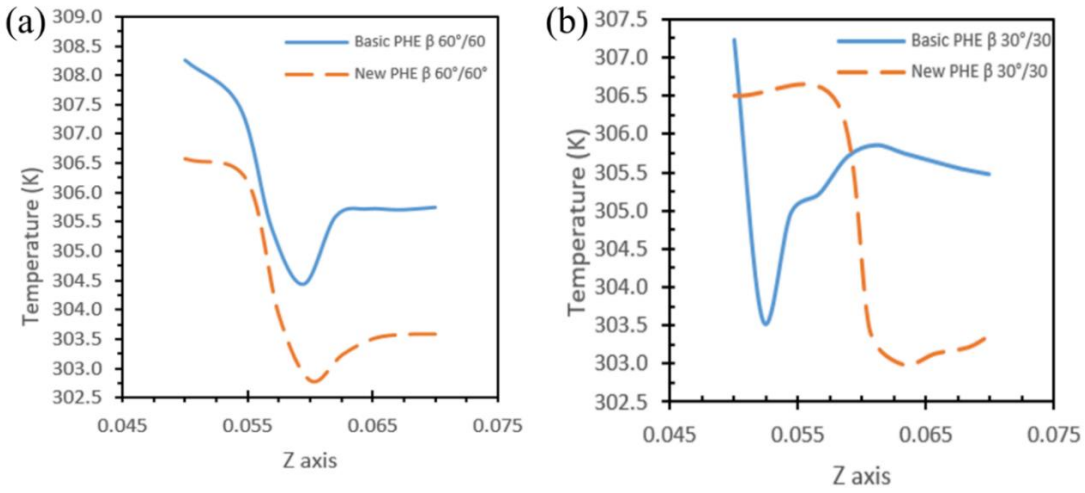

Fig. 3.15: Temperature profile through the hot channel's outlet axis at $Re = 500$ for basic and new CPHEs, (a) For $\beta = 60°/60°$, and (b) For $\beta = 30°/30°$.

3.7.1 Heat transfer correlations

The heat transfer correlations are essential to help the designers to predict the HE's thermal performance and to estimate the required heat transfer area. They are also important for the researcher to compare the harmony level of their data with those in the literature. For the present study, classical Sieder and Tate [155] empirical correlation (3.18) was adopted to predict the Nu correlations. All thermodynamics properties are estimated at the bulk temperature, as shown earlier in Eq. (3.10).

$$Nu = CRe^{p}Pr^{n}\left(\frac{\mu}{\mu_w}\right)^{0.14} \tag{3.18}$$

In order to find the constant values C and p for each CPHE, linear regression technique has been applied to the numerical data in Fig. 3.5(a) and (b). The Pr exponent (n) value ranges from 0.333 up to 0.5 as reported in the literature [41, 42, 45, 156, 157]. However, different values for n have already been tested in Zahrani et al. [47], and 0.333 is found to provide the best approximation. Nu for the basic and the new CPHEs for $\beta = 60°/60°$ is found as follows, respectively.

$$Nu = 0.2354\, Re^{0.6415}Pr^{1/3}\left(\frac{\mu}{\mu_w}\right)^{0.14} \tag{3.19}$$

$$Nu = 0.096\, Re^{0.8273} Pr^{1/3} \left(\frac{\mu}{\mu_w}\right)^{0.14} \quad (3.20)$$

And Nu for the basic and the new CPHEs for $\beta = 30°/30°$ is as follows, respectively.

$$Nu = 0.2332\, Re^{0.6175} Pr^{1/3} \left(\frac{\mu}{\mu_w}\right)^{0.14} \quad (3.21)$$

$$Nu = 0.1134\, Re^{0.7721} Pr^{1/3} \left(\frac{\mu}{\mu_w}\right)^{0.14} \quad (3.22)$$

3.8 Conclusions

Thermal performance of new CPHE for symmetric chevron angles $30°/30°$ and $60°/60°$ has been carried out. A comprehensive validation has been performed with a wide range of published experimental and numerical investigations. A realizable $k-\varepsilon$ turbulence model with scalable wall treatment has been found to provide the most consistent and accurate prediction of the thermal performance of CPHE. The numerical simulations have been conducted for steady-state single phase (water-water), and counter-current flow arrangement.

The CFD results showed that the thermal performance of the new CPHE is significantly higher than that of the well-known CPHE. For the newly developed CPHE, the calculated Nu is up to 75% higher than that available for CPHE. The effectiveness for the new CPHE is significantly higher than that of the well-known CPHE, and generally exhibits a direct proportional relationship with Re. An empirical based correlation for each CPHE is developed to estimate Nu values. The newly developed CPHE would increase the understanding of its thermal behaviour. The findings of the present study could be very useful for many applications, especially for heat recovery applications, where high heat transfer coefficients are required, and for applications where area and weight are limited and require large amount of heat to be removed, such as in ships and airplanes.

Since the performance of the newly developed CPHE is much higher than that of the well-known CPHE, its size can be further reduced for the same heat duty, allowing for a more compact heat exchanger. Further extension of numerical simulations could be performed on the present work to study the difference in size between the new and the

well-known CPHE for the same thermal performance.

Chapter 4: Comparison of Flow Resistance and Port Maldistribution Between Novel and Conventional Plate Heat Exchangers

Research Paper Two:

S. Al-Zahrani, M.S. Islam, S.C. Saha, Comparison of flow resistance and port maldistribution between novel and conventional plate heat exchangers, International Communication in Heat and Mass Transfer, 123 (2021) 105200.

International Communications in Heat and Mass Transfer 123 (2021) 105200

Contents lists available at ScienceDirect

International Communications in Heat and Mass Transfer

journal homepage: www.elsevier.com/locate/ichmt

Comparison of flow resistance and port maldistribution between novel and conventional plate heat exchangers

Salman Al-Zahrani [a,b], Mohammad S. Islam [a], Suvash C. Saha [a,*]

[a] School of Mechanical and Mechatronic Engineering, University of Technology Sydney, Ultimo, NSW 2007, Australia
[b] Mechanical Engineering Department, Faculty of Engineering, Al Baha University, Saudi Arabia

ARTICLE INFO

Keywords:
Corrugated plate heat exchanger
Chevron angle
Heat transfer
Enhancement
Flow resistance
Single-phase

ABSTRACT

Corrugated plate heat exchanger (CPHE) is the most utilized compact heat exchanger (HE) due to its high thermal performance. The present study is conducted for modified CPHEs with chevron angles $\beta = 60°/60°$ and $30°/30°$, and for conventional CPHE with $\beta = 30°/30°$. The characteristics of flow resistance along with other important physical parameters inside the modified and the conventional CPHEs are presented in this study. Acomputational Fluid Dynamics (CFD) approach is employed to conduct the present study, where realizable $k-\varepsilon$ turbulence model is used. The numerical simulations results are validated against available experimental data in the literature. The overall thermal performance is examined by calculating the ratio of the heat transfer rate to the ratio of increase in the pumping power (JF factor). The core pressure drop, fanning friction factor (f), turbulence kinetic energy (TKE), and port maldistribution have been investigated. The findings are compared against those of conventional CPHE with $\beta = 60°/60°$. The modified and the conventional CPHEs are alike in geometrical and physical tests conditions. The simulations are performed for single-phase (water-water), counter-current flow, and for a range of Reynolds number ($Re = 500$ to 2000). The results show that f data of the modified CPHEs are ~4.5–7 fold higher than those of the conventional CPHEs. The data of port maldistribution of conventional CPHEs are found up to ~8 times greater than those of the modified ones. The TKE of the modified CPHEs is found ~2–3 times higher than those of the conventional ones. In addition, due to the high pumping power requirements of the modified CPHEs, their JF data have been found 1.1–1.5 fold lower than those of the conventional CPHEs. The f correlations of the modified and the conventional CPHEs have been established.

4.1 Abstract

Corrugated plate heat exchanger (CPHE) is the most utilized compact heat exchanger (HE) due to its high thermal performance. The present study is conducted for modified CPHEs with chevron angles β = 60°/60° and 30°/30°, and for conventional CPHE with β = 30°/30°. The characteristics of flow resistance along with other important physical parameters inside the modified and the conventional CPHEs are presented in this study. A Computational Fluid Dynamics (CFD) approach is employed to conduct the present study, where realizable $k - \varepsilon$ turbulence model is used. The numerical simulation results are validated against available experimental data in the literature. The overall thermal performance is examined by calculating the ratio of the heat transfer rate to the ratio of increase in the pumping power (JF factor). The core pressure drop, fanning friction factor (f), turbulence kinetic energy (TKE), and port maldistribution have been investigated. The findings are compared against those of conventional CPHE with β = 60°/60°. The modified and the conventional CPHEs are alike in geometrical and physical test conditions. The simulations are performed for single-phase (water-water), counter-current flow, and for a range of Reynolds number (Re = 500 to 2000). The results show that f data of the modified CPHEs are ~ 4.5-7 fold higher than those of the conventional CPHEs. The data of port maldistribution of conventional CPHEs are found up to ~ 8 times greater than those of the modified ones. The TKE of the modified CPHEs is found ~ 2-3 times higher than those of the conventional ones. In addition, due to the high pumping power requirements of the modified CPHEs, their JF data have been found 1.1-1.5 fold lower than those of the conventional CPHEs. The f correlations of the modified and the conventional CPHEs have been established.

Keywords: Corrugated plate heat exchanger; Chevron angle; Heat transfer; Enhancement; Flow resistance; Single-phase.

4.2 Introduction

Due to the continuous growth in economy and population, the demand for energy is globally expanding considerably [16]. Therefore, minimization of energy consumption is desired. Because of that, significant efforts have been devoted to the field of heat transfer enhancement in heat exchangers (HEs) devices. With this regard, passive techniques are usually employed to achieve the enhancement goal [22]. This technique should improve

one or more of the following parameters: weight of the device (i.e. new material), reduction in size of the device for the same heat duty, achievement of energy savings, and feasibility for manufacturing.

The effect of the end plate in frame CPHE and brazed CPHE is investigated by Jin and Hrnjak [158]. Their findings showed, when the number of plates increases, the effect of the end plate becomes insignificant. Heggs and Scheidat [159] reported that the effect of the end plate is diluted when the number of the plates is ≥ 19. For the same test conditions (i.e. same CPHE, and same flow arrangements), the effect of Prandtl number has been investigated by Zahrani et al. [47]. The convective heat transfer and *f* of the water (i.e. Pr = 4.34) are respectively 4 and 1.1 times higher than those of the air (i.e. Pr=0.72). The thermal performance of three different β's (β = 60°/60°, β = 60°/30°, and β = 30°/30°) with U type flow, and single-phase water-water has been studied by Muley and Manglik [42]. They reported that Nu and *f* are strongly affected by Re and β. They incorporated all correlations for all β's into one correlation for Nu and another one for *f*. Similar studies have been carried out to further investigate the effect of different β's on heat transfer characteristics for single-phase heat transfer [46, 51, 160-166]. Heat transfer characteristics of nine CPHEs with different dimensions have been experimentally investigated by Yang et al. [120]. Chevron angle is found the most influencing parameter in their study. Based on the data of the nine CPHEs, they generated individual correlations, and a general correlation as well. An extensive literature review was conducted by Zhang et al. [132] and found that chevron angle is the most influencing parameter.

Recently, Zahrani et al. [167] proposed novel modification in the design of corrugated PHEs. The enhancement in the convective heat transfer of the novel corrugated PHEs is found up to 1.3 times that of the conventional one. Gurel et al. [168] have studied the heat transfer characteristics of lung pattern embossed on the surface of flat plate. Their findings showed 71% increase in the heat transfer rate. Kumar et al. [161] have experimentally studied flow maldistribution in CPHE with β = 60°/60°, U type, water as working fluid, and for single-pass flow arrangement. A direct proportionality between the channel pressure drop and the number of plates set has been found. Kim et al. [169] have studied the thermal performance of two CPHEs. One HE is composed of single-wave, and the other one is composed of double-wave. Their aim was to find a new solution that

could substitute the use of an open-loop cooling tower by a closed-loop one. The result showed that the thermal performance of CPHE with double-wave is 50% higher than that of single-wave. However, double-wave CPHE yields an additional 30% pressure drop. Based on numerical findings, new expressions for calculating heat transfer area, cross-sectional area, and hydraulic diameter of pillow PHE have been proposed by Piper et al. [170]. Experiments have been conducted by Nilpueng et al. [106, 107] on CPHE with plate surface roughness varies from 0.95 μm to 2.75 μm. They reported the correlations of heat transfer and pressure drop for different surface roughness values.

CPHE consists of several geometric parameters, i.e. corrugations' depth, and plate thickness. Dvorak and Vit [171] have numerically studied the effect of plate thickness on the effectiveness of the CPHE for air-air fluid flow. They reported that the material thickness has inverse proportionality to the effectiveness of the CPHE. The effect of the channel's gap size on the flow pattern of air-water fluid flow is investigated by Pipathattakul et al. [172]. It has been found that, as the gap size increases, the flow pattern quickly shifts to the greater value of air velocity. Miura et al. [173] have experimentally investigated 32 flow arrangements to find out the empirical correlation that takes into account the effect of number of flow channels per pass, and number of passes on pressure drop. They also aimed to compare the experimental results with the simulation ones: those obtained by CFD. Good agreement among experimental, empirical, and numerical results is reported. The flow maldistribution from port to channel for small and large PHEs has been investigated by Rao and Das [139, 174]. More severe flow maldistribution is found to take place in the large plate package. In addition, flow maldistribution is also found to take place even for small port cross-sectional area; hence identical sizes between the ports and the connectors is the suggested solution to eliminate/minimize the port maldistribution in small plate packages.

In general, most of the studies in the literature are parametric ones. However, continuous improvement in the design of the HEs is a substantial aim for the developers to meet the continuous expanding of energy demand. Yet, the enhancement in the heat transfer rates of these improved HEs is mostly accompanied with additional pressure drops. Therefore, the present study aims to reveal the thermal characteristics (i.e. flow resistance, and JF factor) of the novel CPHEs proposed [175]. CFD is used to simulate the characteristics of fluid flow inside two modified CPHEs with β = 60°/60° and 30°/30°,

and one conventional CPHE with β = 30°/30°. The findings are compared against those of conventional CPHE with β = 60°/60° from previous study. Simulations are performed for steady-state flow, single-phase (water-water), 500 < Re < 2000, U type counter current flow arrangements, and gravity has been considered for all cases.

4.3 Numerical Approach

4.3.1 Geometry (CAD), mesh, and numerical model.

All of the present CPHEs have been created in Solidworks; two of them represent the modified CPHEs, and one of them represents the conventional CPHE. Fig. 4.1 shows the difference between the shape of thermal plates of the modified and the conventional CPHEs.

Geometry of CPHE is highly complex, because it consists of a large number of curves, and narrow channels. Therefore, tetrahedron mesh elements are adopted for both of the studied CPHEs. All the metrics quality (i.e. skewness, and orthogonal quality) have been checked for all HEs to ensure all meshes are of acceptable quality. All simulations are performed for 500 < Re < 2000, hence the flow is likely to be turbulent in this region [42]. Therefore, a realizable $k - \varepsilon$ has been employed as a turbulence model. Furthermore, a scalable wall is used as the near wall treatment approach. The specifications of the CAD model, mesh generation, mesh test, and the used numerical model are to be found in detail [175].

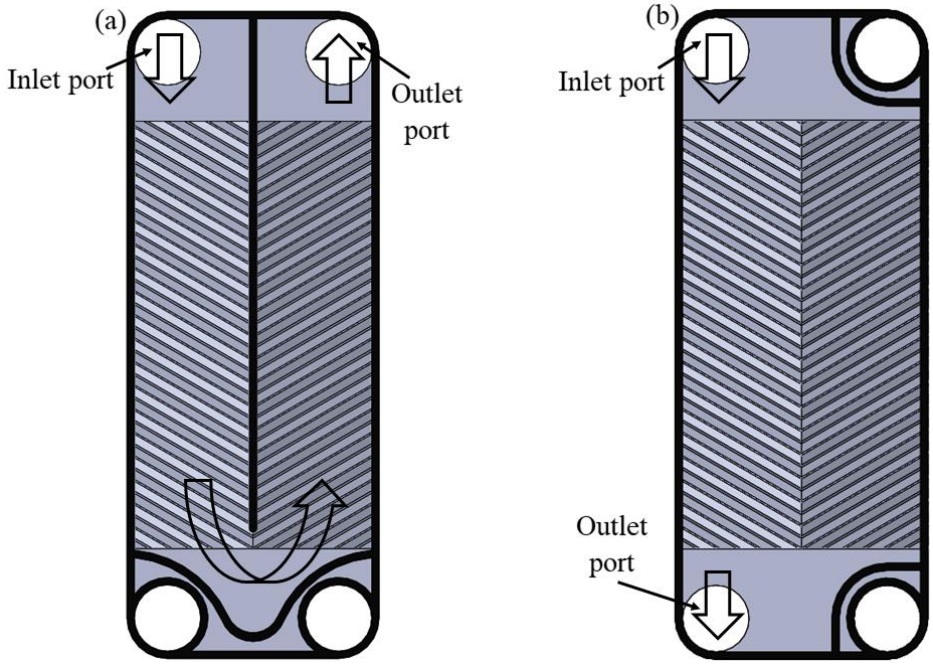

Fig. 4.1: Thermal plate of (a) Modified CPHE, and (b) Conventional CPHE.

4.3.2 Data formulation

The presented calculations are performed for steady-state flow, and for single phase (water-water). The hydraulic diameter (d_e) is calculated as:

$$d_e = 2b \tag{4.1}$$

Where b is the corrugation depth. In addition, Re is estimated as:

$$Re = \frac{\rho\, u\, d_e}{\mu} \tag{4.2}$$

The overall pressure drop across the entire CPHE is estimated as:

$$\Delta P_m = \Delta P_{port} + \Delta P_{core} + \Delta P_{elev.} \tag{4.3}$$

Where ΔP_{port} represents the pressure drop due to the port effect, and ΔP_{core} is the pressure drop inside the channel of the CPHE. In addition, $\Delta P_{elev.}$ is the pressure drop that occurs due to the elevation difference, and it has been ignored in this study because the plate length is small. Based on the Shah and Focke [176] empirical equation, ΔP_{port} is calculated as:

$$\Delta P_{port} = 1.5\left(\frac{\rho V^2{}_{port}}{2}\right) \tag{4.4}$$

From Eq. (4.3), ΔP_{core} is given as:

$$\Delta P_{core} = \Delta P_m - \Delta P_{port} \tag{4.5}$$

Now, loss in shear stress can be expressed by calculating fanning friction factor as follows:

$$f = \frac{\rho d_e \Delta P_{core}}{2 L_P G^2} \tag{4.6}$$

Where L_P, and G are respectively the effective vertical length of the plate, and the mass flux. Moreover, G is estimated as:

$$G = \frac{\dot{m}}{L_w b N} \tag{4.7}$$

Where L_w stands for the width of the flow channel.

4.4 Results and Discussion

4.4.1 Validation

Even at low Reynolds numbers, the flow inside the corrugated channels is more likely expected to be turbulent [42, 152]. A realizable $k-\varepsilon$ model is employed to simulate the flow characteristics inside the corrugated channels. The data of fanning friction factor of conventional CPHE with β = 30°/30° have been compared with the experimental data [26]. The maximum difference between the experimental and the numerical data is found to be ~13% as shown in Fig. 4.2. Lee et al. [39] have studied the difference in Nu and f data for three different ratios between the chevron pitch (the distance between the center of two consecutive corrugations) to the corrugation depth (b). Significant difference among the results has been found. Moreover, Sparrow et al. [151] carried out an experimental study to reveal the impact of small rounding edges on heat transfer and pressure drop. They found even a small difference could attribute in deviation between the results up to 18%. Therefore, the deviation between the present study and the experimental one [26] is likely taking place due to the difference between the geometrical parameters, as CPHE contains a large number of geometrical parameters. Furthermore, f

data of CPHE with β = 60°/60° have been validated with the experimental studies of Kumar [2], and Lee et al. [40] in Zahrani et al. [167]. The maximum deviation between the experimental and the numerical model is found + 9.3%.

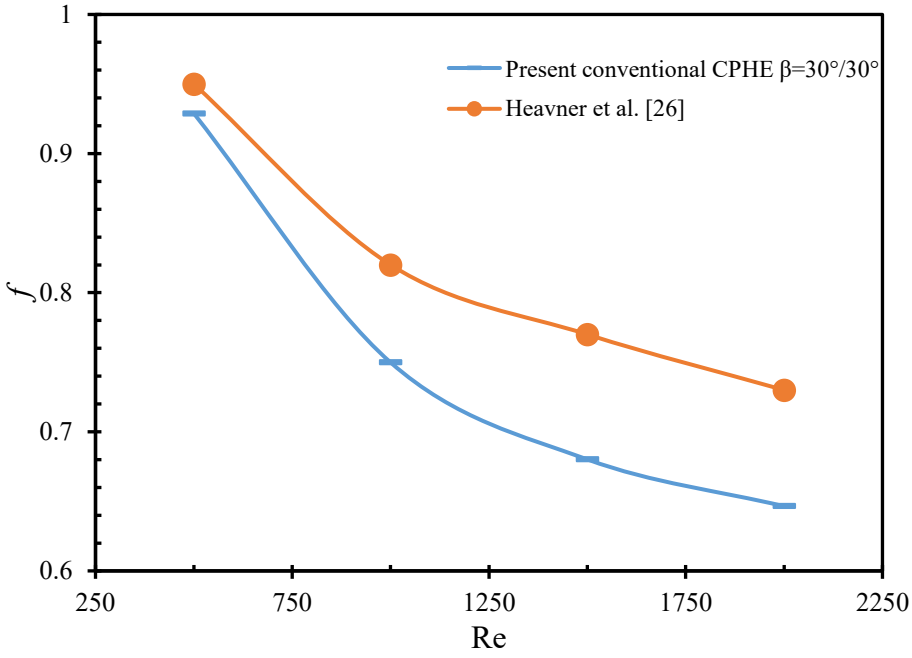

Fig. 4.2: Comparison between numerical data of f and experimental one for CPHE with β = 30°/30°.

4.4.2 Analysis of flow resistance inside hot channel

The flow resistance and overall thermal performance inside the hot channels of modified CPHEs (β = 60°/60°, and β = 30°/30°), and conventional CPHE (β = 30°/30°) are investigated. The results of the conventional CPHE with β = 60°/60° from Zahrani et al. [167] are employed for comparison. All four CPHEs have the same test conditions i.e. same number of channels, and same dimensions.

The change in core pressure drop with different mass flux inside the hot channels of the new and the conventional CPHEs is shown in Fig. 4.3. The core pressure drop of the modified CPHEs is significantly higher than that of the conventional ones. In addition, as velocity increases, more pressure is required to achieve this velocity, hence the trends of all four CPHEs are increasing as mass flux increases, as shown in Fig. 4.3. Moreover, the trends of the conventional CPHEs are linearly increasing while the trends of the modified

CPHEs show non-linear increment with the mass flux increasing. Consequently, the difference between the values of the core pressure drops of the modified and the conventional HEs is quickly expanding with the increase of mass flux, as shown in Fig. 4.3. The pressure drop is increasing as β increases as it has been reported in the literature i.e. $\Delta P_{\beta=60°/60°} > \Delta P_{\beta=30°/30°}$ [177-179]. In the present study, in both modified and conventional CPHEs, chevron angle with β = 60°/60° has the highest pressure drop. That is because as β increases, the water flows with higher velocities, as presented in Fig. 4.7, which eventually causes more pressure drop.

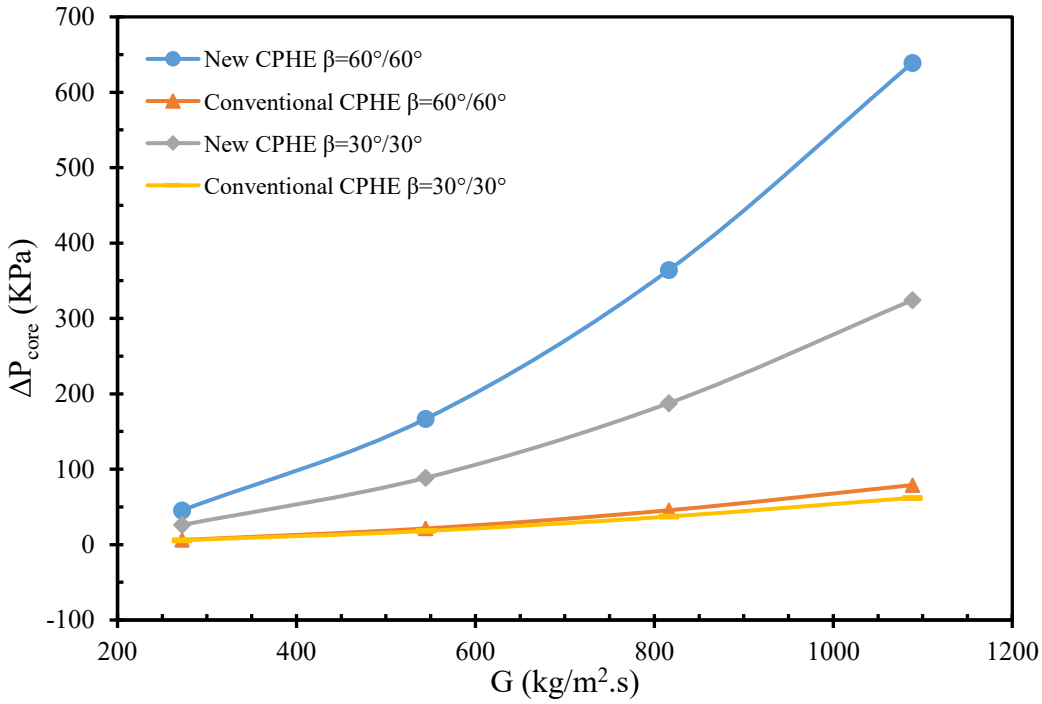

Fig. 4.3: Core pressure drop of modified and conventional CPHEs.

The high-pressure drop of the modified CPHEs is due to the division of the channel into narrower paths as shown in Fig. 4.1(a), hence the fluid will flow with higher velocities. Furthermore, in the modified CPHEs, the fluid moves for a longer distance because it circulates around the plate and leaves from the same side of the entering side, hence more pumping power is required. Both of these two reasons contribute with different percentages in the high pressure drop of the modified CPHE. Furthermore, Fig. 4.4(a) and (c) show the pressure drop contour of the modified CPHE at Re = 1500, and it can be seen high-pressure drop is taking place at the bottom of the channel because the fluid rotates around the bend. Thus, its velocity is further increasing, which would result

in more pressure drop as shown in "*x* area" on Fig. 4.7(a) and (c). In addition, it is noticed from Fig. 4.4(b) and (d) most of the pressure drop is occurring in the corrugation area.

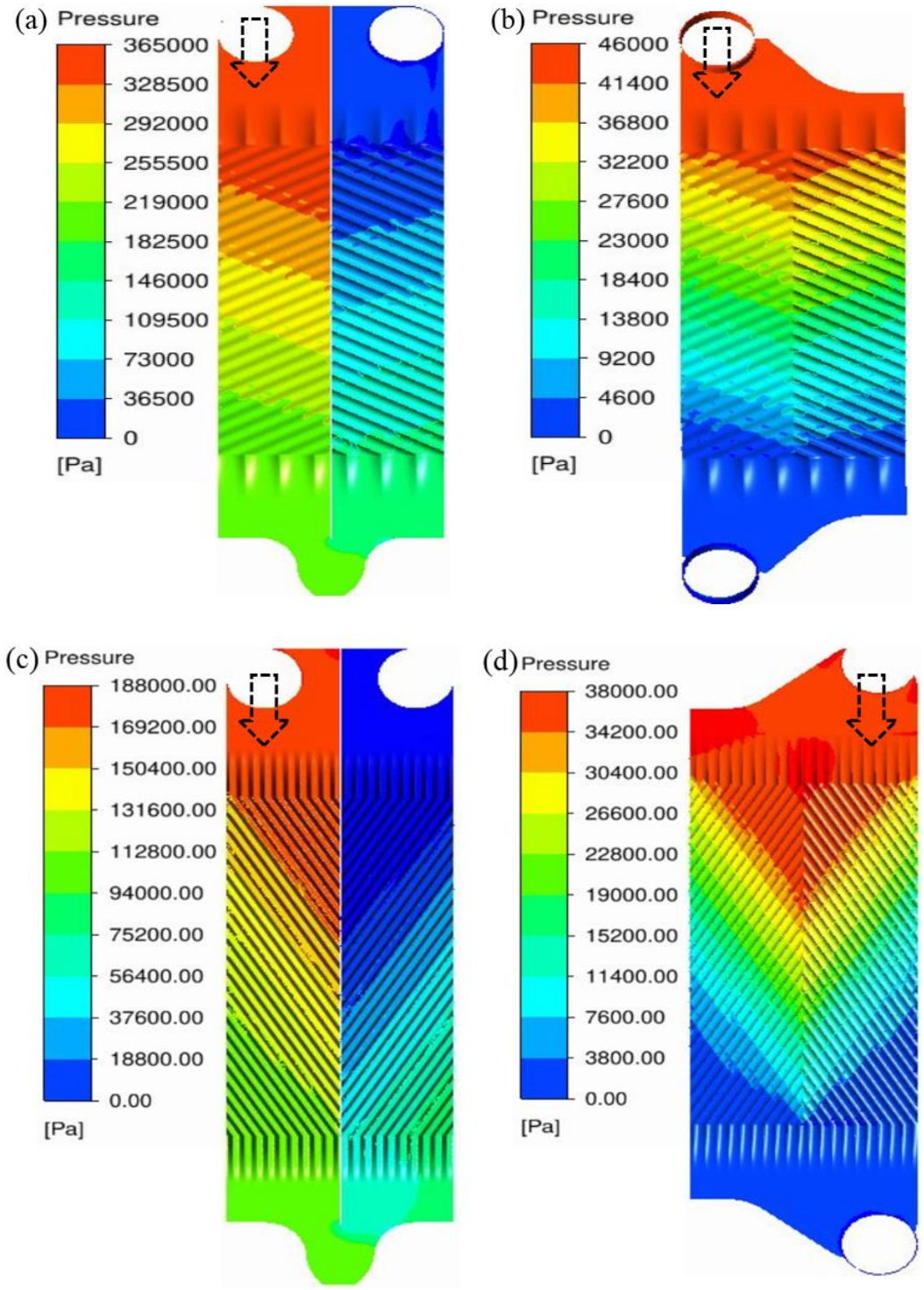

Fig. 4.4: Pressure drop inside (a) Modified channel with β = 60°/60°, (b) Conventional channel with β = 60°/60°, (c) Modified channel with β = 30°/30°, and (d) Conventional channel with β = 30°/30°.

The change in fanning friction factor with Re is presented in Fig. 4.5. Contrary to the data of the core pressure drop, the trends of *f* data are decreasing as Re increases for all CPHEs. That is because as flow velocity increases, the inertia forces become more dominant, and the impact of viscous forces become less influential, hence *f* values decrease. Although all trends are decreasing as Re increases, the trends of the modified CPHEs show faster decrease at the beginning. Generally, *f* data of the modified CPHEs are ~ 4.5-7 fold higher than those of the conventional CPHEs. Moreover, the degree of the linearity of all trends could insinuate the flow is in the turbulent region, though flow visualization is needed to confirm this point. In regards to the type of flow regime, there is vast disagreement in the literature upon the onset point of the turbulent flow inside the corrugated channels. Heavner et al. [26] reported the transition to turbulent flow is started at low Re, i.e. Re = 20, and the flow is fully turbulent at Re > 200. Various studies reported similar results [45, 58]. On the other hand, some other studies [42, 176] reported the critical Re range from 400 to 800. More recently, because the flow inside the corrugated channels is highly irregular, Khan et al. [66] suggested naming the flow "low Re flow", or "high Re flow".

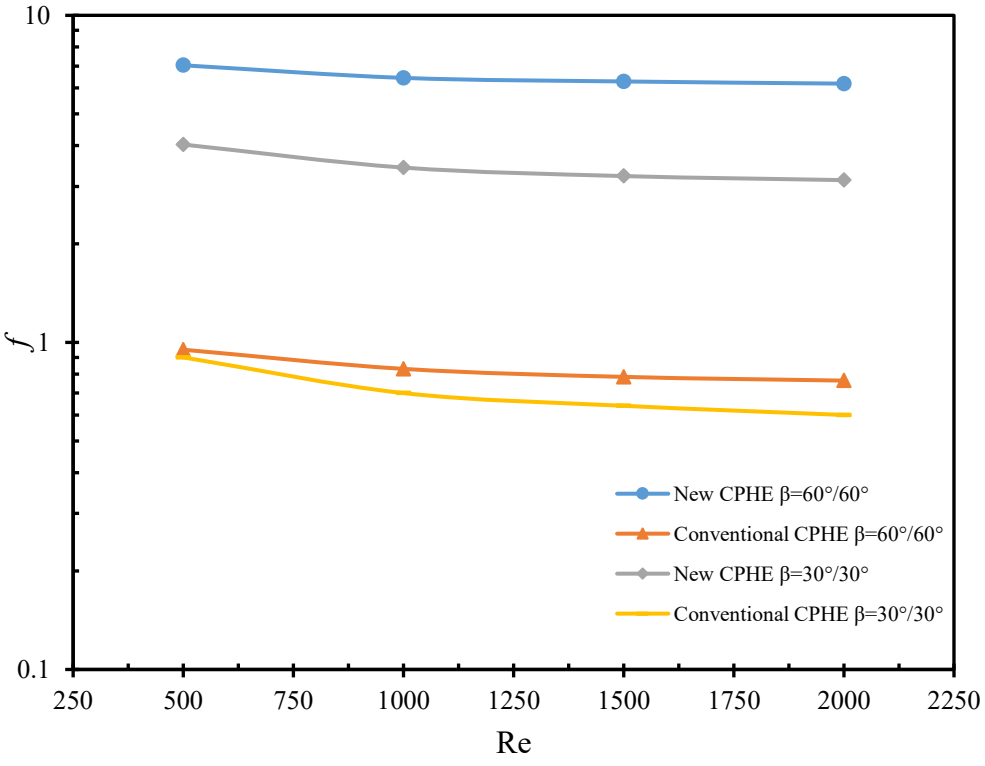

Fig. 4.5: Comparison between f data of the modified and the conventional CPHEs.

In turbulent flow, the kinetic energy that is associated with the eddies is known as turbulence kinetic energy (TKE).

$$TKE = \frac{1}{2}\left(\overline{(u')^2} + \overline{(v')^2} + \overline{(\omega')^2}\right) \tag{4.8}$$

Where u', v', and ω' are the velocity components in x, y, and z directions, respectively.

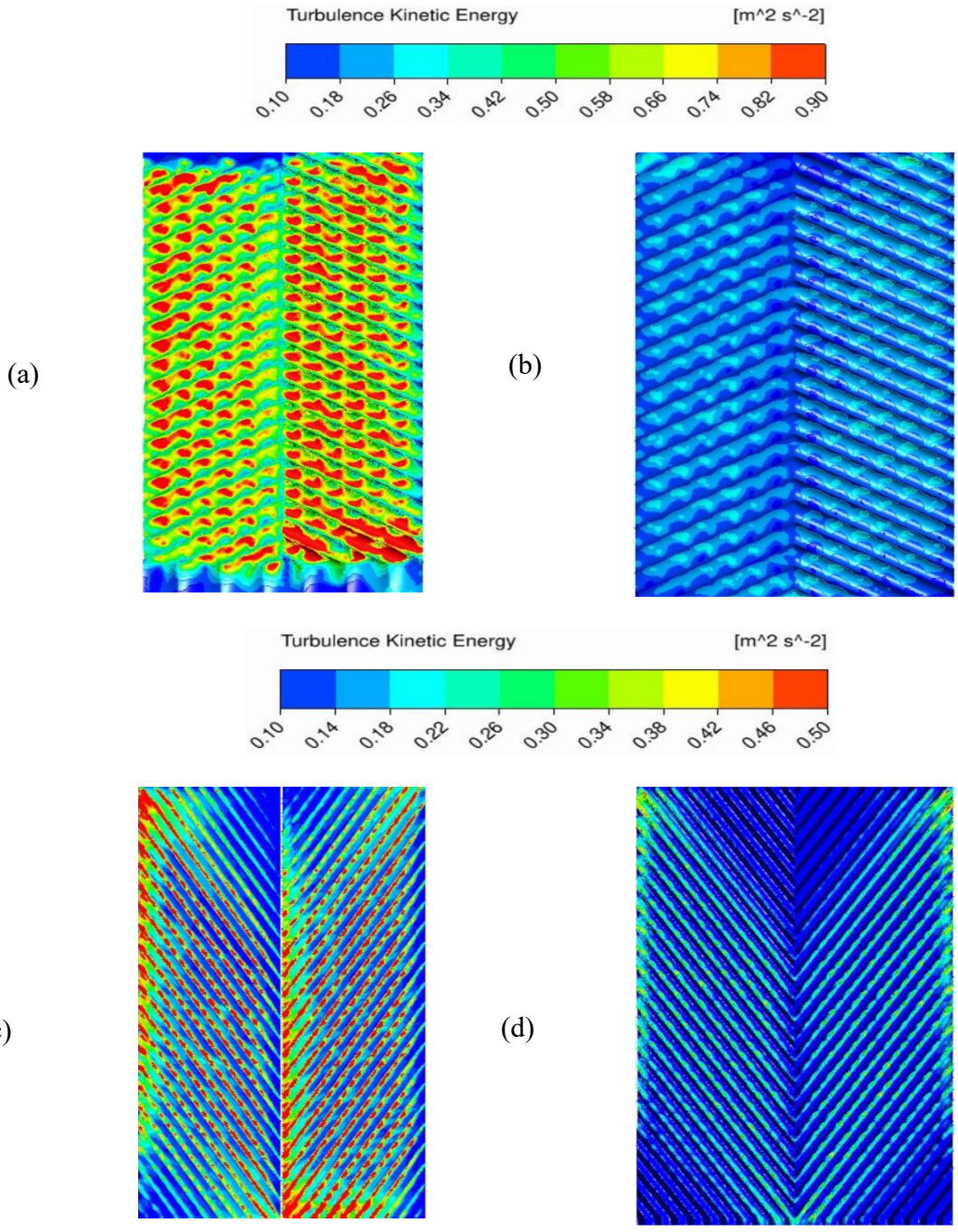

Fig. 4.6: TKE contours at Re = 1500 on the corrugations of (a) Modified plate with β = 60°/60°, (b) Conventional plate with β = 60°/60°, (c) Modified plate with β = 30°/30°, and (d) Conventional plate with β = 30°/30°.

The existence of narrow channels with criss-cross corrugations in CPHEs causes separation of boundary layers, and generation of swirl flow. Eventually this would expedite the flow mixing and cause more pressure drop. At Re = 1500, the TKE on the surface of the corrugations for all CPHEs is presented in Fig. 4.6.

TKE is used as an indicator of the flow mixing degree, hence higher TKE yield higher heat transfer rate [180]. It is conspicuous that the TKE of the modified channels is ~ 2-3 times higher than those of the conventional channels. That is because at the same mass flow rate, the fluid flows with higher velocities inside the modified channels as shown in Fig. 4.7.

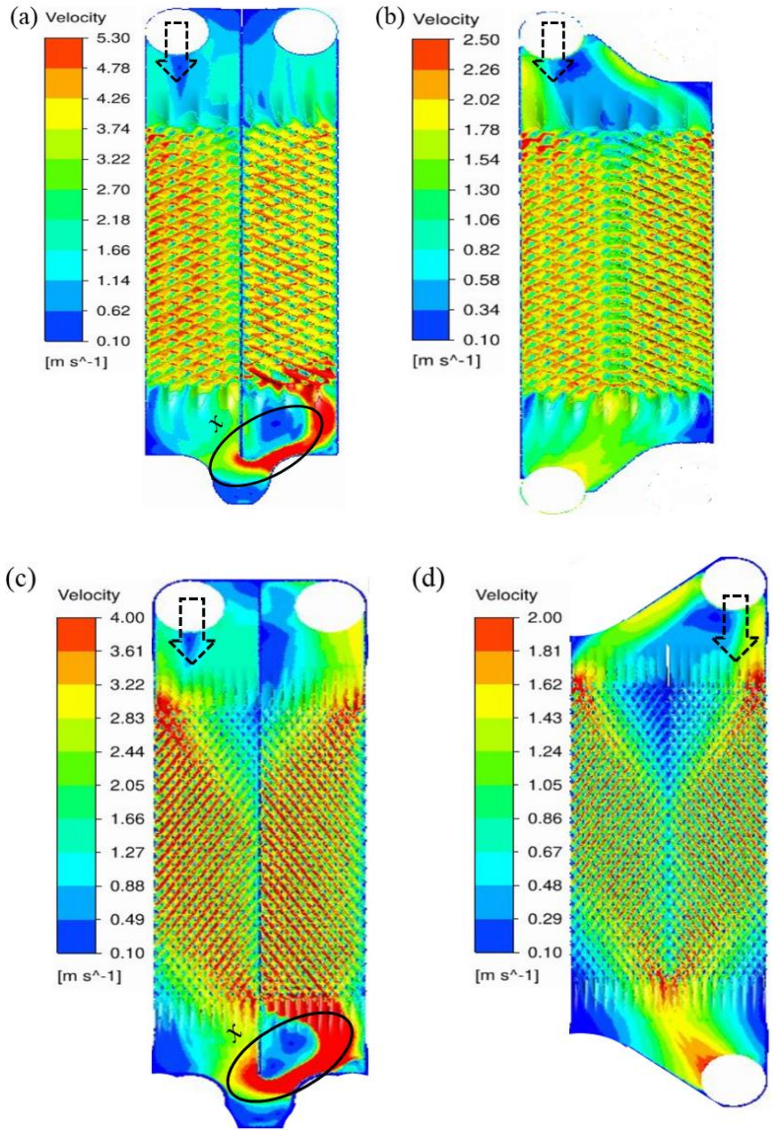

Fig. 4.7: Velocity fluctuation at Re=1500 on the surface of (a) Modified plate with β = 60°/60°, (b) Conventional plate with β= 60°/60°, (c) Modified plate with β = 30°/30°, and

(d) Conventional plate with β = 30°/30°.

In addition, the highest flow velocities' fluctuations are observed on the corrugations' ridges, as can be seen clearly in Fig. 4.6(a).

4.4.3 Overall thermal performance

To investigate the overall quality of the thermal performance of the present CPHEs, JF factor is employed. Higher JF data yield better performance.

$$JF = \frac{(j/j_o)}{(f/f_o)^{1/3}} \tag{4.9}$$

Fig. 4.8 presents JF data of all CPHEs. Because of the high pressure drop that takes place throughout the modified CPHEs, their JF data are lower than those of the conventional CPHEs. The trends of the modified and the conventional CPHEs show unalike behaviours. The conventional CPHEs' trends are decreasing as Re increases, while the trends of the modified CPHEs show direct proportionality with Re. That means, in case of conventional CPHEs, the increase in the rate of pressure drop is greater than the increase in the rate of the convective heat transfer, and vice versa is correct in case of the trends of the modified CPHEs.

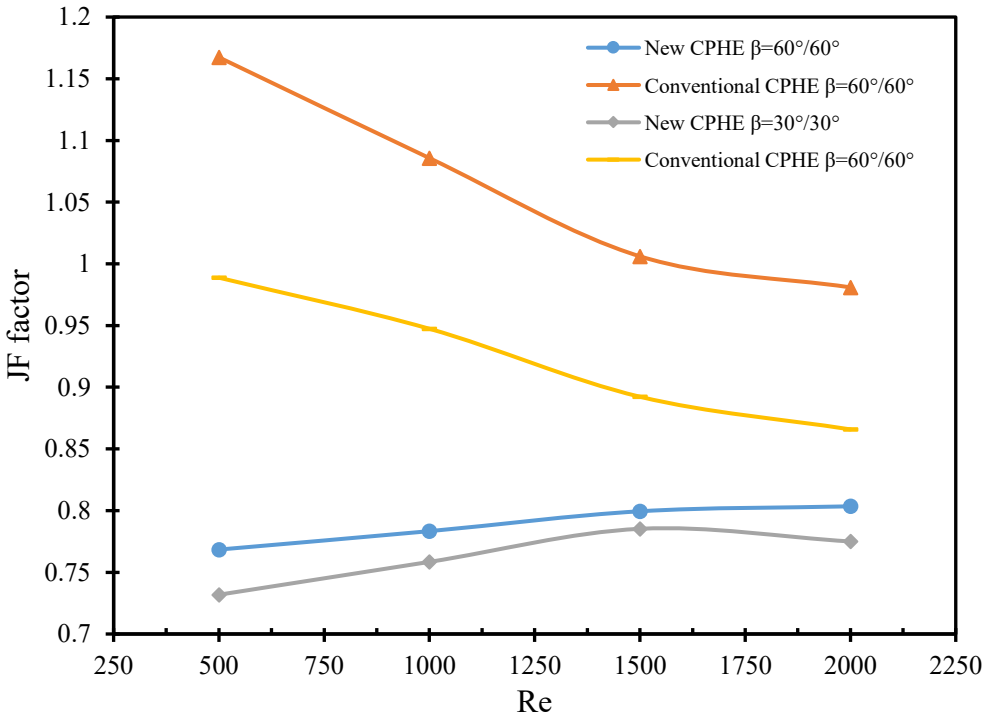

Fig. 4.8: Comparison between JF data of the modified and the conventional CPHEs.

Moreover, conventional CPHE with β = 60°/60° is the only HE that has JF data greater than one. Yet, these JF data are becoming less than one at Re < 1500. Furthermore, in all cases, JF data of CPHEs with β = 60°/60° are greater than those with β = 30°/30°. Generally, JF data of the modified CPHEs are 1.1-1.5 fold lower than those of the conventional CPHEs. However, the convective heat transfer data (Colburn factor "j") of the modified CPHEs are the highest as shown in Fig. 4.9, and also their Nu data are reported the highest in [175].

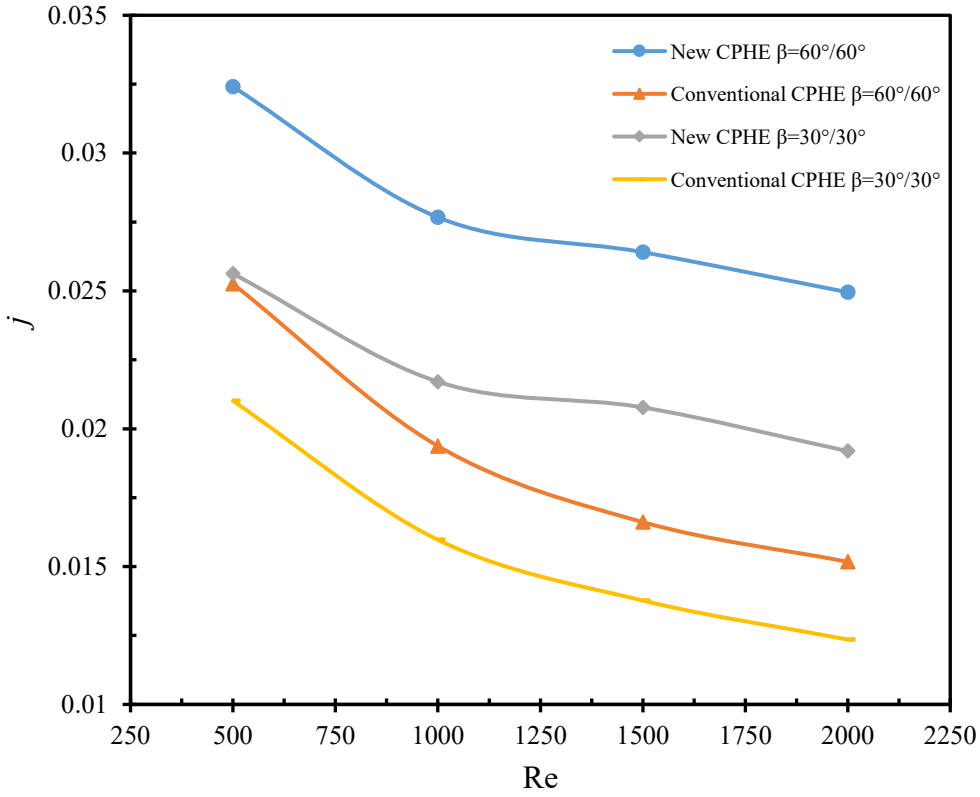

Fig. 4.9: Colburn data of the modified and the conventional CPHEs.

4.4.4 Uniformity of flow distribution from port to channel

There are several types of flow maldistribution that take place in CPHEs. All of them should be considered during the design process of the CPHE. In this study, port-to-channel fluid flow maldistribution (P_{mal}) is investigated. The equation that has been analytically modelled by Bassiouny and Martin [133, 152] is adopted to investigate P_{mal} of the CPHEs in this study. This equation is developed based on the balance between mass and momentum for flow element in inlet and exit ports. The flow distribution is to be considered fully uniform for P_{mal} = 0. Moreover, the flow distribution is to be

considered highly uniform for P_{mal} < 0.01. Generally, higher values of P_{mal} indicate lower flow distribution uniformity. The equation of P_{mal} is as follows:

$$P_{mal} = \left(\frac{NA_{\circ}}{A_p}\right)^2 \frac{d_e}{fL_p} \tag{4.10}$$

Where N, $A_{\circ}$, A_P, and L_p respectively represent the number of channels, cross-section area of the channel, port cross-section area, and effective plate length.

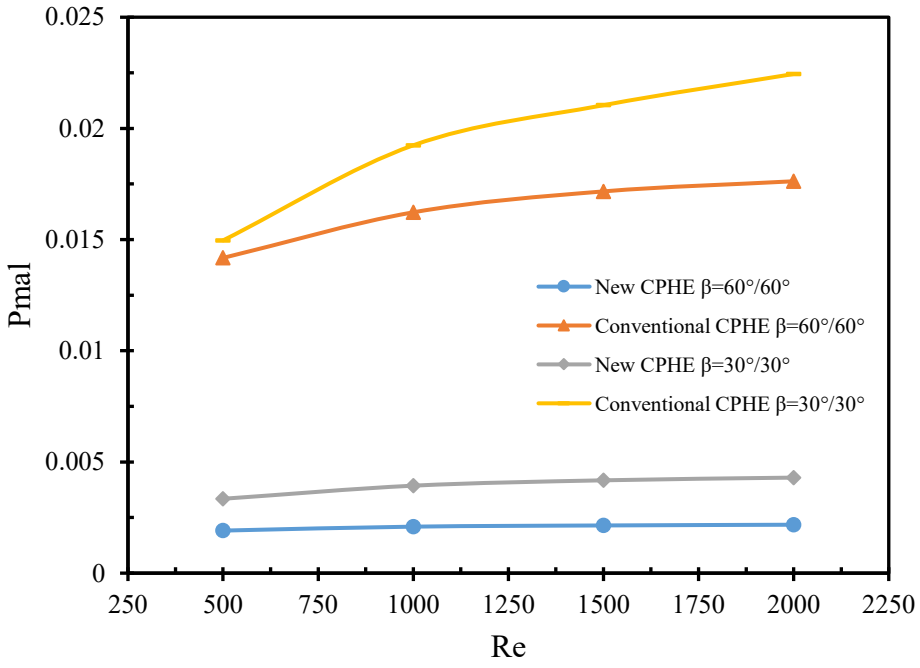

Fig. 4.10: Port maldistribution data of the modified and the conventional CPHEs.

From Fig. 4.10, the difference in P_{mal} values are very pronounced. The port maldistribution in case of the conventional CPHEs is significantly greater than that of the modified ones. In addition, the trends of the conventional CPHEs are increasing as mass flow rate (or Re) increases. On the other hand, the values of P_{mal} of the modified CPHEs are almost the same (i.e. P_{mal}~0.002-0.003) for all Reynolds numbers. In both modified and conventional CPHEs, the P_{mal} data are the lower in case of β = 60°/60°. It is noteworthy to highlight this, the P_{mal} represents one significant disadvantage of CPHE. Several parameters could affect P_{mal}. The number of thermal plates and the pass arrangement should be carefully considered in designing process because as they increase, the P_{mal} becomes more severe [181]. In addition, higher P_{mal} would inversely impact the effectiveness of the CPHE [174].

Each heat exchanger in this study (conventional and modified CPHE) has its own advantages and disadvantages. Most of the advantages of the newly modified CPHE has been disclosed [175] i.e. it yields significantly better convective heat transfer and effectiveness with respect to the conventional one. Therefore, this study is carried out to disclose the disadvantages of the newly modified CPHE. In general, the designers and the developers would now have a comprehensive understanding about the capabilities of the modified CPHE and the cost of these capabilities. Based on that, they can easily make their decision (i.e. based on the allowable pressure drop, available space etc.) as to when to utilize the modified CPHE.

4.4.5 Friction factor correlations

To develop *f* correlations, the common power-law approach is adopted.

$$\boldsymbol{f = CRe^{m}} \tag{4.11}$$

The *f* correlation of the conventional CPHE with β = 60°/60° is provided in Zahrani et al. [167]. For the present modified CPHEs with β = 60°/60°, β = 30°/30°, and for 500 ≤ Re ≤ 2000, the *f* correlations are respectively as follows:

$$f = 12.52Re^{-0.094} \tag{4.12}$$

$$f = 12.48Re^{-0.184} \tag{4.13}$$

For the conventional CPHE with β = 30°/30°, and for 500 ≤ Re ≤ 2000, the *f* correlation is as follows:

$$f = 5.47Re^{-0.2934} \tag{4.14}$$

For the modified CPHEs with β = 60°/60°, β = 30°/30°, and for the conventional CPHE with β = 30°/30°, the maximum deviations between the correlations and the quantitative data of *f* are respectively found < -2%, < -2.2%, and < -3.2%. That means these correlations could predict the fanning friction factor values with good accuracy.

4.5 Conclusions

The current study is carried out to reveal the thermal characteristics (i.e. flow resistance, and JF factor) of the novel CPHE that is proposed [175]. Steady-state numerical study is performed on two modified CPHEs with β = 60°/60°, β = 30°/30°, and

one conventional CPHE with β = 30°/30°. The concluding remarks can be drawn as:

- The data of core pressure drop of the modified CPHEs are significantly higher than those of the conventional ones. Core pressure drop of all HEs shows direct proportionality with the mass flux. However, the trends of core pressure drop in case of the conventional CPHEs are linearly increasing, while these trends show non-linear increment in case of the modified CPHEs.
- The f data of the modified CPHEs are 4.5 to 7 fold higher than those of the conventional CPHEs.
- Because at the same mass flow rate, the fluid flows with higher velocities inside the modified channels. The TKE of the modified channels is found ~ 2 to 3 times higher than those of the conventional ones.
- JF data of the modified CPHEs have been found 1.1 to 1.5 fold lower than those of the conventional CPHEs. The trend of JF data is decreasing as Re increases in case of the conventional CPHEs. Whereas they show direct proportionality with Re in case of the modified CPHEs. In addition, in both modified and conventional CPHEs, β = 60°/60° exhibites higher JF data than that of β = 30°/30°.
- The port maldistribution of conventional CPHEs is found to be up to eight times greater than that of the modified ones. In both modified and conventional CPHEs, the P_{mal} data are lower in case of β = 60°/60°.

Based on these findings, the cost of the high convective heat transfer of the modified CPHE is disclosed in particular. Moreover, in general the characteristics of fluid flow i.e. TKE, and P_{mal} for both conventional and modified HEs are also disclosed. Consequently, this study would ease the selection process between the conventional and the modified CPHEs for engineers. Finally, these modified CPHEs are likely to be most useful in applications where the available space of the HE is very limited and high pressure drop can be tolerated.

Chapter 5: Heat Transfer Enhancement Investigation in a Novel Flat Plate Heat Exchanger

Research Paper Three:

S. Al-Zahrani, M.S. Islam, S.C. Saha, Heat transfer enhancement investigation in a novel flat plate heat exchanger. International Journal of Thermal Sciences, 161 (2021) 106763.

International Journal of Thermal Sciences 161 (2021) 106763

Contents lists available at ScienceDirect

International Journal of Thermal Sciences

journal homepage: http://www.elsevier.com/locate/ijts

Heat transfer enhancement investigation in a novel flat plate heat exchanger

Salman Al zahrani [a,b], Mohammad S. Islam [a], Suvash C. Saha [a,*]

[a] School of Mechanical and Mechatronic Engineering, University of Technology Sydney, Ultimo, NSW, 2007, Australia
[b] Mechanical Engineering Department, Faculty of Engineering, Al Baha University, Saudi Arabia

ARTICLE INFO

Keywords:
Plate heat exchanger
Heat transfer
Enhancement
Nusselt number
Single-phase
Friction factor

ABSTRACT

Plate heat exchangers (PHEs) have become the most popular type of heat exchangers (HEs) for a wide range of daily applications due to their compactness and high thermal performance. The present study aims to expand the understanding of the thermal performance of the basic flat PHE (FPHE) and to develop a more efficient FPHE as well. A new flow arrangement is proposed in order to enhance the thermal performance of the FPHE (modified FPHE). The new flow mechanism is fulfilled by changing the design of the gasket where the inlet and the outlet ports are located on the same side of the thermal plate. Computational fluid dynamics (CFD) has been used to conduct the numerical simulations. The overall simulations have been performed on two FPHEs; the basic and the modified one. Both HEs have identical geometrical dimensions and physical test conditions. Nusselt number (*Nu*), Stanton number (St), Colburn factor j, friction factor (f), and JF factor are employed to evaluate and compare the thermal performance of the presented HEs. Heat transfer data are collected for single phase (water-water), and for Reynolds number (Re) spans from 250 to 2000. The numerical findings have been validated with benchmark experimental data from the literature. The results show that, *Nu* and f data of the modified FPHE are respectively up to 70% and 4.4 times those of the basic FPHE. The critical Reynolds numbers (Re_{cr}) for the modified FPHE are identified. Moreover, JF data of the modified FPHE shows ~0.7%–9% enhancement in the thermal performance with respect to the basic FPHE, hence it could save material and energy for the same heat duty. The findings of the present study have also developed the corresponding correlations for the *Nu* and f for all cases.

5.1 Abstract

Plate heat exchangers (PHEs) have become the most popular type of heat exchangers (HEs) for a wide range of daily applications due to their compactness and high thermal performance. The present study aims to expand the understanding of the thermal performance of the basic flat PHE (FPHE) and to develop a more efficient FPHE as well. A new flow arrangement is proposed in order to enhance the thermal performance of the FPHE (modified FPHE). The new flow mechanism is fulfilled by changing the design of the gasket where the inlet and the outlet ports are located on the same side of the thermal plate. Computational fluid dynamics (CFD) has been used to conduct the numerical simulations. The overall simulations have been performed on two FPHEs: the basic and the modified one. Both HEs have identical geometrical dimensions and physical test conditions. Nusselt number (Nu), Stanton number (St), Colburn factor j, friction factor (*f*), and JF factor are employed to evaluate and compare the thermal performance of the presented HEs. Heat transfer data are collected for single phase (water-water), and for Reynolds number (Re) spans from 250 to 2000. The numerical findings have been validated with benchmark experimental data from the literature. The results show that, Nu and *f* data of the modified FPHE are respectively up to 70% and 4.4 times those of the basic FPHE. The critical Reynolds numbers (Re_{cr}) for the modified FPHE are identified. Moreover, JF data of the modified FPHE shows ~ 0.7% to 9% enhancement in the thermal performance with respect to the basic FPHE, hence it could save material and energy for the same heat duty. The findings of the present study have also developed the corresponding correlations for the Nu and *f* for all cases.

Keywords: Plate heat exchanger; Heat transfer; Enhancement; Nusselt number; Single-phase, Friction factor.

5.2 Introduction

The Plate Heat Exchanger (PHE) was invented in the 1870s [1], yet the basic design has been retained to date. Although PHE was an advanced heat transfer device at that time, it was not commercially used until the late 1920s [2]. PHE consists of a number of series plates either welded or tightened by big bolts with a gasket between each two

consecutive plates. The thermo-hydraulic performance of PHE is high because of the small hydraulic diameter (h_d), and the large surface area where fluids flow on both surfaces of each plate, except the first and the end plates. The maximum allowable pressure was limited to 3 bar, and the maximum allowable temperature was less than 100 °C [2]. Due to these limitations, the PHE was initially limited for milk pasteurization application [150]. However, the PHE's extraordinary performance and compactness motivates more research to be conducted in order to overcome these limitations.In later years, the material technology of PHE has been significantly improved: the current operating pressure can reach up to 40 bar, and the temperature can range from -50 to 350 °C [17]. Nowadays, PHE is employed in pharmaceutical, power generation, dairy, paper/pulp, oil refining and many other applications.

Despite the high thermal performance of PHE, there is no database for the design of PHE. The reasons are, the complexity of PHE channel geometry, diversity of flow and pass arrangements, and the large number of geometrical and physical parameters that affect the performance of the PHE. However, several studies have been carried out to draw a guideline for PHE's design. A number of simplified methods [31-34] have been generated to calculate the required number of the plates. Graphical procedures for optimizing the passes' number and the channels' number per pass were conducted by Jarzebski and Wardas-Koziel [35]. A numerical study for counter current flow, and for a number of different passes arrangements was performed by Kandlikar and Shah. [29]. Their study investigated the impact of number of passes, and number of thermal plates on the number of transfer units (NTU), temperature effectiveness (P), and log mean temperature difference correction factor (F). Their study reports that, 1-1 pass arrangement provides the highest effectiveness for NTU > 5. However, in many industrial applications, multi passes are required due to the differences in the fluid heat capacities and to meet the required heat duty. In addition, similar studies with different approaches, such as experimental measurement [36], physically based mathematical model [37, 87, 182], theoretical based model [183, 184], and numerical data based [39, 40, 177] have been conducted to help the manufacturers and the designers of PHE to predict and analyse the performance of PHE.

Furthermore, an important task for the designer of the HE is to enhance its thermal performance. There are three techniques to fulfil this task; passive, active, and compound

one. Passive technique implies the usage of inserts in the flow passage, wire coils, twisted tapes, dimples, ribs, extended surfaces and many other methods. Active enhancement technique requires an external power input such as induced pulsation, jet impingement, spray, and surface vibration. In the compound technique, both passive and active techniques are employed. Generally, because the active technique requires energy input, and due to the complexity in the design, the passive technique is preferred [15]. Thus, several passive techniques have been proposed to be implemented on PHEs in the literature [94, 167, 168, 185-187]

Initially, a passive technique has been applied to the PHE; corrugations have been created on the surfaces of the plates of FPHE to get the well-known corrugated plate heat exchanger (CPHE). These corrugations increase the projected area, promote the turbulence, and minimize the fouling and stagnant areas. The angle between the corrugation and the main flow axis is known as chevron angle (β). The CPHE's performance is two to five times higher than that of FPHE. Several experimental and numerical studies have been conducted on the CPHE. Most of these studies have investigated the impact of different parameters on the thermal performance of the CPHE i.e. [86, 188-190]. However, there is a lack of studies of FPHE in the literature. Gut and Pinto [36] conducted an experimental measurement on FPHE to obtain the log mean temperature difference correction factor for different configurations. The performance of corrugated, asterisk, and flat PHEs was studied by Durmus et al [101]. Their findings showed the CPHE yields highest values for both the heat transfer rate and friction factor, and FPHE yields lowest values for both the heat transfer rate and the friction factor.

Basically, when heat transfer rate increases, the accompanied pumping power increases. Hence the main challenge is to enhance the heat transfer rate at the minimum pressure drop. The pressure drop in CPHE is 13 to 44 times higher than that of the FPHE [42]. Therefore, the objective of the present study is to introduce a new passive technique that may enhance the thermal performance of the FPHE at the minimum possible pressure drop. In order to quantitatively understand the impact of the modification on the thermo-hydraulic performance of the newly developed FPHE, the thermal performance of the basic FPHE has been numerically investigated by using ANSYS Fluent 19 along with the modified FPHE. For both basic and new FPHEs, Nu, St, and j are calculated to indicate the enhancement in the convective heat transfer rate, and the friction factor is calculated

as an indicator of the pressure drop. In addition, JF factor data are estimated to compare the overall thermal performance of both HEs. The current CAD FPHEs consist of four channels (five plates); two channels belong to the cold side, and the other two belong to the hot side. Both FPHEs have the same geometrical dimensions, and the same physical conditions. Additionally, the port effect is considered for both of them. The steady-state numerical simulations have been conducted on water-water as the working fluids, and for counter current flow arrangements. The cold water represents the utility fluid, and the hot water represents the product fluid. Therefore, the current investigation has been considered for the hot side.

5.3 The Prescription of the Enhancement Approach

The basic design of FPHE has not changed a lot since it was employed in the 1920s [1]. The present modification to the plates of FPHE has been already conducted on the corrugated plates [175], and it showed a significant improvement in the convective heat transfer of the CPHE. Since pressure drop inside the FPHE is much lower than that of the CPHE [191], performing modification to the FPHE could be very useful if the pressure drop is managed to be kept at minimum values. Therefore, this study investigates the impact of the present modification on the thermal performance of FPHE for the first time.

In the well-known flow mechanism of FPHE, the fluid enters from one port and exits from the port that locates on the opposite side to the inlet port either diagonally or vertically as shown in Fig. 5.1. However, in the new design approach, the fluid enters from one port and exits from the port that is located on the same side of the inlet port but from the second half of the plate. On the next plate, the fluid follows exactly the same flow pattern of the previous one but in the opposite direction with respect to the previous fluids (counter current); the same flow mechanism continues to the end plate of the FPHE as shown in Fig. 5.2(a).

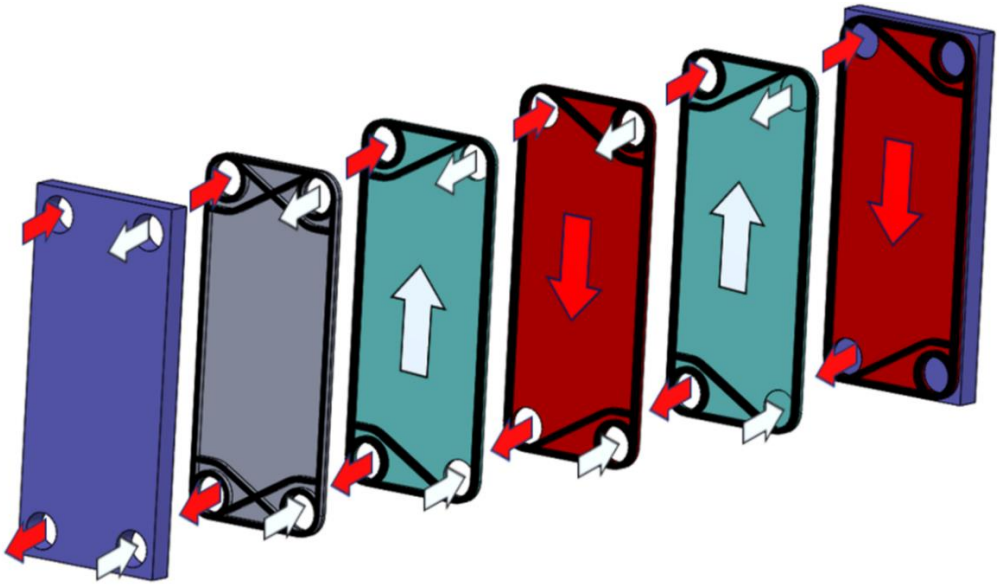

Fig. 5.1: Illustrative schematic for counter current flow mechanism of FPHE.

The new flow mechanism is fulfilled by changing the design of the gasket as shown in Fig. 5.2(b).

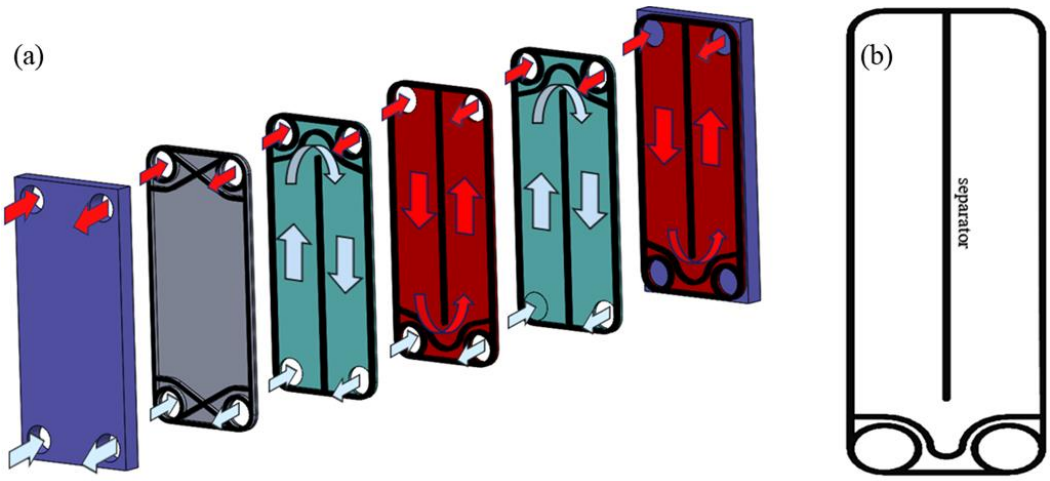

Fig. 5.2: Illustrative schematics for, (a) Counter current flow mechanism of the modified FPHE, and (b) The new gasket.

In the new gasket design, the peripheral of the ports on one side is opened to allow the fluid to enter and leave from these ports, and the peripherals of the ports that are located on the opposite side to the inlet one are closed. At the middle, the gasket "separator" expands from the inlet side and ends before the ports of the opposite side in order to allow the fluid to flow on the second half of the plate.

In the basic design, there is no control on the directions of the fluid over the surface of the plate, hence more fluid maldistribution may occur. However, in the present design, more degree of control on the directions of the fluid flow has been attained, hence lesser fluid maldistribution and higher heat recovery may be achieved compared with the basic FPHE.

5.4 Model Setup

5.4.1 Model's design and mesh generation

Two FPHEs have been created in Solidworks. One of them represents the well-known FPHE, and the other one represents the modified FPHE. Both FPHEs have identical geometrical dimensions. Each FPHE contains four channels divided alternatively and equally between the cold and the hot side, as shown in Fig. 5.1 and Fig. 5.2(a). In addition, the port effect is considered for all cases.

For both FPHEs, an automatic mesh method is used. In this method, both patch conformal method and sweep method are simultaneously enabled for the same geometry. For the present FPHEs, all the plates are sweepable and the fluid domain is a non-sweepable body due to the existence of the multiple edges (the inlet and the outlet ports). The sweepable bodies are automatically identified, and meshed with wedge and hexahedral elements. The sweep meshing technique produces a very stable mesh with a smaller number of nodes in comparison with other techniques, such as the free mesher [146]. Hence the required computational time is reduced. On the other hand, the non-sweepable bodies are meshed by the tetrahedron patch confirming method. In the lateral method, all details are captured, and the mesh element size growth rate is very smooth.

5.4.2 Data formulation

In the present study, Re is the same for cold and hot sides. The mass flow rate is calculated to meet the required Re as:

$$\dot{m} = \frac{\mathrm{Re}\ \mu\ A_{\circ}\ N}{d_e} \tag{5.1}$$

Since the hot side represents the product fluid, then Nu for the hot side is given as:

$$Nu = \frac{h_h d_e}{k} \tag{5.2}$$

The heat transfer coefficient for the hot side (h_h) is calculated from:

$$h_h = \frac{Q_{avg}}{A(T_{h,b} - T_{w,h})} \tag{5.3}$$

Q_c and Q_h should be equal to satisfy the energy balance. However, the difference between them has been always found within $\pm$ 3%. Therefore, Q_{avg} has been considered for all calculations as follows:

$$Q_c = \dot{m}_c c_{p,c}(T_{c,o} - T_{c,i}) \tag{5.4}$$

$$Q_h = \dot{m}_h c_{p,h}(T_{h,i} - T_{h,o}) \tag{5.5}$$

$$Q_{avg} = \frac{Q_c + Q_h}{2} \tag{5.6}$$

$T_{h,b}$ denotes the bulk temperature for the fluid of the hot side, and $T_{w,h}$ denotes the temperature of the plate's wall from the hot side.

The overall pressure drop (ΔP_m) through the FPHE is calculated as:

$$\Delta P_m = \Delta P_{port} + \Delta P_{core} + \Delta P_{elev.} \tag{5.7}$$

Because of the small length of the plate, ΔP_{elev} is ignored. The port losses are evaluated based on shah's empirical equation [176].

$$\Delta P_{port} = 1.5\left(\frac{\rho V^2{}_{port}}{2}\right) \tag{5.8}$$

Therefore, for the shear loss through the flat channels of the hot side, the fanning friction factor (f) is estimated as:

$$f = \frac{\rho d_e \Delta P_{core}}{2 L_P G^2} \tag{5.9}$$

Where G refers to the core mass velocity and is calculated as follows:

$$G = \frac{\dot{m}}{A_\circ N} \tag{5.10}$$

Note, the channel cross-sectional area $A_\circ$ in CPHE is usually calculated as:

$$A_\circ = L_w b \tag{5.11}$$

Where $b = d_e/2$, however, the depth in FPHE equals the hydraulic diameter, therefore $A_\circ$ in FPHE is calculated as:

$$A_\circ = L_w d_e \tag{5.12}$$

The fluid maldistribution from port to channel has been calculated. Bassiouny and Martin. [27, 28] carried out the first study to estimate the intensity of flow maldistribution from port to channel. Later on, different authors conducted similar studies; the formula is given by:

$$P_{mal} = \left(\frac{NA_\circ}{A_p}\right)^2 \frac{d_e}{fL_p} \tag{5.13}$$

Where N is the number of channels for the investigated fluid.

5.4.3 Mesh optimization, numerical model, and boundary conditions setup

A reliable numerical solution is a result of using a stable mesh and a proper boundary condition. A reliable result should reach steady solution and should be the same if additional iterations are applied. Because the modified FPHE is more complicated than the basic one, and to capture both the geometrical important details and boundary layers, the mesh of the modified FPHE is 17.6 times denser than the mesh of the basic FPHE. To ensure the mesh resolution is not affecting the result, a mesh independent test has been carried out for both FPHEs as shown in Table 5.1. A high-performance cluster with nodes consisting of 2.7 GHz, 18 cores, and 180 GB RAM is used.

Various numerical RANS models have been tested. Based on the results, the two equations' realizable $k - \varepsilon$ model with scalable wall function is adopted for this study. For both port sides of each FPHE, mass flow inlet is set as an inlet boundary condition. The cold water temperature is set to 18 °C, and the hot water temperature is set to 40 °C. Pressure outlet as outlet boundary condition with zero gauge pressure has been set for both FPHEs. The turbulence intensity is set to 5%. The plate's material for most studies of PHEs is stainless steel, hence stainless steel properties have been defined as the material of the present FPHEs. In addition, to prescribe the heat exchange between the surfaces of the plates and the fluids at the interface, conjugate heat transfer is defined along with the plate's thickness as $0.5\ mm$.

Table 5.1. Mesh dependency test of the present basic and modified FPHEs.

Basic FPHE			Modified FPHE		
Mesh elements (million)	Outlet cold average temperature (K)	Outlet hot average temperature (K)	Mesh elements (million)	Outlet cold average temperature (K)	Outlet hot average temperature (K)
0.6	291.99	311.3	14.5	292.4	310.2
1.1	**292.13**	**311.54**	**19.4**	**292.83**	**310.65**
2.2	292.14	311.54	23	292.82	310.65

5.4.4 Model validation and verification

There are two major kinds of numerical errors. First one is the linearization error, and the other one is the discretization error. Several methods have been adopted in the present study to check the level of these numerical errors. To assess the linearization error, the solution residuals have been monitored, and maximum solution residual is set to 10^{-5}. Also the conservation of mass has been checked for all cases, and it has been found very close to zero i.e. 10^{-7}. The energy balance has also been checked for all simulations, as mentioned earlier. For both FPHEs, refined meshes have been developed and their results are compared with the original ones to evaluate the discretization error. The results are found very close to each other, as presented in Table 5.1. Finally, to assure the stability of the solution, the results have been checked at different iterations and the same results have been found.

The findings of the present CFD study for the well-known FPHE has been validated with the available experimental data. The empirical data of Nu for the current CFD study is compared with the experimental studies. Fig. 5.3 shows that the CFD data are in good agreement with the experimental correlations. The findings of the CFD study have been compared with the experimental studies of Durmus et al. [101], Gut et al. [36], and Clark [1]. The numerical measurement of the present study shows a maximum of + 15%, + 8%, and + 1.93% deviation respectively with the studies of Durmus et al. [101], Gut et al. [36], and Clark [1].

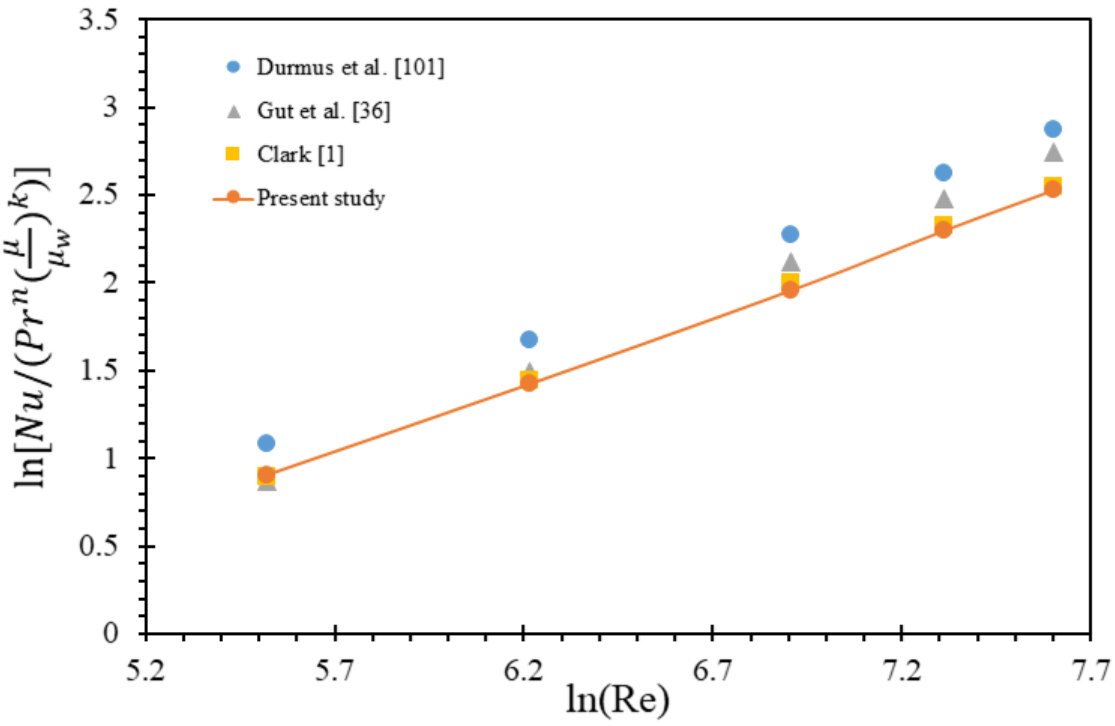

Fig. 5.3: Comparison of present Nu data with other data from literature.

In order to validate the present numerical approach for the calculations of the overall pressure drop (ΔP_m) through the FPHE, the numerical ΔP_m values of the present model have been tested against the experimental ΔP_m values conducted by Al-Zubaydi and Hong [192]. One CAD channel with identical geometrical dimensions to the experimental one has been created and tested numerically using the same physical conditions i.e. air as the working fluid. The FPHE that was experimentally tested in [192] contains 24 channels without inlet and outlet ports (air enters from the top side and leaves from the bottom side). Moreover, Al-Zubaydi and Hong [192] used an induced fan at the outlet side of their heat exchanger to ensure equal flow velocity inside each channel. Therefore, ΔP_m at the outlet of each channel is the same. The maximum deviation between numerical and experimental study is + 10% as shown in Fig. 5.4. An important reason for the deviation is probably due to the fluctuations of the amount of the sucked air at the outlet of the FPHE, along with the uncertainties.

Moreover, a laminar model is used to check the accuracy of the results of the used $k-\varepsilon$ model at very low velocities inside the channels of the basic FPHE. Three simulations at low velocities have been conducted by using a laminar model, and the results have been compared with those conducted by a $k-\varepsilon$ model, as shown in Table 5.2. The highest

solution residual is set to 10^{-5}, and all solutions have converged well. The deviations between the results of both models (laminar model is the baseline) are very small, as presented in Table 5.2, which verifies the validity of the used model in this study.

Table 5.2. Comparison between the results of laminar and realizable $k-\varepsilon$ models at low flow velocities for the basic FPHE.

Model	Velocity m/s	ΔP_m (Pa)	Deviation %	$T_{h,o}$	Deviation %	$T_{c,o}$	Deviation %
Laminar	0.0001	1.9	-	300	-	300.1	-
$k-\varepsilon$	0.0001	1.9	0	300	0	300	+0.033
Laminar	0.0003	1.9	-	299.9	-	300.3	-
$k-\varepsilon$	0.0003	1.88	-1	300	0.033%	300.1	-0.067
Laminar	0.0005	1.99	-	299.8	-	300.5	-
$k-\varepsilon$	0.0005	1.9	+ 4.5	300.1	0.1%	300.1	+ 0.13

Moreover, one case has been studied by using the laminar model to simulate flow characteristics for the modified FPHE at Re = 250. The results are compared with those of the k − ε model. The deviations between the results (laminar model is the baseline) are found insignificant, as shown in Table 5.3.

Table 5.3. Comparison between the results of laminar and realizable $k-\varepsilon$ models at Re = 250 for the modified FPHE.

Model	Re	ΔP_m (Pa)	Deviation %	$T_{h,o}$	Deviation %	$T_{c,o}$	Deviation %
Laminar	250	462	-	310.2	-	292.96	-
$k-\varepsilon$	250	459	+ 0.6	310.2	0	292.95	~0

5.5 Results and Discussions

A thorough thermal performance comparison between the newly modified and the basic FPHEs is conducted. All geometrical dimensions and physical test conditions are identical for both HEs. Each FPHE contains four channels divided alternatively and

equally between the cold and the hot side. The numerical tests are performed on a single phase (water-water). The data are calculated for the hot side of each FPHE. Re ranges from 250 to 2000.

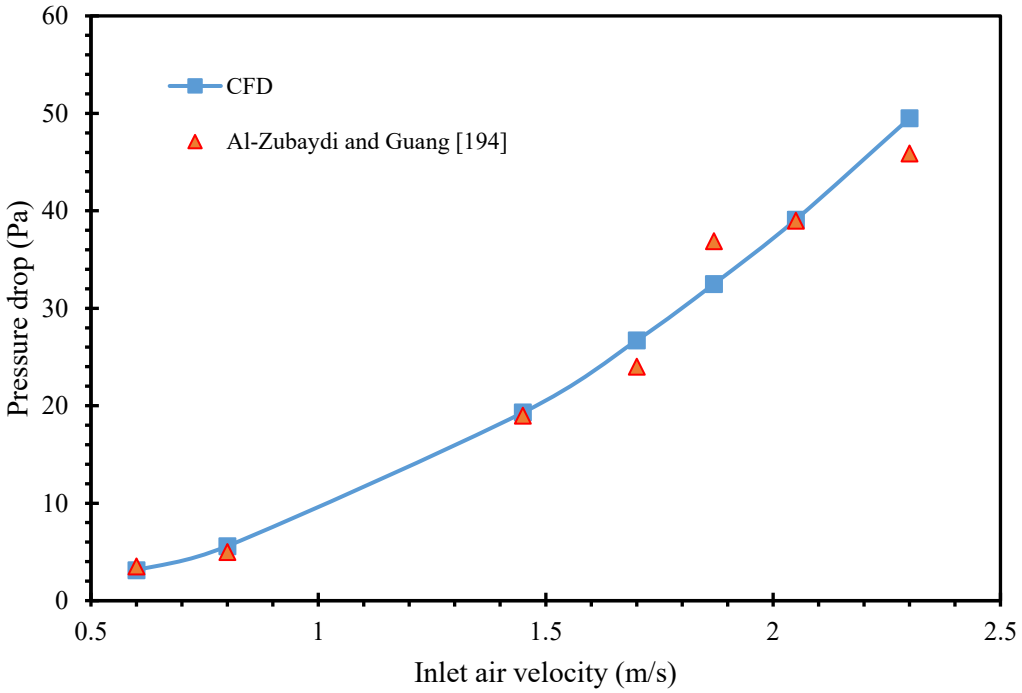

Fig. 5.4: Comparison of numerical pressure drop with experimental one.

5.5.1 Thermal performance evaluation

To understand the impact of the new design on the convective heat transfer, Nu and St have been calculated. Fig. 5.5(a) and (b) shows Nu and St data for the basic and the modified FPHE, respectively. The convective heat transfer rate is significantly higher inside the modified FPHE, and this convective heat transfer (Nu) is increasing as Re increases. In order to clarify the quantitative difference between the modified and the basic FPHE, the improvement (I) in Nu values is estimated and presented in Table 5.4. On the other hand, the amount of the heat transfer to the water to the specific heat of the water (St) is decreasing as Re increases.

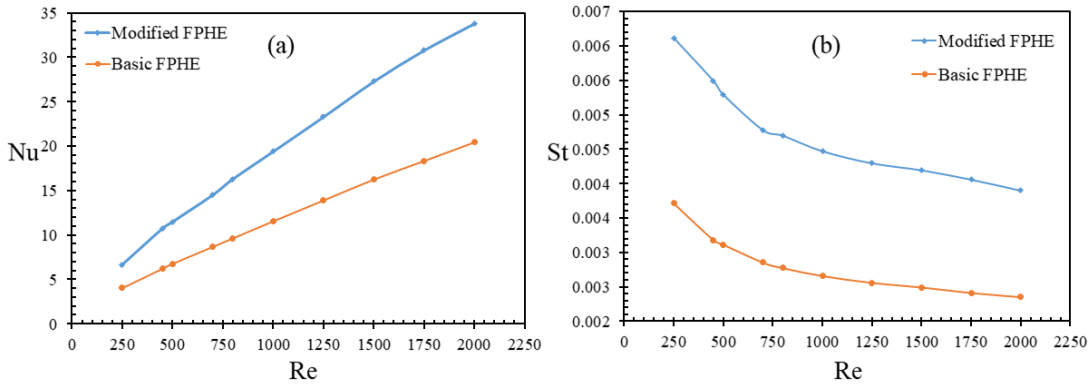

Fig. 5.5: (a) Nu data, and (b) St data versus Re for the modified and the basic FPHEs.

In addition, to comprehensively understand the difference in the overall thermal performance for both HEs, JF factor is considered. JF is calculated as follows:

$$JF = \frac{j}{(f)^{1/3}} \tag{5.14}$$

Fig. 5.6 shows JF data of the modified FPHE are higher than JF data of the basic FPHE in all cases. However, the highest improvement in JF values is about 9% and it takes place at very low Reynolds number i.e. Re = 250. After that, the differences between JF values of the modified and the basic FPHE are very small. Generally, the reason for the better thermal performance of the modified FPHE is related to the augmentation of the flow mixing, the disruption and the thermal boundary layer re-attachment, especially past the bend. Additionally, it could be noted each middle-gasket (the separator) is in full contact with the plate that is located in front of it, which would probably enhance the mechanical strength of the heat exchanger.

Furthermore, the nature of heat transfer and pressure drop are expressed in the form of Colburn factor j and fanning friction factor *f*. In all cases *f* and j data of the modified HE exhibit higher values than these of the basic HE, as presented in Fig. 5.7(a). The augmentation of pressure drop inside the modified FPHE takes place because when the surface of the plate is divided, it becomes narrower; consequently the flow velocity will increase, which in turn results in a greater friction factor. In addition, due to the existence of flow around the bend, secondary flow and vortices are formed past the bend as shown in Fig. 5.9(d), which could contribute to more heat transfer and pressure drop as well. The friction factor for the new FPHE is 3.4 to 4.4 times that of the basic FPHE. The

increase of friction factor values is expected due to the accompanied heat transfer enhancement, however these values are still much smaller than that of the CPHE, where its f is up to 44 times higher than that of the basic FPHE [193].

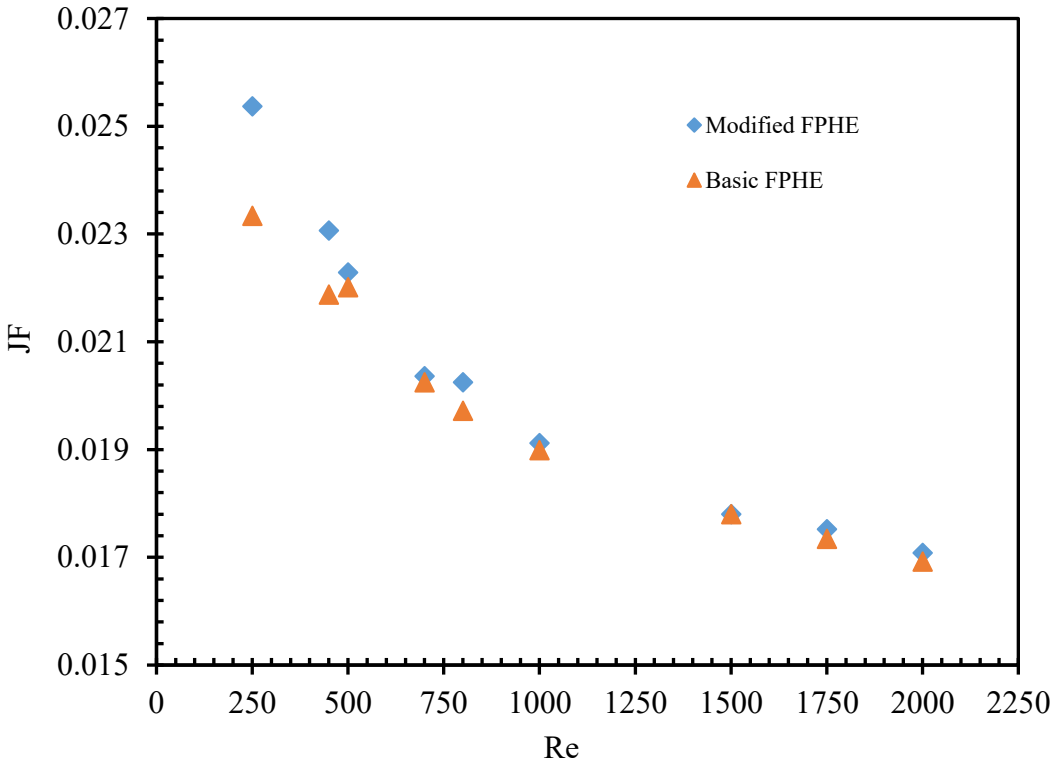

Fig. 5.6: JF data versus Re for the modified and the basic FPHEs.

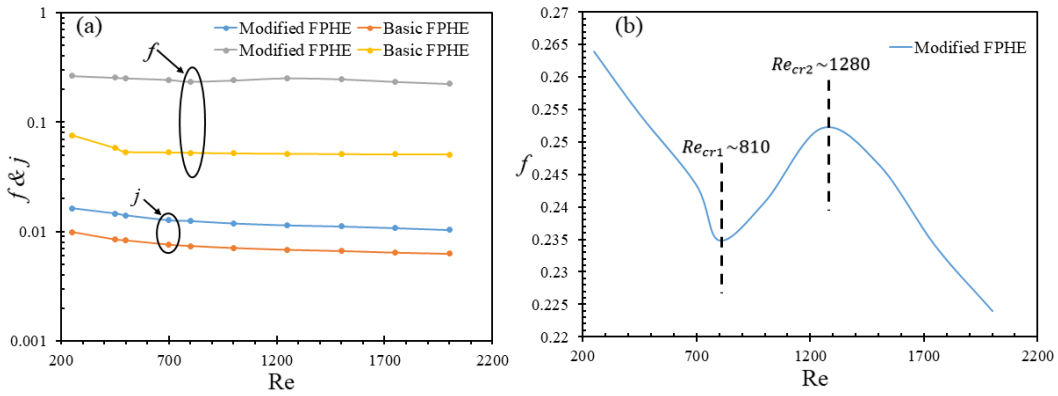

Fig. 5.7: (a) Variation of f and j data with Re for modified and basic FPHEs, and (b) f versus Re for the modified FPHE alone.

In order to explain the flow transition that takes place in the case of the modified FPHE, the friction factor data are plotted alone in Fig. 5.7(b). The flow is laminar for $\mathrm{Re} \leq \mathrm{Re_{cr1}}$ ($\mathrm{Re_{cr1}} \sim 810$). A combination of turbulent and laminar flow may exist in

the region where $\mathrm{Re_{cr1}} \leq \mathrm{Re} \leq \mathrm{Re_{cr2}}$. When Re is high, turbulent flow is achieved, and the concomitant friction factor data decrease with increase of Re. $\mathrm{Re_{cr2}}$ may represent the proper Re functioning as the onset point of the turbulence flow, as the same approach for defining the critical Re that has been identified in the open literature [194, 195].

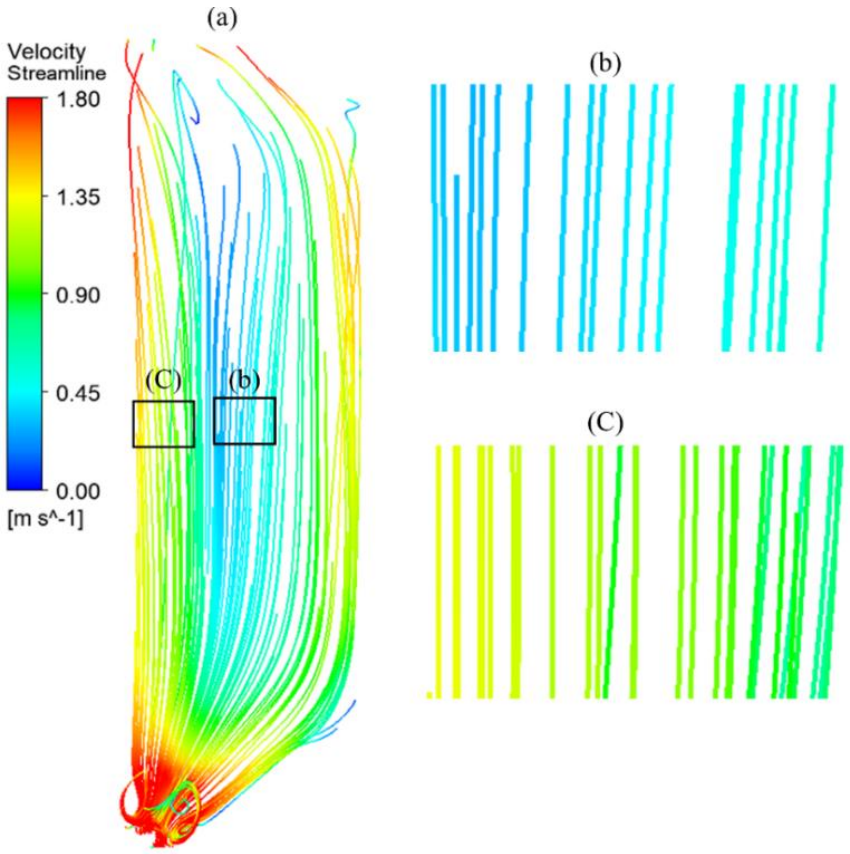

Fig. 5.8: Velocity streamlines of hot fluid inside the basic FPHE channel at Re=1500 for, (a) The whole channel, and magnified pictures of the velocity streamlines at, (b) The middle of the channel, and (c) The right sideway of the channel.

5.5.2 Estimation of fluid flow maldistribution

Fig. 5.8 shows that the fluid flows in adjacent layers (laminar) inside the basic FPHE. At the same Re, Fig. 5.9 shows the contrast where fluid layers agitatedly mix (disordered layers) past the bend of the plate inside the modified FPHE. As a result of the intense mixing of the turbulent boundary layers, swirl flow and large shear stress is formed on the wall. Therefore, the heat transfer rate is higher in the case of turbulent flow.

Table 5.4. Enhancement percentage of Nu data.

Re	Basic FPHE Nu	New FPHE Nu	I%
250	4.03	6.635	65%
500	6.761	11.5	70%
1000	11.546	19.4	68%
1500	16.24	27.3	68%
2000	20.42	33.831	65%

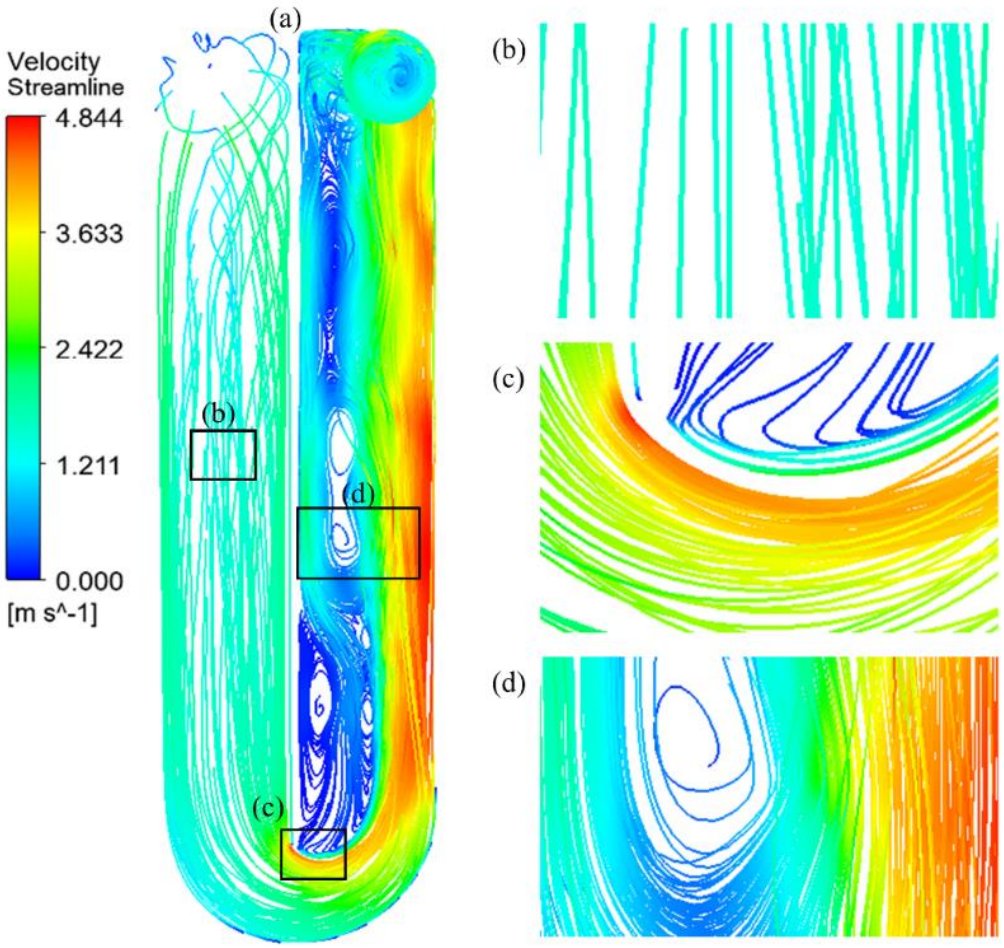

Fig. 5.9: Velocity streamlines of hot fluid inside the modified FPHE channel at Re=1500 for, (a) The whole channel, and magnified picture of the velocity streamlines at, (b) Before the bend, (c) At the bend, and (d) Past the bend.

Flow maldistribution intensity (P_{mal}) implies some parts of theheat transfer surface are not exploited perfectly. Hence, fluid flow misdistribution deteriorates the thermal performance of the HE [139]. The higher the P_{mal} through the PHE's channels, the more loss in heat transfer efficiency [196]. P_{mal} data have been calculated for the present basic and modified FPHEs.

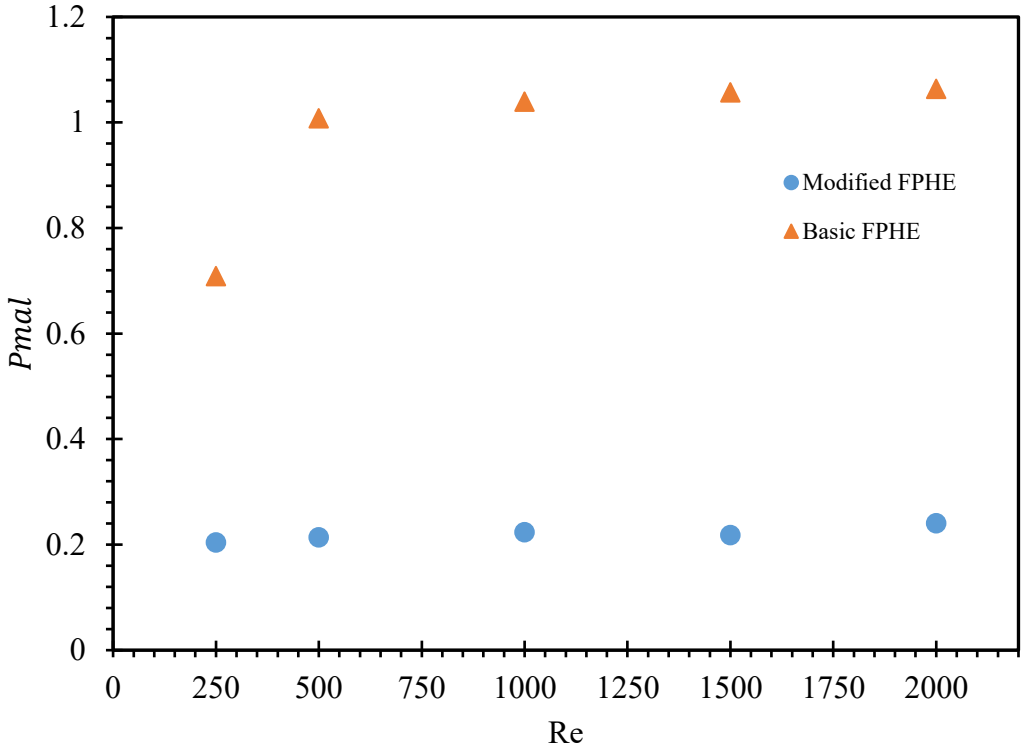

Fig. 5.10: Variation of flow maldistribution intensity versus Re.

Fig. 5.10 shows P_{mal} data for basic FPHE are much higher than those of the modified FPHE. Furthermore, P_{mal} data of the basic FPHE increase with the increase of Re, which is consistent with the findings of [67, 139, 174, 196]. However, in case of the modified FPHE, the variation in P_{mal} data with different Re is insignificant. Moreover, Fig. 5.8(a) shows the tendency of fluid to flow on the sideways of the plates. Similar flow pattern has been experimentally confirmed [141]. On the modified surface, Fig. 5.9(a) and (b) shows laminar flow behaviour on the left side (entrance side) of the plate's surface, however, the flow past the bend (second half of the plate) shows turbulence behaviour as presented in Fig. 5.9(c) and (d). In addition, the velocity of the fluid flow on the modified surface is more than twice the flow velocity on the well-known surface for the same mass flow rate. This is because the width of the modified plate is divided into two halves (the

geometrical modification promotes the status of the fluid flow causing vortices and increment in the fluid velocity).

5.5.3 Shear stress and temperature distribution

Fig. 5.11(a) and (b) present shear stress distribution on the edges of the plates of the modified and the basic hot channels, respectively. The flow inside the basic FPHE is laminar, hence there is no secondary flow. Therefore, the shear stress on the modified edges is about three times higher than that of the basic one. The maximum shear stress attains the edges of the modified plates past the bend on the sidway of the plate. At the bend, the fluid is directed radially outward due to the centrifugal force, as is clear in Fig. 5.9(a). Therefore, at area *x* on Fig. 5.11(a), the velocity and the shear stress attain the maximum values. Fig. 5.12(a) and (b) show temperature distribution at Re = 1500 at the middle hot channel in the modified and the basic FPHEs, respectively. The hot fluid inside the modified FPHE exchanges heat with the cold fluid at higher rate than that of the basic one. Therefore, higher heat recovery, and lesser material requirement could be achieved. In Fig. 5.12(a), the fluid temperature's decreasing rate on the right side is higher than that of the left side because the cold fluid on the adjacent following and preceding channels turns to turbulent flow on the right side past the bend (see Fig. 5.2(a)). In Fig. 5.12(b), the minimum temperature of the hot fluid attains at the right corner from the bottom because cold fluid enters from that direction on the following and the preceding channels (see Fig. 5.1).

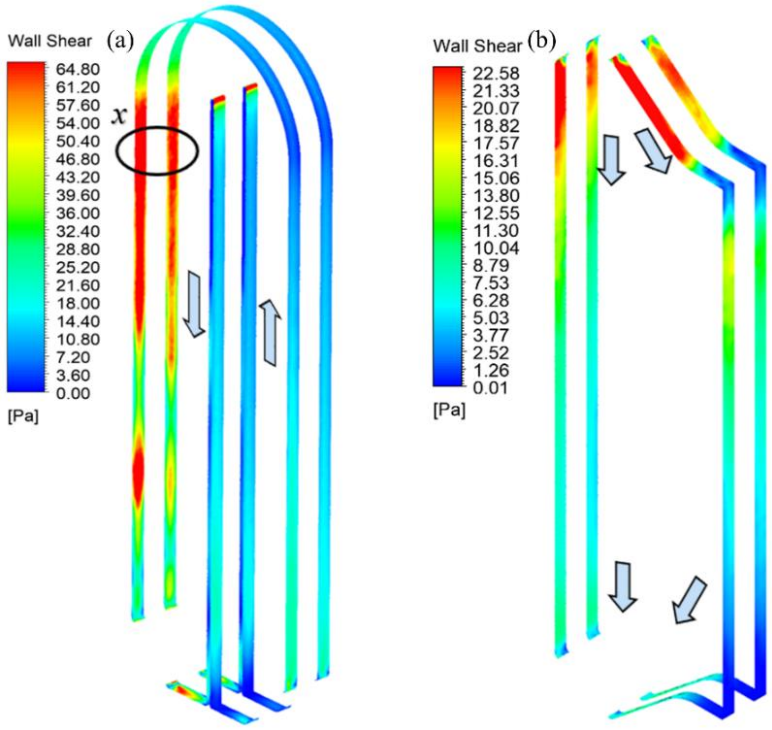

Fig. 5.11: Shear stress distribution at Re = 1500 inside the hot channels of, (a) The modified FPHE, and (b) The basic FPHE.

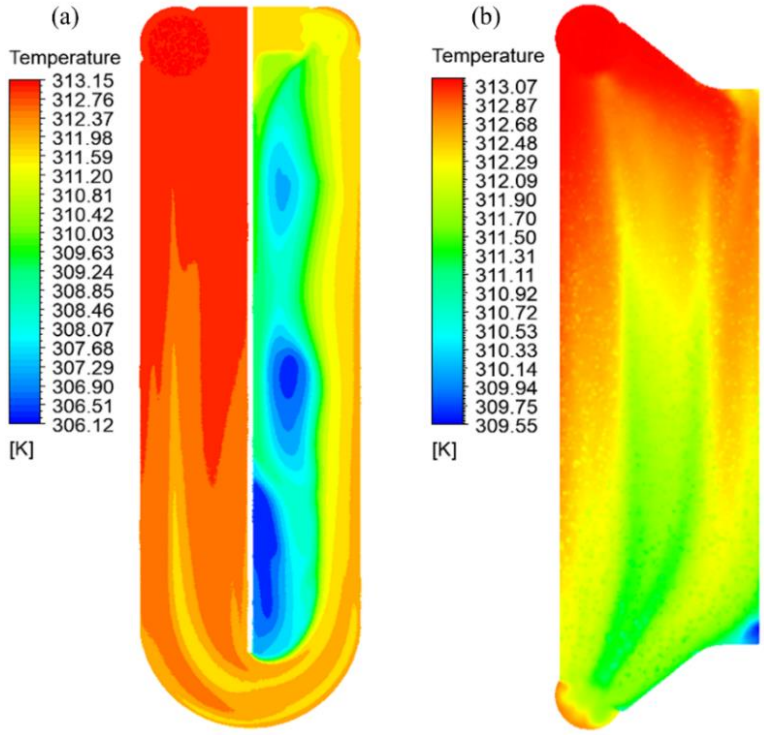

Fig. 5.12: Temperature distribution at Re = 1500 inside the hot channel of (a) The

modified FPHE, and (b) The basic FPHE.

5.5.4 Heat transfer correlations

Sieder empirical correlation (5.15) to estimate Nu has been adopted.

$$Nu = CRe^{p}Pr^{n}\left(\frac{\mu}{\mu_w}\right)^{0.14} \tag{5.15}$$

The constant values ($C, p,$ and n) are independent of the nature of the working fluid [46]. Linear regression analysis is used to find the values of C and p. Moreover, Zahrani et al. [47] examined different values of (n) for different fluids, and findings showed 1/3 granted the most accurate result. The present study introduces Nu and *f* for the present modified FPHE as follows:

For $250 \geq \text{Re} \geq 810$

$$Nu = 0.0617\ Re^{0.76}Pr^{1/3}\left(\frac{\mu}{\mu_w}\right)^{0.14} \tag{5.16}$$

$$f = 0.396\ Re^{-0.0742} \tag{5.17}$$

For $1280 \geq \text{Re} \geq 2000$

$$Nu = 0.0518\ Re^{0.79}Pr^{1/3}\left(\frac{\mu}{\mu_w}\right)^{0.14} \tag{5.18}$$

$$f = 1.6\ Re^{-0.26} \tag{5.19}$$

Nu and *f* for the basic FPHE are as follows:

For $250 \geq \text{Re} \geq 2000$

$$Nu = 0.0296\ Re^{0.7953}Pr^{1/3}\left(\frac{\mu}{\mu_w}\right)^{0.14} \tag{5.20}$$

$$f = 0.184\ Re^{-0.176} \tag{5.21}$$

5.6 Conclusions

The present study proposes a new modified FPHE. A numerical study of the modified and the basic FPHEs has been performed. A realizable $k-\varepsilon$ with scalable wall function has been adopted. The numerical data have been validated with the available limited

experimental data. Moreover, one case has been numerically studied by using the laminar model, and the results are found very close to those of $k-\varepsilon$ model. All simulations have been conducted for single phase (water-water), and for Re ranges from 250 up to 2000.

At the same flow rate, Nusselt number, Stanton number, and j factor of the modified HE are enhanced up to 70% in comparison with the same parameters of the basic HE. JF data of the newly modified HE are greater than those of the basic HE for all cases. However, the maximum enhancement of JF data is about 9% at $\mathrm{Re}=250$. Re is strongly affecting the heat transfer characteristics. Generally, Stanton number, j, and JF data decrease as Re increases, while Nusselt number increases as Re increases. In addition, the fanning friction factor of the modified HE is distinctively different from that of the basic HE. In the basic HE, the flow is always laminar for the present range of Re and the friction factor decreases with the increase of Re. In the modified HE, the friction factor decreases with the increase of Re and attain the minimum value at $\mathrm{Re}_{\mathrm{cr1}}\sim 810$. $\mathrm{Re}_{\mathrm{cr1}}$ could represent the onset of the transition flow. The friction factor rises in the transitional region and attains the maximum at $\mathrm{Re}_{\mathrm{cr2}}\sim 1280$ and then it decreases with the increases of Re. $\mathrm{Re}_{\mathrm{cr2}}$ could represent the beginning of the turbulent flow.

The velocity of the fluid flow on the modified surface is more than twice the flow velocity on the well-known surface for the same mass flow rate. Therefore, the turbulent flow could be achieved faster, which would result in swirl flow, and large shear could be formed on the walls of the plates. Moreover, due to the formation of the secondary flow past the bend inside the modified HE, shear stress is about three times higher than that of the basic HE. Friction factor data of the modified HE are about 3.4 to 4.4 greater than that of the basic HE. In addition, the port-to-channel flow maldistribution of the modified HE is much smaller than that of the basic HE. The numerical findings developed new correlations for Nu and *f* for the modified and the basic HEs.

Because *f* of the basic FPHE is small, the proposed modification to the surface of the flat plate could be very promising since the increase of *f* is still in an acceptable region. Additionally, the proposed modification provides more contact areas between each two consecutive plates from the middle, which could enhance the mechanical strength of the HE. Thus, this modification could be utilized to minimize the size of the heat exchanger and consequently reduce the material cost. However, further studies could be conducted to investigate how much size the modified HE could save, in comparison with the basic

HE for the same heat duty.

Chapter 6: Heat Transfer Augmentation in Retrofitted Corrugated Plate Heat Exchanger

Research Paper Four:

S. Al-Zahrani, M.S. Islam, S. C. Saha, Heat transfer augmentation in retrofitted corrugated plate heat exchanger, International Journal of Heat and Mass Transfer, 161 (2020) 120226.

International Journal of Heat and Mass Transfer 161 (2020) 120226

Contents lists available at ScienceDirect

International Journal of Heat and Mass Transfer

journal homepage: www.elsevier.com/locate/hmt

Heat transfer augmentation in retrofitted corrugated plate heat exchanger

Salman Al zahrani [a,b], Mohammad S. Islam [a], Suvash C. Saha [a,*]

[a] School of Mechanical and Mechatronic Engineering, University of Technology Sydney, Ultimo, New South Wales 2007, Australia
[b] Mechanical Engineering Department, Faculty of Engineering, Al baha University, Saudi Arabia

ARTICLE INFO

Article history:
Received 13 May 2020
Revised 27 June 2020
Accepted 20 July 2020

Keywords:
Plate heat exchanger
Chevron angle
Heat transfer
Enhancement
Nusselt number
Single-phase

ABSTRACT

Corrugated plate heat exchangers (CPHEs) have been extensively adopted especially for systems that require high thermal efficiencies such as aerospace and gas turbine power plants. According to several factors (i.e. required heat duty), CPHEs can be optimized to meet the application requirements. However, the number of the required thermal plates (N_p) could be very large (N_p>40) which in turn would cause several disadvantages (i.e. sever flow maldistribution). Therefore, the present study aims to introduce an innovative modification that can boost the thermal performance of the basic CPHE which in turn would reduce the number of required plates for the same heat duty. The thermal performance of the modified CPHE has been numerically investigated by using Computational Fluid dynamics (CFD) software. The numerical data have been validated with experimental measurement from the literature. The impact of the new modification has been studied on Nusselt number (Nu), fanning friction factor (*f*), Stanton number (St), Turbulence kinetic energy (TKE), flow maldistribution, j factor, and quality index factor (JF). The result has been compared with previously reported data of the basic corrugated and flat PHEs. At the same mass flow rate, Nu, *f*, and TKE of the modified CPHE are respectively 1.3, 1.7, and 3.5 times greater than those of the basic CPHE. Moreover, JF data of the modified CPHE are 1.4, and 64 times greater than those of the basic corrugated and flat PHEs, respectively. In addition to the superior thermal performance, the present modification offers larger contact area between the plates which could boost the overall mechanical integrity of the heat exchanger. Thus, this modification could pave the way for CPHEs to be incorporated in new applications that require more compact and durable HEs. The heat transfer correlations of the modified CPHE have been developed.

6.1 Abstract

Corrugated plate heat exchangers (CPHEs) have been extensively adopted especially for systems that require high thermal efficiencies, such as aerospace and gas turbine power plants. According to several factors (i.e. required heat duty), CPHEs can be optimized to meet the application requirements. However, the number of the required thermal plates (N_p) could be very large ($N_p > 40$), which in turn would cause several disadvantages (i.e. sever flow maldistribution). Therefore, the present study aims to introduce an innovative modification that can boost the thermal performance of the basic CPHE, which in turn would reduce the number of required plates for the same heat duty. The thermal performance of the modified CPHE has been numerically investigated by using Computational Fluid dynamics (CFD) software. The numerical data have been validated with experimental measurements from the literature. The impact of the new modification has been studied on Nusselt number (Nu), fanning friction factor (*f*), Stanton number (St), Turbulence kinetic energy (TKE), flow maldistribution, j factor, and quality index factor (JF). The result has been compared with previously reported data of the basic corrugated and flat PHEs. At the same mass flow rate, Nu, *f*, and TKE of the modified CPHE are respectively 1.3, 1.7, and 3.5 times greater than those of the basic CPHE. Moreover, JF data of the modified CPHE are 1.4 times those of the basic CPHE. In addition to the superior thermal performance, the present modification offers larger contact area between the plates, which could boost the overall mechanical integrity of the heat exchanger. Thus, this modification could pave the way for CPHEs to be incorporated in new applications that require more compact and durable HEs. The heat transfer correlations of the modified CPHE have been developed.

Keywords: Plate heat exchanger; Chevron angle; Heat transfer; Enhancement; Nusselt number; Single-phase.

6.2 Introduction

The continuous global demand on energy represents a driving force to develop a new generation of the compact heat exchangers (CHEs). In the next two decades, the global demand on energy is expected to increase by 37% [16]. CPHE is the most common type of CHE, which was introduced in the 1920s and it was mainly used for milk pasteurization. Firstly, CPHE was made from cast metal plates stacked inside a frame.

The temperature and pressure limitations were the main disadvantages for PHE to be used in more aggressive applications i.e. acid coolers. However, the advancement in the material technology allows CPHE to be used for higher pressure and temperature applications [197]. Although the thermal performance of CPHE is extraordinary, the air conditioning and refrigerant companies could not adopt this technology immediately because of the use of the gaskets for sealing [14]. However, welded PHE has been introduced to eliminate the gaskets' use. Nowadays, welded CPHEs are used for heating, ventilation, and air conditioning systems (HVAC) and ammonia cooling units [14]. In addition to the high thermal efficiency of CPHE, its weight and volume are respectively 20% and 30% compared to shell and tube heat exchanger for the same heat transfer area [23].

Also, for the same thermal performance, the volume of CPHE is 50% and 60% less than finned tube and serpentine HEs [22], respectively. Therefore, CPHE has been widely spread out for chemical processing, pharmaceutical, polymers, industrial and many other applications.

Fluid flow visualization is highly important in order to reveal flow pattern, transition and turbulence onset points, stagnation areas etc. Fluid flow visualization inside CPHE has been conducted by Fock and Knibbe [154]. A spiral flow was observed on the corrugations of each wall. Furthermore, the visual inspection inside the corrugated channel that has been carried out by Tokgoz and Sahin [198] has reported that the sharp corners are the main source for turbulence generation. Lozano et al. [141] have both experimentally and numerically investigated the fluid flow pattern for oil-water inside the channels of CPHE. The planar laser-induced fluorescent (PLIF), and the particle image velocimetry (PIV) are employed to visualize the flow structure and the flow velocity respectively. The numerical and experimental results were consistent and they showed that the flow is not uniform for both oil and water and it tends to flow along the lateral sides of the plates. The flow distribution and pressure drop inside two channels of CPHE were studied numerically by Tsai et al. [142]. The port effect was considered, and the fluid maldistribution formula that is proposed by Bssiouny and Martin [28] was adopted. However, the friction factor was used instead of the channel frictional coefficient (ζ_c) that is used in the genuine formula of Bssiouny and Martin [28]. An experimental study on the flow maldistribution was performed by Rao et al. [139]. The flow maldistribution

was found to be affected by the flow rate, the port size, and the number of channels. An important finding is that the number of the plates should be carefully calculated, because at a certain point it will only cause a significant pressure drop rather than increasing the heat transfer area [139].

A comparison between different types of plate was carried out by Durmus et al. [101]. The chevron plate type is found to provide the highest heat transfer rate and pressure drop among the other types. Lin and Huang [119] have characterized the heat transfer performance of CPHE by deriving dimensionless correlations using the Buckingham Pi theorem. The results show that both mean and local Nu are greatly affected by Reynolds number (Re) and inclination angle "β". The basic features of the chevron plate are presented in Fig. 6.1. Fock et al. [50] investigated the effect of different $\beta's$ on heat transfer and pressure drop. The result showed that β is the most important factor that strongly affects the heat transfer process. The reason is that β changes the flow direction and consequently the performance of the CPHE. According to the same study, the maximum heat transfer rate occurred at $\beta = 80°$. Similar experimental studies have been carried out to further investigate the effect of chevron angle on the thermo-hydraulic performance of the CPHE [107, 199]. However, there is a significant variation between the results of the heat transfer correlations that have been provided by different researchers [46, 50]. As CPHE consists of consecutive plates, where each plate is rotated by 180° with respect to the adjacent plate, this forms a complicated 3-D criss-cross channel. Thus, each channel is made up from many geometrical parameters such as the corrugation depth, pitch, and roundness. Hence, different geometrical dimensions could contribute to the deviation between the previous studies [151].

Several techniques have been adopted by researchers in order to improve the thermal performance of the HEs. Gurel et al. [168] have applied the human lung pattern on the surfaces of the plates of the FPHE. They reported this design could enhance the heat transfer by about 71.3%. Modified design of the corrugated and the flat PHEs have been proposed by Zahrani et al. [175, 200]. The findings show the convective heat transfer has been enhanced by ~75% and ~70% for corrugated and flat PHEs, respectively. Aliabadi et al. [201] have studied the quality of different passive techniques. They have found that the winged wavy plates could provide the best thermal performance in comparison to other types of wavy plates i.e. perforated ones. In addition, several studies [202-205] have

investigated the impact of adding various types of nanofluids (i.e. metal oxide nanofluids copper–water nanofluid, and carbon–water nanofluid) to the base fluid to improve the thermal performance of the CPHE. Generally, the findings show similar trends where the heat transfer rate increases when they add nanofluids. However, the pressure drop is also increasing. Moreover, energy saving is an intrinsic aspect to be considered along with the operational and maintenance cost of the HE. Therefore, exergy loss analysis studies are necessary. Pandey and Nema [206] investigated the exergy loss of the CPHE with sinusoidal and rectangular corrugations' profiles. The results show that less exergy loss and better contact between solid and fluid are achieved in case of sinusoidal profile. Similar findings have been found by Ipek et al. [207] when they investigated exergy loss for different corrugations' profiles. Arsenyeva et al. [208] developed a mathematical model to be used to optimize the shape of the corrugation. Furthermore, Lee et al. [209] optimized the heat transfer area of the water side of the CPHE that was implemented in the low temperature heat pump system. An efficiency index for energy consumption of CPHE is proposed by Zhang et al. [210]. The formula of the efficiency index is proposed based on the single-phase heat transfer data of 281 CPHEs.

Several items of software have been developed to predict the behavior of the fluid flow and/or to resolve the boundary layers at the area of interest. CFD has been adopted to numerically predict different types of complicated phenomena i.e. air flow over wing. Two approaches have been used to simulate fluid flow and heat transfer inside the CPHE: unitary cell and full-scale CPHE. A representative computational cell or a unitary cell is the smallest segment of the corrugated channel. To save a significant amount of the computational cost, several studies considered the periodicity of the heat transfer and the fluid flow pattern inside the channels of the CPHE by adopting the unitary cell approach [193, 211]. However, the validity of this approach is still questionable. Because there are various parameters that could affect the performance of CPHE, these parameters are not included in the unitary cell approach such as the port effect and the flow maldistribution on the plate's surface. Numerical study for the performance of the full-scale CPHE is carried out by Zahrani et al. [47]. Air and water as the process fluids have been investigated to explore the impact of Prandtl number (Pr) on the pressure drop and the heat transfer process.

Nowadays, the heat transfer enhancement is an essential target in order to reduce both

the overall volume of the heat exchanger and the fuel consumption. The active technique requires an external input power such as surface vibration and jet impingement. On the other hand, the passive technique can be achieved either by using inserts such as twisted tape, or by performing a geometrical modification to the flow passage that could either enhance the flow mixing or reduce the pressure drop. Furthermore, the active technique is complicated in design, and hence the passive technique is the preferred one [15]. In PHEs, generally, the large number of thermal plates (N > 40) would lead to two significant disadvantages [29]. These disadvantages are: severe flow maldistribution is more likely to take place, and the increase in overall heat transfer coefficient is negligible. In addition, the space for the HE to be installed will be larger and the cost of the HE will be higher. Therefore, the present study aims to present a new passive technique that could simultaneously boost the thermo-hydraulic performance and the mechanical strength of the current well-known CPHE. Consequently, the number of the required thermal plates for the same heat duty would be less, which in turn would save materials and mitigate the flow maldistribution. This modification has been applied on the surface of each thermal plate of the CPHE. Furthermore, the present modification could be implemented in any PHE without affecting the flow arrangements.

The effect of the present modification has been studied numerically. The results have been compared with the previously reported results of the basic corrugated [175] and flat [200] PHEs. For all three HEs, the geometrical dimensions, the physical properties, and the boundary conditions are identical. To attain a reliable result, the inlet/outlet ports, and the sinusoidal shape of the corrugations are considered in the numerical model. Each HE of the present PHEs comprises of four channels divided equally between the cold and the hot fluid. The numerical simulations have used single-phase water/water as the working fluids, U-type counter-current flow arrangement, $250 \leq Re \leq 2500$ and $\beta = 60°/60°$. Nusselt number, Stanton number, j factor, fanning friction factor, flow maldistribution intensity index, and JF factor are calculated to assess the thermal performance for each HE.

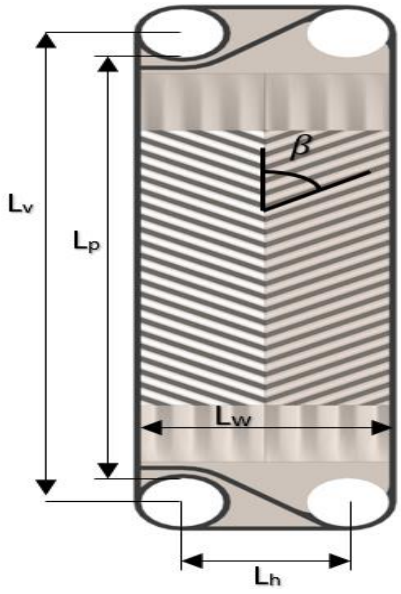

Fig. 6.1: Basic geometrical features of chevron plate.

6.3 Description of the New Modification PHE.

CPHE is compact in nature, yet the present study suggests a new passive technique that would allow the CPHE to be even more compact. The flow in the well-known CPHE is either vertical or diagonal. However, the new CPHE can be employed for both vertical and diagonal flow. In addition, the flow arrangement used in this study is U-type counter-current flow. Yet, the new CPHE can also be employed in any flow arrangement e.g., Z-type, and parallel flow arrangement.

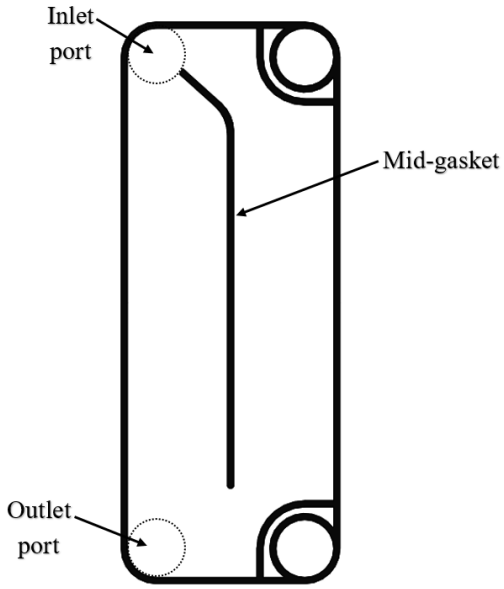

Fig. 6.2: The new gasket design.

A gasket is a mechanical seal, and mostly it is desirable to be made from materials that have the ability to deform and tightly seal the space between two or more mating surfaces. In the well-known CPHE, the gasket is compressed 25% of its original thickness to seal the space (the channel) between each two consecutive plates [130]. Furthermore, the gasket regulates the fluid flow inside the channels of CPHE. In the new CPHE, the gasket is also used for the same objectives, but there is an additional gasket (mid-gasket) that starts from the corner of the inlet port from the middle side of the plate and ends right before the outlet port as shown in Fig. 6.2. As fluid enters from the inlet port, it gets separated between the two sides of the plate, then all fluids mix at the end of the middle gasket and exit from the outlet port. Simultaneously, on the adjacent plate, the other fluid follows the same flowing mechanism but in the opposite direction (counter-current) as shown in Fig. 6.3.

Fig. 6.3: Schematic of flow mechanism inside the modified CPHE.

6.4 Numerical Approach

6.4.1 Governing equations and turbulence model

For numerical simulations, pressure-velocity coupling with the SIMPLE algorithm have been adopted. For pressure, momentum, and energy, second order discretization is used. For turbulent kinetic energy, and turbulent dissipation rate, first order discretization

is used. ANSYS Fluent employs the finite volume method (FVM). By this method, the partial differential equations (PDEs) are presented in the form of algebraic equations.

In order to calculate the changes in the physical and chemical properties of the fluid, ANSYS Fluent solves all the governing equations. Navier Stokes equation (NS) (6.1) characterizes the fluid's motion.

$$\frac{\partial}{\partial x_j}\left(\rho u_i u_j\right) = -\frac{\partial p}{\partial x_i} + \frac{\partial}{\partial x_j}\left[(\mu + \mu_t)\frac{\partial u_i}{\partial x_j}\right] \tag{6.1}$$

The left-hand side of NS represents the acceleration of the fluid, while the right-hand side represents the pressure and viscous forces that act on the fluid. An analytical solution may exist for special cases i.e. linear PDEs, or imposing simplified assumptions. Complicated flow problems have no analytical solution yet. However, CFD has the capabilities to numerically solve NS along with all other governing equations at each grid point in milliseconds until the solution gets converged.

For the fluid's flow, the mass of the fluid is always conserved regardless of the complexity of the channel or the flow direction. This fundamental principle is known as continuity of the flow. NS equations are always solved along with the continuity equation (6.2).

$$\frac{\partial}{\partial x_i}(\rho u_i) = 0 \tag{6.2}$$

In addition, Fluent solves the energy equation (6.3) in order to resolve the heat transfer that occurs inside the heat exchanger.

$$\rho C_p \frac{\partial}{\partial x_j}\left(u_j T\right) = k_{eff}\frac{\partial^2 T}{\partial x_j^2} + (T_{ij})_{eff}\frac{\partial u_i}{\partial x_j} \tag{6.3}$$

All the numerical models (i.e. LES, DES, standard $k-\varepsilon$, and SST $k-\omega$) that are incorporated in the Fluent solver have been tested in Zahrani et al. [175]. A realizable $k-\varepsilon$ with scalable wall function has been found the most accurate model. Thus, it is employed for the current investigation. More details about the turbulence model, and the transport equations, are provided in Zahrani et al. [175].

6.4.2 Model Setup

The model has been generated by using Solidworks. The basic CPHE is the same one that was studied in Zahrani et al. [175]. The chevron angle is chosen as $60°/60°$ for both models. Furthermore, the geometrical dimensions are identical for both models. Each CPHE consists of four channels that are divided equally between the cold and the hot sides. The sinusoidal shapes have been created to construct the corrugations. Moreover, ports of the inlet and the outlet of both cold and hot sides will affect the flow distribution [174] inside the channels of the CPHE. Consequently, this would affect the pressure drop and the overall heat transfer process. Thus, the effect of the ports are considered in this study.

ANSYS meshing module is adopted for grid creation. A good mesh's metric qualities are difficult to be achieved for corrugated PHEs due to the existence of a large number of curved narrow passages. Thus, unstructured tetrahedral mesh elements are used, as they are dedicated for complicated geometries where they can provide a good mesh quality easier than hexahedral elements [146]. The transition of tetrahedral elements from small mesh size in the narrow passage and holes to larger size elsewhere is smoother and problem-free in comparison with hexahedral elements. However, the hexahedral produces fewer elements and consequently a faster solution. More efficient hexahedral mesh is achieved when the structured mesh is aligned to the physics [146]. Furthermore, to ensure the result is not affected by the grid's resolution, a grid sensitivity test has been performed as presented in Table 6.1 for the new corrugated PHE.

All simulations have been carried out for steady-state flow. The physical conditions are identical for both CPHEs. The plate's material is stainless steel. The cold and the hot sides have the same Reynolds number. Mass flow inlet is set at the inlet ports as the inlet boundary condition. The pressure at the outlet of the ports is set to be equal to the atmospheric pressure (zero gauge pressure) as the outlet boundary condition to prevent the occurrence of the reverse flow. An effective design of modern heat exchanger requires an efficient heat transfer in fluids and solids [212]. Usually, fluids carry energy and solids are needed to allow the heat transfer to take place between the fluids without being mixed. Therefore, a conjugate heat transfer is set for both CPHEs with plate thickness equal to 0.5 mm.

In the current investigation, the hot side is considered as the process fluid, therefore, all calculations are performed on the hot side.

Table 6.1. Mesh sensitivity test of the modified CPHE.

Grid's element (Million)	$T_{c,o}$	$T_{h,o}$	f
40	296.44	304.82	1.52
53	296.44	304.61	1.46
60.5	296.5	304.64	1.47

6.5 Results and Discussion

6.5.1 Numerical approach validation

To validate the thermal performance of the present CPHEs, non-dimensional standards parameters are adopted. Nu and *f* have been calculated and compared with other Nu and *f* data from the literature.

Although the differences in the geometrical parameters and physical conditions (e.g. corrugation's depth, wavelength, fluid viscosity, and density) could attribute in the deviation between the results, the present Nu data for the basic CPHE with $\beta = 60°/60°$ have been extensively validated in Zahrani et al. [175].

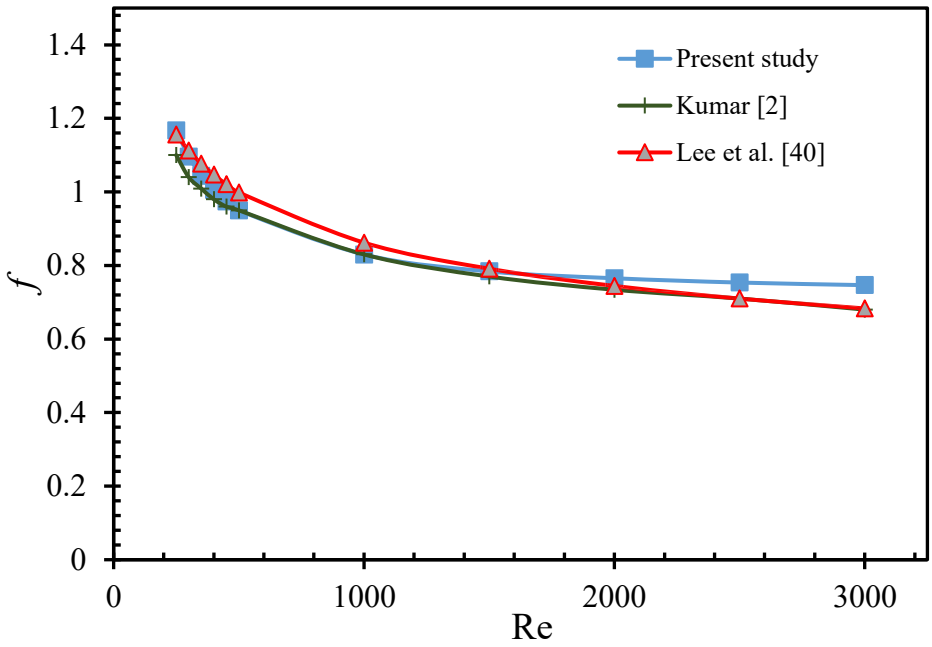

Fig. 6.4: Numerical versus experimental data of friction factor.

The numerical data of *f* for the basic CPHE with $\beta = 60°/60°$ are validated with the experimental correlation of Lee et al. [40], and Kumar [2]. The *f's* experimental correlation of Lee et al [40] is presented in Eq. (6.4) as follows:

$$f = 3.7235\, Re^{-0.2118} \tag{6.4}$$

Fig. 6.4 shows that the present numerical *f* data are in good agreement with other *f* data from the literature. The enhancement of flow velocity results in the reduction of all the trends. The maximum deviation is + 9.2%, and + 9.3% with respect to the *f* data of Lee et al [40], and Kumar [2], respectively. The variation could be attributed to the difference in the geometrical dimensions (i.e. corrugation aspect ratio, and enlargement factor) where small difference could cause high variation in heat transfer and friction factor data [151].

6.5.2 Thermal performance evaluation

In the present study, a new modification to the design of the plates' surfaces is presented. The impact of this modification on the thermal performance of the CPHE has been numerically investigated. The result has been compared with the previous studies of the basic corrugated and the flat PHEs [175, 213]. Fig. 6.5 illustrates the difference among

the modified, basic, and smooth thermal plates. Hot and cold water are considered to be the working fluids.

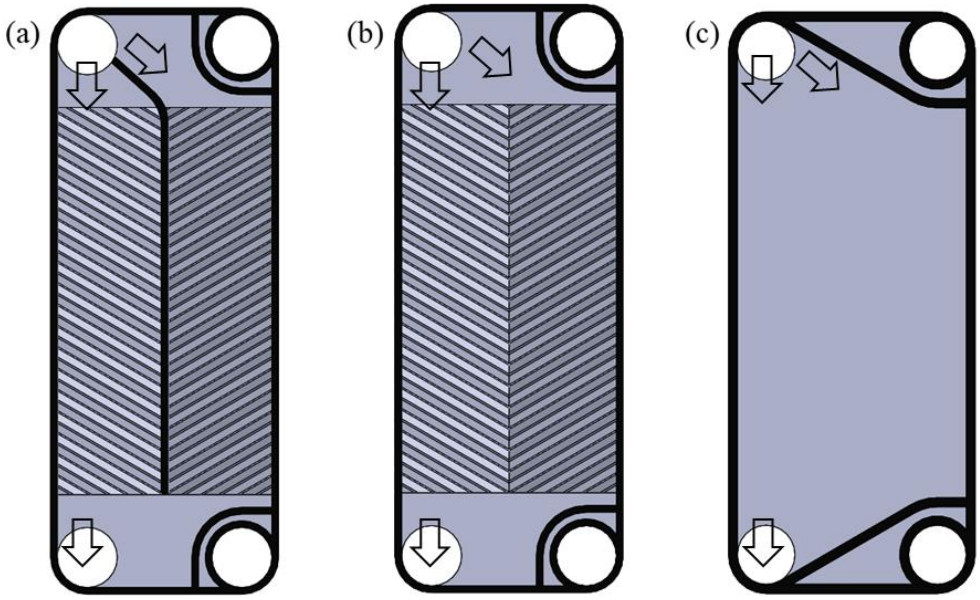

Fig. 6.5: Thermal plate of (a) Modified CPHE, (b) Basic CPHE, and (c) Smooth FPHE.

All calculations are performed to the hot side as the process fluid. Although, the geometrical and physical conditions of all studies are identical, dimensionless physical quantities are estimated in order to provide the most accurate data that are independent of the geometrical dimensions. Nu data with different Re are presented in Fig. 6.6. Nu data of the newly modified CPHE are found to be the highest. The enhancement in the convective heat transfer is up to 1.3 and 4 times greater than that of the basic corrugated and smooth PHEs, respectively.

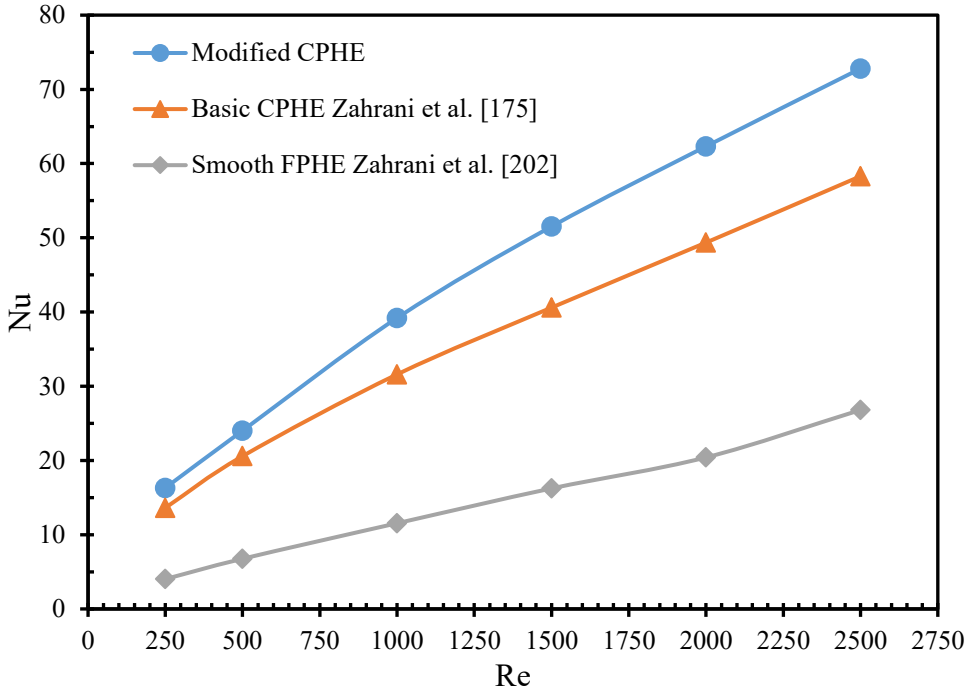

Fig. 6.6: Nu data versus Re for all investigated HEs.

In addition, in all cases Nu increases as Re increases because of the increase of mass flow rate ($\dot{m}$) where more $\dot{m}$ will lead to higher heat transfer coefficient (h).

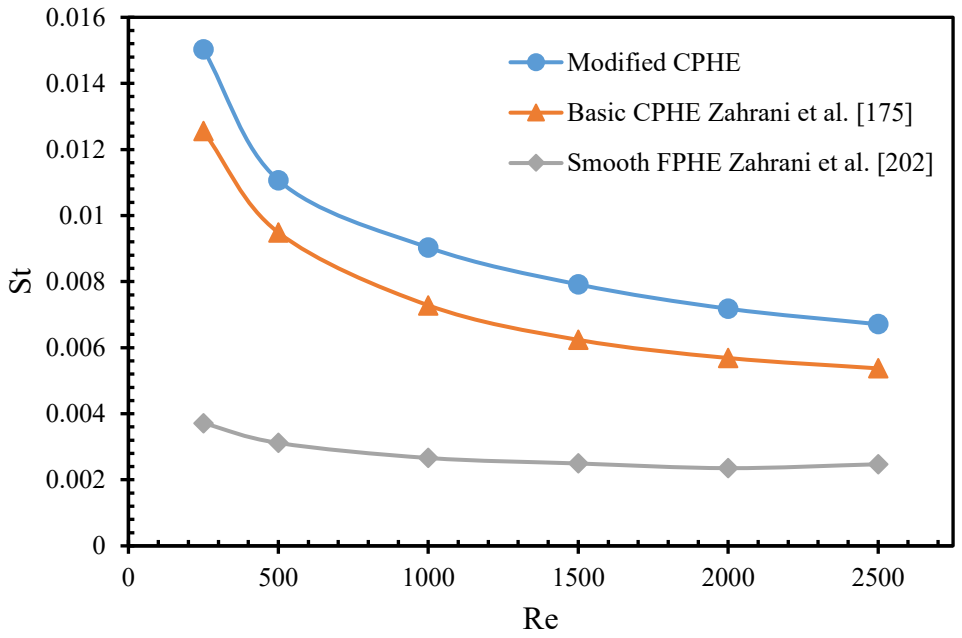

Fig. 6.7: St data versus Re for all investigated HEs.

Furthermore, the thickness of the thermal boundary layers reduces as the mass flow

rate increases, hence less thermal resistance is exerted by those boundary layers [47]. St is estimated and presented in Fig. 6.7. St of the modified HE yields the highest values with varying Re. From Nu and St figures, it is pronounced that the convective heat transfer rate inside the modified channels is higher than that of the basic channels. However, because the enhancement varies with Re, the enhancement percentage in the convective heat transfer due to the present new modification is estimated at different Re as:

$$Enhancement = \frac{(Nu - Nu_o)_{Modified} - (Nu - Nu_o)_{Basic}}{(Nu - Nu_o)_{Basic}} \times 100 \qquad (6.5)$$

Where Nu_o refers to Nusselt number of the FPHE (smooth channel). Fig. 6.8 shows the enhancement is fluctuating with Re. The minimum and the maximum enhancement in the convective heat transfer are taking place at Re~460 (16.7%) and Re~1600 (27%), respectively. In addition, at Re < 460 and Re > 1600 the enhancement's trend decreases. The reason could be that, the new modification boost the flow mixing at this range of Re i.e. 460 < Re < 1600, whereas the flow regimes in the modified and the basic channels at Re < 460 and Re > 1600 are similar i.e. laminar (Re < 460), and turbulent (Re > 1600). Furthermore, the entropy generation in this range (460 < Re < 1600) could be the lowest. However, the convective heat transfer rate inside the modified channel is greater than those of the basic one for all Re.

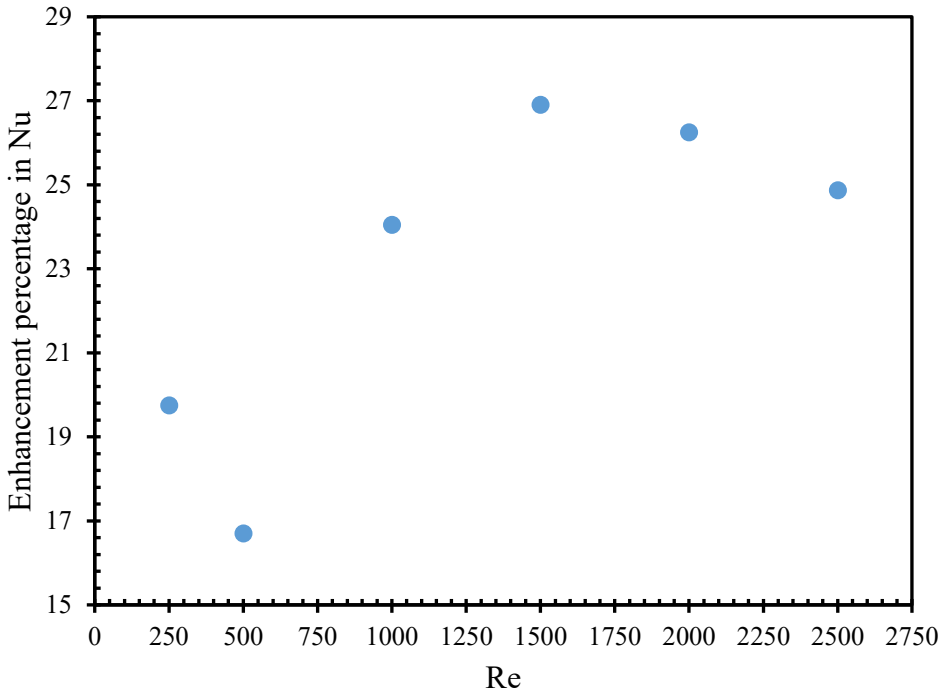

Fig. 6.8: The enhancement percentage of Nu versus Re.

The Colburn j factor is an index of thermal performance of the HEs and it is presented in Fig. 6.9 along with the fanning friction factor for each HE. The j and f data of the modified CPHE are greater than those of the basic CPHE and smooth PHE for all cases. The increase in the f data of the modified CPHE is up to 1.7 greater than that of the basic CPHE, and it is up to 25 times greater than that of the smooth PHE. Moreover, the f data of the basic CPHE are found 14 to 18 times higher than that of the smooth PHE.

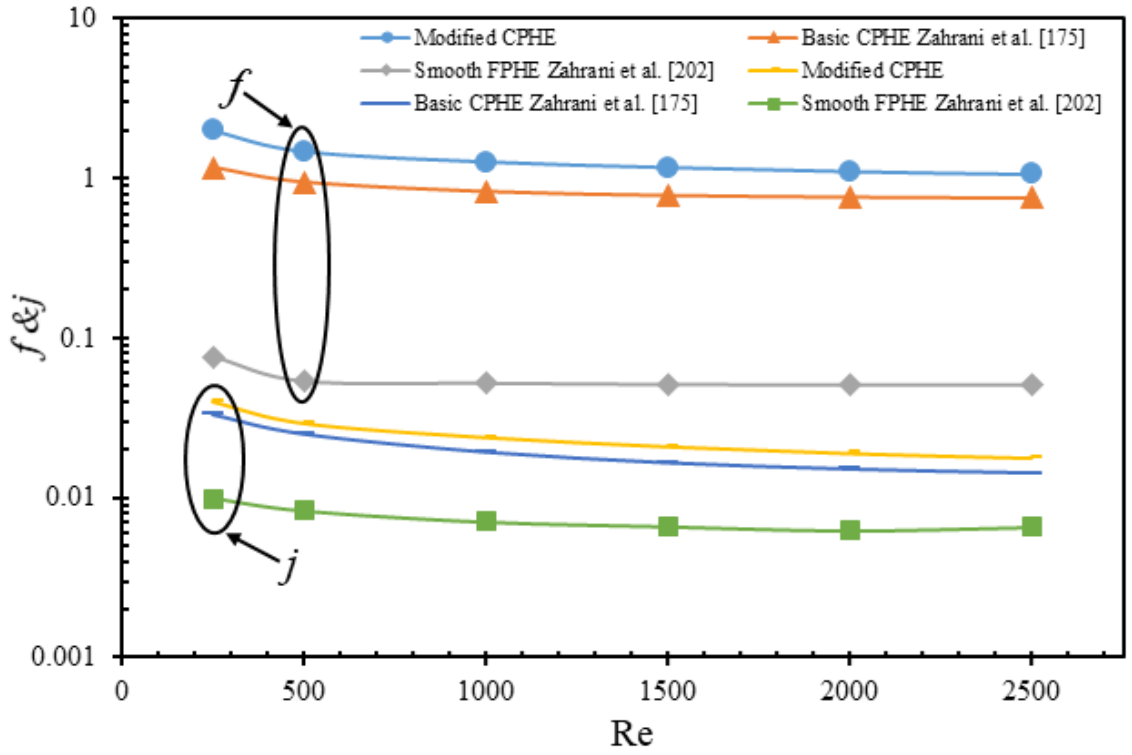

Fig. 6.9: Coulborn j and f data versus Re for all investigated HEs.

Furthermore, JF factor is a comprehensive index of thermal performance of HE.

$$JF = \frac{(j/j_o)}{(f/f_o)^{1/3}} \tag{6.6}$$

Fig. 6.10 shows that the heat transfer rate of the modified CPHE is greater than the resistance of the fluid flow (i.e. JF > 1). Thus, JF data of the modified CPHE are up to 1.4 times JF data of the basic CPHE.

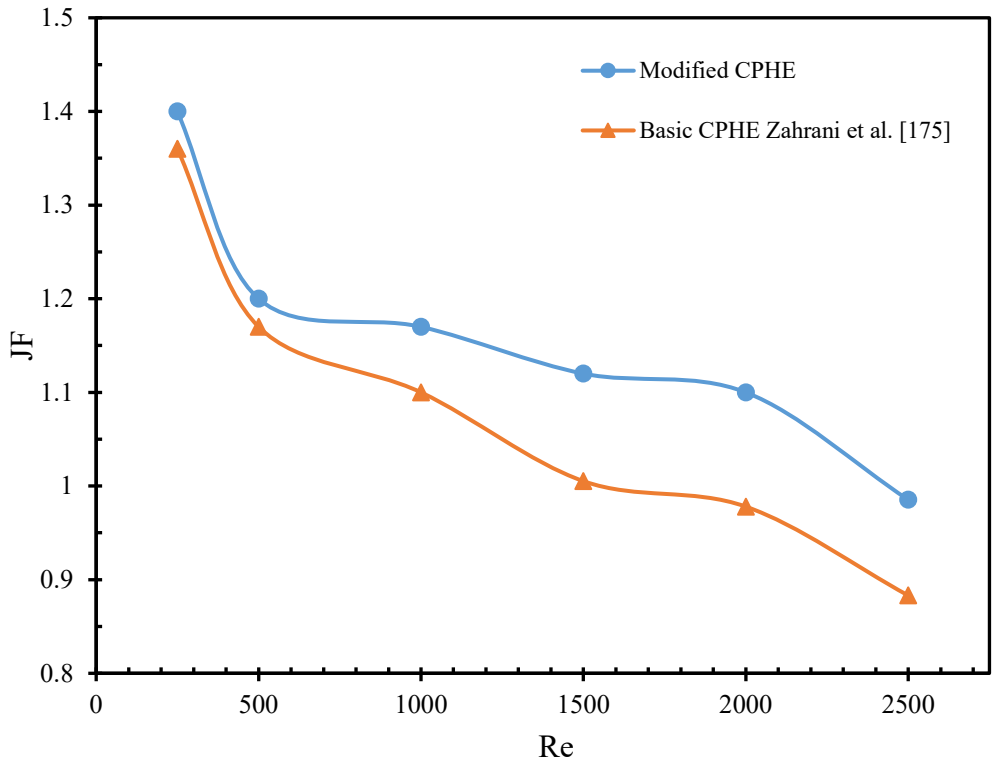

Fig. 6.10: Overall performance index versus Re.

Turbulence kinetic energy is an indicator of flow mixing and vortex generation. Fig. 6.11 shows TKE contours for all investigated HEs in the present study inside the same hot channel at Re = 2500. It is pronounced that the TKE of the smooth PHE is very low due to the smoothness of its surface. An important observation is that the TKE at the middle of the channel of the basic CPHE is almost zero, which refers to the weakness of the fluid flow in this area. Therefore, the present modification exploits this area to simultaneously promote the flow mixing and enhance the mechanical strength of the HE, as each gasket in this area is fully in contact with the previous thermal plate. The TKE attains the maximum values at the corrugation's ridge in both modified and the basic CPHEs. In general, at the same flow rate, the intensity of velocity (TKE) of the modified CPHE is about 3.5 times greater than that of the well-known CPHE.

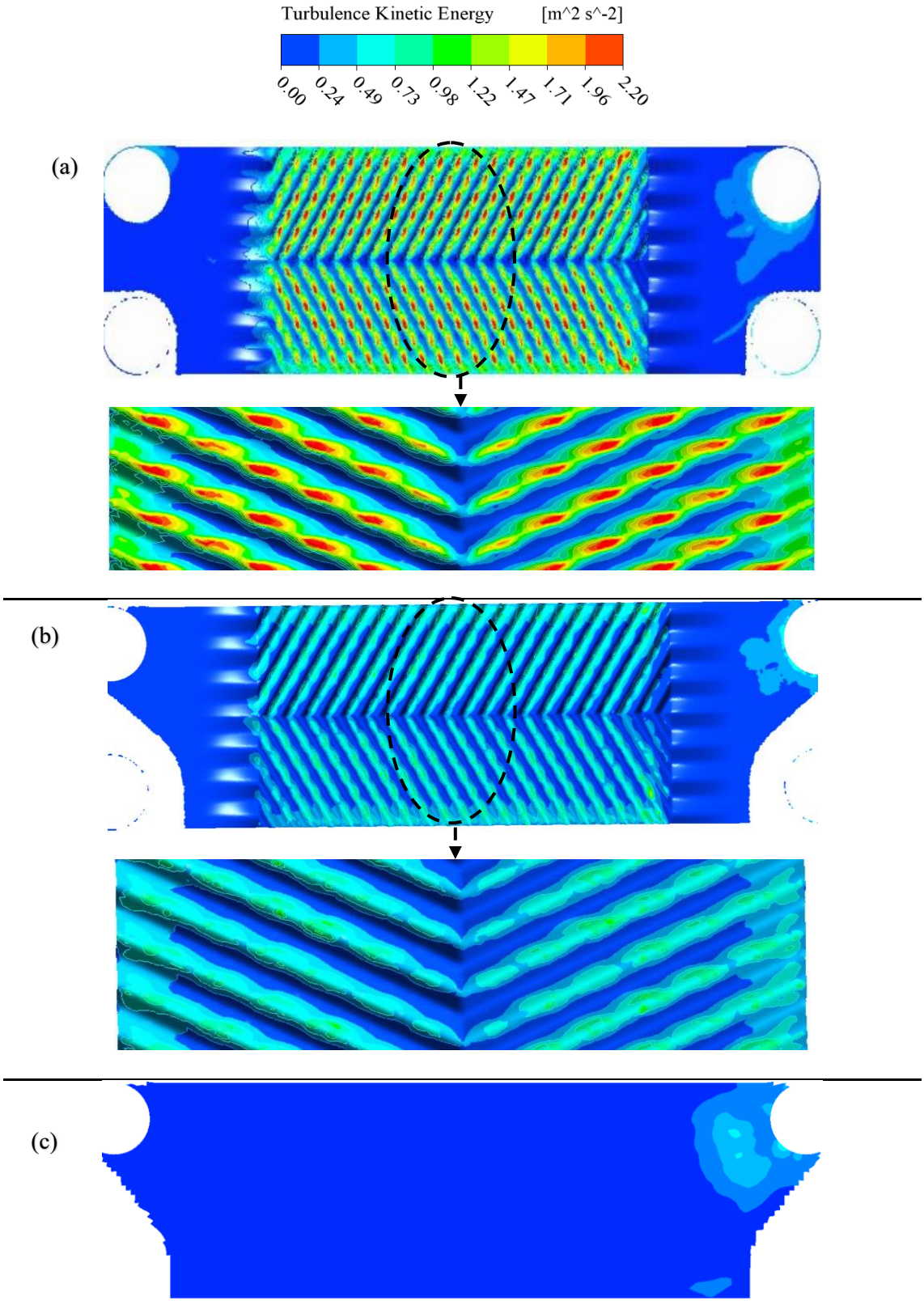

Fig. 6.11: TKE contours inside the middle hot channel for (a) Modified CPHE "enlarge cut part is vertical", (b) Basic CPHE "enlarge cut part is vertical", and (c) Smooth PHE.

Moreover, the variation in TKE with different Re inside the modified and the basic hot channel are presented in Fig. 6.12. This shows that the TKE of the modified channel is 3.3 to 4 times higher than that of the basic channel, which is similar to the TKE data shown in Fig. 6.11. An important point is this, Fig. 6.12 shows the maximum enhancement in TKE of the modified channel is taking place at Re = 1500. It is ~ 2.4 times higher than TKE data at Re = 1000, which is consistent with the data provided in Fig. 6.8. Therefore, this Re (i.e. Re = 1500 to 1600) is the optimum one.

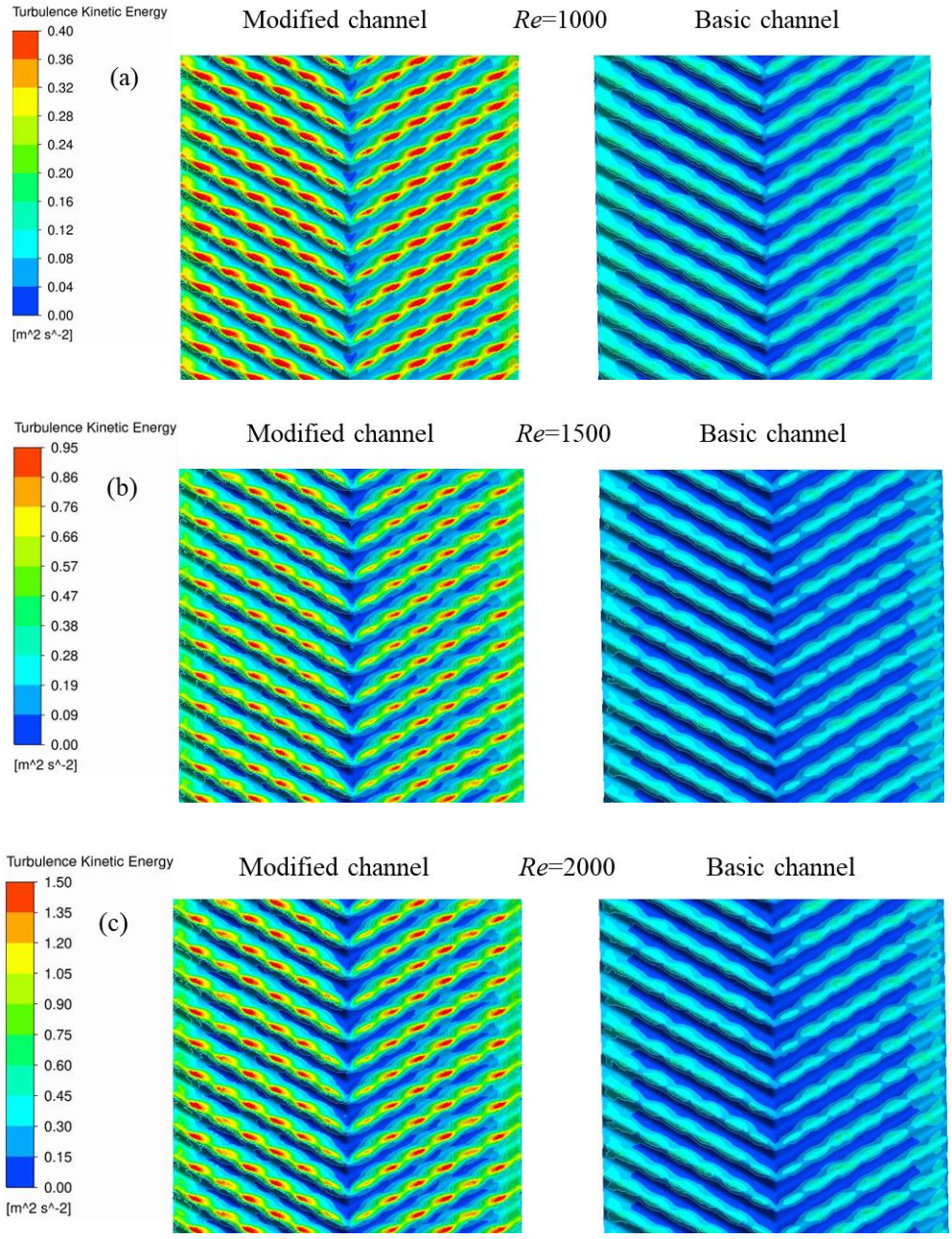

Fig. 6.12: TKE variation insdie the modified and the basic hot channel at (a) Re = 1000, (b) Re = 1500, and (c) Re = 2000.

Furthermore, in Fig. 6.13 the velocity vectors at the same location and same mass flow rate inside the hot channel are shown. The velocity vectors inside the modified channel have the greatest magnitude, which is consistent with the TKE data in Fig. 6.11 and Fig. 6.12. Therefore, it is clear that the turbulence rate of the flow has a direct proportionality on the overall thermo-hydraulic performance of the HE, which is also confirmed widely in the literature [180].

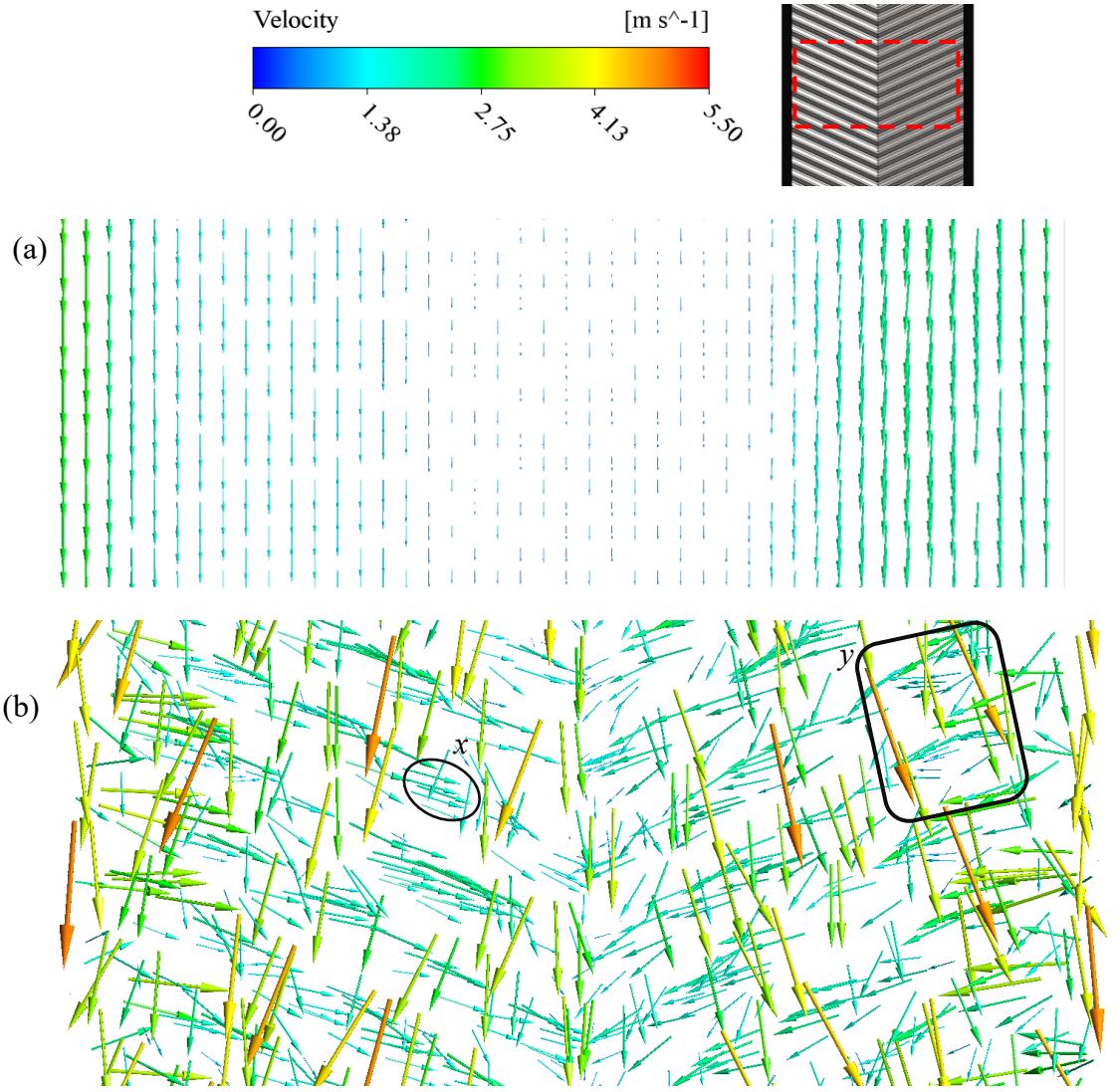

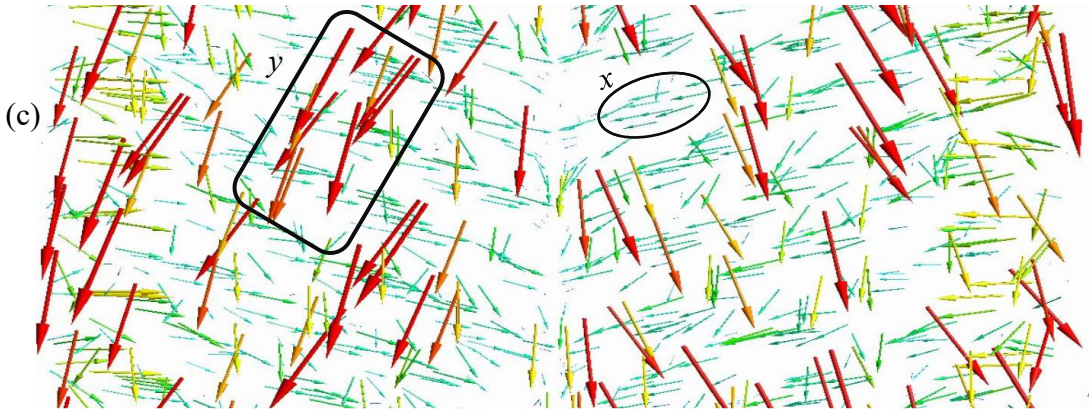

Fig. 6.13: Velocity vectors at the middle hot channel for all of the present PHEs.

6.5.3 Fluid flow distribution

The intensity of the randomness of the fluid distribution (P_{mal}) from port to channel is calculated for all the studied HEs. The higher the P_{mal} is, the more deterioration in the thermal performance of the HE. P_{mal} is calculated based on Bassiouny and Martin [28] correlation. The ports' diameters of the inlet and the outlet are identical, thus P_{mal} is:

$$P_{mal} = \left(\frac{NA_\circ}{A_p}\right)^2 \frac{d_e}{fL_p} \tag{1}$$

where N represents the channels number of the investigated fluid, $A_\circ$ and A_p are the cross-sectional areas of the channel flow and the inlet port, respectively. Fig. 6.14 shows the variation of P_{mal} with different Re.

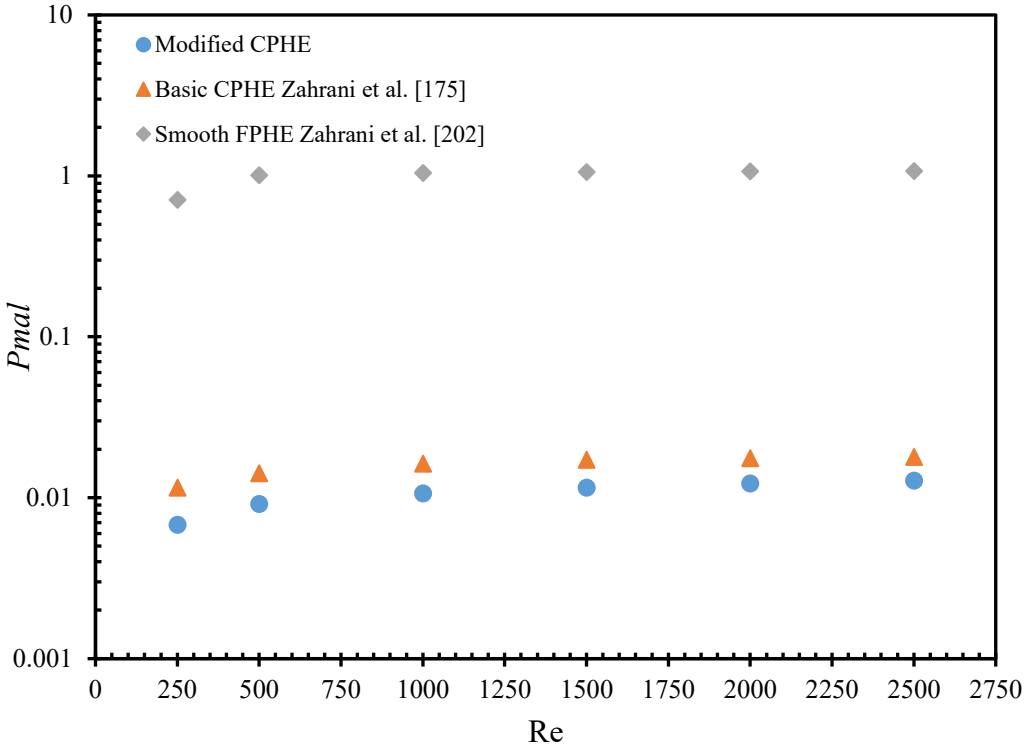

Fig. 6.14: P_{mal} for all of the present PHEs.

The fluid flow maldistribution of the smooth PHE is the highest. It is up to 70 and 110 times greater than that of the basic and the modified CPHEs, respectively. In addition, for all HEs as Re increases, the P_{mal} increases. However, the P_{mal} increasing rate of the modified CPHE is the lowest. The P_{mal} data of all HEs are listed in Table 6.2.

Table 6.2. P_{mal} data variation with different Re for all HEs.

Re	P_{mal} FPHE	P_{mal} basic CPHE	P_{mal} modified CPHE
250	0.709006	0.011540637	0.006768
500	1.008267	0.01418115	0.009133
1000	1.039793	0.016230325	0.01063
1500	1.057469	0.017182923	0.011513
2000	1.063817	0.017599768	0.01223
2500	1.067612	0.017873346	0.01275

Additionally, Fig. 6.13(a) shows that the fluid with high magnitude tends to flow on the sides of the smooth surface while this magnitude is gradually decreasing till it almost vanishes as the fluid moves toward the middle. Similar flow behavior is observed on the surfaces of the basic and the modified CPHEs. The fluid of the higher magnitude flows transversely to the corrugations toward the sides of the plate as highlighted in (*y*) areas on Fig. 6.13(b) and (c). Furthermore, the fluid of the low magnitude follows the corrugation path as highlighted in (*x*) areas on Fig. 6.13(b) and (c). A similar flow pattern has been experimentally found by Lozano et al. [141]. In addition, Fig. 6.11 shows the TKE contours are consistent with the fluid flow magnitude and the flow direction on the plate's surface. Thus, installing the middle gasket could perform multi-purposes. Mainly it could enhance the thermal performance of the CPHE as it has been demonstrated from all aforementioned heat transfer data. Also lower fluid flow maldistribution from port to channel is achieved. In addition, the fluid flow velocity on the left and the right side of the modified plate has higher magnitude than the velocity on the surface of the basic CPHE, as shown in Fig. 6.13(c). Therefore, this could promote the flow mixing, turbulence intensity, and expedite disruption and re-attachment of the thermal boundary layers resulting in a better heat exchanging process. Another important aspect is that each middle gasket will be in contact with the previous plate, which would increase the mechanical strength of the heat exchanger. Thus, a larger range of the maximum operating pressure and temperature could be fulfilled.

6.5.4 Heat transfer correlations

Nusselt number correlation has been developed based on Sieder empirical correlation [155], as follows:

$$Nu = C_1 Re^p Pr^n \left(\frac{\mu}{\mu_w}\right)^{0.14} \tag{6.7}$$

Where C_1 represents the constant of the straight line, and p represents the slope of the line. Additionally, the fanning friction factor correlation has been developed based on Kumar empirical correlation [74]:

$$\boldsymbol{f = C_2 Re^m} \tag{6.8}$$

Nusselt number and fanning friction factor correlations for the basic CPHE and the smooth PHE have been reported in Zahrani et al. [175, 213]. By applying regression

technique on the numerical data of the present modified CPHE, Nu and *f* are found as follows:

For $250 \leq Re \leq 2500$

$$Nu = 0.26\, Re^{0.6573} Pr^{1/3} \left(\frac{\mu}{\mu_w}\right)^{0.14} \tag{6.9}$$

$$f = 8.09\, Re^{-0.2638} \tag{6.10}$$

The maximum difference between the numerical data of Nu and *f* and the provided correlations are respectively + 4% and + 5%.

6.6 Conclusions

Most studies that are performed on PHEs in the literature have investigated the thermal performance of the basic PHEs. However, the current study has presented a newly modified CPHE. The thermal performance of the modified CPHE has been numerically investigated by using a CFD approach. To evaluate the impact of the new modification, the result has been compared with the previously reported results of the basic corrugated and smooth PHEs. The geometrical dimensions, physical properties, and boundary conditions are identical for all three HEs. All calculations are performed to the hot side as the process fluid. The essential remarks of this study can be drawn as follows:

- Nusselt number data of the newly modified CPHE are the highest of all three HEs. The enhancement in the convective heat transfer is up to 1.3 and 4 times greater than that of the basic corrugated and the smooth PHEs, respectively.
- The increase in the fanning friction factor data of the modified CPHE is up to 1.7 greater than that of the basic one.
- The TKE attains the maximum values at the corrugation's ridge in both modified and basic CPHEs. The velocity vectors have revealed consistent behavior with the TKE data. The intensity of the TKE inside the modified channel is ~ 3.5 times the TKE inside the basic channel. Thus, TKE is strongly related to the thermo-hydraulic performance of the HE.
- Maximum enhancement in TKE and convective heat transfer of the modified CPHE is taking place at Re~1600.
- In both modified and basic channels, the fluid of the higher magnitude flows

transversely with respect to the corrugations toward the sides of the plate, whereas the fluid of the low magnitude follows the corrugation path.

- The P_{mal} values are significantly reduced in the modified CPHE where they yield the lowest values. In addition, for all HEs as Re increases the P_{mal} increases. However, the P_{mal} increasing rate of the modified CPHE is the lowest of all three HEs.
- JF data of the modified CPHE are up to 1.4 times JF data of the basic CPHE.

Generally, the present modification could simultaneously boost the thermal performance and the maximum allowable operating pressure and temperature due to the presence of contact areas at the middle between the plates. In addition, the present modification could be applied for any type of PHE e.g., welded PHE and for any flow arrangement. Thus, it could open up new application areas that require high heat transfer efficiency and could handle high-pressure drop. Finally, further studies are recommended to disclose the additional enhancement in the overall thermal performance of the current modified CPHE when different types of nanofluids are added to the base fluid, and also when different chevron angles (i.e. 30°/30°, and 60°/30°) are used.

Chapter 7: Heat Transfer Enhancement of Modified Flat Plate Heat Exchanger

Research Paper Five:

S. Al-Zahrani, M.S. Islam, S.C. Saha, Heat transfer enhancement of modified flat plate heat exchanger, Applied Thermal Engineering, 186 (2021) 116533.

Applied Thermal Engineering 186 (2021) 116533

Contents lists available at ScienceDirect

Applied Thermal Engineering

journal homepage: www.elsevier.com/locate/apthermeng

Heat transfer enhancement of modified flat plate heat exchanger

Salman Al zahrani [a,b], Mohammad S. Islam [a], Suvash C. Saha [a,*]

[a] School of Mechanical and Mechatronic Engineering, University of Technology Sydney, Ultimo, NSW 2007, Australia
[b] Mechanical Engineering Department, Faculty of Engineering, Al Baha University, Saudi Arabia

ARTICLE INFO

Keywords:
Flat plate heat exchanger
Corrugated plate heat exchanger
Heat transfer enhancement
Nusselt number
Flow maldistribution

ABSTRACT

Flat plate heat exchanger (FPHE) can tolerate more mass flow rate, significantly yield lesser pressure drop, and it is easier for manufacturing than the corrugated plate heat exchanger (CPHE). However, the overall thermal performance of FPHE is poor due to its low heat transfer rate. Therefore, the aim of the current study is to improve the thermal performance of the existing conventional FPHE ($FPHE_C$). Thus, two newly developed modified FPHEs are introduced ($FPHE_{m1}$ and $FPHE_{m2}$). A computational fluid dynamics (CFD) technique is applied to numerically test the performance of the heat exchangers (HEs). Moreover, experiments are carried out to confirm the validity of the numerical results obtained in this study. The performance of $FPHE_{m2}$ significantly outperforms that of $FPHE_C$ and $FPHE_{m1}$. Hence, the results of $FPHE_{m2}$ are compared with those of the conventional corrugated plate heat exchanger ($CPHE_C$). Data of Nusselt number (Nu), fanning friction factor (f), turbulence intensity, JF factor, severity of temperature gradient of the plate (ΔTp), and average temperature through the plate (Tp,avg) are employed to quantify the best performance among all four HEs. The numerical results show that $FPHE_{m2}$ has the best temperature uniformity and average temperature (the lowest values), and it has the highest Nu, JF, and turbulence intensity among all four HEs. Also, the f data of the $FPHE_{m2}$ are 18.7% to 33.2% lower than those of the $CPHE_C$. Thus, $FPHE_{m2}$ could be a probable replacement of its counterparts of both $FPHE_C$ and $CPHE_C$. Critical Reynolds numbers (Re_{cr}) of $FPHE_{m2}$, heat transfer correlations and the flow distribution along with other details have been analysed numerically.

7.1 Abstract

Flat plate heat exchanger (FPHE) can tolerate more mass flow rate, significantly yield lesser pressure drop, and it is easier for manufacturing than the corrugated plate heat exchanger (CPHE). However, the overall thermal performance of FPHE is poor due to its low heat transfer rate. Therefore, the aim of the current study is to improve the thermal performance of the existing conventional FPHE ($FPHE_C$). Thus, two newly developed modified FPHEs are introduced ($FPHE_{m1}$ and $FPHE_{m2}$). A computational fluid dynamics (CFD) technique is applied to numerically test the performance of the heat exchangers (HEs). Moreover, experiments are carried out to confirm the validity of the numerical results obtained in this study. The performance of $FPHE_{m2}$ significantly outperforms that of $FPHE_C$ and $FPHE_{m1}$. Hence, the results of $FPHE_{m2}$ are compared with those of the conventional corrugated plate heat exchanger ($CPHE_C$). Data of Nusselt number (Nu), fanning friction factor (*f*), turbulence intensity, JF factor, severity of temperature gradient of the plate (ΔTp), and average temperature through the plate (Tp,avg) are employed to quantify the best performance among all four HEs. The numerical results show that, $FPHE_{m2}$ has the best temperature uniformity and average temperature (the lowest values), and it has the highest Nu, JF, and turbulence intensity among all four HEs. Also, the *f* data of the $FPHE_{m2}$ are 18.7% to 33.2% lower than those of the $CPHE_C$. Thus, $FPHE_{m2}$ could be a probable replacement of its counterparts of both $FPHE_C$ and $CPHE_C$. Critical Reynolds numbers (Re_{cr}) of $FPHE_{m2}$, heat transfer correlations and the flow distribution along with other details have been analysed numerically.

Keywords: Flat plate heat exchanger; Corrugated plate heat exchanger; Heat transfer enhancement; Nusselt number; flow maldistribution;

7.2 Introduction

The global industrial market has been experiencing continuous innovations and growth in several numbers of applications such as concentrated solar power (CSP), recovery systems, combined power plants, food and dairy industries, oil cooling and refineries. HEs are essential parts of all power applications and implemented in many industrial processes for cooling and heating. However, environmental legalizations, energy cost, and safety regulations represent great challenges for the designers of the HEs.

In 2012, the global demand for HEs was about USD $42.7 billion, and it is expected to reach USD $78.2 billion by the end of the current year 2020 [214].

The type of fluid and its cleanness degree varies according to the application. Generally, the relative degree of cleanness is required for the cryogenic applications. At the same time, high degree clean fluids are required in chemical applications [215]. Furthermore, the heat duty, the allowable pressure drop, and the available space along with many other specifications are important factors to assist the designers in choosing the most suitable HE. Thus, the suitable choice of the HE would minimize both the capital and the maintenance cost. HEs are classified into conventional and compact HEs. When the ratio of the heat transfer area (A_h) of the process fluid to the volume occupied by the process fluid exceed 700 m^2/m^3, or when the hydraulic diameter is < 6 mm, the HE is considered as a compact one [13]. Shell and tube as conventional HE occupies the first market share by about 40% [17]. On the other hand, plate type HE occupies the first market share in comparison with all different types of compact HEs [17]. Various significant advantages have contributed to the increasing demand on the PHEs. Some of these advantages are: low weight and area requirements, fast in start-up and shut down due to the small filling space in the channels, its modular nature offering high degree of flexibility to adjust the number of plates to meet the heat duty or to conduct maintenance and cleaning process, and it offers large A_h and high heat transfer coefficient.

Both corrugated and flat PHEs consist of a number of adjacent plates that are assembled in similar manner inside one unit. However, in corrugated PHE, each plate contains corrugations on its surface. These corrugations promote swirl flow, especially near the contact points [216, 217], increase the projected heat transfer area, expedite flow mixing where turbulence flow could be achieved at relatively low Re, and mitigate fouling. Several fouling deposition mechanisms inside heat exchangers have been investigated by several authors [218-223]. Arsenyeva et al. [224] have defined the fouling accumulation inside the channel of the corrugated PHE as the ratio of fouling deposition rate to the fouling removing rate. They also developed an equation that describes the variation of the fouling resistance rate with time. In addition, these corrugations are tilted with an angle known as chevron angle "β". As β increases, the heat transfer rate and pressure drop increase [175, 225]. The thermal performance of nine brazed plate heat exchangers has been experimentally studied by Yang et al. [120]. They have found that

chevron angle is the most influential geometrical parameter. Moreover, the thermal performances of two identical β's (i.e. 30°/30°, 60°/60°) and one mixed β (i.e. 30°/60°) have been investigated by Khan et al. [46, 66]. Their findings confirm that larger β yields both higher heat transfer rate and pressure drop.

The effect of the channel height has been studied by Islamoglu and Parmaksizoglu [226]. The result shows the channel with larger height yields both higher Nu and friction factor. In addition, Zahrani et al. [47] investigated the effect of Prandtl number (Pr) on Nu and friction factor inside corrugated PHE with single β = 60°/60°. The findings disclosed that Nu and the friction factor data of water (Pr = 4.34) are respectively up to 4 and 1.1 times greater than those of air (Pr = 0.72). Arsenyeva et al. [227, 228] conducted a comparison between the thermal performance of the $CPHE_C$ and novel PHE called Pillow PHE. They reported that the flow moves with higher velocities inside the Pillow PHE's channel. Also, Piper et al. [229] have proposed the use of Pillow PHE to enhance the flow mixing near the walls. However, the thermal performance of Pillow PHE with respect to the $CPHE_C$ has not been provided. Hu et al. [190] have investigated the capability of various numerical models to simulate the thermo-hydraulic characteristics of $CPHE_C$. The findings disclosed that, the realizable $k-\varepsilon$ model is providing the best match with the experimental data. A new design of the surface of the PHE called capsule PHE has been proposed by Zhang et al. [94]. It has been reported that Nu data of the capsule PHE are greater than those of the $CPHE_C$.

Tao and Ferreira [230] conducted a review on the heat transfer and pressure drop correlations in PHEs during condensation. The correlations that are provided by Longo et al. [231] and Kuo et al. [232] respectively reported the best correlations. In addition, the melting and solidification temperatures of phase-change-materials in $CPHE_C$ have been widely investigated [233-235]. However, Medrano et al. [236] reported that double pipe HE is much better as a heat store than PHE because the ratio of PCM heat capacity to the empty heat exchanger heat capacity is very low in the case of PHE.

On the other hand, FPHE yields lower heat transfer rate in comparison with CPHE. However, the pressure drop inside FPHE's channels is lower than that inside the corrugated channels. Muley and Manglik [42] have compared their *f* data of the $CPHE_C$ with the *f* correlation of the $FPHE_C$ that is provided by Kakac et al. [191]. They found *f* data of FPHE are 13-44 times lower than that of the CPHE. In addition, Zahrani et al.

[167] carried out numerical study for corrugated and flat PHEs where both have identical dimensions and boundary conditions. The results showed the *f* data of FPHE are 14-18 times lower than that of the CPHE. Thus, due to the low pumping power requirement of FPHE, it has been implemented in various applications such as air dryer, and free cooling applications [6, 237-240]. Gurel et al. [168] have adopted a biomimetic approach by applying lung pattern on the surfaces of the FPHE. Enhancement in heat transfer by 71.3% and decrease in pressure drop by 67.8% in their newly designed PHE have been reported. An experimental study on FPHE has been performed by Gut et al. [241] to come up with generalized heat transfer correlations. However, they reported that there is lack of data when multiple configuration is used, such as flow maldistribution that takes place inside the channels of the FPHE.

The aim of the current study is to develop FPHE with superior thermal performance. To achieve this objective, a new passive technique has been implemented to the plates' surfaces of the FPHE. In this regard, the modified design that already showed promising capabilities on the CPHE [242] has been replicated on the $FPHE_{m1}$. In addition, a new novel design "$FPHE_{m2}$" is proposed in the current study. The goodness of each design has been evaluated based on the following parameters:

(a) The enhancement in the convective heat transfer (Nu).
(b) The increase in *f* data.
(c) The uniformity of the fluid flow distribution on the surface of the channel.
(d) The fluid flow velocity, and its turbulence intensity inside the channel.
(e) The average temperature of the plates of the HE (Tp,avg).
(f) The severity of the temperature gradient across the walls of the HE (ΔTp).
(g) The overall heat performance index (JF).

The findings have been compared against those of the $FPHE_C$ and $CPHE_C$ that has been reported in [175]. All four HEs have identical dimensions. The numerical simulations have been performed for Re range from 250 to 2000, and for counter-current flow. An experiment has also been conducted to validate the numerical approach.

7.3 The Present Passive Technique Description

Several studies [37, 141] show the fluid is flowing randomly on the surfaces of the PHEs. Consequently, this would deteriorate the thermal performance of the HE. To

mitigate this obstacle, the current study introduces two passive techniques (modified geometries) as an endeavour to improve the flow distribution and the overall heat transfer process. Fig. 7.1 shows the first modification; for simplicity it has been named "$FPHE_{m1}$".

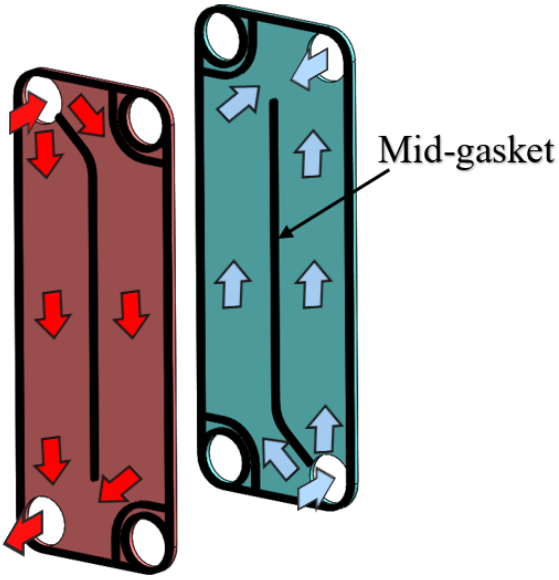

Fig. 7.1: Schematic drawing of flow mechanism of $FPHE_{m1}$.

The fluid mechanism on the surfaces of the $FPHE_{m1}$ is as follows: the fluid enters from the inlet port and then it gets separated on the right and left sides of the thermal plate by the help of new gasket installed at the middle called "mid-gasket" as shown in Fig. 7.1. Otherwise, the flow mechanism is precisely the same with that (counter-current flow) of the $FPHE_C$. The fluid will enter and exit from the same ports as in the case of $FPHE_C$.

Another modified FPHE named as $FPHE_{m2}$ is generated to enable us to have more degree of control over the fluid flow direction, as shown in Fig. 7.2(a). The flow will be guided inside the smooth channel by the use of the modified gasket as it is shown schematically on Fig. 7.2(a). In addition, all the details of $FPHE_{m2}$'s thermal plate are outlined in Fig. 7.2(b). As the pressure drop of the FPHE is significantly smaller than that of the CPHE, this modification could be more useful in case of FPHE. In addition, it is the first study that investigates the effectiveness of these modifications on the smooth surfaces.

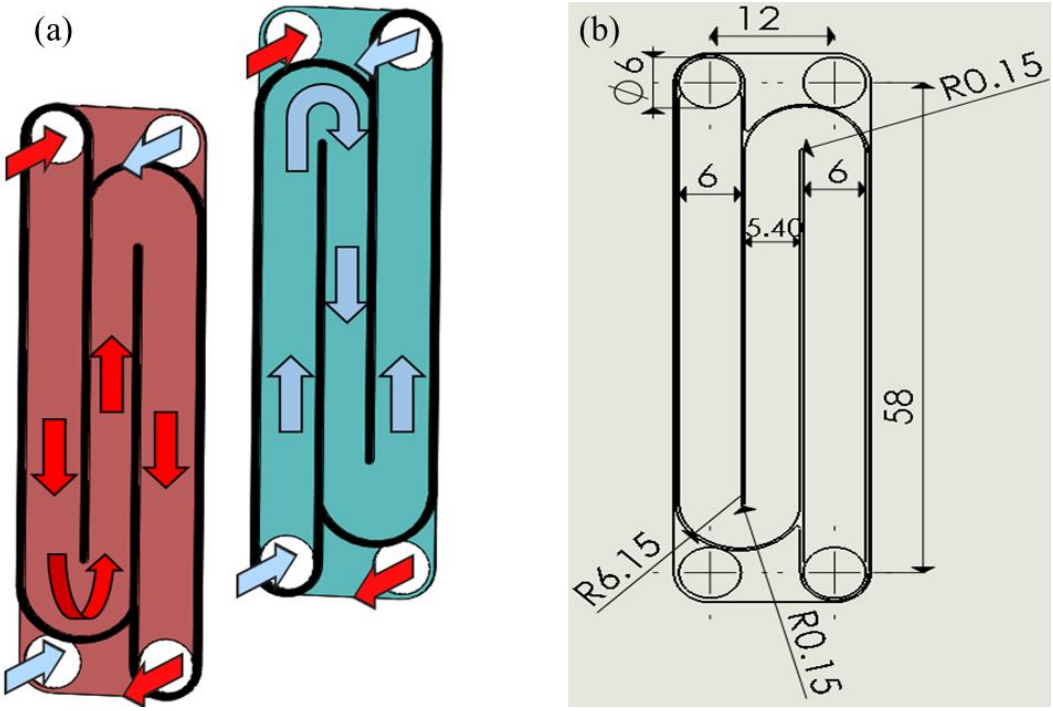

Fig. 7.2: Schematic drawing of, (a) Flow mechanism of $FPHE_{m2}$, and (b) Detailed sketch of $FPHE_{m2}$'s thermal plate (all dimensions are in mm).

The purposes of the use of the mid gasket and the modified gasket are to:

- Mitigate the flow maldistribution where fluid is flowing over a smaller cross-sectional area without reducing the size of the thermal plate.
- Boost the heat transfer rate. Because the modified surface is divided, at the same mass flow rate ($\dot{m}$) the fluid will flow with higher velocity in comparison with that of the conventional surface. Consequently, this would increase the rate of the flow mixing and boundary layer separation.
- The gasket of each thermal plate is in contact with the gasket that is installed on the surfaces of the preceding and the following thermal plates. Hence the overall mechanical strength of the FPHE is expected to increase.

7.4 Experimental Model

7.4.1 Experiment set-up and procedure

The aim of this experiment is to verify the reliability of the numerical model that is implemented in this study. Fig. 7.3(a) and (b) shows the experimental model, which consists of five stainless steel thermal plates. The capacity of the hot water tank is 9 l, and

it contains 1*2500 W heater. The cold water flows in via fluid control valve through a needle valve to the HE. The hot water has an electric heater with an adjustable controller to set the temperature. It is circulated through a closed-loop from the tank through a needle to the HE. Eight experiments have been performed for water-water, counter-current flow, and flow rate range from 0.5 to 4 litre per minute (lpm). The tubes and the HE are insulated with polyethylene foam. The flow rate of each side is controlled by the flow control valve, and the temperature of the hot side is controlled by using a thermostat. Four thermocouples (type-K) of an accuracy $\pm$ 0.15 °C are installed at the inlet and the outlet of each side. These thermocouples are used to measure the temperature at each port. The geometrical specification of the HE is presented in Table 7.1.

Table 7.1. Geometrical dimensions of the experimental FPHE.

Vertical distance including the ports, L_v *(mm)*	132
Horizontal distance including the ports, L_w *(mm)*	50
Port diameter, *dp (mm)*	12
Plate thickness, *t (mm)*	1

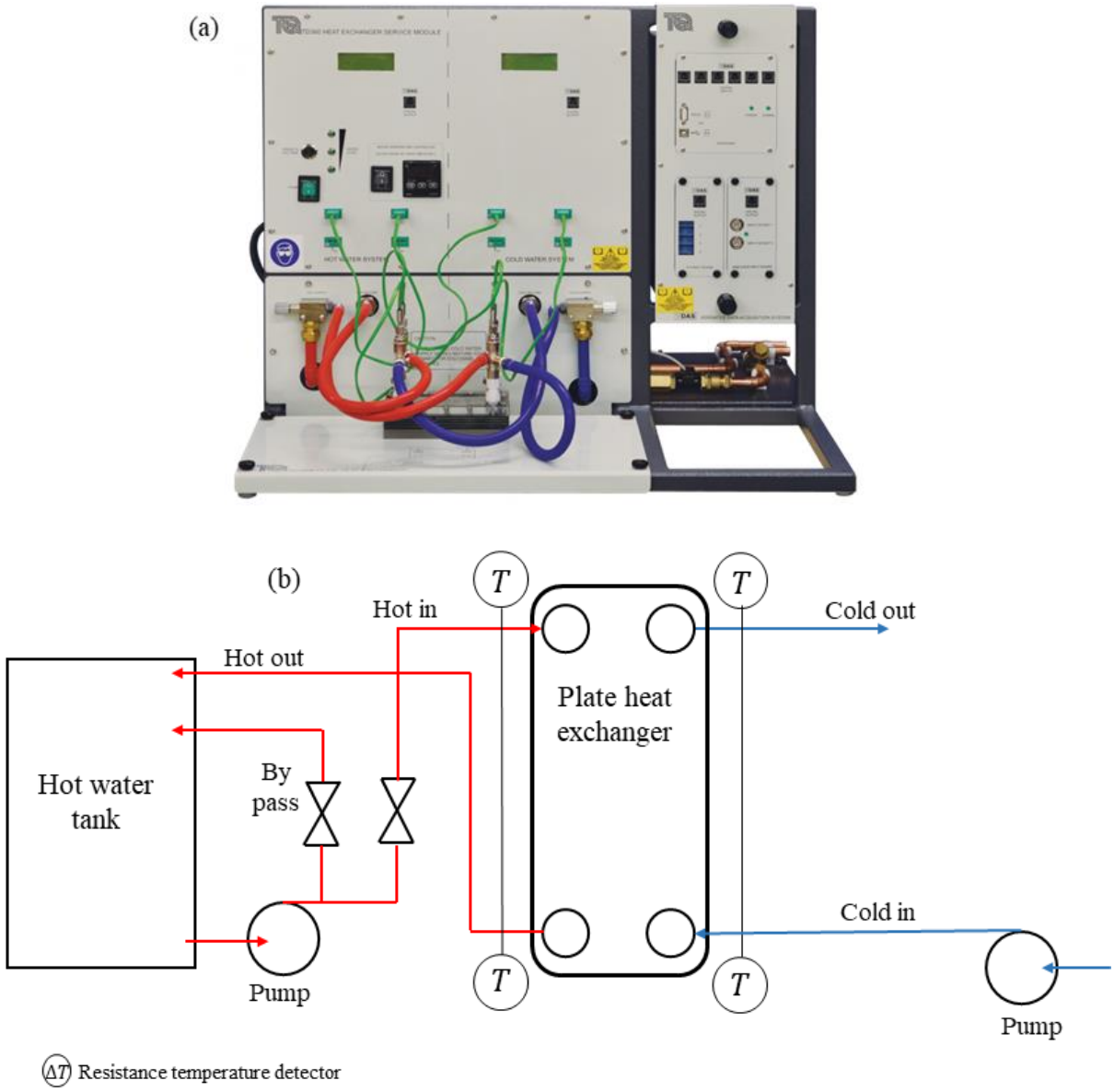

Fig. 7.3: (a) Front view of the experimental rig, and (b) schematic drawing of the experimental test.

7.4.2 Uncertainties

An instrumentation calibration has been carried out by the manufacturer to eliminate the systematic error. In addition, multiple readings of each experiment have been conducted and then averaged to reduce the random error. Moreover, the uncertainty analysis has been checked. The effect of the uncertainties U_R has been evaluated based on the expression that is proposed by Kline and McClintock [243].

$$U_R = \sqrt{\sum_{k=0}^{n} \left(\frac{\partial R}{\partial x_k} U_k \right)^2} \quad (7.1)$$

The total uncertainties are listed in Table 7.2.

Table 7.2. Uncertainty analysis of the experimental variables.

Variable	Uncertainty
Fluid temperature of hot inlet, $T_{h,i}$	$\pm$ 0.15 °C
Fluid temperature of cold inlet, $T_{c,i}$	$\pm$ 0.15 °C
Fluid temperature of hot outlet, $T_{h,o}$	$\pm$ 0.15 °C
Fluid temperature of cold outlet, $T_{c,o}$	± 0.15 °C
Mass flow rate of hot side, $\dot{m}_{h,i}$	$\pm$ 3%
Mass flow rate of cold side, $\dot{m}_{c,i}$	$\pm$ 3%
Channel equivalent diameter, d_e	$\pm$ 2%
Heat transfer rate of hot side, $\dot{Q}_h$	$\pm$ 6%

7.5 Numerical Approach

7.5.1 CAD models, and mesh distribution

Four FPHEs have been created by using Solidworks CAD. Each HE consists of four channels where two of them are pertaining to the cold side and the other two for the hot side. The first CAD model is identical with the experimental model. Each thermal plate of the experimental model contains three disturbers on its surface to promote the fluid flow, as shown in Fig. 7.4. The second FPHE ($FPHE_{m1}$) is the modified one, where mid-gasket is installed on its surfaces as shown in Fig. 7.1. The third FPHE ($FPHE_{m2}$) is also a modified one with narrow paths as shown in Fig. 7.2(a). The fourth FPHE represents the conventional FPHE ($FPHE_C$) where its thermal plates are smooth, as presented in Fig. 7.9(a).

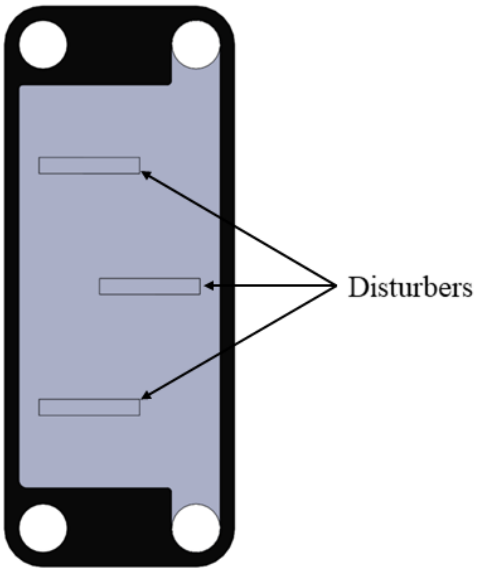

Fig. 7.4: CAD thermal plate identical with the experimental one.

Meshing is an essential process that directly affects the accuracy of the solution and its speed of convergence. Thus, the most appropriate mesh technique for each engineering problem that is reliable and stable should be achieved. In the beginning, the CAD models have to be clean where small flaws of geometry that have no impact on the physics of the problem, such as slivers and holes, could negatively impact the accuracy of the result. Therefore, it is recommended to remove these flaws from the CAD models. If the automated tools that are integrated into the meshing in ANSYS Fluent could provide high qualities metrics (such as orthogonal quality and skewness), that means a more accurate and faster solution is more likely to be achieved [244]. Therefore, the global mesh technique is adopted for all HEs of the present study. This technique offers a large number of options for the user, starting from fully automated mesh up to mesh that is controllable up to a certain level. Moreover, very valuable functions that are known as advanced size functions are integrated into ANSYS where they can refine the mesh in the areas that probably would experience high gradients. The curvature function is enabled for the present study, where the size of the cell is defined based on the growth rate. Also, the minimum and maximum sizes of the element that is generated by the size function have been tested against different sizes until good metrics qualities are achieved. Because PHE consists of thin plates and narrow channels, a small cell sizes i.e. 0.015 mm, and 0.01 mm have been used to cover these small thin and narrow areas and consequently reduce the discretization error. Samples of mesh at different locations on $FPHE_{m2}$ are shown in Fig.

7.5. In addition, the mesh dependency test has been conducted by measuring the local velocity at the hot outlet port of all HEs, as shown in Table 7.3.

Table 7.3. Mesh test of $FPHE_{m1}$ and $FPHE_{m2}$.

$FPHE_{m1}$		$FPHE_{m2}$	
Mesh elements (million)	Local velocity (m/s)	Mesh elements (million)	Local velocity (m/s)
11	0.431	10	0.317
19	0.425	19	0.352
25.5	**0.404**	**24**	**0.421**
29	0.402	32	0.420

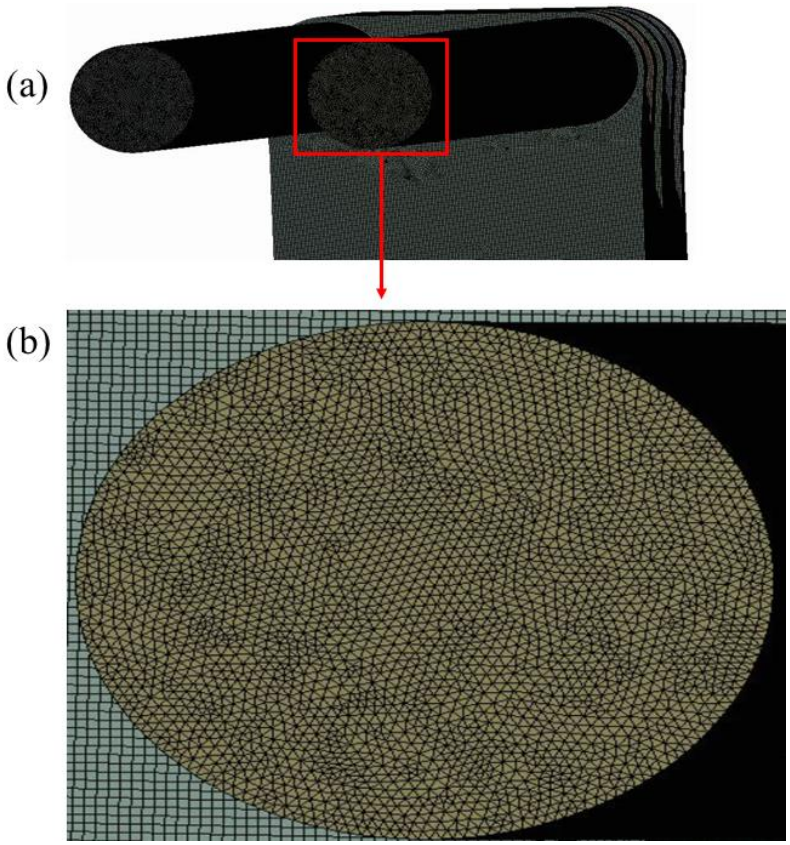

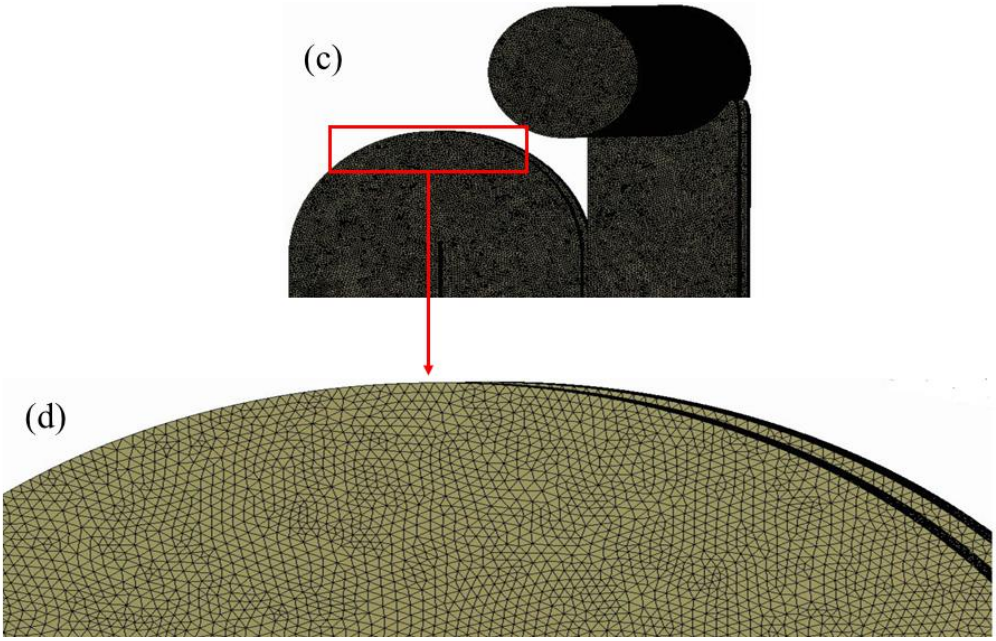

Fig. 7.5: Samples of $FPHE_{m2}$'s grid at, (a) Upper side of the entire HE, (b) Close view at the inlet port, (c) Upper side of the hot channels, and (d) Close view at the outer bend inside the hot channel.

7.5.2 Boundary conditions, and turbulence model

There is no single option of boundary conditions that could be implemented for all engineering problems. CFD provides multi-options of boundary conditions to be adapted according to the physics of the problem. The current study employed realistic boundary conditions that are very close to that one in real life. Mass flow rate ($\dot{m}$) of each fluid along with its temperature for the hot and the cold sides is set as the inlet boundary condition. For both outlets, zero gauge pressure is set as the outlet boundary condition. The walls and the flow domains' thicknesses have been defined to enable CFD to calculate the conjugate heat transfer.

To simulate the flow characteristics of the current study, $k-\varepsilon$ model is adopted. This model comprises two partial differential equations "transport equations". In addition, the realizable approach is enabled along with scalable near-wall treatment function. Shih et al. [245] is the first one who came up with the fact that the coefficient of the model (C_μ) is not constant in the case of large mean strain (e.g. $Sk/\varepsilon > 3.7$ where $S = \sqrt{S_{ij}S_{ij}}$). In the same study [245], the performance of the realizable against the standard $k-\varepsilon$ model has been experimentally tested under different flow conditions. The findings showed realizable $k-\varepsilon$ model provides more accurate results in all cases. More details about the

transport equations, eddy viscosity (μ_t), and the capability of this model, as well as its suitability tests, are to be found in Zahrani et al. [175].

7.5.3 Data reduction

Equal Reynolds number (Re) is considered for both fluid streams, and it is calculated as follows:

$$Re = \frac{\rho\, u\, d_e}{\mu} \tag{7.2}$$

Where ρ, and μ are the fluid density and dynamic viscosity, respectively. Also, u represents the fluid flow velocity, and d_e represents the equivalent diameter. For $CPHE_C$, d_e equals twice the depth of the corrugation.

$$d_e = 2b \tag{7.3}$$

Where b represents the corrugation depth. Additionally, in case of all FPHEs (i.e. $FPHE_{m1}$, $FPHE_{m2}$, and $FPHE_C$) d_e equals the distance between the surfaces of two consecutive thermal plates as shown in Fig. 7.6. Note, d_e of all present heat exchangers is the same.

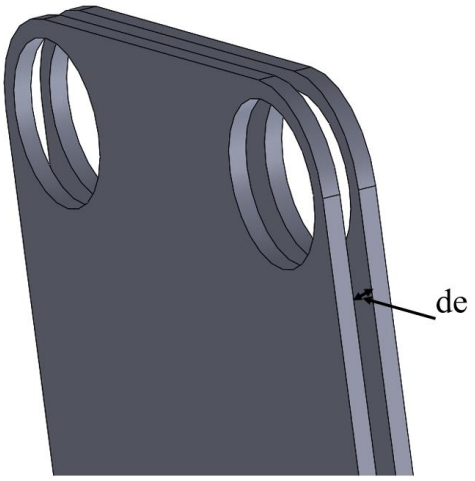

Fig. 7.6: Schematic drawing of de of FPHE.

Heat transfer rates of cold and hot streams are respectively calculated as follows:

$$Q_c = \dot{m}_c c_{p,c}\left(T_{c,o} - T_{c,i}\right) \tag{7.4}$$

$$Q_h = \dot{m}_h c_{p,h}\left(T_{h,i} - T_{h,o}\right) \tag{7.5}$$

Where $c_{p,c}$, and $c_{p,h}$ are respectively representing the specific heat of cold and hot

streams, and they have been calculated at the bulk temperature:

$$T_{c,b} = \frac{(T_{c,i} + T_{c,o})}{2} \tag{7.6}$$

$$T_{h,b} = \frac{(T_{h,i} + T_{h,o})}{2} \tag{7.7}$$

The maximum deviation between the data of Q_c, and Q_h is found ± 3%, hence the average value is calculated.

$$Q_{avg} = \frac{Q_c + Q_h}{2} \tag{7.8}$$

Note, hot side is considered as the process fluid in this study, hence all calculations belong to the hot side. Now, heat transfer coefficient is calculated as:

$$h_h = \frac{Q_{avg}}{A(T_{h,b} - T_{w,h})} \tag{7.9}$$

Where $T_{w,h}$ is the temperature of the hot sides of the thermal plates walls. Consequently, Nu is given by:

$$Nu = \frac{h_h d_e}{k} \tag{7.10}$$

The total pressure drop (ΔP_m) throughout the heat exchanger is given by:

$$\Delta P_m = \Delta P_{port} + \Delta P_{core} + \Delta P_{elev.} \tag{7.11}$$

Where ΔP_{port} represents the pressure drop due to the port effect, and it is evaluated based on the equation of Shah and Focke [176] as follows:

$$\Delta P_{port} = 1.5\left(\frac{\rho V^2{}_{port}}{2}\right) \tag{7.12}$$

$\Delta P_{elev.}$ is ignored as the plate length is small. Now, ΔP_{core} can be calculated as:

$$\Delta P_{core} = \Delta P_m - \Delta P_{port} \tag{7.13}$$

The isothermal fanning friction factor is calculated based on the Kakac et al. [114] equation as:

$$f = \frac{\rho d_e \Delta P_{core}}{2 L_P G^2} \tag{7.14}$$

Where L_P is the effective length of the thermal plate, and G is mass flux and it is evaluated as:

$$G = \frac{\dot{m}}{L_w bN} \tag{7.15}$$

Where L_w, and N are respectively the width of the plate and the number of the channels.

7.6 Results and Discussion

7.6.1 CFD model validation

The fluid of the hot side has been considered as the process fluid for the whole study. To achieve high sensible heat transfer rate, the temperature difference between the inlet and the outlet ports of the same side (i.e. the hot side) is desired to be as large as possible. Therefore, the outlet temperature (To) is of significant importance where it can be employed as an indicator of the quality of the heat transfer process. To validate the numerical approach that is adopted for this study, the local outlet temperature $(Th,o)_L$ and the local heat transfer rate (Q_L) of the hot side are employed to compare the experimental data with the numerical ones. The mesh test of the numerical model that is identical with the experimental one is presented in Table 7.4. Comparison between $(Th,o)_L$ of the experimental and numerical data versus different volume flow rates are presented in Fig. 7.7. The trends of both studies are increasing as the volume flow rate increases, and the maximum deviation is found to be - 1%. In addition, comparison between Q_L of the experimental and numerical data versus different volume flow rates are presented in Fig. 7.8. The maximum difference is found + 13%, and both trends are increasing as mass flow rate increases.

Table 7.4. Mesh test of the experimental CAD model.

Mesh elements (million)	Local temperature (K)
10	47.6
13	48.1
18	48.36
21	48.37

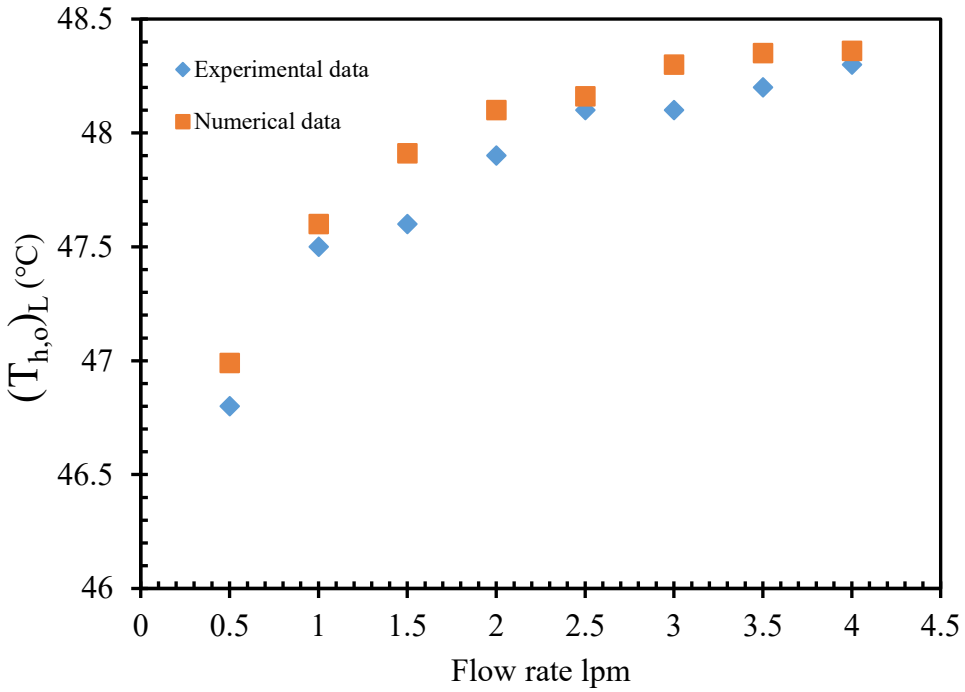

Fig. 7.7: Hot outlet temperature versus flow rate for experimental and numerical data.

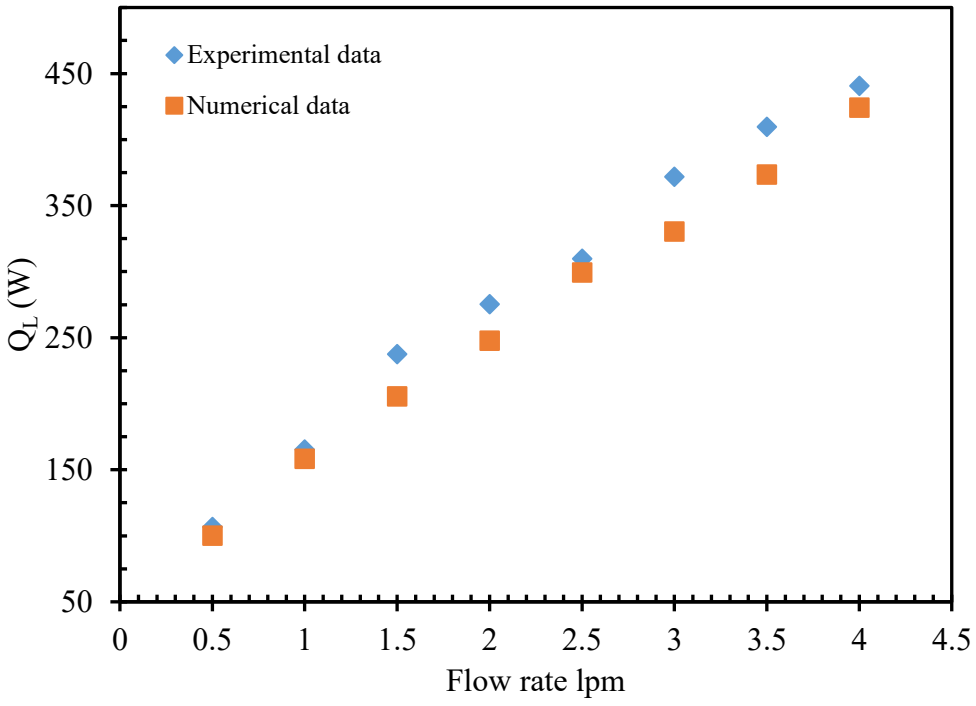

Fig. 7.8: Comparison between local heat transfer rate versus flow rate of experimental and numerical data

The numerical data of pressure drop (realizable $k-\varepsilon$ model) have been validated against the experimental data of Al-Zubaydi and Hong [192]. The same channel that has

been used in the experiment [192] is replicated numerically in Fluent. Moreover, the experimental test conditions, i.e. flow velocity and air as the working fluid, have been used in the numerical model. The experimental and numerical pressure drop data are found close to each other with maximum difference 10 % as presented in Table 7.5.

Table 7.5. Comparison between experimental and numerical data of pressure drop.

Inlet velocity m/s	Pressure drop Experiment (Pa)	Pressure drop numerical (Pa)	Deviation %
0.6	3.5	3.16	9.71%
0.8	5.1	5.6	-9.80%
1.45	19	19.3	-1.58%
1.7	24.6	26.7	-8.54%
1.87	35.8	32.5	9.22%
2.05	39	39.1	-0.26%
2.3	45.9	49.5	-7.84%
2.63	60.5	65	-7.44%

7.6.2 Evaluation of thermo-hydraulic performance of HEs

The thermo-hydraulic performance of two modified FPHEs along with the $FPHE_C$ is numerically inspected. The results are compared with those of the $CPHE_C$ [175]. All four HEs have undergone the same conditions i.e. same material, and same boundary conditions. The geometrical dimensions (port diameters, length and width of the plates etc.) are also the same. The numerical tests are performed on single phase (hot water-cold water), steady flow, Re varies from 250 to 2000, and the calculations belong to the hot side as the process fluid for all HEs. The surfaces of all HEs are presented in Fig. 7.9.

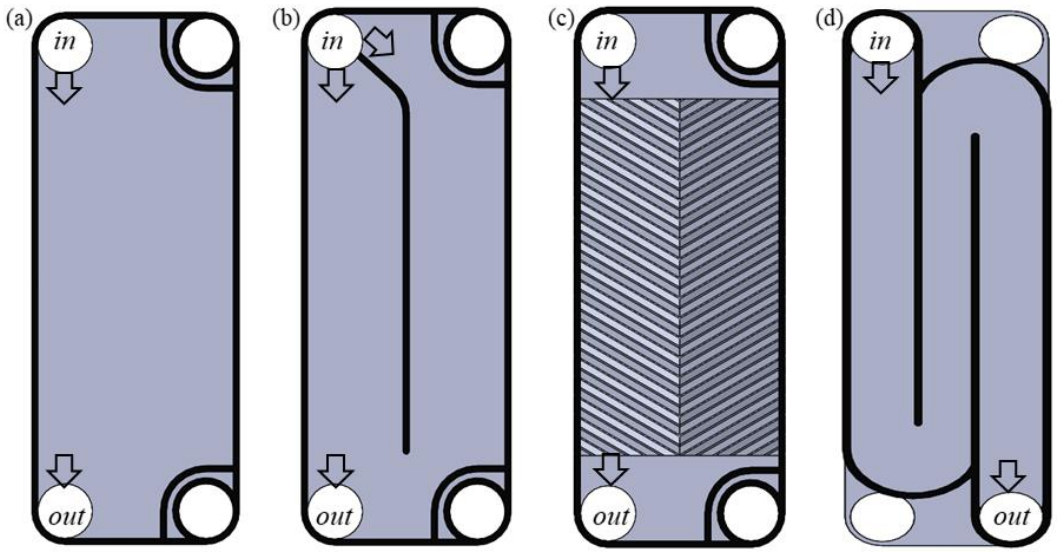

Fig. 7.9: Schematic drawing for thermal plates of , (a) $FPHE_C$., (b) $FPHE_{m1}$, (c) $CPHE_C$, and (d) $FPHE_{m2}$.

The Nu data for the cooling of the hot water inside the four tested HEs are presented in Fig. 7.10. Nu data of $FPHE_{m1}$ are almost identical with the Nu data of the $FPHE_C$. In addition, $FPHE_{m2}$ shows superior enhancement in the convective heat transfer rate in comparison with the other two FPHEs.

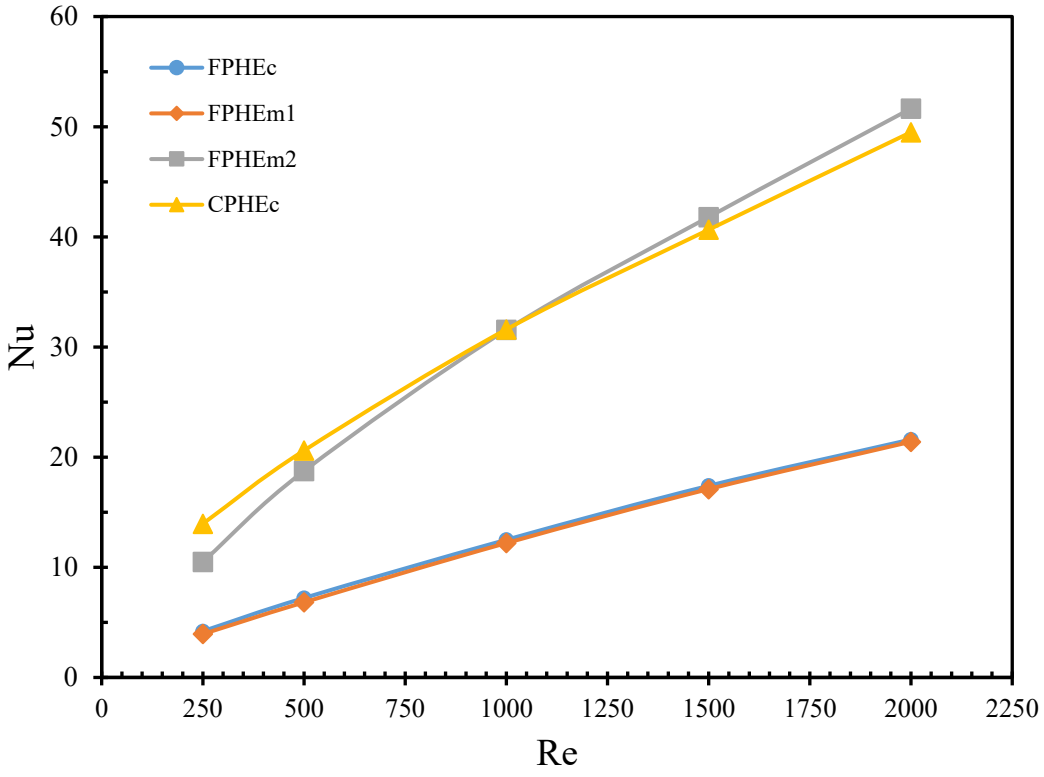

Fig. 7.10: Comparison of Nu data for different designs of the PHE.

The data of the Nu of $FPHE_{m2}$ and $CPHE_C$ are close to each other. For 250 < Re < 1000, Nu data of $FPHE_{m2}$ are less than those of the $CPHE_C$, and Nu data of these two HEs intersect at Re = 1000. For Re > 1000, Nu data of the $FPHE_{m2}$ are higher than those of the $CPHE_C$. That is because the flow inside the $FPHE_{m2}$ probably become turbulent, as is explained in the forthcoming discussion.

The increase in the convective heat transfer occurs at the expense of increase in pressure drop. The fanning friction factor (*f*) is used in the current study as a metric of pressure drop. Fig. 7.11(a) shows *f* data of the hot water for all HEs. The trends of both $FPHE_{m1}$ and $FPHE_C$ are almost identical, where the difference between them is insignificant, and their *f* data values are the lowest. On the other hand, the *f* data of the $FPHE_{m2}$ and the $CPHE_C$ are respectively up to 16 and 27 times greater than those of the $FPHE_{m1}$ and $FPHE_C$. Furthermore, the *f* data of the $CPHE_C$ are 18.7% to 33.2% greater than those of the $FPHE_{m2}$ for all Re range.

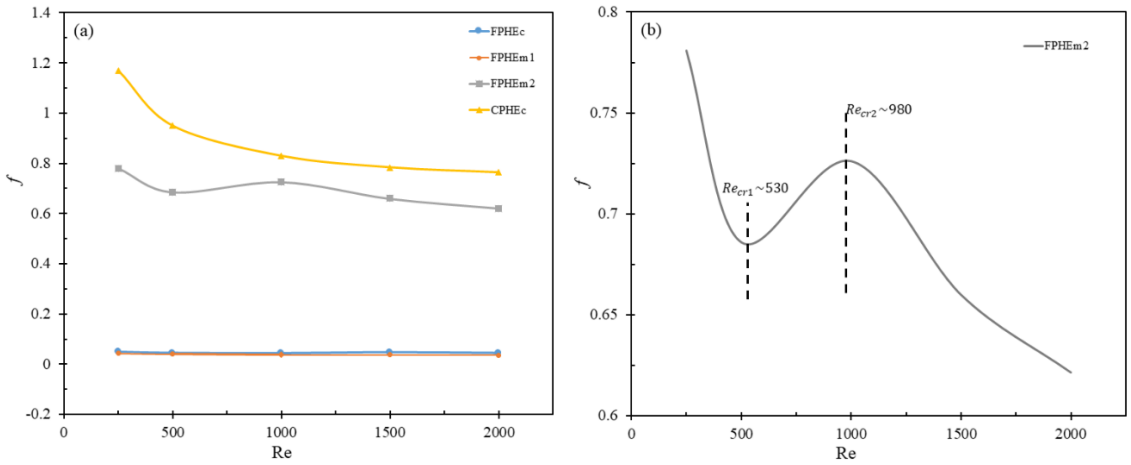

Fig. 7.11: (a) Comparison of *f* data for different designs of the PHE, and (b) *f* data for $FPHE_{m2}$ alone.

Fig. 7.11(a) shows that the trends of *f* data for all HEs are decreasing as Re increases except for $FPHE_{m2}$. It has been reported that, the flow in the $FPHE_C$ is likely laminar for Re < 2000 [191]. However, this might not be applicable in the case of $FPHE_{m2}$. Fig. 7.11(b) shows the flow is probably laminar for Re < 530, after that, steep increase takes place for $Re_{cr1} \leq Re \leq Re_{cr2}$. The flow transition inside the channels of the $FPHE_{m2}$ is most likely taking place due to the existence of the rotating paths, as shown in Fig. 7.2(a) and Fig. 7.9(d). These rotating paths cause formation of vortices, as shown in Fig. 7.14(b) which will expedite the boundary layer separation and consequently this will enhance the

disturbance of the fluid flow, causing both more heat transfer rate and pressure drop. The point at which the secondary transition ends (onset point of turbulent flow) is usually unclear [194]. However, the *f* data trend of the $FPHE_{m2}$ is stably decreasing for Re > 980. Thus, this could insinuate that the flow is leaving the transition zone ($Re_{cr1} \leq Re \leq Re_{cr2}$) to the turbulent one at Re > 980. Yet, experimental visualization is needed to confirm the type of flow inside the channels of $FPHE_{m2}$. The approach used in this study to identify the critical Re is well-known in the literature and has been implemented in other studies i.e. [194, 195].

To depict the fluid flow distribution characteristics, Fig. 7.12 shows streamlines of the fluid flow inside the middle hot channel (between two cold channels) for $FPHE_{m1}$ and $FPHE_C$ at Re = 1000. The flow inside the channels of the $FPHE_{m1}$ and the $FPHE_C$ has a similar pattern, where it tends to flow away from the centre of the channel toward its sides as shown in Fig. 7.12(c).

Moreover, it can be seen from Fig. 7.13 that the flow of the $CPHE_C$ also shows tendency to flow away from the centre of the corrugated channel because of the contact points. Similar findings of fluid pattern have been reported in the literature [141]. In addition, even though the fluid is not distributing perfectly inside the channel of the $FPHE_{m2}$, it shows the best flow distribution pattern among all four HEs, as shown in Fig. 7.14(a). In fact, an essential aim of the channel design of $FPHE_{m1}$ and $FPHE_{m2}$ is to control the direction of the fluid flow to achieve better fluid flow distribution. However, this aim has been partially fulfilled in the $FPHE_{m2}$ but not for $FPHE_{m1}$ where the impact of modification is insignificant.

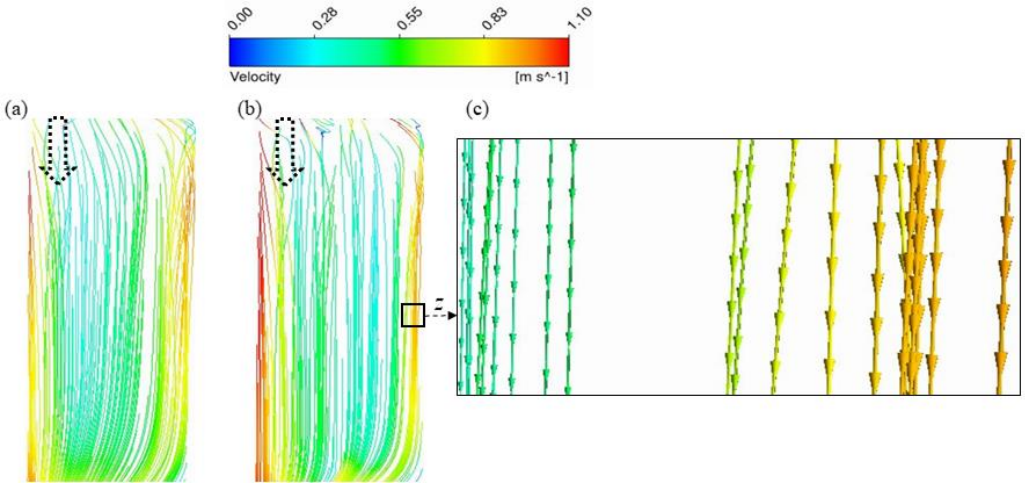

Fig. 7.12: Fluid flow distribution at Re = 1000 for (a) $FPHE_C$, (b) $FPHE_{m1}$, and (c) Magnified

streamlines at the left side of the $FPHE_{m1}$ channel.

Fig. 7.14 shows that the fluid inside the channels of the $FPHE_{m2}$ flows with the highest velocity among all HEs because the surface is divided into three regions. Thus, at the same mass flow rate, the fluid inside $FPHE_{m2}$ channel flows 3 to 4.5 times greater than those of the other three HEs. In addition, when fluid is flowing in a circular path, it experiences a centrifugal force that directs the flow outward away from the centre of the path. Hence the highest flow velocity takes place on the outer wall right after the bend as shown in Fig. 7.14(a).

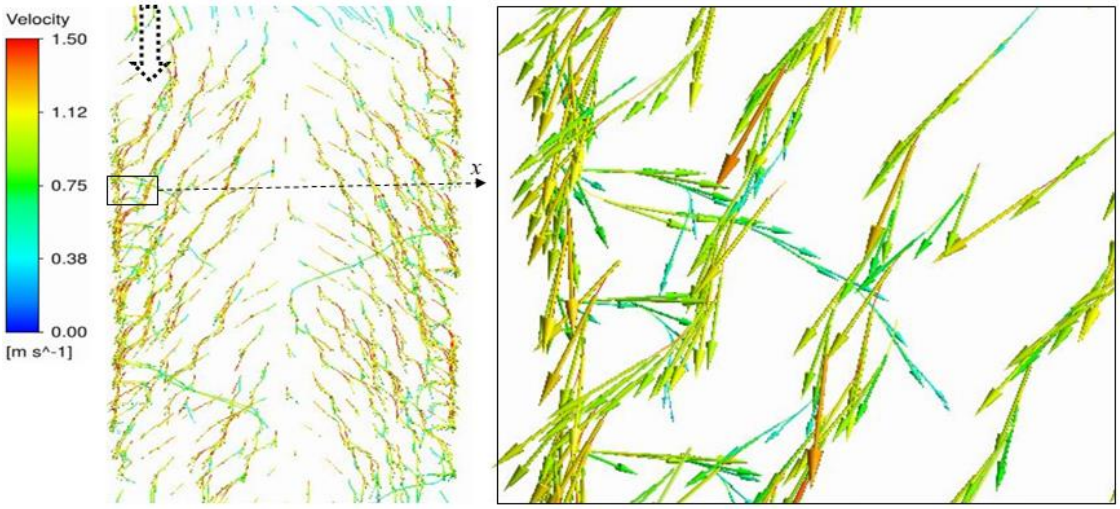

Fig. 7.13: Velocity vectors inside the middle hot channel of $CPHE_C$ at Re = 1000.

The turbulence intensity is an indicator of the ratio between the velocity fluctuations of the root-mean-square to the main flow velocity. Furthermore, as the turbulence intensity increases, the heat transfer rate increases [246]. Fig. 7.15 illustrates the turbulence intensity at the same hot channel (middle channel) at Re = 1000 for all four HEs. In addition, to find the average turbulence intensity inside these hot channels, three vertical lines are plotted inside them as shown in Fig. 7.16. Each line consists of 30 points, and the values of these points (90 points) are averaged (mean value) inside the hot channel of each HE, as presented in Table 7.6. The turbulence intensity average values of both $FPHE_{m1}$ and $FPHE_C$ are close to each other; they are 7.63% and 6.57%, respectively. On the other hand, the average turbulence intensity of the $CPHE_C$ is 16.6%. Its highest turbulence intensity is found to take place at the left side (entrance side) which refers to flow maldistribution inside this corrugated channel. It also has been found that several points along the three lines inside the corrugated channel yield zero turbulence intensity;

these points are likely contact points.

Table 7.6. Average values of turbulence intensity.

Type of HE	$FPHE_C$	$FPHE_{m1}$	$FPHE_{m2}$	$CPHE_C$
Turbulence Intensity %	6.57	7.63	20.56	16.65

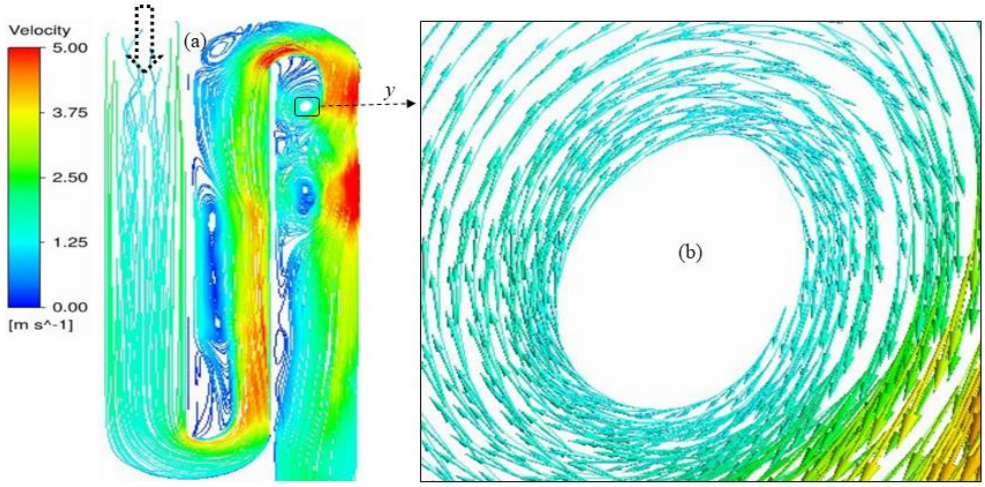

Fig. 7.14: Fluid flow distribution of $FPHE_{m2}$ at Re = 1000 for, (a) The entire channel, and (b) Magnified streamlines beyond the bend.

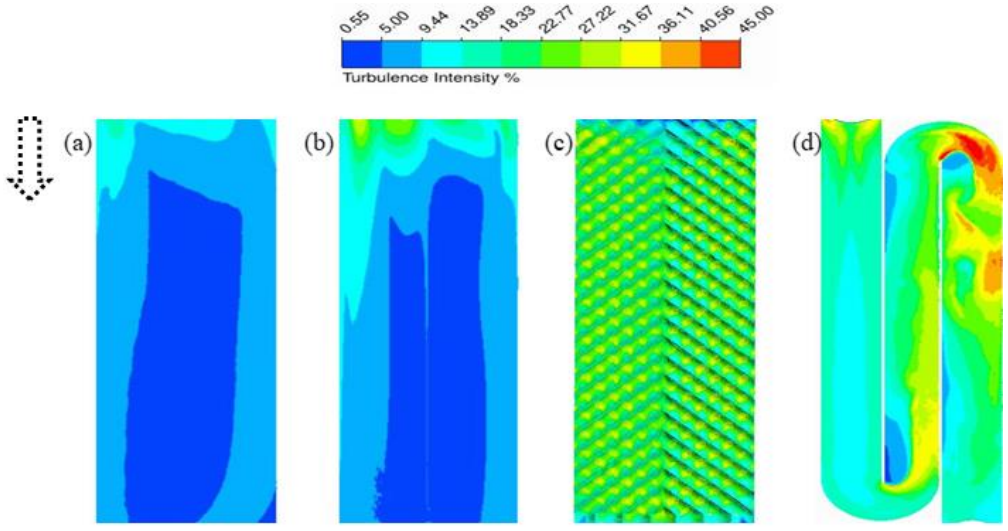

Fig. 7.15: Contours of turbulence intensity at Re = 1000 inside the middle hot channel of, (a) $FPHE_{C.}$, (b) $FPHE_{m1}$, (c) $CPHE_{C.}$, and (d) $FPHE_{m2}$.

In addition, Fig. 7.15(d) shows that the turbulence intensity inside the hot channel of the $FPHE_{m2}$ yields significant enhancement in comparison to that of the $FPHE_C$. The

turbulence intensity is to be considered high when it is greater than 10% [244]. Nevertheless, the average turbulence intensity inside the channel of the $FPHE_{m2}$ is found 20.6%. Moreover, from the field of the predicted turbulence intensity (Fig. 7.15(d)), it can be observed that the highest turbulence intensity takes place at the outer walls beyond the bends inside the channels of the $FPHE_{m2}$ which is consistent with the data shown in Fig. 7.14(a).

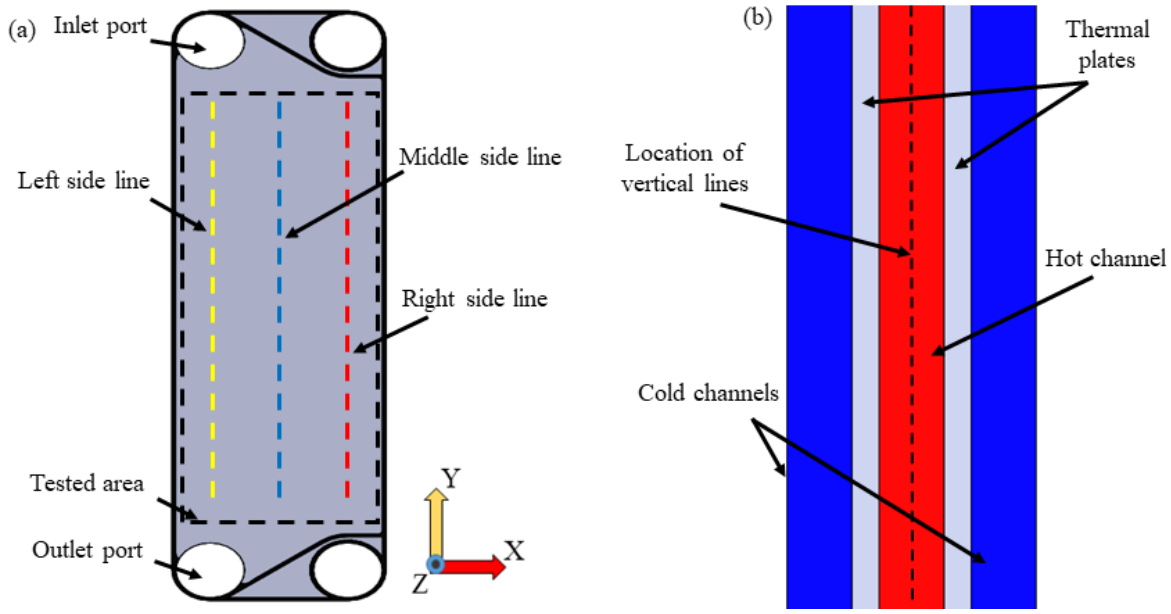

Fig. 7.16: Illustrative diagram for the direction of flow, location of the tested area, and location of the vertical lines to measure the turbulence intensity inside the middle hot channel, (a) Front view, and (b) Side view.

7.6.3 Effect of the design on temperature distribution and pumping power

The main purpose of indirect HEs such as PHEs is to allow the maximum amount of heat to be transferred through their walls at the possible minimum pumping power. In addition, one of the modern design criteria of HEs is to make sure the temperature of the HE's wall is as low as possible during the heat transfer process. The reasons of the significance of this criteria are:

- To reduce thermal stresses. These stresses affect the walls of the HE due to the presence of temperature gradient at these walls. Furthermore, they could cause the walls to change their shape (expansion/contraction), and with daily cycling, this would degrade the lifetime of the HE and the entire cycle where the HE is

employed. Thus, it is required to keep the temperature gradient of the wall surfaces as low as possible.

- Usually HEs are insulated (adiabatic), hence a heat exchange process is taking place between the fluids and the walls of HEs. Higher wall temperatures lead to lesser heat exchange process between the fluids on the sides of these walls and vice versa. Therefore, it is required to come up with novel ways to keep the temperatures of these walls as low as possible.

In addition to the above-mentioned metrics (Nu, *f*, turbulence intensity), three further criteria are considered to evaluate the overall performance of the HEs. The first one is the average temperature of the middle thermal plate (Tp,avg). Second criteria is the difference between the maximum and minimum temperature spots on the middle plate (ΔTp).

$$\Delta T_p = T_{p,max} - T_{p,min} \tag{7.16}$$

Both the first and the second criterion are measured from the same middle thermal plate that locates exactly between hot and cold water, as shown in Fig. 7.17. Moreover, these measures are taken by plotting three vertical lines at the middle of the thermal plate itself, as shown in Fig. 7.16(a). The same number of points that have been used in the case of turbulence intensity measurements, is also used for temperature measurements where each line consists of 30 points. The third criterion represents the measurements of the overall thermal performance (JF factor). JF factor is a ratio between the rate of the increase in the convective heat transfer to the rate of the increase in the pumping power, and it is calculated as:

$$JF = \frac{(j/j_o)}{(f/f_o)^{1/3}} \tag{7.17}$$

Where j_o and f_o are respectively j factor and fanning friction factor of the $FPHE_C$ (the baseline).

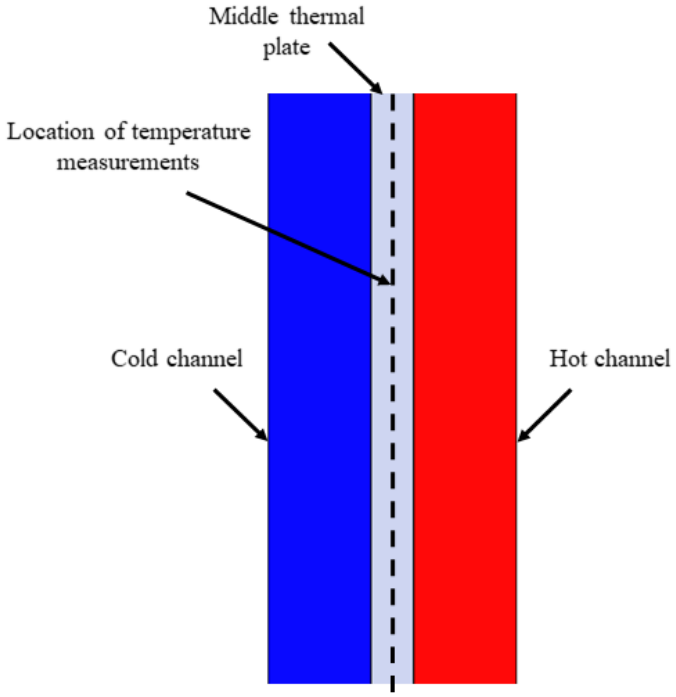

Fig. 7.17: Illustrative side view for the location of temperature measurements at the middle of the thermal plate.

The measurements of the maximum, minimum, and average temperatures inside the same location for all four HEs are presented in Table 7.7. These measurements are taken for Re 250, 1000, and 2000. ΔTp is employed as an indicator of the temperature gradient intensity throughout the plate. This ΔTp has been found to have the highest values in case of $CPHE_C$ for all Re range, which probably indicates severe randomness in flow distribution. In addition, the average temperatures (Tp,avg) of $FPHE_C$, $FPHE_{m1}$, and $CPHE_C$ are found increasing as Re increases, which is expected because as Re increases the effect of the viscous forces to dissipate heat decreases.

On the other hand, significant improvement in temperature measurements are achieved in the case of $FPHE_{m2}$. Its ΔTp is the lowest (best temperature distribution) where the difference with the closest ΔTp of other HEs is still significant. Also, Tp,avg in the case of $FPHE_{m2}$ is the lowest, and the change of Tp,avg with Re is insignificant. Furthermore, being Tp,min of $FPHE_{m2}$ the highest refers to best heat transfer process, which is likely due to the best flow distribution. Also, being Tp,max, ΔTp, and Tp,avg of the $FPHE_{m2}$ the lowest indicate that the best heat transfer process and the lowest thermal stresses are taking place throughout this HE.

Table 7.7. Results of temperature measurements for middle thermal plates of the tested PHEs.

Re	Type of HE	Tp,max (K)	Tp,min (K)	ΔTp (K)	Tp,avg (K)
250	$FPHE_C$	307.1	296.03	11.07	301.45
	$CPHE_C$	312.84	296.8	16.04	301.3
	FPHEm1	307.8	295.13	12.67	301.37
	FPHEm2	304.72	297.82	6.9	300.62
1000	$FPHE_C$	306.53	296.51	10.02	301.72
	$CPHE_C$	312.79	299.03	13.76	302.8
	FPHEm1	305.81	296.15	9.66	301.8
	FPHEm2	304.39	297.99	6.40	300.82
2000	$FPHE_C$	306.76	296.94	9.82	302.18
	$CPHE_C$	312.81	299.84	12.97	303.48
	FPHEm1	306.23	295.98	10.25	301.94
	FPHEm2	304.34	296.5	7.84	300.78

The rate of the enhancement in convective heat transfer to the rate of increase in the pumping power is shown in Fig. 7.18. JF factor has been employed to compare the overall performance of different HEs or configurations in the literature [40, 247-250].

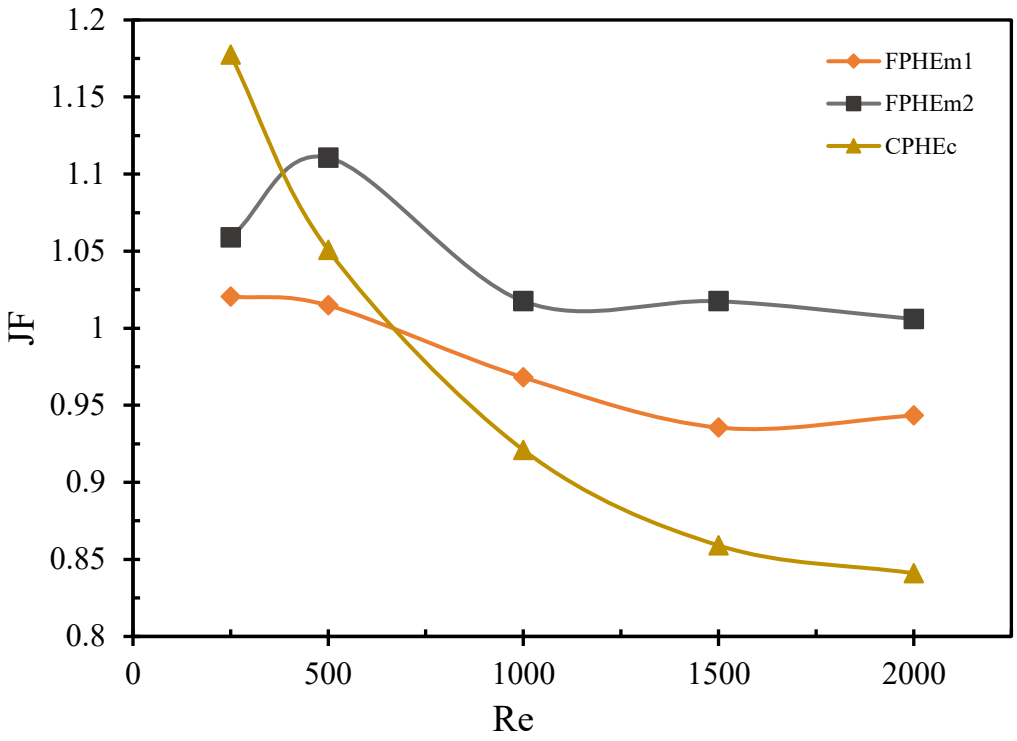

Fig. 7.18: JF data versus Re of the tested PHEs.

For Re = 250, Fig. 7.18 shows $CPHE_C$ can provide the highest JF. However, it has the lowest JF data right after Re > 670. The trend of JF data of $CPHE_C$ is decreasing as Re increases. Also, the amount of pumping power given to the $CPHE_C$ is greater than the rate of the heat removed, starting from Re > 670. In $CPHE_C$, the flow is likely turbulent for Re > 400 [176], thus it yields very high pressure drop, which causes low JF data. In addition, JF data of $FPHE_{m1}$ are generally better than those of the $CPHE_C$. However, because Nu and *f* data of $FPHE_{m1}$ and $FPHE_C$ (the baseline) are close to each other, JF data of $FPHE_{m1}$ are close to 1. Moreover, JF data of $FPHE_{m2}$ are generally the highest. At Re < 530, JF data of $FPHE_{m2}$ shows steep increasing and when Re is greater than 530 JF, data shows steep decreasing until Re = 980. The reason is probably that the flow is laminar at Re < 530, hence less pumping power is required (lower pressure drop), and the flow is probably in the transitional zone at 530 < Re < 980 as shown earlier, hence higher pressure drop is taking place. After that, the change in the JF data of $FPHE_{m2}$ is insignificant where the flow is most likely fully turbulent in this region, i.e. Re > 980.

7.6.4 Heat transfer correlations of $FPHE_{m2}$

Nu and *f* correlations have been developed in the turbulent region for $FPHE_{m2}$. These correlations are applicable for single-phase flow, and for 980 < Re < 2000. Nu and *f* correlations have been developed based on the Sieder [155] and Kumar [74] empirical correlations, respectively.

$$Nu = C_1 Re^p Pr^n \left(\frac{\mu}{\mu_w}\right)^{0.14} \tag{7.18}$$

$$f = C_2 Re^m \tag{7.19}$$

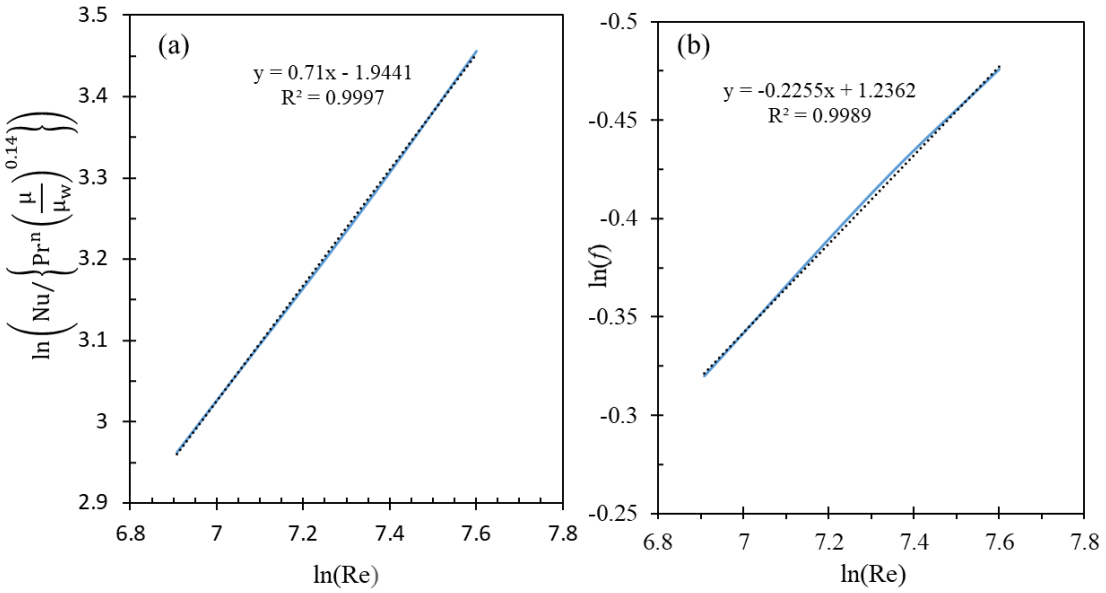

Fig. 7.19: Log-log scale of, (a) Nu data of $FPHE_{m2}$, and (b) f data $FPHE_{m2}$.

The correlations of Nu and *f* are extracted by performing curve fitting on Fig. 7.19(a) and (b), respectively. The maximum deviation between the data of correlations of Nu and *f* and the exact values are respectively 0.46% and 0.30%. Finally, Nu and *f* correlations of $FPHE_{m2}$ are:

$$Nu = 0.14311 Re^{0.71} Pr^{1/3} \left(\frac{\mu}{\mu_w}\right)^{0.14} \tag{7.20}$$

$$f = 3.444 Re^{-0.2255} \tag{7.21}$$

7.7 Conclusions

The thermal performance of two newly developed modified FPHEs have been investigated in this study. The results have been compared with those of the conventional corrugated and the conventional flat PHEs. All four HEs have the same dimensions and have been studied at the same physical conditions. The main findings can be drawn as follows:

- Nu data of $FPHE_{m2}$ are the highest except for Re < 530 where $CPHE_C$ yield the highest Nu data at this Re range. In addition, Nu and *f* data of $FPHE_{m1}$ and $FPHE_C$ are very close to each other, and they are the lowest.
- $CPHE_C$ is found to have the highest *f* data for all Re range. Its *f* data are 18.7% to 33.2% greater than those of the $FPHE_{m2}$. Moreover, critical Reynolds numbers of $FPHE_{m2}$ have been determined. The flow is found to be likely laminar at Re < 530 (Re_{cr1}), and turbulent at Re > 980 (Re_{cr2}).
- The fluid flow inside the channels of $FPHE_C$, $FPHE_{m1,}$ and $CPHE_C$ shows strong tendency to move toward the sides of these channels. At the same time, the flow inside the $FPHE_{m2}$'s channels shows best flow uniformity.
- The average turbulence intensity has been calculated by plotting three vertical lines distributed equally through the investigated channels. The average intensity inside the channel of $FPHE_{m2}$ is the highest; it is 1.2 to 3.1 greater than those of the other three HEs.
- The severity of temperature gradient (ΔTp), and the average temperature (Tp,avg) have been calculated inside middle thermal plate at different Reynolds numbers. Both ΔTp, and Tp,avg of $FPHE_{m2}$ are found to be the lowest at all investigated Re range, which indicates the best temperature distribution, and the lowest temperature gradient. Consequently, thermal plates of $FPHE_{m2}$ would be subjected to the lowest thermal stresses.
- At low Re i.e. Re < 380 JF data of $CPHE_C$ are the highest. After that, they sharply decrease as Re increases and become the lowest (JF < 1). Reversely, JF data of $FPHE_{m2}$ are generally the highest in comparison to those of $FPHE_{m1}$ and $CPHE_C$. They are greater than 1 for all Re range.

Based on all aforementioned parameters, $FPHE_{m1}$ is found to have poor thermal performance, which is very close to the thermal performance of $FPHE_C$. On the contrary, $FPHE_{m2}$ shows the most superior thermal performance, thus it could be a probable replacement of its counterparts. In $FPHE_{m2}$, fluids flow with higher velocities with respect to the $CPHE_C$, hence further studies could be conducted to investigate the fouling rate inside the channels of the $FPHE_{m2}$ where this rate probably will be mitigated.

Chapter 8: Conclusions and Recommendations

8.1 Conclusions

In this thesis, novel corrugated and flat plate heat exchangers have been presented for the first time. Due to the flaws of the active enhancement techniques (i.e. complexity in design, and large power consumption requirements), passive enhancement technique is the employed approach for all HEs that have been presented in this thesis.

To verify the superiority of these novel HEs, a CFD code has been adopted. Moreover, the code has been extensively validated with benchmark experimental studies from the open literature. Furthermore, an experiment is conducted for further validation of the used numerical approach. The maximum deviation is always found in an acceptable range i.e. maximum deviation < 15%.

All numerical models have been generated by using Solidworks software. A full CAD model approach is the one used. Each HE consists of five plates and four channels (two cold, and two hot channels). For accuracy purposes, the dimensions of the corrugations are fully controllable, and ports' effect have been considered. Thus, these CAD models can effectively reflect the physical phenomena that take place in real life. The meshes have been developed in ANSYS software. Several sophisticated mesh techniques have been adopted for the presented HEs in order to minimize the discretization errors. Moreover, all the models of the solver have been tested, and the realizable $k-\varepsilon$ with scalable wall treatment is found the best numerical model that can provide the most accurate data.

To assess the thermo-hydraulic performance of the HEs in this thesis, several quantitative and qualitative data are used. Turbulence kinetic energy, intensity of fluid flow maldistribution and turbulence intensity, along with other parameters, are used. However, the most common parameters that are used to assess the thermal performance of the HEs are Nusselt number (to assess the enhancement in the convective heat transfer), and fanning friction factor (to assess the pressure drop inside the HE's channels). To assure the accuracy of the comparisons among the investigated HEs, all HEs contain the same number of cold and hot channels, have identical dimensions, the same fluid properties, and stainless steel is appointed as the material of all HEs.

In general, five independent studies have been carried out to disclose the impact of the used passive techniques on the thermal performance of the PHEs. Briefly, the enhancement that has been achieved by each study could be concluded as follows:

- For the modified CPHE (Chapter 3, and Chapter 4), the enhancement in Nu and E are respectively up to 75%, and 42% in comparison with those of the conventional CPHE. The *f* data of the modified CPHEs are up to ~ 4.5 to 7 fold higher than those of the conventional CPHEs. Moreover, JF data of the modified CPHEs have been found 1.1 to 1.5 fold lower than those of the conventional CPHEs.
- For the modified FPHE (Chapter 5), the enhancement in Nu and JF factor are respectively up to 70%, and 9% in comparison with those the conventional FPHE.
- For the modified CPHE (Chapter 6), Nu, *f*, JF, and TKE are respectively 1.3, 1.7, 1.4, and 3.5 times those of the conventional CPHE.
- For the modified FPHE ($FPHE_{m2}$) (Chapter 7), Nu data are up to 2.7 times those of the conventional FPHE. Due to the high thermal performance of $FPHE_{m2}$, the findings have been compared with those of the conventional corrugated PHE. Although Nu data of $FPHE_{m2}$ are generally close to those of the conventional CPHE, its *f* data are ~ 18.7% to 33.2% fold lower than those of the conventional CPHE. Generally, $FPHE_{m2}$ has the best fluid flow distribution, the lowest thermal stresses, and the highest JF factor.

Accordingly, this thesis presents these novel PHEs to the users, the designers, and particularly the developers. The performance of these modified PHEs differs from one to another. That is unequivocally either due to the use of different type surfaces (corrugated/flat), or the different modification approaches. Thus, the selection of the PHE must be carefully performed as it depends on several parameters i.e. the heat duty of the desired application, and the available space.

8.2 Future Work

Although this thesis has introduced novel PHEs with thorough illustration, particularly in regard with heat transfer features, further studies could be performed to expand the understanding of all aspects of these PHEs. Some of the future suggestions are:

- All the proposed newly modified PHEs yield better heat transfer rates, hence their sizes can be further reduced. Therefore, further studies could be performed to disclose the difference in area density between the conventional and the modified PHEs.
- The newly modified PHEs offer larger contact areas between the consecutive thermal plates with respect to the conventional ones. Hence this would likely boost the mechanical integrity of the entire heat exchanger and maximize the allowable pressure drop. Therefore, new study is suggested to disclose the difference in mechanical integrity and maximum allowable pressure drop between the conventional and the modified PHEs.
- In study of $FPHE_{m2}$ (Chapter 7), further studies could be conducted to optimize the widths of the fluid flow paths inside the channels of the $FPHE_{m2}$.
- In all proposed modified PHEs, fluids flow with higher velocities with respect to those of the conventional channels at the same Reynolds numbers. This would likely result in fouling mitigation. Therefore, further study is suggested to disclose the difference in the fouling rates inside the modified and the conventional channels.
- Experiments are encouraged to be performed on the novel PHEs to disclose the deviation between the numerical and the experimental findings.

References

[1] D. Clark, Plate heat exchanger design and development. Brewer, 1976.

[2] H. Kumar. The plate heat exchanger: construction and design. in Institute of Chemical Engineering Symposium Series. 1984.

[3] R. Seligman, Surface heat exchange apparatus for fluids. 1935, Google Patents.

[4] R.S. Andhare, A. Shooshtari, S.V. Dessiatoun, and M.M. Ohadi, Heat transfer and pressure drop characteristics of a flat plate manifold microchannel heat exchanger in counter flow configuration. Applied Thermal Engineering, 2016. **96**: p. 178-189.

[5] J. Cerezo, M. Bourouis, M. Vallès, A. Coronas, and R. Best, Experimental study of an ammonia–water bubble absorber using a plate heat exchanger for absorption refrigeration machines. Applied thermal engineering, 2009. **29**(5-6): p. 1005-1011.

[6] M. Rajagopal, R. Dinesh Babu, V. Antony Aroul Raj, and R. Velraj, Investigation on phase change material-based flat plate heat exchanger modules for free cooling applications in energy-efficient buildings. Advances in Building Energy Research, 2017. **11**(2): p. 282-304.

[7] J.J. Chan, R. Best, J. Cerezo, M.A. Barrera, and F.R. Lezama, Experimental study of a bubble mode absorption with an inner vapor distributor in a plate heat exchanger-type absorber with NH3-LiNO3. Energies, 2018. **11**(8): p. 2137.

[8] J. Peng, F. Chen, L. Liu, Y. Ge, H. Wu, and W. Liu, Experimental Research on Plate Heat Exchanger in OTEC System. Journal of Applied Science and Engineering, 2020. **23**(1): p. 21r29.

[9] H. Jeong, J. Oh, and H. Lee, Experimental investigation of performance of plate heat exchanger as organic Rankine cycle evaporator. International Journal of Heat and Mass Transfer, 2020. **159**: p. 120158.

[10] O.P. Arsenyeva, L.L. Tovazhnyansky, P.O. Kapustenko, and G.L. Khavin, Optimal design of plate-and-frame heat exchangers for efficient heat recovery in process industries. Energy, 2011. **36**(8): p. 4588-4598.

[11] G.M.I. Inc., Heat exchanger market size, share & trends analysis report by product (plate & frame (brazed, gasketed, welded), shell & tube, air cooled), by end use

(chemical, power generation), by region, and segment forecasts, 2020 - 2027. 2019.

[12] G.M.I. Inc., Plate and frame heat exchangers market size, share & trends analysis report by product (gasketed, welded, brazed), by application (chemical, HVAC & refrigeration, power generation), and segment forecasts, 2020 - 2027. 2019.

[13] R. Shah, Compact heat exchanger technology and applications. Heat exchange engineering, 1991. **2**: p. 1-23.

[14] Z.H. Ayub, Plate heat exchanger literature survey and new heat transfer and pressure drop correlations for refrigerant evaporators. Heat Transfer Engineering, 2003. **24**(5): p. 3-16.

[15] A. Dewan, P. Mahanta, K.S. Raju, and P.S. Kumar, Review of passive heat transfer augmentation techniques. Proceedings of the Institution of Mechanical Engineers, Part A: Journal of Power and Energy, 2004. **218**(7): p. 509-527.

[16] 2014 World Energy Outlook, Executive Summary, Access date 08.11.2020 https://eneken.ieej.or.jp/data/5794.pdf.

[17] M. Reppich, Use of high performance plate heat exchangers in chemical and process industries. International Journal of Thermal Sciences, 1999. **38**(11): p. 999-1008.

[18] F. Harvey, Plate heat exchanger. 1936, Google Patents.

[19] 2017 International Energy Outlook, Executive Summary, Access date 08.11.2020 https://www.eia.gov/outlooks/ieo/pdf/exec_summ.pdf.

[20] N. Patel, Heat transfer. 2010: Alfa Lafa.

[21] T. Zaleski and K. Klepacka, Plate heat exchangers—method of calculation, charts and guidelines for selecting plate heat exchanger configurations. Chemical Engineering and Processing: Process Intensification, 1992. **31**(1): p. 49-56.

[22] Q. Li, G. Flamant, X. Yuan, P. Neveu, and L. Luo, Compact heat exchangers: A review and future applications for a new generation of high temperature solar receivers. Renewable and Sustainable Energy Reviews, 2011. **15**(9): p. 4855-4875.

[23] B. Sundén and R.M. Manglik, Plate heat exchangers: design, applications and performance. Vol. 11. 2007: Wit Press.

[24] S. Wand, Practical design tips for plate heat exchangers in ammonia refrigerants systems. Proceeding of the IIAR 16th Annual Meeting, St Louis, Missouri, 1994.

[25] M. Young, Plate heat exchangers as liquid cooling evaporators in ammonia refrigeration system. Proceeding of the IIAR 16th Annual Meeting, St Louis, 1994.

[26] R. Heavner, H. Kumar, and A. Wanniarachchi. Performance of an industrial plate heat exchanger: effect of chevron angle. in AICHE Symposium series. 1993. American Institute of Chemical Engineers.

[27] M. Bassiouny and H. Martin, Flow distribution and pressure drop in plate heat exchangers—II Z-type arrangement. Chemical Engineering Science, 1984. **39**(4): p. 701-704.

[28] M. Bassiouny and H. Martin, Flow distribution and pressure drop in plate heat exchangers—I U-type arrangement. Chemical Engineering Science, 1984. **39**(4): p. 693-700.

[29] S. Kandlikar and R. Shah, Multipass plate heat exchangers—effectiveness-NTU results and guidelines for selecting pass arrangements. Journal of Heat Transfer, 1989. **111**(2): p. 300-313.

[30] J. Huang, Performance analysis of plate heat exchangers used as refrigerant evaporators. 2011.

[31] R. Buonopane, R. Troupe, and J. Morgan, Heat transfer design method for plate heat exchangers. Chemical Engineering Progress, 1963. **59**(7): p. 57-61.

[32] B. Jackson and R. Troupe. Plate heat exchanger design by epsilon-NTU METHOD(Heat transfer effectiveness-number of transfer unit relations determined, using differential equations to obtain temperature profile of each channel in exchanger). in Chemical Engineering Progress, Symposium Series. 1966.

[33] F. Lawry, Plate-type heat exchangers. Chemical Engineering, 1959. **29**: p. 89-94.

[34] K. Raju and J. Bansal, Design of plate heat exchangers. Low Reynolds Number Flow Heat Exchangers, 1983: p. 932-913.

[35] A. Jarzebski and E. Wardas-Koziel, Dimensioning of plate heat exchangers to give minimum annual operating costs. Chemical Engineering Research and Design, 1985. **63**(4): p. 211-218.

[36] J.A. Gut and J.M. Pinto, Modeling of plate heat exchangers with generalized configurations. International Journal of Heat and Mass Transfer, 2003. **46**(14): p. 2571-2585.

[37] D. Dović, B. Palm, and S. Švaić, Generalized correlations for predicting heat transfer and pressure drop in plate heat exchanger channels of arbitrary geometry. International Journal of Heat and Mass Transfer, 2009. **52**(19-20): p. 4553-4563.

[38] A. Wright and P. Heggs, Rating calculation for plate heat exchanger effectiveness and pressure drop using existing performance data. Chemical Engineering Research and Design, 2002. **80**(3): p. 309-312.

[39] J. Lee and K.-S. Lee, Flow characteristics and thermal performance in chevron type plate heat exchangers. International Journal of Heat and Mass Transfer, 2014. **78**: p. 699-706.

[40] J. Lee and K.-S. Lee, Friction and Colburn factor correlations and shape optimization of chevron-type plate heat exchangers. Applied Thermal Engineering, 2015. **89**: p. 62-69.

[41] K. Okada, M. Ono, T. Tomimura, T. Okuma, H. Konno, and S. Ohtani, Design and heat transfer characteristics of new plate heat exchanger. Heat Transfer Japanese Research, 1972. **1**(1): p. 90-95.

[42] A. Muley and R. Manglik, Experimental study of turbulent flow heat transfer and pressure drop in a plate heat exchanger with chevron plates. Journal of Heat Transfer, 1999. **121**(1): p. 110-117.

[43] A. Savostin and A. Tikhonov, Investigation of characteristics of plate-type heating surfaces. Thermal Engineering, 1970. **17**(9): p. 113-122.

[44] L. Tovazhnyanski, P. Kapustenko, and V. Tsibulnik, Heat transfer and hydraulic resistance in channels of plate heat exchangers. Energetika, 1980. **9**(7): p. 123-125.

[45] A. Wanniarachchi, U. Ratnam, B. Tilton, and K. Dutta-Roy, Approximate correlations for chevron-type plate heat exchangers. 1995, American Society of Mechanical Engineers, New York, NY (United States).

[46] T. Khan, M. Khan, M.-C. Chyu, and Z. Ayub, Experimental investigation of single phase convective heat transfer coefficient in a corrugated plate heat exchanger for multiple plate configurations. Applied Thermal Engineering, 2010. **30**(8-9): p. 1058-1065.

[47] S. Al-Zahrani, M.S. Islam, and S.C. Saha, A thermo-hydraulic characteristics investigation in corrugated plate heat exchanger. Energy Procedia, 2019. **160**: p. 597-605.

[48] R. Crozier, J. Booth, and J. Stewart, Heat transfer in plate and frame heat exchangers. Chemical Engineering Progress, 1964. **60**(8): p. 43-45.

[49] W. Emerson, The Thermal and Hydrodynamic Performance of a Plate Heat Exchanger: Flat Plates-An APV Exchanger-A De Lavel Exchanger-A Rosenblad Exchanger. 1967: National Engineering Laboratory.

[50] W. Focke, J. Zachariades, and I. Olivier, The effect of the corrugation inclination angle on the thermohydraulic performance of plate heat exchangers. International Journal of Heat and Mass Transfer, 1985. **28**(8): p. 1469-1479.

[51] I. Gherasim, N. Galanis, and C.T. Nguyen, Heat transfer and fluid flow in a plate heat exchanger. Part II: Assessment of laminar and two-equation turbulent models. International Journal of Thermal Sciences, 2011. **50**(8): p. 1499-1511.

[52] J. Girstmair, A. Zakrzewski, F. Lapraz, M. Handberg-Thorsager, P. Tomancak, P.G. Pitrone, F. Simpson, and M.J. Telford, Light-sheet microscopy for everyone? Experience of building an OpenSPIM to study flatworm development. BMC Developmental Biology, 2016. **16**.

[53] M.M. Gobble, News and Analysis of the Global Innovation Scene. Research Technology Management, 2013. **56**(5): p. 2-8.

[54] J. Hesselgreaves, The impact of compact heat exchangers on refrigeration technology and CFC replacement, in ASHRAE-Purdue CFC Conference. 1990, 500-492.

[55] M.B. Kim and C.Y. Park, An experimental study on single phase convection heat transfer and pressure drop in two brazed plate heat exchangers with different chevron shapes and hydraulic diameters. Journal of Mechanical Science and Technology, 2017. **31**(5): p. 2559-2571.

[56] M.E. Steinke and S.G. Kandlikar. Single-phase heat transfer enhancement techniques in microchannel and minichannel flows. in ASME 2004 2nd International Conference on Microchannels and Minichannels. 2004. American Society of Mechanical Engineers.

[57] A.C. Talik, Heat transfer and pressure drop characteristics of a plate heat exchanger. 1995, Texas A&M University.

[58] B. Thonon, R. Vidil, and C. Marvillet, Recent research and developments in plate heat exchangers. Journal of Enhanced Heat Transfer, 1995. **2**(1-2).

[59] P. Vlasogiannis, G. Karagiannis, P. Argyropoulos, and V. Bontozoglou, Air–water two-phase flow and heat transfer in a plate heat exchanger. International Journal of Multiphase Flow, 2002. **28**(5): p. 757-772.

[60] R.L. Webb and N.-H. Kim, Principles Enhanced Heat Trans. 2004: Garland Science.

[61] J.T. Cieśliński, A. Fiuk, K. Typiński, and B. Siemieńczuk, Heat transfer in plate heat exchanger channels: Experimental validation of selected correlation equations. Archives of Thermodynamics, 2016. **37**(3): p. 19-29.

[62] E. Richter, Hausen, H., Wärmeübertragung im Gegenstrom, Gleichstrom und Kreuzstrom, 2., neubearb. Aufl., Berlin-Heidelberg-New York. Springer-Verlag. 1976. 429 S., 215 Abb., DM 148,–. US $60.70. ZAMM-Journal of Applied Mathematics and Mechanics/Zeitschrift für Angewandte Mathematik und Mechanik, 1979. **59**(4): p. 213-213.

[63] E. Sparrow and J. Comb, Effect of interwall spacing and fluid flow inlet conditions on a corrugated-wall heat exchanger. International Journal of Heat and Mass Transfer, 1983. **26**(7): p. 993-1005.

[64] M. Ciofalo, M. Collins, and J. Stasiek, Flow and heat transfer predictions in flow passages of air preheaters: assessment of alternative modelling approaches. Developments in Heat Transfer, 1997. **1997**: p. 169-225.

[65] I. Lioumbas, A. Mouza, and S. Paras, Local velocities inside the gas phase during counter-current two-phase flow in a narrow vertical channel. Chemical Engineering Research and Design, 2002. **80**(6): p. 667-673.

[66] T.S. Khan, M.S. Khan, and Z.H. Ayub, Single-phase flow pressure drop analysis in a plate heat exchanger. Heat transfer engineering, 2017. **38**(2): p. 256-264.

[67] D. Chisolm and A. Wanniarachchi, Maldistribution in single-pass mixed-channel plate heat exchangers. ASME, NEW YORK, NY(USA). 1992. **201**: p. 95-99.

[68] A.G. Kanaris, A.A. Mouza, and S.V. Paras, Flow and heat transfer prediction in a corrugated plate heat exchanger using a CFD code. Chemical Engineering & Technology, 2006. **29**(8): p. 923-930.

[69] M. Pantzali, A. Kanaris, K. Antoniadis, A. Mouza, and S. Paras, Effect of nanofluids on the performance of a miniature plate heat exchanger with modulated surface. International Journal of Heat and Fluid Flow, 2009. **30**(4): p. 699-691.

[70] Y.-C. Tsai, F.-B. Liu, and P.-T. Shen, Investigations of the pressure drop and flow distribution in a chevron-type plate heat exchanger. International Communications in Heat and Mass Transfer, 2009. **36**(6): p. 578-574.

[71] Z. Zhang and Y. Li, CFD simulation on inlet configuration of plate-fin heat exchangers. Cryogenics, 2003. **43**(12): p. 678-673.

[72] A. Kanaris, A. Mouza, and S. Paras, Flow and heat transfer in narrow channels with corrugated walls: a CFD code application. Chemical Engineering Research and Design, 2005. **83**(5): p. 460-468.

[73] S. Jain, A. Joshi, and P. Bansal, A new approach to numerical simulation of small sized plate heat exchangers with chevron plates. Journal of Heat Transfer, 2007. **129**(3): p. 291-297.

[74] H. Kumar. Evaporation in Plate Heat Exchangers. in AICHE Symposium Series. 1993. American Institute Of Chemical Enginners.

[75] G.F. Hewitt, G.L. Shires, and T.R. Bott, Process heat transfer. Vol. 113. 1994: CRC press Boca Raton, FL.

[76] R. Shah and W. Focke, Plate heat exchangers and their design theory. Heat Transfer Equipment Design, 1988. **227**(6): p. 254.

[77] G. Croce and P. d'Agaro, Numerical analysis of forced convection in plate and frame heat exchangers. International Journal of Numerical Methods for Heat & Fluid Flow, 2002. **12**(6): p. 756-771.

[78] S. O'Halloran and A. Jokar, CFD Simulation of Single-Phase Flow in Plate Heat Exchangers. ASHRAE Transactions, 2011. **117**(1).

[79] M. Asif, H. Aftab, H. Syed, M. Ali, and P. Muizz, Simulation of corrugated plate heat exchanger for heat and flow analysis. International Journal of Heat and Technology, 2017. **35**(1): p. 205-210.

[80] J. Skočilas and I. Palaziuk, CFD simulation of the heat transfer process in a chevron plate heat exchanger using the SST turbulence model. 2015.

[81] D.B. Wang, Z.X. Liang, J.J. Zhou, and H.B. Wang. The simulation research on the performance of chevron-type corrugated plate heat exchanger. in Advanced Materials Research. 2012. Trans Tech Publ.

[82] C. Guo, W. Du, and L. Cheng, Characteristics of heat transfer and resistance of double chevron plate heat exchanges with different corrugation pitch, in Business, Economics, Financial Sciences, and Management. 2012, Springer. p. 169-174.

[83] Y.H. Zhao, Y.F. Wu, H.J. Cheng, and G.L. Zhu. Numerical simulation of corrugated depth on the performance of plate heat exchanger. in Advanced Materials Research. 2014. Trans Tech Publ.

[84] Y. Zhicheng, W. Lijun, Y. Zhaokuo, and L. Haowen, Shape optimization of welded plate heat exchangers based on grey correlation theory. Applied Thermal Engineering, 2017. **123**: p. 761-769.

[85] Y. Zhao, Y. Wu, H. Cheng, and G. Zhu. Numerical simulation of corrugated inclination angle on the performance of plate heat exchanger. in 2014 International Conference on Mechatronics, Electronic, Industrial and Control Engineering (MEIC-14). 2014. Atlantis Press.

[86] M. Kan, O. Ipek, and B. Gurel, Plate heat exchangers as a compact design and optimization of different channel angles. Acta Physica Polonica A, 2015. **12**: p. 49-52.

[87] L. Vafajoo, K. Moradifar, S.M. Hosseini, and B. Salman, Mathematical modelling of turbulent flow for flue gas–air Chevron type plate heat exchangers. International Journal of Heat and Mass Transfer, 2016. **97**: p. 596-602.

[88] K. Sarraf, S. Launay, and L. Tadrist, Complex 3D-flow analysis and corrugation angle effect in plate heat exchangers. International Journal of Thermal Sciences, 2015. **94**: p. 126-138.

[89] A.G. Kanaris, A.A. Mouza, and S.V. Paras, Flow and heat transfer prediction in a corrugated plate heat exchanger using a CFD code. Chemical Engineering & Technology: Industrial Chemistry-Plant Equipment-Process Engineering-Biotechnology, 2006. **29**(8): p. 923-930.

[90] J. Lee and K.-S. Lee, Correlations and shape optimization in a channel with aligned dimples and protrusions. International Journal of Heat and Mass Transfer, 2013. **64**: p. 444-451.

[91] W. Han, K. Saleh, V. Aute, G. Ding, Y. Hwang, and R. Radermacher, Numerical simulation and optimization of single-phase turbulent flow in chevron-type plate heat exchanger with sinusoidal corrugations. HVAC&R Research, 2011. **17**(2): p. 186-197.

[92] J. Jayakumar, S. Mahajani, J. Mandal, P. Vijayan, and R. Bhoi, Experimental and CFD estimation of heat transfer in helically coiled heat exchangers. Chemical engineering research and design, 2008. **86**(3): p. 221-232.

[93] A. Abbas, H. Lee, A. Sengupta, and C.-C. Wang, Numerical investigation of thermal and hydraulic performance of shell and plate heat exchanger. Applied Thermal Engineering, 2020. **167**: p. 114705.

[94] Y. Zhang, C. Jiang, Z. Yang, Y. Zhang, and B. Bai, Numerical study on heat transfer enhancement in capsule-type plate heat exchangers. Applied Thermal Engineering, 2016. **108**: p. 1237-1242.

[95] J. Song, F. Wang, and L. Cheng, Experimental study and analysis of a novel multi-media plate heat exchanger. Science China Technological Sciences, 2012. **55**(8): p. 2157-2162.

[96] W. Li, Y. Yan, S. Shen, and Y. Hai. C565/027/99 An investigation on heat transfer performance of a new type of plate heat exchanger with dimples. in IMECHE Conference Transactions. 1999. Mechanical Engineering Publications.

[97] C. Ji, L. Wu, J. Li, and X. Wang. Experimental research on heat transfer characteristics of Dimple plate heat exchanger. in 5th International Conference on Advanced Design and Manufacturing Engineering. 2015. Atlantis Press.

[98] A.M. Alqutub, M.T. Linjawi, and I.M. Alrawi. Performance Study of a Dimpled-Protruded Air-to-Air Plate Heat Exchanger. in ASME Power Conference. 2015. American Society of Mechanical Engineers.

[99] W. Du, F. Wang, G. Xin, S. Zhang, and L. Cheng. Numerical Investigation and Thermodynamic Analysis on a Novel Regular Hexagonal Plate Heat Exchanger. in International Heat Transfer Conference. 2010.

[100] J.Y. Jeong, H. ki Hong, S.K. Kim, and Y.T. Kang, Impact of plate design on the performance of welded type plate heat exchangers for sorption cycles. International journal of refrigeration, 2009. **32**(4): p. 705-711.

[101] A. Durmuş, H. Benli, İ. Kurtbaş, and H. Gül, Investigation of heat transfer and pressure drop in plate heat exchangers having different surface profiles. International Journal of Heat and Mass Transfer, 2009. **52**(5-6): p. 1451-1457.

[102] C. Zhang, D. Wang, Y. Han, Y. Zhu, and X. Peng, Experimental and numerical investigation on the exergy and entransy performance of a novel plate heat exchanger. Experimental Heat Transfer, 2017. **30**(2): p. 162-177.

[103] N. Azhagcsan, P. Balachandran, and A. Haq, Heat transfer characteristics and pressure drop in bubble finned plate heat exchanger and correlation development. Int. J. Heat Technol., 2007. **25**: p. 1-8.

[104] H.H.S. Villanueva and P.E.B. de Mello, Heat transfer and pressure drop correlations for finned plate ceramic heat exchangers. Energy, 2015. **88**: p. 118-125.

[105] D.B. Monteiro and P.E.B. de Mello, Thermal performance and pressure drop in a ceramic heat exchanger evaluated using CFD simulations. Energy, 2012. **45**(1): p. 489-496.

[106] K. Nilpueng and S. Wongwises, Experimental study of single-phase heat transfer and pressure drop inside a plate heat exchanger with a rough surface. Experimental Thermal and Fluid Science, 2015. **68**: p. 268-275.

[107] K. Nilpueng, T. Keawkamrop, H.S. Ahn, and S. Wongwises, Effect of chevron angle and surface roughness on thermal performance of single-phase water flow inside a plate heat exchanger. International Communications in Heat and Mass Transfer, 2018. **91**: p. 201-209.

[108] J. Wajs and D. Mikielewicz. Effect of surface roughness on thermal-hydraulic characteristics of plate heat exchanger. in Key Engineering Materials. 2014. Trans Tech Publ.

[109] J. Wajs and D. Mikielewicz, Influence of metallic porous microlayer on pressure drop and heat transfer of stainless steel plate heat exchanger. Applied Thermal Engineering, 2016. **93**: p. 1337-1346.

[110] A.E. Bergles, J.H. Lienhard V, G.E. Kendall, and P. Griffith, Boiling and evaporation in small diameter channels. Heat Transfer Engineering, 2003. **24**(1): p. 40-18.

[111] R.K. Shah and D.P. Sekulic, Fundamentals of heat exchanger design. 2003: John Wiley & Sons.

[112] A.E. Bergles, J.H. Lienhard V, G.E. Kendall, and P. Griffith, Boiling and evaporation in small diameter channels. Heat transfer engineering, 2003. **24**(1): p. 18-40.

[113] F.-B. Liu and Y.-C. Tsai, An experimental and numerical investigation of fluid flow in a cross-corrugated channel. Heat and mass transfer, 2010. **46**(5): p. 585-593.

[114] S. Kakac, H. Liu, and A. Pramuanjaroenkij, Heat exchangers: selection, rating, and thermal design. 2002: CRC press.

[115] M.-A. Hessami, An experimental investigation of the performance of cross-corrugated plate heat exchangers. Journal of enhanced heat transfer, 2003. **10**(4).

[116] A. Kanaris, A. Mouza, and S. Paras, Optimal design of a plate heat exchanger with undulated surfaces. International Journal of Thermal Sciences, 2009. **48**(6): p. 1184-1195.

[117] B. Kılıç and O. İpek, Experimental investigation of heat transfer and effectiveness in corrugated plate heat exchangers having different chevron angles. Heat and Mass Transfer, 2017. **53**(2): p. 725-731.

[118] Y.-S. Lee, C.-C. Su, Y.-M. Sun, and J.-C. Ye, Experimental study on heat transfer in wavy channels. Journal of Enhanced Heat Transfer, 2003. **10**(1).

[119] J. Lin, C. Huang, and C. Su, Dimensional analysis for the heat transfer characteristics in the corrugated channels of plate heat exchangers. International communications in heat and mass transfer, 2007. **34**(3): p. 304-312.

[120] J. Yang, A. Jacobi, and W. Liu, Heat transfer correlations for single-phase flow in plate heat exchangers based on experimental data. Applied Thermal Engineering, 2017. **113**: p. 1547-1557.

[121] H. Martin, A theoretical approach to predict the performance of chevron-type plate heat exchangers. Chemical Engineering and Processing: Process Intensification, 1996. **35**(4): p. 301-310.

[122] A. Cooper and J.D. Usher, Heat exchanger design handbook, in Method Surf. Area Calc. 1983, VDI-Verlag, Hemisphere Publishing Ltd.

[123] I. Maria, heat transfer to non-newtonian food fluids in plate heat exchanger, in Chemical and biological engineering. 2012, University of Porto.

[124] S. Kakac, H. Liu, and A. Pramuanjaroenkij, Heat exchangers: selection, rating, and thermal design. 2012: CRC press.

[125] K. Raju and J. Chand, Consider the plate heat-exchanger. Chemical Engineering, 1980. **87**(16): p. 133-144.

[126] M. Reppich, Use of high performance plate heat exchangers in chemical and process industries. International Journal of Thermal Sciences, 1999. **38**(11): p. 1008-1999.

[127] K. Rafferty, Direct use geothermal applications for brazed plate heat exchangers. 1992, Oregon Inst. of Tech., Klamath Falls, OR (United States). Geo-Heat Center.

[128] A. Engineering. Proper cleaning procedure for the brazed plate evaporator. 1995, July 14; Available from: https://www.advantageengineering.com/fyi/149/pdf/advantageFYI149.pdf.

[129] Z.H. Ayub, Plate heat exchanger literature survey and new heat transfer and pressure drop correlations for refrigerant evaporators. Heat Transfer Engineering, 2003. **24**(5): p. 16-13.

[130] M. Mehrabian, Construction, performance, and thermal design of plate heat exchangers. Proceedings of the Institution of Mechanical Engineers, Part E: Journal of Process Mechanical Engineering, 2009. **223**(3): p. 123-131.

[131] P. Heggs, P. Sandham, R. Hallam, and C. Walton, Local transfer coefficients in corrugated plate heat exchanger channels. Chemical Engineering Research and Design, 1997. **75**(7): p. 641-645.

[132] J. Zhang, X. Zhu, M.E. Mondejar, and F. Haglind, A review of heat transfer enhancement techniques in plate heat exchangers. Renewable and Sustainable Energy Reviews, 2019. **101**: p. 305-328.

[133] G. Biswas, K. Torii, D. Fujii, and K. Nishino, Numerical and experimental determination of flow structure and heat transfer effects of longitudinal vortices in a channel flow. International Journal of Heat and Mass Transfer, 1996. **39**(16): p. 3441-3451.

[134] P. Saha, G. Biswas, and S. Sarkar, Comparison of winglet-type vortex generators periodically deployed in a plate-fin heat exchanger–A synergy based analysis. International Journal of Heat and Mass Transfer, 2014. **74**: p. 292-305.

[135] A. Sinha, K.A. Raman, H. Chattopadhyay, and G. Biswas, Effects of different orientations of winglet arrays on the performance of plate-fin heat exchangers. International Journal of Heat and Mass Transfer, 2013. **57**(1): p. 202-214.

[136] L. Sirovich and S. Karlsson, Turbulent drag reduction by passive mechanisms. Nature, 1997. **388**(6644): p. 753.

[137] T. Rush, T. Newell, and A. Jacobi, An experimental study of flow and heat transfer in sinusoidal wavy passages. International journal of heat and mass transfer, 1999. **42**(9): p. 1541-1553.

[138] C.-C. Wang, W.-S. Lee, and W.-J. Sheu, A comparative study of compact enhanced fin-and-tube heat exchangers. International Journal of Heat and Mass Transfer, 2001. **44**(18): p. 3565-3573.

[139] B.P. Rao and S.K. Das, An experimental study on the influence of flow maldistribution on the pressure drop across a plate heat exchanger. Journal of Fluids Engineering, 2004. **126**(4): p. 680-691.

[140] R. Troupe, J. Morgan, and J. Prifiti, The plate heater versatile chemical engineering tool. Chemical Engineering Progress, 1960. **56**(1): p. 124-128.

[141] A. Lozano, F. Barreras, N. Fueyo, and S. Santodomingo, The flow in an oil/water plate heat exchanger for the automotive industry. Applied Thermal Engineering, 2008. **28**(10): p. 1109-1117.

[142] Y.-C. Tsai, F.-B. Liu, and P.-T. Shen, Investigations of the pressure drop and flow distribution in a chevron-type plate heat exchanger. International communications in heat and mass transfer, 2009. **36**(6): p. 574-578.

[143] E. Elshafei, M. Awad, E. El-Negiry, and A. Ali, Heat transfer and pressure drop in corrugated channels. Energy, 2010. **35**(1): p. 101-110.

[144] R. Gugulothu, K.V.K. Reddy, N.S. Somanchi, and E.L. Adithya, A review on enhancement of heat transfer techniques. Materials Today: Proceedings, 2017. **4**(2): p. 1051-1056.

[145] D. Walraven, B. Laenen, and W. D'haeseleer, Comparison of shell-and-tube with plate heat exchangers for the use in low-temperature organic Rankine cycles. Energy conversion and management, 2014. **87**: p. 227-237.

[146] Ansys, Ansys fluent 12.0 user's guide. 2009.

[147] F. Menter and T. Esch. Elements of industrial heat transfer predictions. in 16th Brazilian Congress of Mechanical Engineering (COBEM). 2001. sn.

[148] D.C. Wilcox, Formulation of the kw turbulence model revisited. AIAA journal, 2008. **46**(11): p. 2823-2838.

[149] I. Gherasim, M. Taws, N. Galanis, and C.T. Nguyen, Heat transfer and fluid flow in a plate heat exchanger part I. Experimental investigation. International Journal of Thermal Sciences, 2011. **50**(8): p. 1492-1498.

[150] B. Thonon. Design method for plate evaporators and condensers. in BHR Group Conference Series Publication. 1995. Mechanical Engineering Publications Limited.

[151] E. Sparrow and L. Hossfeld, Effect of rounding of protruding edges on heat transfer and pressure drop in a duct. International Journal of Heat and Mass Transfer, 1984. **27**(10): p. 1715-1723.

[152] H. Blomerius and N. Mitra, Numerical investigation of convective heat transfer and pressure drop in wavy ducts. Numerical Heat Transfer: Part A: Applications, 2000. **37**(1): p. 37-54.

[153] S. Won and P. Ligrani, Comparisons of flow structure and local Nusselt numbers in channels with parallel-and crossed-rib turbulators. International journal of heat and mass transfer, 2004. **47**(8-9): p. 1573-1586.

[154] W. Focke and P. Knibbe, Flow visualization in parallel-plate ducts with corrugated walls. Journal of Fluid Mechanics, 1986. **165**: p. 73-77.

[155] E.N. Sieder and G.E. Tate, Heat transfer and pressure drop of liquids in tubes. Industrial & Engineering Chemistry, 1936. **28**(12): p. 1429-1435.

[156] G. Longo and A. Gasparella, Refrigerant R134a vaporisation heat transfer and pressure drop inside a small brazed plate heat exchanger. International journal of refrigeration, 2007. **30**(5): p. 821-830.

[157] A. Talik, L. Fletcher, N. Anand, and L. Swanson, Heat transfer and pressure drop characteristics of a plate heat exchanger using a propylene-glycol/water mixture as the working fluid. 1995, American Society of Mechanical Engineers, New York, NY (United States).

[158] S. Jin and P. Hrnjak, Effect of end plates on heat transfer of plate heat exchanger. International Journal of Heat and Mass Transfer, 2017. **108**: p. 740-748.

[159] P.J. Heggs and H.-J. Scheidat, Thermal performance of plate heat exchangers with flow maldistribution. ASME, New York, NY(USA). 1992. **201**: p. 87-93.

[160] S. Mohebbi and F. Veysi, An experimental investigation on the heat transfer and friction coefficients of a small plate heat exchanger with chevron angle. Heat and Mass Transfer, 2020. **56**(3): p. 849-858.

[161] B. Kumar and S. Singh, Study of pressure drop in single pass U-type plate heat exchanger. Experimental Thermal and Fluid Science, 2017. **87**: p. 40-49.

[162] B. Kumar, A. Soni, and S. Singh, Effect of geometrical parameters on the performance of chevron type plate heat exchanger. Experimental Thermal and Fluid Science, 2018. **91**: p. 126-133.

[163] K.G. Patel, U.S. Modi, P.D. Panchal, and S.L. Padalia, Heat Transfer Analysis of Corrugated Plate Heat Exchanger. IJRAR-International Journal of Research and Analytical Reviews (IJRAR), 2019. **6**(2): p. 59-64-59-64.

[164] R. Shanmugam and C.R. William, Comparative study of Nusselt number for a single phase fluid flow using plate heat exchanger. Thermal Science, 2016. **20**(suppl. 4): p. 929-935.

[165] M. Asadi and R.H. Khoshkhoo, Effects of chevron angle on thermal performance of corrugated plate heat exchanger. International Journal of Engineering Practical Research, 2014. **3**(1): p. 8.

[166] S. Sohn, J.-H. Shin, J. Kim, S.H. Yoon, and K.H. Lee, A Numerical Study on the Pressure Drop and Heat Transfer in the Hot Channel of Plate heat Exchanger with Chevron Shape. Korean Journal of Air-Conditioning and Refrigeration Engineering, 2018. **30**(4): p. 175-185.

[167] S. Al-Zahrani, M.S. Islam, and S.C. Saha, Heat transfer augmentation in retrofitted corrugated plate heat exchanger. International Journal of Heat and Mass Transfer, 2020. **161**: p. 120226.

[168] B. Gürel, V.R. Akkaya, M. Göltaş, Ç.N. Şen, O.V. Güler, M.İ. Koşar, and A. Keçebaş, Investigation on flow and heat transfer of compact brazed plate heat exchanger with lung pattern. Applied Thermal Engineering, 2020: p. 115309.

[169] M. Kim, Y.-J. Baik, S.-R. Park, H.-S. Ra, and H. Lim, Experimental study on corrugated cross-flow air-cooled plate heat exchangers. Experimental thermal and fluid science, 2010. **34**(8): p. 1265-1272.

[170] M. Piper, A. Olenberg, J. Tran, and E. Kenig, Determination of the geometric design parameters of pillow-plate heat exchangers. Applied Thermal Engineering, 2015. **91**: p. 1168-1175.

[171] V. Dvořák and T. Vít, Numerical investigation of counter flow plate heat exchanger. Energy Procedia, 2015. **83**: p. 341-349.

[172] M. Pipathattakul, O. Mahian, A.S. Dalkilic, and S. Wongwises, Effects of the gap size on the flow pattern maps in a mini-gap annular channel. Experimental thermal and fluid science, 2014. **57**: p. 420-424.

[173] R.Y. Miura, F.C. Galeazzo, C.C. Tadini, and J.A. Gut, The effect of flow arrangement on the pressure drop of plate heat exchangers. Chemical Engineering Science, 2008. **63**(22): p. 5386-5393.

[174] B.P. Rao and S.K. Das, Effect of flow distribution to the channels on the thermal performance of the multipass plate heat exchangers. Heat Transfer Engineering, 2004. **25**(8): p. 48-59.

[175] S. Al-Zahrani, M.S. Islam, F. Xu, and S.C. Saha, Thermal performance investigation in a novel corrugated plate heat exchanger. International Journal of Heat and Mass Transfer, 2020. **148**: p. 119095.

[176] R. Shah and W. Focke, Plate heat exchangers and their design theory. Heat Transfer Equipment Design, 1988. **227**: p. 254.

[177] X. Zhu and F. Haglind, Relationship between inclination angle and friction factor of chevron-type plate heat exchangers. International Journal of Heat and Mass Transfer, 2020. **162**: p. 120370.

[178] S.K. Saha and A.H. Khan, Numerical Study on the Effect of Corrugation Angle on Thermal Performance of Cross Corrugated Plate Heat Exchangers. Thermal Science and Engineering Progress, 2020: p. 100711.

[179] A. Sharif, B. Ameel, I. T'Jollyn, S. Lecompte, and M. De Paepe, Comparative performance assessment of plate heat exchangers with triangular corrugation. Applied Thermal Engineering, 2018. **141**: p. 186-199.

[180] Y. Wang, F. Houshmand, D. Elcock, and Y. Peles, Convective heat transfer and mixing enhancement in a microchannel with a pillar. International Journal of Heat and Mass Transfer, 2013. **62**: p. 553-561.

[181] P.R. Bobbili, B. Sunden, and S.K. Das, An experimental investigation of the port flow maldistribution in small and large plate package heat exchangers. Applied Thermal Engineering, 2006. **26**(16): p. 1919-1926.

[182] O.P. Arsenyeva, L. Čuček, L.L. Tovazhnyanskyy, P.O. Kapustenko, Y.A. Savchenko, S.K. Kusakov, and O.I. Matsegora, Utilisation of waste heat from exhaust gases of drying process. Frontiers of Chemical Science and Engineering, 2016. **10**(1): p. 131-138.

[183] M. Bobič, B. Gjerek, I. Golobič, and I. Bajsić, Dynamic behaviour of a plate heat exchanger: Influence of temperature disturbances and flow configurations. International Journal of Heat and Mass Transfer, 2020. **163**: p. 120439.

[184] J. Ham, Y. Shin, and H. Cho, Theoretical investigation of the influence of pipe diameter and exit channel width in welded plate heat exchanger on heat exchanger performance. Heat and Mass Transfer, 2020. **56**(3): p. 759-771.

[185] H. Arasteh, R. Mashayekhi, M. Ghaneifar, D. Toghraie, and M. Afrand, Heat transfer enhancement in a counter-flow sinusoidal parallel-plate heat exchanger

partially filled with porous media using metal foam in the channels' divergent sections. Journal of Thermal Analysis and Calorimetry, 2019: p. 1-17.

[186] D.P. Soman, S. Karthika, P. Kalaichelvi, and T. Radhakrishnan, Experimental study of turbulent forced convection heat transfer and friction factor in dimpled plate heat exchanger. Applied Thermal Engineering, 2019. **162**: p. 114254.

[187] K. Nilpueng, L.G. Asirvatham, A.S. Dalkılıç, O. Mahian, H.S. Ahn, and S. Wongwises, Heat transfer and fluid flow characteristics in a plate heat exchanger filled with copper foam. Heat and Mass Transfer, 2020: p. 1-11.

[188] S. Chtourou, H. Djemel, M. Kaffel, and M. Baccar. A CFD Investigation of a Turbulent Flow in a Corrugated Plate Heat Exchanger. in International Conference on Advances in Mechanical Engineering and Mechanics. 2019. Springer.

[189] S. Gusew and R. Stuke, Pressure Drop in Plate Heat Exchangers for Single-Phase Convection in Turbulent Flow Regime: Experiment and Theory. International Journal of Chemical Engineering, 2019. **2019**.

[190] Z. Hu, X. He, L. Ye, M. Yang, and G. Qin, Full-scale research on heat transfer and pressure drop of high flux plate heat exchanger. Applied Thermal Engineering, 2017. **118**: p. 585-592.

[191] S. Kakaç, R.K. Shah, and W. Aung, Handbook of single-phase convective heat transfer. 1987.

[192] A.Y.T. Al-Zubaydi and G. Hong, Experimental investigation of counter flow heat exchangers for energy recovery ventilation in cooling mode. International Journal of Refrigeration, 2018. **93**: p. 132-143.

[193] R. Manglik and J. Ding, Laminar flow heat transfer to viscous powerlaw fluids in double-sine ducts. International Journal of Heat and Mass Transfer, 1997. **40**(6): p. 1379-1390.

[194] Y.-H. Wang, J.-L. Zhang, and Z.-X. Ma, Experimental determination of single-phase pressure drop and heat transfer in a horizontal internal helically-finned tube. International Journal of Heat and Mass Transfer, 2017. **104**: p. 240-246.

[195] Y.-H. Wang, J.-L. Zhang, and Z.-X. Ma, Experimental study on single-phase flow in horizontal internal helically-finned tubes: The critical Reynolds number for turbulent flow. Experimental Thermal and Fluid Science, 2018. **92**: p. 402-408.

[196] L. Huang. Port flow distribution in plate heat exchangers. in Proceedings of the Third International Conference on Compact Heat Exchangers and Enhancement Technology for the Process Industries, Davos, Switzerland. 2001.

[197] A. Syed, The use of plate heat exchangers as evaporators and condensers in process refrigeration. Heat Exchange Engineering, 1992.

[198] N. Tokgoz and B. Sahin, Experimental studies of flow characteristics in corrugated ducts. International Communications in Heat and Mass Transfer, 2019. **104**: p. 41-50.

[199] H. Mohammed, A.M. Abed, and M. Wahid, The effects of geometrical parameters of a corrugated channel with in out-of-phase arrangement. International Communications in Heat and Mass Transfer, 2013. **40**: p. 47-57.

[200] S. Al-Zahrani, M.S. Islam, and S.C. Saha, Heat transfer enhancement investigation in a novel flat plate heat exchanger. International Journal of Thermal Sciences, 2021. **161**: p. 106763.

[201] M. Khoshvaght-Aliabadi, A. Jafari, O. Sartipzadeh, and M. Salami, Thermal–hydraulic performance of wavy plate-fin heat exchanger using passive techniques: perforations, winglets, and nanofluids. International Communications in Heat and Mass Transfer, 2016. **78**: p. 231-240.

[202] M.A. Khairul, M.A. Alim, I.M. Mahbubul, R. Saidur, A. Hepbasli, and A. Hossain, Heat transfer performance and exergy analyses of a corrugated plate heat exchanger using metal oxide nanofluids. International Communications in Heat and Mass Transfer, 2014. **50**: p. 8-14.

[203] M. Goodarzi, A. Amiri, M.S. Goodarzi, M.R. Safaei, A. Karimipour, E.M. Languri, and M. Dahari, Investigation of heat transfer and pressure drop of a counter flow corrugated plate heat exchanger using MWCNT based nanofluids. International communications in heat and mass transfer, 2015. **66**: p. 172-179.

[204] A. Bhattad, J. Sarkar, and P. Ghosh, Discrete phase numerical model and experimental study of hybrid nanofluid heat transfer and pressure drop in plate heat exchanger. International Communications in Heat and Mass Transfer, 2018. **91**: p. 262-273.

[205] M. Sarafraz, B. Yang, O. Pourmehran, M. Arjomandi, and R. Ghomashchi, Fluid and heat transfer characteristics of aqueous graphene nanoplatelet (GNP)

nanofluid in a microchannel. International Communications in Heat and Mass Transfer, 2019. **107**: p. 24-33.

[206] S.D. Pandey and V. Nema, An experimental investigation of exergy loss reduction in corrugated plate heat exchanger. Energy, 2011. **36**(5): p. 2997-3001.

[207] O. İpek, B. Kılıç, and B. Gürel, Experimental investigation of exergy loss analysis in newly designed compact heat exchangers. Energy, 2017. **124**: p. 330-335.

[208] O. Arsenyeva, P. Kapustenko, L. Tovazhnyanskyy, and G. Khavin, The influence of plate corrugations geometry on plate heat exchanger performance in specified process conditions. Energy, 2013. **57**: p. 201-207.

[209] H. Lee, K. Saleh, Y. Hwang, and R. Radermacher, Optimization of novel heat exchanger design for the application to low temperature lift heat pump. Energy, 2012. **42**(1): p. 204-212.

[210] Y. Zhang, C. Jiang, B. Shou, W. Zhou, Z. Zhang, S. Wang, and B. Bai, A quantitative energy efficiency evaluation and grading of plate heat exchangers. Energy, 2018. **142**: p. 228-233.

[211] H. Metwally and R.M. Manglik, Enhanced heat transfer due to curvature-induced lateral vortices in laminar flows in sinusoidal corrugated-plate channels. International Journal of Heat and Mass Transfer, 2004. **47**(10-11): p. 2283-2292.

[212] A.S. Dorfman, Conjugate problems in convective heat transfer. 2009: CRC Press.

[213] S. Al-Zahrani, M.S. Islam, and S.C. Saha, Heat transfer enhancement investigation in a novel flat plate heat exchanger. International Journal of Thermal Sciences, 2020. **161**: p. 106763.

[214] Acmite, Global Heat Exchanger Market Report. 2013.

[215] P. Stehlík and V.V. Wadekar, Different strategies to improve industrial heat exchange. Heat Transfer Engineering, 2002. **23**(6): p. 36-48.

[216] S. Chapaloglou, A. Nikolopoulos, N. Nikolopoulos, S. Karellas, and P. Vourliotis, Numerical analysis of a GPHE's hydrodynamic and thermal characteristics, by applying an iterative procedure for the thermal boundary conditions. International Journal of Heat and Mass Transfer, 2018. **118**: p. 88-102.

[217] H.J. Lee and S.H. Lee, Effect of Secondary Vortex Flow Near Contact Point on Thermal Performance in the Plate Heat Exchanger with Different Corrugation Profiles. Energies, 2020. **13**(6): p. 1328.

[218] B.O. Hasan, G.J. Nathan, P.J. Ashman, R.A. Craig, and R.M. Kelso, The effects of temperature and hydrodynamics on the crystallization fouling under cross flow conditions. Applied Thermal Engineering, 2012. **36**: p. 210-218.

[219] A. Karabelas, S. Yiantsios, B. Thonon, and J. Grillot, Liquid-side fouling of heat exchangers. An integrated R & D approach for conventional and novel designs. Applied Thermal Engineering, 1997. **17**(8-10): p. 727-737.

[220] S.N. Kazi, G. Duffy, and X.D. Chen, Fouling mitigation of heat exchangers with natural fibres. Applied thermal engineering, 2013. **50**(1): p. 1142-1148.

[221] S. Peyghambarzadeh, A. Vatani, and M. Jamialahmadi, Application of asymptotic model for the prediction of fouling rate of calcium sulfate under subcooled flow boiling. Applied Thermal Engineering, 2012. **39**: p. 105-113.

[222] E.K. Tamakloe, G.T. Polley, and M. Picón-Núñez, Design of Compabloc exchangers to mitigate refinery fouling. Applied thermal engineering, 2013. **60**(1-2): p. 441-448.

[223] G. Polley, D. Wilson, B. Yeap, and S. Pugh, Use of crude oil fouling threshold data in heat exchanger design. Applied Thermal Engineering, 2002. **22**(7): p. 763-776.

[224] O.P. Arsenyeva, B. Crittenden, M. Yang, and P.O. Kapustenko, Accounting for the thermal resistance of cooling water fouling in plate heat exchangers. Applied Thermal Engineering, 2013. **61**(1): p. 53-59.

[225] M. Shirzad, M.A. Delavar, S.S.M. Ajarostaghi, and K. Sedighi, Evaluation the effects of geometrical parameters on the performance of pillow plate heat exchanger. Chemical Engineering Research and Design, 2019. **150**: p. 74-83.

[226] Y. Islamoglu and C. Parmaksizoglu, The effect of channel height on the enhanced heat transfer characteristics in a corrugated heat exchanger channel. Applied Thermal Engineering, 2003. **23**(8): p. 979-987.

[227] O. Arsenyeva, J. Tran, M. Piper, and E. Kenig, An approach for pillow plate heat exchangers design for single-phase applications. Applied Thermal Engineering, 2019. **147**: p. 579-591.

[228] O. Arsenyeva, M. Piper, A. Zibart, A. Olenberg, and E.Y. Kenig, Investigation of heat transfer and hydraulic resistance in small-scale pillow-plate heat exchangers. Energy, 2019. **181**: p. 1213-1224.

[229] M. Piper, A. Zibart, E. Djakow, R. Springer, W. Homberg, and E. Kenig, Heat transfer enhancement in pillow-plate heat exchangers with dimpled surfaces: A numerical study. Applied Thermal Engineering, 2019. **153**: p. 142-146.

[230] X. Tao and C.A.I. Ferreira, Heat transfer and frictional pressure drop during condensation in plate heat exchangers: Assessment of correlations and a new method. International Journal of Heat and Mass Transfer, 2019. **135**: p. 996-1012.

[231] G.A. Longo, G. Righetti, and C. Zilio, A new computational procedure for refrigerant condensation inside herringbone-type Brazed Plate Heat Exchangers. International Journal of Heat and Mass Transfer, 2015. **82**: p. 530-536.

[232] W. Kuo, Y. Lie, Y. Hsieh, and T. Lin, Condensation heat transfer and pressure drop of refrigerant R-410A flow in a vertical plate heat exchanger. International Journal of Heat and Mass Transfer, 2005. **48**(25-26): p. 5205-5220.

[233] B. GÜREL, A numerical investigation of the melting heat transfer characteristics of phase change materials in different plate heat exchanger (latent heat thermal energy storage) systems. International Journal of Heat and Mass Transfer, 2020. **148**: p. 119117.

[234] B. Gürel, Thermal performance evaluation for solidification process of latent heat thermal energy storage in a corrugated plate heat exchanger. Applied Thermal Engineering, 2020: p. 115312.

[235] H.J. Juaifer, M.B. Ayani, and M. Poursadegh, Melting process of paraffin wax inside plate heat exchanger: experimental and numerical study. Journal of Thermal Analysis and Calorimetry, 2020: p. 1-12.

[236] M. Medrano, M. Yilmaz, M. Nogués, I. Martorell, J. Roca, and L.F. Cabeza, Experimental evaluation of commercial heat exchangers for use as PCM thermal storage systems. Applied energy, 2009. **86**(10): p. 2047-2055.

[237] G.B. Abadi, C. Moon, and K.C. Kim, Experimental study on single-phase heat transfer and pressure drop of refrigerants in a plate heat exchanger with metal-foam-filled channels. Applied Thermal Engineering, 2016. **102**: p. 423-431.

[238] H. Ghasemkhani, A. Keyhani, M. Aghbashlo, S. Rafiee, and A.S. Mujumdar, Improving exergetic performance parameters of a rotating-tray air dryer via a simple heat exchanger. Applied Thermal Engineering, 2016. **94**: p. 13-23.

[239] M. Sarafraz, V. Nikkhah, S. Madani, M. Jafarian, and F. Hormozi, Low-frequency vibration for fouling mitigation and intensification of thermal performance of a

plate heat exchanger working with CuO/water nanofluid. Applied Thermal Engineering, 2017. **121**: p. 388-399.

[240] J. Vogel, J. Felbinger, and M. Johnson, Natural convection in high temperature flat plate latent heat thermal energy storage systems. Applied Energy, 2016. **184**: p. 184-196.

[241] J.A. Gut, R. Fernandes, J.M. Pinto, and C.C. Tadini, Thermal model validation of plate heat exchangers with generalized configurations. Chemical Engineering Science, 2004. **59**(21): p. 4591-4600.

[242] S. Al zahrani, M.S. Islam, and S.C. Saha, Heat transfer augmentation in retrofitted corrugated plate heat exchanger. International Journal of Heat and Mass Transfer, 2020(Accepted for publication).

[243] S.J. Kline and F.A. McClintock, Describing uncertainties in single-sample experiments, Mech. 1953, Engng.

[244] Fluent 6.3 user manual, Access date 13.11.2018 (https://www.sharcnet.ca/Software/Fluent6/html/ug/main_pre.htm).

[245] T.-H. Shih, W.W. Liou, A. Shabbir, Z. Yang, and J. Zhu, A new k-epsilon eddy viscosity model for high Reynolds number turbulent flows: Model development and validation. 1994.

[246] X. Li, J. Sun, C. Xu, Y. Li, R. Zhang, L. Qian, and Y. Chen, Visualization of bubble flow in the channel of a dimple-type embossing plate heat exchanger under different fluid inlet/outlet ports. International Journal of Heat and Mass Transfer, 2019. **145**: p. 118750.

[247] X. Liu and J. Niu, Effects of geometrical parameters on the thermohydraulic characteristics of periodic cross-corrugated channels. International Journal of Heat and Mass Transfer, 2015. **84**: p. 542-549.

[248] X. Zhang, Y. Wang, M. Li, S. Wang, and X. Li, Improved flow and heat transfer characteristics for heat exchanger by using a new humped wavy fin. Applied Thermal Engineering, 2017. **124**: p. 510-520.

[249] H. Wang, Y.-w. Liu, P. Yang, R.-j. Wu, and Y.-l. He, Parametric study and optimization of H-type finned tube heat exchangers using Taguchi method. Applied Thermal Engineering, 2016. **103**: p. 128-138.

[250] D.H. Park, D.B. Lee, E.R. Seo, and Y.J. Park, Study on the heat transfer and fluid flow characteristics in V-shaped corrugated composite fin. Applied Thermal Engineering, 2016. **102**: p. 293-301.